Linear Stability and Transient Behaviour of Viscoelastic Fluids in Boundary Layers

submitted by

Martina Cracco

for the degree of Doctor of Philosophy

of the

CARDIFF UNIVERSITY

November 2019

Declaration

This work has not been submitted in substance for any other degree or award at this or any other university or place of learning, nor is being submitted concurrently in candidature for any degree or other award.

Signed . . . . (candidate) Date . . . .

STATEMENT 1
This thesis is being submitted in partial fulfilment of the requirements for the degree of PhD.

Signed . . . . (candidate) Date . . . .

STATEMENT 2
This thesis is the result of my own independent work/investigation, except where otherwise stated. Other sources are acknowledged by explicit references. The views expressed are my own.

Signed . . . . (candidate) Date . . . .

STATEMENT 3
I hereby give consent for my thesis, if accepted, to be available for photocopying and for inter-library loan, and for the title and summary to be made available to outside organisations.

Signed . . . . (candidate) Date . . . .

Abstract

The linear stability analysis of Rivlin-Ericksen fluids of second order is investigated for boundary layer flows, where a semi-infinite wedge is placed symmetrically with respect to the flow direction. Second order fluids belong to a larger family of fluids called Order fluids, which is one of the first classes proposed to model departures from Newtonian behaviour. Second order fluids can represent non-zero normal stress differences, which is an essential feature of viscoelastic fluids.

The linear stability properties are studied for both signs of the elasticity number K, which characterises the non-Newtonian response of the fluid. Stabilisation is observed for the temporal and spatial evolution of two-dimensional disturbances when $K > 0$, in terms of increase of critical Reynolds numbers and reduction of growth rates, whereas the flow is less stable when $K < 0$. By extending the analysis to three-dimensional disturbances, we show that a positive elasticity number K destabilises streamwise independent waves, while the opposite happens for $K < 0$.

We show that, as for Newtonian fluids, the nonmodal amplification of streamwise independent disturbances is the most dangerous mechanism for transient energy growth which is enhanced when $K > 0$ and reduced when $K < 0$.

A preliminary study of boundary layer flows of UCM, Oldroyd B, Phan-Thien Tanner and Giesekus fluids is performed. Asymptotic Suction Boundary Layer theory allows us to simplify the governing equations and obtain analytical solutions for the UCM and Oldroyd B models. The mean flow obtained can be used as a starting point for a modal and nonmodal linear stability analysis, following the analysis performed for second order models.

Acknowledgments

I would like to thank my supervisors Dr Chris Davies and Prof Tim Phillips for their invaluable guidance and support throughout the years of my PhD. Their knowledge and patience has been key to my academic growth.

I would also like to thank Dr Paul Griffiths for meeting me through the UK Fluids Network and for his precious insights and encouragements.

I thank the EPSRC for funding this research and the School of Mathematics for hosting it.

My gratitude also goes to my academic brothers, Scott and Alex. It was a pleasure to share an office, conference trips and inspiring conversations about maths and about life.

It is impossible to express how grateful I am for my years in Cardiff, which so many friends made special. I thank all the international friends I crossed path with, who opened my mind and will stay always with me even if far away. In particular, I thank my academic cousin, Lorenzo, and the inexhaustible source of energy who is my flatmate Carlotta.

Finally, but not last, I would like to thank my father and brother. They always welcomed me back home and made sure I found the best food. They accompanied me in endless and regenerating walks in our amazing mountains.

Contents

List of Figures

Introduction

The aim of this thesis is to investigate the hydrodynamic stability of viscoelastic fluids in boundary layers.

Viscoelastic fluids are examples of non-Newtonian fluids. The mechanical behaviour of many real fluids is well described by the Navier-Stokes theory. This theory is based on the assumption of a Newtonian constitutive equation. More specifically, the extra-stress tensor can be expressed as a linear, isotropic function of the components of the velocity gradient. Many common fluids, such as water and air can be assumed to be Newtonian. However, many rheologically complex fluids such as polymer solutions, soaps, blood, paints, shampoo, ketchup are not well described by a Newtonian constitutive equation.These fluids exhibit a variety of non-Newtonian behaviours that cannot be captured using the Navier-Stokes equations.

The branch of fluid mechanics which studies the deformation and flow of materials is known as *Rheology*. The emergence of rheology as a separate field can be dated back to 1929 with the formation of the Society of Rheology, due to an increased interest in understanding the mechanical behaviour of industrial materials like rubber, plastics, paints and many biological fluids like blood. Since then, several constitutive equations have been proposed to model departures from Newtonian behaviour. Most of them take into account the microstructure to better represent complex responses of the materials.

In this work, we focus on viscoelastic fluids, which exhibit both viscous and elastic properties when undergoing deformation (Phan-Thien [**59**]). Viscous fluids resist forces exerted upon them through internal friction and they instantaneously forget the shape they are in. For these fluids, the stress is directly proportional to the rate of

strain and satisfies the Newtonian law. Elastic solids always remember the shape they start from and, when the stress is removed, they relax back to their original shape. The stress experienced by the solid is directly proportional to the strain. Viscoelastic fluids undergo a gradual deformation and recovery when they are subjected to loading and unloading. The stress is neither directly proportional to the strain nor the rate of strain, the relationship is more complex.

One of the first class of material models proposed consists of fluids of differential type (Owens and Phillips [54]). In this thesis, we consider a subclass of differential type fluids known as the *Rivlin-Ericksen fluids of second order*. In these models, only an infinitesimal part of the history of the deformation gradient has an influence on the stress. The extra-stress is a function of the velocity gradient and its higher time derivatives. These materials lack a gradually fading memory and they cannot represent the phenomenon of *stress relaxation*. However, they can predict *non-zero normal stress differences*. The presence of non-zero normal stress differences is an important feature of viscoelastic fluids, which is responsible for interesting phenomena such as *rod-climbing* and *die swell* (Boger and Walters [10]). The rod-climbing effect, also referred to as Weissenberg effect, can occur when a rod is rotated into a beaker containing a viscoelastic fluid. For Newtonian fluids, inertia would dominate and the fluid would move to the edges of the container. For viscoelastic fluids, the rotation produces a tension along the circular streamlines and forces the fluid up the rod. The phenomenon of die-swell can occur when a viscoelastic fluid is extruded from a capillary. For viscoelastic fluids, the extrudate diameter tends to swell considerably more than for Newtonian fluids. In the tube, a tension along the streamlines associated with the normal stresses is present. At the extrusion, the viscoelastic fluid relaxes the tension along the streamlines by expanding radially.

The aim of the first part of this thesis is to understand the linear stability behaviour of such fluids in boundary layers and to study how the presence of non-zero normal stress differences affects the stability properties. Specifically, a configuration of a flow over a semi-infinite wedge is investigated.

Free Stream
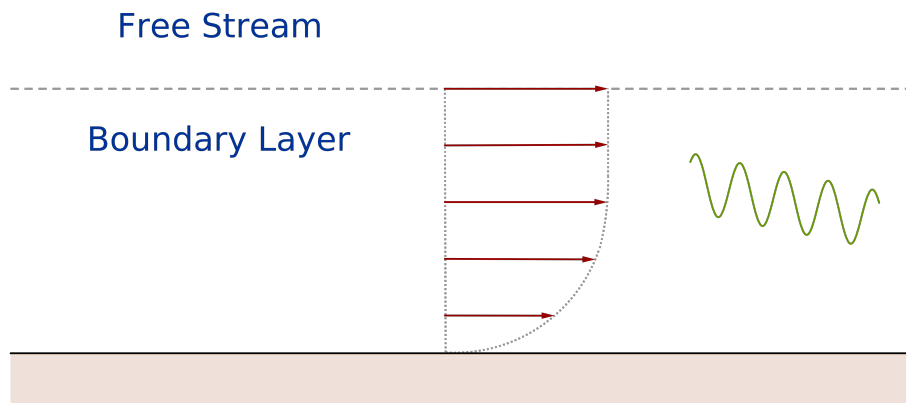
Boundary Layer

FIGURE 0.1. Illustration of disturbances in the boundary layer.

The second order fluid model has been chosen for its mathematical simplicity and the possibility of applying a boundary layer approximation similar to Newtonian fluids. Later in the thesis, we consider more complex viscoelastic models such as the Upper-Convected Maxwell, Oldroyd B, Phan-Thien Tanner and Giesekus models. We start investigating the undisturbed flow profile as the first necessary step in order to apply a linear stability analysis. By means of a theory known as asymptotic suction boundary layer (ASBL), which assumes homogeneous suction at the wall, we are able to considerably simplify the governing equations and obtain analytical solutions for the Uprper-Convected Maxwell and the Oldroyd B models. Analytical velocity profiles are not common. To the best of our knowledge, this has not been done in the past.

Boundary layers are thin layers near the surface of an object where the velocity varies from zero at the wall to the full velocity at a certain distance from the wall (see Figure 0.1). Boundary layer theory was presented by Prandtl during the Heidelberg mathematical congress in 1904 (Anderson [3]). His related paper [62], published a year later, showed how viscosity affects the flow at high Reynolds numbers. The Reynolds number is a dimensionless quantity defined as $Re = UL/\nu$, where U and L are the characteristic velocity and length, respectively, and ν is the kinematic viscosity of the fluid. It represents the ratio of inertial forces to viscous forces.

Prandtl suggested that the fluid adheres to the surface of an object so its velocity adjacent to the wall is zero and that the viscosity becomes important only in a thin layer near the surface (Schlichting and Gersten [**73**]). Prandtl's work enabled the Navier-Stokes equations to be reduced to a much simpler form.

In 1908, Blasius [**9**] solved the boundary layer equations for the two-dimensional flow over a flat plate by reducing the system of partial differential equations to a single ordinary differential equation by means of a similarity transformation. In 1931, Falkner and Skan [**28**] extended the work to include the case of the plate forming a wedge with respect to the flow direction.

Boundary layer theory has many practical applications, such as the calculation of the friction drag of bodies in a flow (Schlichting and Gersten [**73**]), and therefore it is natural to extend it to non-Newtonian fluids. In this thesis, we apply a boundary layer approximation to the case of a non-Newtonian fluid of second order.

We are interested in studying how disturbances propagate in the boundary layer region. The subject which concerns the stability and instability of motion of fluids is known as *hydrodynamic stability theory*. It began in the late 19th century with the important work of Reynolds and Lord Rayleigh (Schmid and Henningson [**77**]). If the flow returns to its original laminar state after being disturbed with a perturbation of small or finite amplitude, the flow is said to be *stable*. If the disturbance grows, the flow is said to be *unstable*. An unstable flow often evolves into a state of motion called *turbulence*, which is characterised by chaotic three-dimensional variations with a broad spectrum of spatial and temporal scales.

The first step in stability analysis is to consider the disturbances to be very small and to linearise the equations about a given base flow, which allows one to simplify the equations considerably (Schmid and Henningson [**77**]). As the disturbances grow, nonlinear effects become important and cannot be ignored. Throughout this thesis we focus our attention on linear stability. The linear stability equations have

limited validity but they are important in identifying physical growth mechanisms and the particular disturbance which grows the most.

In this work we conduct a local stability analysis where we assume a normal mode form for the disturbances, which is equivalent to taking the Fourier transform of the linearised equations. Following this approach, for two-dimensional Newtonian fluids the classical *Orr-Sommerfeld equation* is obtained. Later in the thesis, we present a modified Orr-Sommerfeld equation for second order fluids.

For Newtonian fluids, an important result known as *Squire's theorem* justifies the study of two-dimensional instead of three-dimensional disturbances (Drazin [**23**]). However, an equivalent Squire's theorem for second order fluids cannot be proven. Therefore, we extend the analysis to the study of three-dimensional disturbances for second order fluids.

Classical linear stability analysis is based on eigenvalues. However, in hydrodynamic stability and in many other physical situations dominated by nonnormal systems, eigenvalues prove to be misleading and they do not describe correctly the whole dynamics (Trefethen *et al.* [**90**]). In nonnormal systems, such as Poiseuille, Couette and Blasius flows, it can be seen that there can be short-time growth of energy even if all the eigenvalues decay exponentially (Butler and Farrell [**14**]). This phenomenon is known as *transient growth*.

For Newtonian fluids, the possibility of transient growth has been known since the 1980s (Landahl [**49**]). Some work has been done regarding the transient growth of viscoelastic fluids in channel flows (Brandt [**11**]). Therefore, in this work we analyse the transient growth of second order fluids in boundary layers.

Outline of this thesis

Chapter 1 provides a linear stability analysis of Rivlin-Ericksen fluids of second order. First, a mean flow profile is obtained by applying Prandtl's boundary layer approximation to the governing equations. This allows the PDEs to be simplified and a pseudo-similarity transformation is introduced to reduce them to an ODE. The ODE obtained

retains a dependency on the streamwise direction. However, this problem is overcome by introducing an elasticity number, K, based on the displacement thickness. Secondly, we derive a modified Orr-Sommerfeld equation which governs the development of two-dimensional disturbances for second order fluids. This equation reduces to the Newtonian Orr-Sommerfeld equation when the elasticity number $K = 0$, and has extra-terms which account for non-Newtonian effects.

The mean flow and the Orr-Sommerfeld equations are solved numerically. The results are represented in terms of neutral stability curves and critical Reynolds numbers, taking into account both the temporal and the spatial evolution of disturbances. Finally, the linear stability analysis is extended to three-dimensional disturbances.

In Chapter 2, the linear stability equations are written as an initial-value problem. This allows one to study the short-time behaviour of disturbances and their tendency to grow transiently. We derive the initial-value problem for second order fluids and analyse how non-zero normal stress differences affect the transient growth. We compare the maximum possible amplification of energy density in the Newtonian and non-Newtonian cases and analyse which type of disturbances grows the most. In order to confirm the transient growth results we solve the initial-value problem by marching in time with a numerical scheme.

Chapter 3 is dedicated to the confirmation of the results obtained in Chapter 1 using Direct Numerical Simulations (DNS). The governing equations are written using a compact velocity-vorticity formulation, where the number of variables in the system is reduced. We follow the approach of Davies and Carpenter [19] and derive velocity-vorticity equations for second order fluids. The flow is disturbed by a temporally localised forced impulse. We represent the solutions in terms of Chebyshev polynomials and integrate the equations twice. Finally, the discretised system of equations is solved by marching in time with a predictor-corrector method. We present a comparison between the temporal growth rates obtained through the simulations and the ones given by the eigenvalue analysis described in Chapter 1.

Chapter 4 is a preliminary study of the flow of more complex viscoelastic fluids. We take into consideration the Upper-Convected Maxwell, Oldroyd B, Phan-Thien Tanner and Giesekus models and begin by expressing their constitutive equations as one single constitutive equation which can represent them all. These models are characterised by more complicated governing equations and the application of a boundary layer, as for the Newtonian and second order fluids, is not straightforward. Instead, we apply an asymptotic suction boundary layer and obtain mean flow profiles that can be used as a starting point for a linear stability analysis.

Chapter 5 describes the numerical methods employed throughout this thesis. The main technique used to approximate derivatives in the wall-normal direction is the Chebyshev collocation method. For this purpose, we map the semi-infinite domain into a finite interval. The type of mappings considered in this work naturally clusters the grid points near the wall. This property is particularly suitable for the problems studied, where more points near the wall are required to resolve the rapid changes happening inside the boundary layer. We perform numerical tests to determine what kind of mapping is best to solve numerically the linear stability equations described in Chapters 1 and 2.

A literature survey is given at the beginning of each chapter and covers the main work already done on the topic.

CHAPTER 1

Linear stability analysis of second order fluids

In this chapter, we present a linear stability analysis performed on fluids of second order. This kind of analysis is the starting point to understand the stability properties of a fluid in a specific geometry.

Second order fluids belong to a larger family of fluids called *Order fluids* that can be classified as fluids of differential type or Rivlin-Ericksen fluids (Rivlin and Ericksen [**70**]). The constitutive equation is a polynomial function of the Rivlin-Eriksen tensors $\{A_k\}$. The tensors $\{A_k\}$ are frame-indifferent measures of higher rates of material straining. Since the tensor A_k has physical dimension t^{-k}, where t is the time, order fluids can be derived by arranging the terms in the polynomial function as reciprocal powers of t. By terminating the expansion at first order, we obtain the Newtonian fluid while at second order we obtain the second order fluid.

This class of constitutive equations is one of the first proposed to model departures from Newtonian behaviour. In such models, only an infinitesimal part of the history of the deformation gradient has an influence on the stress. In fact, the extra-stress tensor is a function of the velocity gradient and its time derivatives. Therefore, while these models are able to describe the phenomenon of creep, they cannot represent the phenomenon of stress relaxation (Dunn and Rajagopal [**26**]). However, second order models can capture non-zero normal stress differences. As models to describe viscoelastic fluids, Order fluids are suitable to describe slightly elastic fluids, where the fluid's behaviour weakly departs from the Newtonian one and flows for which the Rivlin-Ericksen tensors vary slowly (Owens and Phillips [**54**]).

9

In this chapter, we perform a linear stability analysis of a second grade fluid past a semi-infinite wedge by solving a modified Orr-Sommerfeld equation around a steady and parallel mean flow, which is obtained by numerically solving a local ODE. We study the non-Newtonian effects on stability by comparing the growth rates in the Newtonian and non-Newtonian cases and we quantify this effect by computing the neutral stability curves and the critical Reynolds numbers. We show the stabilising effect of elasticity in the second grade model, and the destabilising effects in the second order model, for all the geometrical configurations considered.

Section 1.1 provides an introduction to second order models and a brief literature review. In Section 1.2, we present the governing equations and the geometrical configuration. In Section 1.3, we derive the mean flow by applying a boundary layer approximation and in Section 1.4 we apply a two-dimensional linear stability analysis. The results can be found in Section 1.5. In Section 1.6, we apply energy theory to the non-Newtonian models considered. Section 1.7 extends the linear stability analysis to three-dimensional disturbances. In Section 1.8, we comment briefly on the results obtained in this chapter.

1.1. Second order fluids

The Cauchy stress tensor $\boldsymbol{\sigma}$ in a fluid of second grade has the form (Rivlin and Ericksen [70], Owens and Phillips [54])

$$\boldsymbol{\sigma} = -p\mathbf{I} + \mu\mathbf{A}_1 + \alpha_1\mathbf{A}_2 + \alpha_2\mathbf{A}_1^2, \qquad (1.1)$$

where p is the pressure, μ is the dynamic viscosity, α_1 and α_2 (SI: Kg/m) are the material moduli usually referred to as *normal stress moduli*. The spherical stress $-p\mathbf{I}$ is due to the constraint of incompressibility, while $\mathbf{A}_1$ and $\mathbf{A}_2$ are the Rivlin-Ericksen tensors of order 1 and order 2 respectively[1]

$$\mathbf{A}_1 = \nabla\mathbf{v} + \nabla\mathbf{v}^T, \quad \mathbf{A}_2 = \frac{\mathrm{D}\mathbf{A}_1}{\mathrm{D}t} + (\nabla\mathbf{v})\mathbf{A}_1 + \mathbf{A}_1(\nabla\mathbf{v})^T, \qquad (1.2)$$

---

[1]For the gradient velocity tensor $\nabla\mathbf{v}$ we use the following definition

$$(\nabla\mathbf{v})_{i,j} = \frac{\partial v_j}{\partial x_i}.$$

where $\mathbf{v}$ denotes the velocity field and $\mathrm{D}/\mathrm{D}t$ denotes the material time derivative.

Rivlin and Ericksen [70] proved that, if the extra-stress tensor depends only on the velocity gradients and higher time-derivatives, then there exists a polynomial in $\mathbf{T} = \boldsymbol{\sigma} + p\mathbf{I}$, the deviatoric stress, and the Rivlin-Ericksen tensors $\{\mathbf{A}_k\}$. These are frame-indifferent measures of higher rates of material straining. In general, the Rivlin-Ericksen tensor $\mathbf{A}_k$ of order k is defined as the k-th time derivative of the Cauchy-Green strain tensor

$$\mathbf{C} = \mathbf{F}^T\mathbf{F},$$

where $\mathbf{F}$ is the deformation gradient tensor. It can be seen that $\mathbf{A}_1$ is the rate-of-strain tensor and there exists a recurrence relation that permits us to calculate $\mathbf{A}_{k+1}$ as the lower-convected derivative of the previous kinematic tensor $\mathbf{A}_k$. Since the tensor $\mathbf{A}_k$ has physical dimension t^{-k} where t is the time, the second order models can be obtained by truncating the polynomial expansion for $\mathbf{T}$ at second order.

The sign of the material parameters in this model has been a source of some controversy (Dunn and Rajagopal [26]). Henceforth, we will refer to the model with a positive material parameter α_1 as the "second grade model" and to the model with a negative α_1 as the "second order model", in line with the literature. However, sometimes we will talk about "second order models" to indicate both cases and this will be clear from the context.

In this work, we consider both the cases $\alpha_1 > 0$ and $\alpha_1 < 0$. The second grade model, for which $\alpha_1 > 0$, is taken into account because of its compatibility with thermodynamics. Since the form (1.1) is properly frame-indifferent, it can be used as an exact model. In this view, Dunn and Fosdick [25], Fosdick and Rajagopal [29] justified some assumptions on the coefficients of the second order constitutive equation. In order for the fluid model to be compatible with thermodynamics, in the sense that all motions of the fluid satisfy the Clausius-Duhem inequality and the assumption that the specific Helmholtz free energy be a minimum in equilibrium, it then follows that

$$\mu \geq 0, \quad \alpha_1 \geq 0 \quad \text{and} \quad \alpha_1 + \alpha_2 = 0. \tag{1.3}$$

A detailed discussion on these assumptions can be found in the critical review of Dunn and Rajagopal [26].

The second order model, for which $\alpha_1 < 0$, is studied because it gives the right sign for the first normal stress difference, as shown in the next section. Moreover, in terms of linear stability, it is a consistent approximation to a proper stress-relaxing fluid, such as the Maxwell fluid, at small elasticity numbers and when the disturbance time scale is large compared to the characteristic time scale of the fluid (Porteous and Denn [61]).

1.1.1. Second order fluids in boundary layers. In theoretical work, Rajagopal *et al.* [66] showed that it is possible to apply Prandtl's boundary layer theory to the case of a non-Newtonian fluid of second grade. In particular, they showed that the equations of motion of a second grade fluid can be satisfied by an irrotational flow and they identified suitable assumptions to obtain a consistent theory. In the case of fluids of differential type the equations of motion are an order higher than the Navier-Stokes equations, and thus the no-slip and no-penetration boundary conditions are insufficient to determine the solution completely (Rajagopal and Kaloni [67] and Rajagopal [64]). The same is also true for the boundary layer approximation. In order to overcome this difficulty, in their study of an incompressible fluid of liquid B' near a stagnation point, Beard and Walters [6] suggested a perturbation method. This method was also adopted by Rajagopal *et al.* [65] in their analysis of the flow past a wedge of an incompressible fluid of second grade. The perturbation method reduces the order of the problem, but is only valid for small values of the non-Newtonian parameter. This parameter multiplies the higher order spatial derivatives in the equation.

While studying flow near a stagnation point and flow past a wedge, Garg and Rajagopal [31, 32] suggested that it would be preferable to use an augmented boundary condition justified by physically reasonable assumptions. The augmented condition, based on smoothness properties of the solution at infinity, was also adopted by Vajravelu and Roper [92] in their study of the flow and heat transfer in a second grade fluid over

a stretching sheet and by Vajravelu and Rollins [**91**] while studying hydromagnetic flow of a second grade fluid over a stretching sheet.

Another difficulty that arises is the impossibility of finding a similarity solution to the boundary layer equations as in the Newtonian case, with the exception of stagnation flow. Garg and Rajagopal [**32**] showed that a pseudo-similarity solution is possible and solved numerically the local ODE obtained.

1.1.2. Linear stability of second order fluids. To the best of our knowledge, little work has been done on the stability of second grade/order fluids in boundary layers unlike the situation for channel flows. In 1968, Chun and Schwarz [**15**] studied the stability of plane Poiseuille flow of a second order fluid ($\alpha_1 < 0$). Their analysis yields an Orr-Sommerfeld equation modified by adding a non-Newtonian term. The mean flow is a parabolic profile as in the Newtonian case. They showed that the critical Reynolds number decreases as the magnitude of the non-Newtonian parameter increases. Later Sadeghy *et al.* [**71**] solved the same modified Orr-Sommerfeld equation for the plane Poiseuille flow of a second grade fluid ($\alpha_1 > 0$). They showed that non-Newtonian effects in this model are stabilising. Rafiki *et al.* [**63**] studied the hydrodynamic stability of plane Poiseuille flow of second order and second grade fluids in the presence of a transverse magnetic field. The combined effects of magnetic field and elasticity on the stability are investigated. The analysis is performed by solving the modified Orr-Sommerfeld equation using a collocation method. In agreement with previous literature, Rafiki *et al.* [**63**] found that elasticity is stabilising for second grade fluids ($\alpha_1 > 0$) and destabilising for second order fluids ($\alpha_1 < 0$).

Regarding the linear stability of non-Newtonian fluids in boundary layers, Griffiths [**34**] recently studied the effect of shear-thinning on the linear stability of flow over an inclined flat plate. Shear-thinning is shown to delay instability for the two material models considered.

Regarding the stability of viscoelastic fluids, some results were obtained for channel flows but, to the best of our knowledge, not much

has been done for boundary layer flows. Porteous and Denn [61] studied the linear stability analysis of plane Poiseuille flow for the second order and Maxwell fluids. They showed that the second order model is a consistent approximation to the Maxwell model in the limit of small elasticity and when the disturbance time scale is large compared to the characteristic time scale of the fluid. The results shows a destabilisation process due to elasticity. At high values of the elasticity number, the stability is qualitatively different from that for Newtonian fluids because it results from the second mode of the Orr-Sommerfeld equation.

Sureshkumar and Beris [80] used an Arnoldi-based orthogonalization algorithm to investigate the linear stability of Poiseuille flow. The models investigated are Upper Convected Maxwell (UCM), Oldroyd B and Chilcott-Rallison fluids. The results show that the destabilisation caused by elasticity for the UCM fluid is reduced when effects of solvent viscosity and finite extensibility are taken into account. Zhang *et al.* [96] showed that, when the polymer relaxation time is shorter than the instability time scale, the Poiseuille flow of FENE-P fluids appears to be less stable. However, in the opposite case, the strong elastic effect stabilises the flow.

1.2. Governing equations

The field equations for an incompressible second order fluid can be derived by substituting expression (1.1) for the Cauchy stress into the balance of linear momentum

$$\rho \frac{\mathrm{D}\mathbf{v}}{\mathrm{D}t} = \nabla \cdot \boldsymbol{\sigma}, \tag{1.4}$$

where ρ is the density of the fluid and $\nabla \cdot \boldsymbol{\sigma}$ denotes the divergence of the stress tensor[2]. Since the fluid is incompressible, i.e. $\frac{D\rho}{Dt} = 0$, we require all possible motions be isochoric and hence for the conservation of mass the continuity equation reduces to

$$\nabla \cdot \mathbf{v} = 0. \tag{1.5}$$

---

[2]The divergence of the tensor $\boldsymbol{\sigma}$ is defined by

$$(\nabla \cdot \boldsymbol{\sigma})_j = \frac{\partial \boldsymbol{\sigma}_{i,j}}{\partial x_j},$$

where Einstein summation convention is adopted.
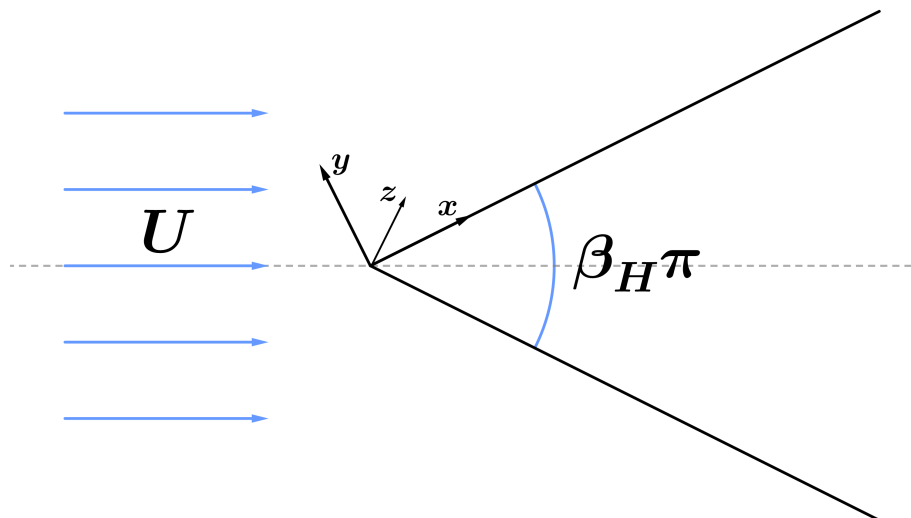
FIGURE 1.1. Semi-infinite wedge flow configuration ($\beta_H > 0$).

The geometric configuration considered consists of a wedge of angle $\beta_H\pi$ which is placed symmetrically with respect to the direction of the uniform velocity field, as shown in Figure 1.1. The x-axis is chosen to be in the streamwise direction, the z-axis in the spanwise direction and the y-axis in the wall-normal direction. Due to the symmetric nature of the problem, we can restrict our analysis to the case $y \geq 0$.

The angle parameter β_H is known as *Hartree parameter*. Notice that, if $\beta_H = 0$, we recover the case of flow over a semi-infinite flat plate, while $\beta_H = 1$ corresponds to the case of a stagnation point flow. When $\beta_H > 1$ we have the flow into an acute corner, $\beta_H < 0$ gives a flow past a corner and $0 < \beta_H < 1$ is the flow past an acute wedge.

Consider the case of steady two-dimensional flow described by the velocity field $\mathbf{v} = (u, v)$. After a straightforward manipulation of equations (1.4) and (1.5), which can be found in Appendix A.1, we obtain the following governing equations

$$\frac{\partial u}{\partial x} + \frac{\partial v}{\partial y} = 0, \tag{1.6a}$$

$$u\frac{\partial u}{\partial x} + v\frac{\partial u}{\partial y} = -\frac{1}{\rho}\frac{\partial p}{\partial x} + \frac{\mu}{\rho}\left(\frac{\partial^2 u}{\partial x^2} + \frac{\partial^2 u}{\partial y^2}\right) \tag{1.6b}$$

$$+ \frac{\alpha_1}{\rho}\left[2\frac{\partial^2}{\partial x^2}\left(u\frac{\partial u}{\partial x} + v\frac{\partial u}{\partial y}\right) + \frac{\partial^2}{\partial y^2}\left(u\frac{\partial u}{\partial x} + v\frac{\partial u}{\partial y}\right)\right.$$

$$+ \frac{\partial^2}{\partial x \partial y}\left(u\frac{\partial v}{\partial x} + v\frac{\partial v}{\partial y}\right) + 2\frac{\partial}{\partial y}\left(\frac{\partial u}{\partial x}\frac{\partial u}{\partial y} + \frac{\partial v}{\partial x}\frac{\partial v}{\partial y}\right)$$

$$\left.+ \frac{\partial}{\partial x}\left(\left(\frac{\partial v}{\partial x}\right)^2 - \left(\frac{\partial u}{\partial y}\right)^2 - 2\left(\frac{\partial u}{\partial x}\right)^2 - 2\frac{\partial v}{\partial x}\frac{\partial u}{\partial y}\right)\right],$$

$$u\frac{\partial v}{\partial x} + v\frac{\partial v}{\partial y} = -\frac{1}{\rho}\frac{\partial p}{\partial y} + \frac{\mu}{\rho}\left(\frac{\partial^2 v}{\partial x^2} + \frac{\partial^2 v}{\partial y^2}\right) \tag{1.6c}$$

$$+ \frac{\alpha_1}{\rho}\left[2\frac{\partial^2}{\partial y^2}\left(u\frac{\partial v}{\partial x} + v\frac{\partial v}{\partial y}\right) + \frac{\partial^2}{\partial x^2}\left(u\frac{\partial v}{\partial x} + v\frac{\partial v}{\partial y}\right)\right.$$

$$+ \frac{\partial^2}{\partial x \partial y}\left(u\frac{\partial u}{\partial x} + v\frac{\partial u}{\partial y}\right) + 2\frac{\partial}{\partial x}\left(\frac{\partial u}{\partial x}\frac{\partial u}{\partial y} + \frac{\partial v}{\partial x}\frac{\partial v}{\partial y}\right)$$

$$\left.+ \frac{\partial}{\partial y}\left(\left(\frac{\partial u}{\partial y}\right)^2 - \left(\frac{\partial v}{\partial x}\right)^2 - 2\left(\frac{\partial v}{\partial y}\right)^2 - 2\frac{\partial v}{\partial x}\frac{\partial u}{\partial y}\right)\right].$$

1.2.1. Viscometric flow. The stress components can be completely determined in steady viscometric flows of isotropic simple fluids (Phan-Thien [**59**]), such as the order fluids. Viscometric flows are flows in very simple geometries that allow us to have an idea of the main non-Newtonian characteristics. It can be seen that the constitutive equation of an incompressible fluid of order 2 can be determined uniquely from its viscometric functions. Here, we derive the stress for two viscometric flows, simple shear flow and uniaxial extensional flow.

1.2.1.1. *Simple shear flow.* Consider a steady simple shear flow $\mathbf{v} = (\dot{\gamma}_{xy}y, 0, 0)$, where $\dot{\gamma}_{xy}$ is the constant shear-rate, as represented in Figure 1.2. The first two Rivlin-Ericksen tensors become

$$\mathbf{A}_1 = \begin{bmatrix} 0 & \dot{\gamma}_{xy} & 0 \\ \dot{\gamma}_{xy} & 0 & 0 \\ 0 & 0 & 0 \end{bmatrix}, \qquad \mathbf{A}_2 = \begin{bmatrix} 0 & 0 & 0 \\ 0 & 2\dot{\gamma}_{xy}^2 & 0 \\ 0 & 0 & 0 \end{bmatrix}.$$
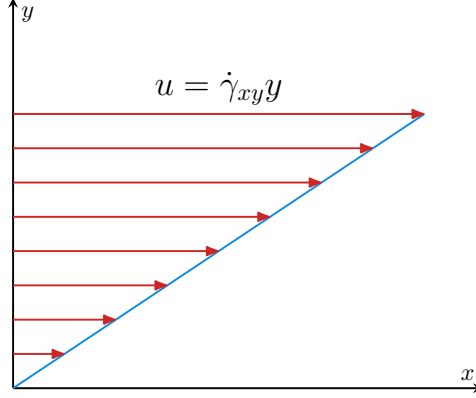
FIGURE 1.2. Steady simple shear flow.

Therefore, the extra-stress tensor $\mathbf{T} = p\mathbf{I} + \boldsymbol{\sigma}$ becomes

$$\mathbf{T} = \mu \begin{bmatrix} 0 & \dot{\gamma}_{xy} & 0 \\ \dot{\gamma}_{xy} & 0 & 0 \\ 0 & 0 & 0 \end{bmatrix} + \alpha_1 \begin{bmatrix} 0 & 0 & 0 \\ 0 & 2\dot{\gamma}_{xy}^2 & 0 \\ 0 & 0 & 0 \end{bmatrix} + \alpha_2 \begin{bmatrix} \dot{\gamma}_{xy}^2 & 0 & 0 \\ 0 & \dot{\gamma}_{xy}^2 & 0 \\ 0 & 0 & 0 \end{bmatrix}.$$

Hence, we can write the components of the extra-stress tensor $\mathbf{T}$ in terms of three functions of the rate-of-strain $\dot{\gamma}_{xy}$, the so-called *viscometric functions* η, N_1 and N_2, as follows

$$T_{xy} = \eta(\dot{\gamma}_{xy})\dot{\gamma}_{xy} = \mu\dot{\gamma}_{xy},$$

$$T_{xx} - T_{yy} = N_1(\dot{\gamma}_{xy}) = -2\alpha_1\dot{\gamma}_{xy}^2,$$

$$T_{yy} - T_{zz} = N_2(\dot{\gamma}_{xy}) = \alpha_1\dot{\gamma}_{xy}^2,$$

$$T_{xz} = T_{yz} = 0,$$

where η is called *shear viscosity* and N_1 and N_2 are, respectively, the *first* and *second normal stress differences*.

This model predicts constant viscosity and non-zero normal stress differences. Non-zero normal stress differences are a feature of nonlinear models and are responsible for interesting phenomena such as *rod-climbing* and *die swell* (Boger and Walters [10]). The main limitation of the second grade model ($\alpha_1 > 0$) is that it predicts negative N_1 and positive N_2, while experiments indicate that N_1 should be expected to be positive and N_2 small in comparison to N_1 and non-positive for

polymeric fluids (see Owens and Phillips [54]). On the contrary, the second order model with $\alpha_1 < 0$ predicts a positive first normal stress difference as physically observed.

1.2.1.2. *Extensional flow.* Consider a uniaxial extensional flow $\mathbf{v} = \left(\dot{\epsilon}x, -\frac{\dot{\epsilon}}{2}y, -\frac{\dot{\epsilon}}{2}z\right)$, where $\dot{\epsilon}$ is the constant extensional strain-rate. The Rivlin-Ericksen tensors of order 1 and 2 become

$$\mathbf{A}_1 = \begin{bmatrix} 2\dot{\epsilon} & 0 & 0 \\ 0 & 0 & 0 \\ 0 & 0 & 0 \end{bmatrix}, \qquad \mathbf{A}_2 = \begin{bmatrix} 0 & 0 & 0 \\ 0 & 2\dot{\gamma}_{xy}^2 & 0 \\ 0 & 0 & 0 \end{bmatrix}.$$

Therefore, the components of the stress tensor become

$$\boldsymbol{\sigma}_{xx} = -p + 2\mu\dot{\epsilon} + 4\alpha_1\dot{\epsilon}^2 + 4\alpha_2\dot{\epsilon}^2,$$

$$\boldsymbol{\sigma}_{yy} = -p - \mu\dot{\epsilon} + \alpha_1\dot{\epsilon}^2 + \alpha_2\dot{\epsilon}^2,$$

$$\boldsymbol{\sigma}_{zz} = -p - \mu\dot{\epsilon} + \alpha_1\dot{\epsilon}^2 + \alpha_2\dot{\epsilon}^2,$$

$$\boldsymbol{\sigma}_{xy} = \boldsymbol{\sigma}_{xz} = \boldsymbol{\sigma}_{yz} = 0.$$

The *extensional viscosity* η_{E} is defined as

$$\eta_{\mathrm{E}} = \frac{\boldsymbol{\sigma}_{xx} - \boldsymbol{\sigma}_{yy}}{\dot{\epsilon}} = \frac{\boldsymbol{\sigma}_{xx} - \boldsymbol{\sigma}_{zz}}{\dot{\epsilon}},$$

and in this case, remembering that $\alpha_1 + \alpha_2 = 0$, it becomes

$$\eta_{\mathrm{E}} = 3\mu + 3(\alpha_1 + \alpha_2)\dot{\epsilon} = 3\mu.$$

For a Newtonian fluid the *Trouton ratio*, which is the ratio between the extensional viscosity η_{E} and the shear viscosity μ, is equal to 3 and does not depend on shear rate $\dot{\gamma}_{xy}$ or extension rate $\dot{\epsilon}$. The second order models predicts a Newtonian constant extensional viscosity. However, for a viscoelastic fluid the extensional viscosity generally depends on the extension rate and can be very large. Trouton ratios can reach values as high as 10^3 or 10^4. For example, dilute polymer solutions may have high Trouton ratios because they are *tension-thickening*, i.e. their extensional viscosity increases substantially with $\dot{\epsilon}$ (Phan-Thien [59], Owens and Phillips [54]).

1.3. Mean flow

In this section, we present the derivation of the undisturbed flow profile. This is the necessary first step in order to perform the stability analysis. The mean flow is obtained by applying a boundary layer approximation as is usually done for Newtonian fluids.

Boundary layer theory was presented by Prandtl during the Third International Congress of Mathematics held at Heidelberg, Germany in 1904 (Schlichting and Gersten [73], Tani [81], Anderson [3]). The related paper [62] was published in the Proceedings of the Congress a year later and is one of the most important contributions to fluid dynamics. This paper showed how viscosity affects the flow at high Reynolds numbers. Prandtl theorised that the fluid adheres to the surface of an object so its velocity adjacent to the wall is zero and that the viscosity becomes important only in a thin layer near the surface. This region is characterised by a transition from zero at the wall to the full velocity at a certain distance from the wall. Outside the boundary layer the flow was irrotational, essentially inviscid and widely studied for centuries. In other words, boundary layer theory deals with the asymptotic behaviour of flows at large Reynolds numbers (Van Dyke [93]). It is also the first example of a singular perturbation method applied to solve a partial differential equation.

Prandtl's work enabled the aerodynamic drag to be calculated and the Navier-Stokes equations to be reduced to a simpler form. In 1908, Blasius [9], who was Prandtl's student, solved the boundary layer equations for 2D flow over a flat plate by reducing the PDEs to a single ordinary differential equation. In 1931, Falkner and Skan [28] extended the work to the case in which the free-stream velocity varies according to a power law.

1.3.1. Potential flows. It is important to clarify the assumption of an irrotational flow in the free stream. It is common to associate irrotational flows with inviscid fluids. They are in fact two distinct properties, the former relates to the flow and the last is a material property. For Newtonian fluids, irrotational flows satisfy the full viscous

and incompressible PDEs with no need to impose zero viscosity, as remarked by Joseph [46]. Viscous effects are still present in irrotational flows but they balance internally and they do not enter the equations of motion. In this work, we do not deal with the viscous effects in the outer layer and how they affect the inner layer since we consider flows at high Reynolds numbers. We refer to Joseph [45] for further reading.

Regarding viscoelastic fluids, Joseph and Liao [47] provided a condition for the extra-stress tensor for an irrotational flow to satisfy the equations. Not many constitutive equations are compatible with irrotational solutions. The flow is said to be irrotational when the vorticity is zero, i.e.

$$\boldsymbol{\omega} = \nabla \times \mathbf{v} = \mathbf{0}.$$

If the domain is simply-connected, there exists a velocity potential $\phi(\mathbf{x}, t)$ such that $\mathbf{v} = \nabla\phi$. The opposite is trivially true. In this case, the momentum equation (1.4) can be written as follows

$$\nabla \left(\rho \frac{\partial \phi}{\partial t} + \rho \frac{|\nabla \phi|^2}{2} + p \right) = \nabla \cdot \mathbf{T},$$

where $\mathbf{T}$ is the extra-stress tensor. Here we ignore body forces, but the conclusion is still valid provided that they are conservative. Therefore, the following condition must hold

$$\nabla \times (\nabla \cdot \mathbf{T}) = \mathbf{0}. \tag{1.7}$$

In other words, the divergence of the deviatoric tensor $\mathbf{T}$ is the gradient of a function $\mathcal{T}$. The pressure can be determined by a generalised Bernoulli equation, i.e.

$$p = -\rho \frac{\partial \phi}{\partial t} - \rho \frac{|\nabla \phi|^2}{2} + \mathcal{T} + C(t),$$

where C is a constant depending on time only. Condition (1.7) is satisfied by inviscid and viscous Newtonian fluids, linear viscoelastic fluids and for second order fluids.

1.3.2. Boundary layer approximation. Rajagopal *et al.* [66] pointed out some assumptions regarding the flow in order to apply Prandtl's boundary layer theory to the case of a non-Newtonian fluid of second grade. It is necessary that, not only the ratio of the inertial

forces to the forces due to the tangential stresses be large (high Reynolds number), as in the Newtonian case, but also the ratio of the inertial forces to the forces due to the normal stresses should be large. This implies the following assumptions for a second order fluid

$$Re \gg 1 \quad \text{and} \quad \frac{Re}{Wi} \gg 1,$$

where $Re = \frac{\rho U L}{\mu}$ is the Reynolds number, and $Wi = \frac{\alpha_1 U}{\mu L}$ is the Weissenberg number. Here U is a characteristic velocity, that is usually taken to be the free-stream velocity, and L is a characteristic length. White [95] first introduced the Weissenberg number while analysing the dimensionless groups of fluids of second grade. It quantifies the nonlinearity of the rheological response and does not coincide, in general, with the Deborah number (Poole [60], Dealy [22]).

Rajagopal *et al.* [66] suggested the possibility of having a boundary layer with a two-deck structure. In addition to the viscous boundary layer, they hypothesised an "elastic boundary layer" where inertia and pressure forces balance the forces due to normal stresses. This possibility was investigated further by Pakdemirli [55] who showed that a multiple deck boundary layer theory is not possible for the second order model. Therefore, here we consider the conventional viscous boundary layer theory, where we have one inner expansion and an outer expansion which is irrotational.

Inside the boundary layer the velocity gradient normal to the wall, $\partial u / \partial y$, is very large and therefore viscous forces cannot be neglected. Requiring the viscous term to be of the same order of magnitude as the inertia and pressure forces leads to

$$\frac{\delta}{L} = O\left(\sqrt{\nu}\right), \quad \text{or equivalently} \quad \frac{\delta}{L} = O\left(\frac{1}{\sqrt{Re}}\right),$$

where δ denotes a typical value of the thickness of the boundary layer and $\nu = \mu/\rho$ is the kinematic viscosity. At the same time, requiring the non-Newtonian normal stress forces to balance the inertia and therefore the viscous forces, we obtain

$$\frac{\delta}{L} = O\left(\sqrt{\frac{\alpha_1}{\rho}}\right), \quad \text{and so} \quad \alpha_1 = O\left(\mu\right).$$

This is equivalent to saying that the Weissenberg number Wi needs to be of order 1 to have a valid boundary layer theory.

The key idea of Prandtl's order of magnitude argument is to recognise that boundary layers are thin in comparison to their length of development, hence $\delta/L \ll 1$. This is true at reasonably high Reynolds numbers. From the continuity equation (1.6a), it follows that $\frac{\partial v}{\partial y}$ is of order U/L and v is of order $\delta U/L$ in the boundary layer, where U is the chosen characteristic velocity. Thus, the component of the velocity v in the y-direction is small compared to the velocity u in the direction of the plate.

Applying the boundary layer approximation, as shown in Appendix A.2, to the two-dimensional field equations (1.4) and (1.5), we obtain

$$
\begin{cases}
\dfrac{\partial u_*}{\partial x_*} + \dfrac{\partial v_*}{\partial y_*} = 0, \\[2mm]
u_* \dfrac{\partial u_*}{\partial x_*} + v_* \dfrac{\partial u_*}{\partial y_*} = \quad -\dfrac{1}{\rho}\dfrac{\partial p_*}{\partial x_*} + \dfrac{\mu}{\rho}\dfrac{\partial^2 u_*}{\partial y_*^2} + \dfrac{\alpha_1}{\rho}\left[v_* \dfrac{\partial^3 u_*}{\partial y_*^3} \right. \\[4mm]
\qquad\qquad\qquad \left. + \dfrac{\partial}{\partial x_*}\left(u_* \dfrac{\partial^2 u_*}{\partial y_*^2} \right) + \dfrac{\partial u_*}{\partial y_*}\dfrac{\partial^2 v_*}{\partial y_*^2} \right],
\end{cases}
\tag{1.8}
$$

where starred dependent and independent variables indicate dimensional variables. If the plate forms an angle $\beta_H \pi/2$ with respect to the uniform velocity field as in Figure 1.1, the free-stream velocity varies with distance to the leading edge according to potential flow theory (Batchelor [5]) as a power law

$$
U_e(x_*) = a x_*^m,
$$

where a is a positive constant and the exponent m is related to the Hartree parameter $\beta_H = \frac{2m}{m+1}$.

After the following boundary layer transformation

$$
\eta = \frac{y_*}{\delta}, \qquad \psi_* = \delta U_e(x_*) f(\eta),
$$

where

$$
\delta = \sqrt{\frac{\nu}{a(m+1)}}\, x_*^{\frac{1-m}{2}}
\tag{1.9}
$$

is a measure for the displacement thickness and ψ_* is the stream function introduced to satisfy the continuity equation, the boundary layer equations (1.8) are transformed into the following local ordinary differential equation for $f(\eta)$

$$2(m+1)f''' + (m+1)ff'' + 2m - 2mf'^2 =$$
$$\frac{\alpha_1 a}{\rho\nu}(m+1)x_*^{m-1}\Big[(m+1)\,f^{iv}f + 2(1-3m)f'f''' + (3m-1)(f'')^2\Big],$$
$$\text{(1.10)}$$

where $'$ indicates the derivative with respect to the boundary layer variable, η. The key idea is to solve this equation numerically for fixed values of x^* in order to obtain a local solution. It can be easily seen that a similarity solution is possible only for stagnation point flow, where $m = 1$ (Garg and Rajagopal [**31**,**32**]) and, trivially, for Newtonian fluids. Notice that, when $\alpha_1 = 0$, equation (1.10) reduces to the well-known third order equation known as the *Falkner-Skan equation* (Falkner and Skan [**28**]). Instead, in the non-Newtonian case the equation to solve is of fourth order. For the stability analysis, equation (1.10) will be transformed and the dependency on the streamwise position x^* will be included in the elasticity parameter, which will be defined later in this section.

For Newtonian fluids, in the case of slightly decelerating flow, that is, $-0.091 < m < 0$ ($-0.199 < \beta_H < 0$), there are two solutions, one exhibit points of inflection while the other one has a region of reversed flow near the boundary (Schlichting and Gersten [**73**]). If $m \leq -0.091$ ($\beta_H \leq -0.199$) separation occurs and profiles have a vanishing wall shear stress. For zero and positive pressure gradients, where $m \geq 0$, the Falkner-Skan equation has a unique solution without a point of inflection. In this work, we are not concerned with the existence and uniqueness of the solution of the local ODE (1.10), since we will always consider solutions that are small departures from the Newtonian solutions. Using Rayleigh's inflection point criterion (Rayleigh [**68**]), we can conclude that, in the inviscid limit, the boundary layer with an adverse pressure gradient could exhibit exponential instabilities whereas for zero and positive pressure gradients inviscid unstable solutions do not exist. In

this section, we also analyse the non-Newtonian effects on inflection points since they play a crucial role in the stability.

The stability analysis is traditionally performed, for a Newtonian fluid, by choosing a fixed streamwise position $x_* = x_0$, as first proposed by Tollmien [84] in 1929. The approach consists of finding the longitudinal velocity at that station, ignoring the relatively small transverse velocity, and then solving the Orr-Sommerfeld equation for the resulting base profile.

Following the example of Schmid and Henningson [77], we apply the same procedure to the second grade fluid and we define a displacement thickness δ_0, at position x_0, as follows

$$\delta_0 = C\delta(x_0) = C\sqrt{\frac{\nu}{a(m+1)}}x_0^{\frac{1-m}{2}}, \tag{1.11}$$

where δ is defined by equation (1.9) and C is a constant given by

$$C = \int_0^\infty \left(1 - f'_{\text{Newt}}(\eta)\right) d\eta$$

calculated in the Newtonian case. This choice was made in order to easily compare non-Newtonian solutions with Newtonian solutions. The Reynolds number based on the displacement thickness is

$$Re_0 = \frac{U_e(x_0)\delta_0}{\nu} \tag{1.12}$$

and satisfies the following important relation

$$\frac{x_0}{\delta_0} = \frac{m+1}{C^2}Re_0.$$

The Reynolds number Re_0 is related to the Reynolds number Re_{x_0} based on the downstream distance x_0 by

$$Re_0 = C\sqrt{\frac{Re_{x_0}}{m+1}}.$$

Using these relations, equation (1.10) at the fixed position x_0 can be rewritten as

$$2(m+1)f''' + (m+1)ff'' + 2m - 2mf'^2 =$$
$$K_0C^2\Big[(m+1)f^{iv}f + 2(1-3m)f'f''' + (3m-1)(f'')^2\Big], \tag{1.13}$$

where

$$K_0 = \frac{\alpha_1}{\rho \delta_0^2} \tag{1.14}$$

is a non-dimensional parameter known as the *elasticity number*, that can be interpreted as representing the ratio of non-Newtonian normal stress forces to inertial forces. In fact, we can write

$$K_0 = \frac{Wi_0}{Re_0},$$

where $Wi_0 = \frac{\alpha_1 U_e(x_0)}{\mu \delta_0}$ is the Weissenberg number based on the displacement thickness δ_0. We also notice that K_0 relates to the Weissenberg number based on the streamwise distance x_0, as follows

$$K_0 = \frac{m+1}{C^2} Wi_{x_0}.$$

Equation (1.13) is solved numerically by applying a Chebyshev collocation method, as described in Section 5.2. The base flow for the stability analysis is non-dimensionalised by using the free-stream velocity U_e, hence the velocity in the x-direction is

$$U_B = \frac{u_*}{U_e(x_*)} = f'.$$

The wall-normal velocity V_B is

$$V_B = \frac{v_*}{U_e(x_*)} = \frac{1}{2} \frac{1}{\sqrt{(m+1)Re_{x_*}}} \big[(1-m)\, \eta f' - (m+1)f \big].$$

It is clear that this flow is nearly parallel because the transverse velocity V_B is smaller than U_B by a factor of $Re_{x_*}^{-1/2}$, so it will be neglected in order to perform the stability analysis. This is a valid approximation when the Reynolds number $Re_{x_*} = U x_*/\nu$ is large.

1.3.2.1. *Boundary conditions.* In the case of fluids of differential type the equations of motion are an order higher than the Navier-Stokes equations, and thus the adherence boundary conditions are insufficient to determine the solution completely. The same is also true for the boundary layer approximation given by equation (1.8) and the ODE (1.10). In order to overcome this difficulty, in their study of an incompressible fluid of second order near a stagnation point, Beard and Walters [**6**] suggested a perturbation method. This method was followed

also by Rajagopal *et al.* [**65**] in their analysis of the Falkner-Skan flow of an incompressible fluid of second order.

The perturbation method reduces the order of the problem, but it is valid only for small values of the parameter K_0. This parameter multiplies the higher order spatial derivatives in the equation. Garg and Rajagopal [**31, 32**] suggested that it would be preferable to use an augmented boundary condition justified by physically reasonable assumptions. Therefore, equation (1.13) is solved by applying the usual boundary conditions that ensure no-slip and no-penetration at the wall and matching with the free-stream velocity at infinity

$$f(\eta) = 0, f'(\eta) = 0 \qquad \text{at } \eta = 0,$$
$$f'(\eta) \to 1 \qquad \text{as } \eta \to \infty,$$

augmented by the condition

$$f''(\eta) \to 0 \qquad \text{as } \eta \to \infty. \tag{1.15}$$

Condition (1.15) is derived by imposing $\frac{\partial u_*}{\partial y_*} \to 0$ at infinity and is equivalent to requiring that the solution approaches the free-stream velocity smoothly far from the wall (Garg and Rajagopal [**31, 32**]).

1.3.3. Mean flow characteristics. The effect of elasticity on the velocity profile changes with the geometrical configuration. For the second grade model (i.e. when $K_0 > 0$), we can see from Figures 1.3(a),(b) that the velocity at all points in the boundary layer is larger in the non-Newtonian case for the flow over a flat plate ($\beta_H = 0$) and the greater variation appears at the wall. Instead, for the second order model (i.e. when $K_0 < 0$) the velocity at all points in the boundary layer is smaller in the non-Newtonian case for the flow over a flat plate. Figures 1.3(c),(d) show that for a wedge angle of $\pi/2$ there is a smaller relative variation than for the flat plate observed in Figure 1.3(a),(b). When $K_0 > 0$ the non-Newtonian velocity is slightly smaller inside the boundary layer while, when $K_0 < 0$, the non-Newtonian velocity is larger. In both cases the greater deviation from the Newtonian profile happens at a distance $\eta \approx 2$ from the wall. In Figures 1.3(e),(f) we see that the effect of increasing $|K_0|$ for the stagnation point flow ($\beta_H = 1$) is the opposite of the flat plate case.

Figures 1.4(a),(b) show how the inflection point (where $U_B'' = 0$) for a flow past a corner ($\beta_H = -0.07, -0.14$) moves towards the wall upon increasing the non-Newtonian parameter K_0. On the contrary, for the second order model ($K_0 < 0$), decreasing the non-Newtonian parameter K_0 moves the inflection point away from the wall. In fact, even the flat plate profile has an inflection point for negative K_0, as can be seen from Figure 1.4(d).

Notice that, the non-Newtonian parameter K_0 in these graphs has been chosen to be large enough to be able to distinguish clearly the non-Newtonian effects on the mean flow. However, as already mentioned in Section 1.3.2, we need $|K_0| \ll 1$ for the boundary layer theory to be valid.

Furthermore, it is possible to quantify the different effects of elasticity on the velocity profile by measuring displacement thickness, initial slope and shape factor. The initial slope $f''(0)$ is physically important because it determines the local wall shear stress and thus the friction drag. The friction drag is the force experienced by the plate opposite to the direction of the flow and it is calculated as the integral over the surface of the local shear stress τ at the wall, that is given by

$$\tau(x_*)\big|_{y_*=0} = \mu \frac{\partial u_*}{\partial y_*}\bigg|_{y_*=0} = \frac{\mu U_e}{\delta} f''(\eta = 0).$$

Figure 1.5(a) shows that, for the second grade model ($K > 0$), increasing the non-Newtonian parameter decreases the initial slope $f''(0)$ for large value of β_H ($\beta_H = 0.5, 1, 1.2$), while it increases for smaller angles ($\beta_H = 0.25, 0, -0.07, -0.14$). The opposite is true for the second order model ($K < 0$), as shown in Figure 1.5(b).

The displacement thickness is a measure of the displacement action of the viscosity and it is defined as the distance by which the surface should be moved in an inviscid fluid stream of velocity U_e to have the same mass flow rate of the viscous fluid. It is calculated as follows

$$\delta_* = \int_0^\infty \left(1 - \frac{u_*}{U_e}\right) dy_* = \delta_1 \delta, \tag{1.16}$$
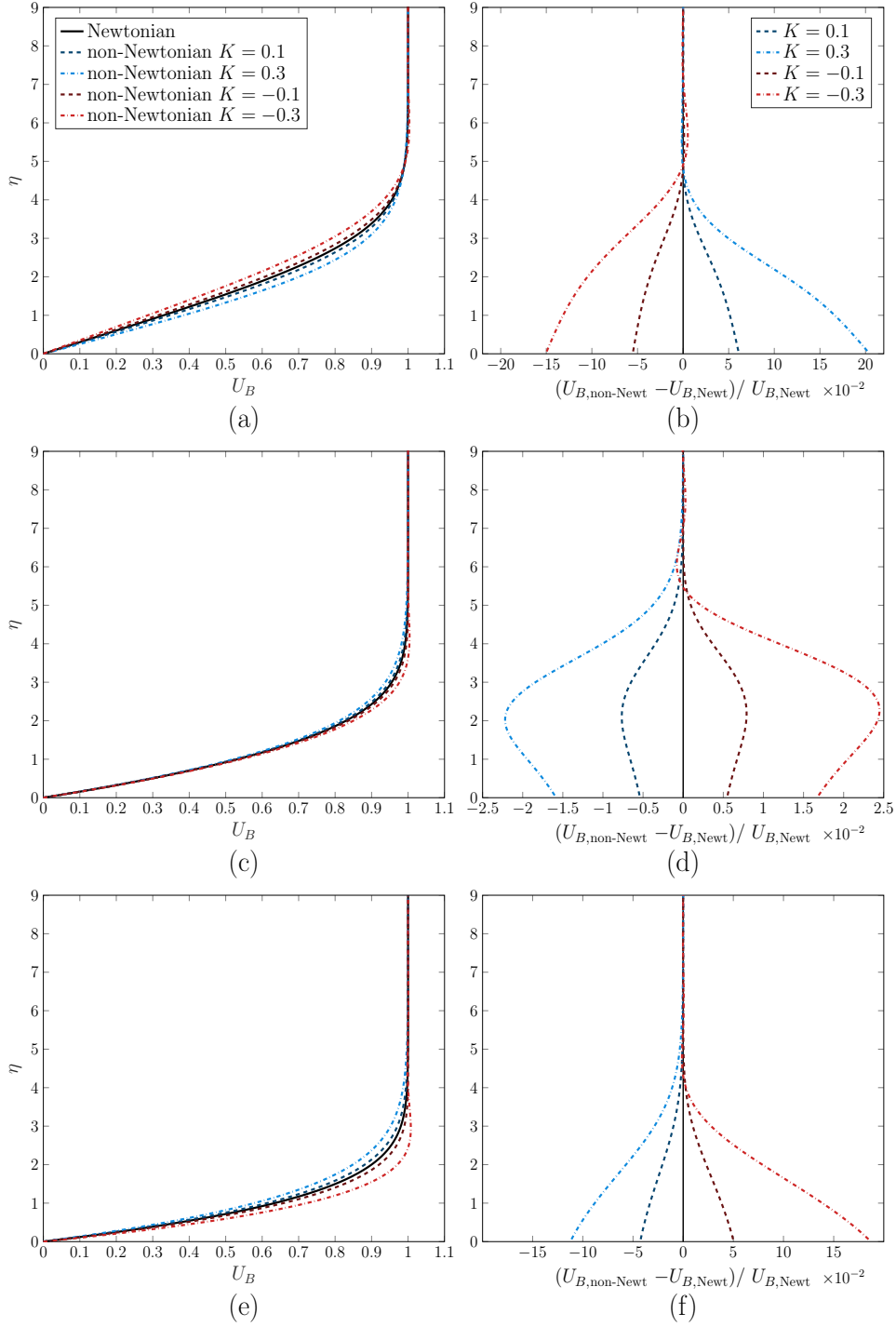
FIGURE 1.3. Velocity profile and relative variation with respect to the Newtonian profile for increasing and decreasing values of the parameter $K = K_0 C^2$. (a), (b) $\beta_H = 0$ (flat plate); (c), (d) $\beta_H = 0.5$ (flow past a wedge); (e), (f) $\beta_H = 1$ (stagnation flow).
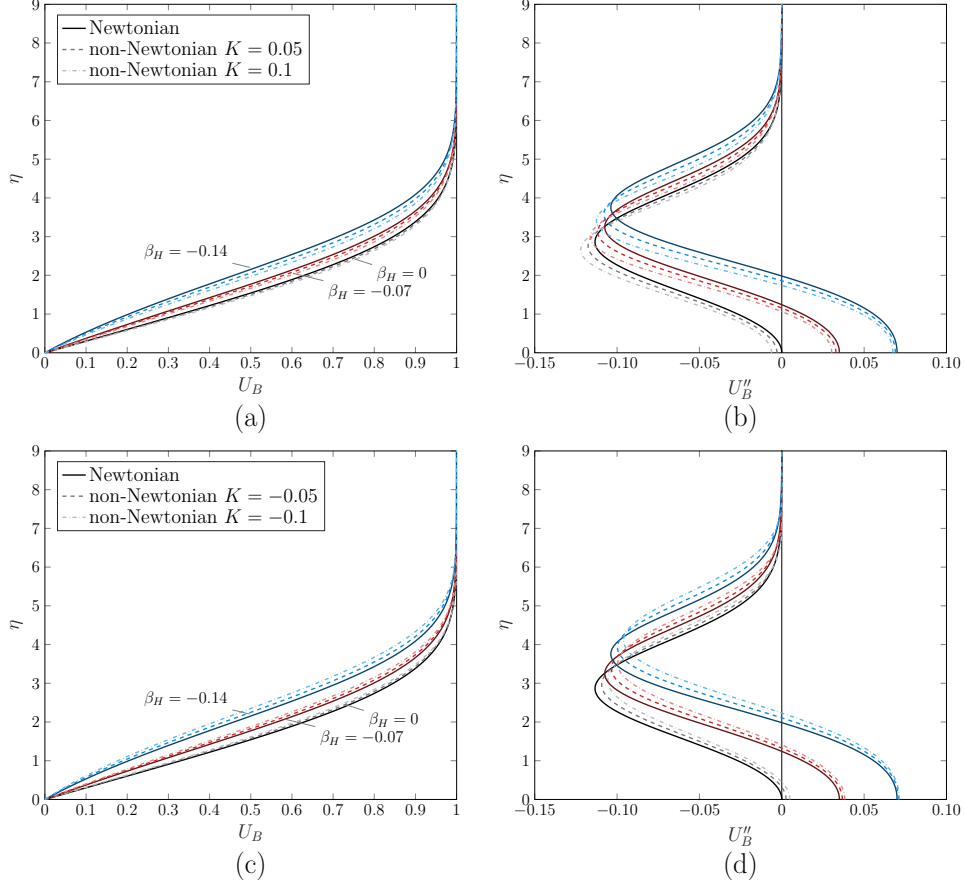
FIGURE 1.4. Velocity profiles (a),(c) and second derivatives (b),(d) for flows with an inflection point (flow past a corner) and increasing (a),(b) or decreasing (c),(d) values of the parameter $K = K_0 C^2$.

where
$$\delta_1 = \int_0^\infty (1 - f') \, d\eta = \lim_{\eta \to \infty} (\eta - f(\eta)). \tag{1.17}$$
and $\delta = y_*/\eta$ is defined by equation (1.9). In Figures 1.5(c),(d) we plot the constant factor δ_1. For small values of the angle parameter β_H, elasticity in the second grade model ($K > 0$) makes the boundary layer thinner, while it makes the boundary layer thicker for larger values of β_H. The opposite behaviour is observed for the second order model ($K < 0$).

The values at $K = 0$ agree with the ones found in the literature, see for example Schlichting and Gersten [73]. For the second grade fluid, our numerical results agree with those obtained by Garg and
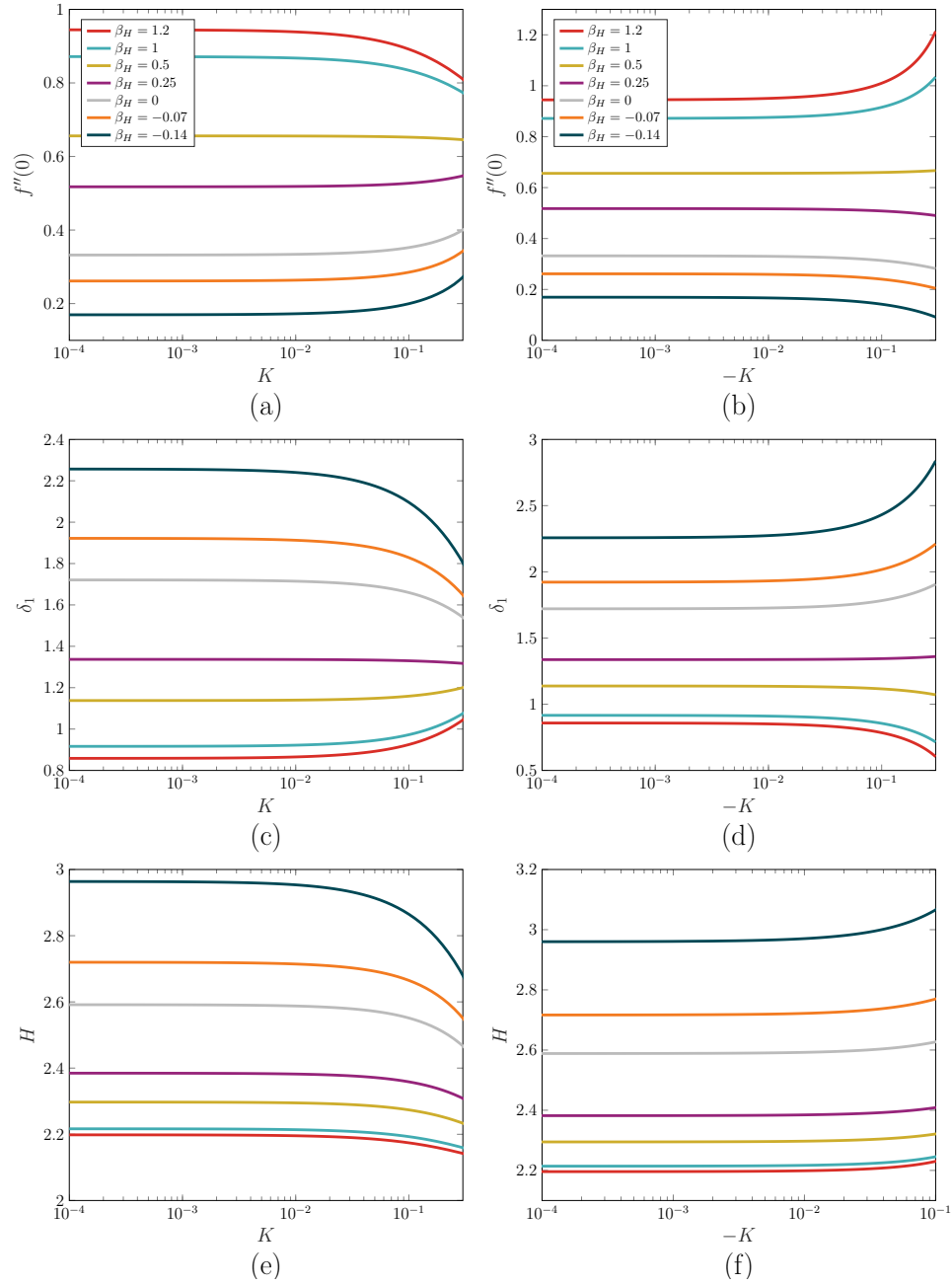
FIGURE 1.5. Values of the initial slope (a),(b), displacement thickness (c),(d) and shape factor (e),(f) for different angle parameters β_H, increasing the non-Newtonian parameter K in (a),(c),(e) and decreasing K in (b),(d),(f).

Rajagopal [**32**] for $\beta_H = 0, 0.25, 0.5, 1$. Moreover, we calculated the shape factor H, which is calculated as the ratio between displacement thickness, given by equation (1.16), and momentum thickness as follows

$$H = \frac{\delta_*}{\theta_*},$$

where θ_* is the momentum thickness, defined by

$$\theta_* = \int_0^\infty \left(\frac{u_*}{U_e} \left(1 - \frac{u_*}{U_e} \right) \right) dy_* = \delta \int_0^\infty \left(f' \left(1 - f' \right) \right) d\eta. \qquad (1.18)$$

The momentum thickness represents the distance by which a surface would have to be displaced perpendicular from the reference plane in an inviscid fluid to have the same total momentum. From Figures 1.5(e),(f) we see uniform behaviour over all the values of the parameter β_H, that consists in a decrease of the shape factor for the second grade model and an increase of the shape factor for the second order model. It is interesting to notice that H varies more steeply for small values of β_H.

In conclusion, the non-Newtonian effects in the second grade ($K_0 > 0$) and the second order model ($K_0 < 0$) have almost opposite effects on the mean flow.

1.4. Two-dimensional linear stability analysis

In this section, we apply a linear stability analysis to study the non-Newtonian effects on two-dimensional disturbances.

The full unsteady and two-dimensional governing equations derived from equations (1.4), (1.5) and Definition (1.1) can be written as follows

$$\begin{cases} \dfrac{\partial u_*}{\partial x_*} + \dfrac{\partial v_*}{\partial y_*} = 0, \\[2mm] \dfrac{D u_*}{D t_*} = -\dfrac{1}{\rho}\dfrac{\partial p_*}{\partial x_*} + \dfrac{\mu}{\rho}\Delta u_* + \dfrac{\alpha_1}{\rho}\left(\dfrac{\partial \tau_{xx}^*}{\partial x_*} + \dfrac{\partial \tau_{xy}^*}{\partial y_*} \right), \\[2mm] \dfrac{D v_*}{D t_*} = -\dfrac{1}{\rho}\dfrac{\partial p_*}{\partial y_*} + \dfrac{\mu}{\rho}\Delta v_* + \dfrac{\alpha_1}{\rho}\left(\dfrac{\partial \tau_{xy}^*}{\partial x_*} + \dfrac{\partial \tau_{yy}^*}{\partial y_*} \right), \end{cases} \qquad (1.19)$$

where τ_{xx}^*, τ_{xy}^* and τ_{yy}^* are components of $\boldsymbol{\tau}^*$, the non-Newtonian part of the stress tensor $\boldsymbol{\sigma}$, such that we can rewrite the stress tensor $\boldsymbol{\sigma}$ defined

in (4.2) as follows

$$\boldsymbol{\sigma} = -p_* \mathbf{I} + \frac{\mu}{\rho} \mathbf{A}_1^* + \frac{\alpha_1}{\rho} \boldsymbol{\tau}^*,$$

where $\mathbf{A}_1^* = \nabla \mathbf{u}_* + \nabla \mathbf{u}_*^T$ is the rate-of-strain tensor. Using identities derived in Appendix A.1, we have

$$\tau_{xx}^* = 2\frac{\partial^2 u_*}{\partial t_* \partial x_*} + 2u_* \frac{\partial^2 u_*}{\partial x_*^2} + 2v_* \frac{\partial^2 u_*}{\partial x_* \partial y_*} + \left(\frac{\partial v_*}{\partial x_*}\right)^2 - \left(\frac{\partial u_*}{\partial y_*}\right)^2,$$

$$\tau_{xy}^* = \frac{\partial^2 u_*}{\partial t_* \partial y_*} + \frac{\partial^2 v_*}{\partial t_* \partial x_*} + u_* \frac{\partial^2 u_*}{\partial x_* \partial y_*} + v_* \frac{\partial^2 u_*}{\partial y_*^2} + u_* \frac{\partial^2 v_*}{\partial x_*^2}$$
$$+ v_* \frac{\partial^2 v_*}{\partial x_* \partial y_*} + 2\frac{\partial u_*}{\partial x_*}\frac{\partial u_*}{\partial y_*} + 2\frac{\partial v_*}{\partial x_*}\frac{\partial v_*}{\partial y_*},$$

$$\tau_{yy}^* = 2\frac{\partial^2 v_*}{\partial t_* \partial y_*} + 2v_* \frac{\partial^2 v_*}{\partial y_*^2} + 2u_* \frac{\partial^2 v_*}{\partial x_* \partial y_*} + \left(\frac{\partial u_*}{\partial y_*}\right)^2 - \left(\frac{\partial v_*}{\partial x_*}\right)^2.$$

Notice that the components $\tau_{xx}^*, \tau_{xy}^*, \tau_{yy}^*$ of the non-Newtonian stress tensor $\boldsymbol{\tau}^*$ include time derivatives and several nonlinear terms.

We scale the velocities with the constant free-stream velocity $U_e(x_0)$ and the lengths with the displacement thickness δ_0 defined by equation (1.11), relative to the fixed streamwise location x_0. The new dimensionless variables are

$$\begin{aligned} x &= \frac{x_*}{\delta_0}, & y &= \frac{y_*}{\delta_0}, & t &= \frac{U_e(x_0)t_*}{\delta_0}, \\ u &= \frac{u_*}{U_e(x_0)}, & v &= \frac{v_*}{U_e(x_0)}, & p &= \frac{p_*}{\rho U_e(x_0)^2}. \end{aligned} \qquad (1.20)$$

Hence, the non-dimensional governing equations are

$$\begin{cases} \dfrac{\partial u}{\partial x} + \dfrac{\partial v}{\partial y} = 0, \\[2mm] \dfrac{Du}{Dt} = -\dfrac{\partial p}{\partial x} + \dfrac{1}{Re_0}\Delta u + K_0 \left(\dfrac{\partial \tau_{xx}}{\partial x} + \dfrac{\partial \tau_{xy}}{\partial y}\right), \\[2mm] \dfrac{Dv}{Dt} = -\dfrac{\partial p}{\partial y} + \dfrac{1}{Re_0}\Delta v + K_0 \left(\dfrac{\partial \tau_{xy}}{\partial x} + \dfrac{\partial \tau_{yy}}{\partial y}\right), \end{cases}$$

where τ_{xx}, τ_{xy} and τ_{yy} are non-dimensional components of the non-Newtonian part of the extra-stress tensor $\boldsymbol{\tau}$. In these equations $Re_0 = U_e(x_0)\delta_0/\nu$, $K_0 = \alpha_1/(\rho\delta_0^2)$ are, respectively, the Reynolds and elasticity numbers defined as before. In order to perform a local linear stability analysis we assume the undisturbed flow to be steady and parallel, neglecting the transverse component of the velocity. The velocity of

the base flow in the streamwise direction is taken to be $U_B(y) = f'(\eta)$, i.e. the solution of the ODE (1.13) resulting from the boundary layer approximation at the fixed location x_0, as shown in Section 1.3. However, derivatives of U_B require additional scaling due to the following relations

$$y = \frac{y_*}{\delta_0}, \eta = \frac{y_*}{\delta} \implies \eta = Cy,$$

where η is the boundary layer variable and C is the constant

$$C = \int_0^\infty (1 - f'_{\text{Newt}}) \, d\eta. \tag{1.21}$$

Therefore,

$$\frac{dU_B}{dy} = Cf''(\eta), \frac{d^2U_B}{dy^2} = C^2 f'''(\eta), \frac{d^3U_B}{dy^3} = C^3 f^{iv}(\eta), \frac{d^4U_B}{dy^4} = C^4 f^v(\eta).$$

We can now introduce the non-dimensional stream function ψ, so that the continuity equation is satisfied identically, and decompose it into base flow ψ_B and perturbation $\tilde{\psi}$ as follows

$$\psi(x, y, t) = \psi_B(y) + \tilde{\psi}(x, y, t),$$

where $\psi_B = \delta_0 f$ is the stream function relative to the parallel and steady base flow. The pressure p is expressed in the same way, i.e.

$$p(x, y, t) = P_B(x) + \tilde{p}(x, y, t).$$

Next, we assume the normal mode form for the disturbances, as follows

$$\psi(x, y, t) = \phi(y)e^{i(\alpha x - \omega t)}, \qquad \tilde{p}(x, y, t) = \hat{p}(y)e^{i(\alpha x - \omega t)},$$

where α is the wavenumber in the x-direction and ω is the frequency of the disturbance. In general, both α and ω can be considered complex numbers.

When the fluid is Newtonian, the assumption of a parallel base flow and the neglect of the nonlinear terms allow the normal mode decomposition to be applied. This is equivalent to taking the Fourier transform and allows the PDEs to be transformed into an ordinary differential equation called the *Orr-Sommerfeld equation*. We can easily see that this is also true for the non-Newtonian model considered in this work. The equation obtained is the Orr-Sommerfeld equation with

an additional term due to the non-Newtonian correction

$$(U_B - c)(\phi'' - \alpha^2 \phi) - U_B'' \phi = \frac{1}{i\alpha Re_0} \left[\phi^{iv} - 2\alpha^2 \phi'' + \alpha^4 \phi \right]$$
$$+ K_0 \left[(U_B - c)(\phi^{iv} - 2\alpha^2 \phi'' + \alpha^4 \phi) - U_B^{iv} \phi \right], \quad (1.22)$$

where $'$ represents differentiation with respect to the wall-normal coordinate y and $c = \omega/\alpha$ is the phase speed. This equation has been derived by Chun and Schwarz [15] for the stability analysis of a Poiseuille flow of a second order fluid ($\alpha_1 < 0$) and used later by Sadeghy *et al.* [71] and Rafiki *et al.* [63]. More details can be found in Appendix A.4, where equation (1.22) is derived as a particular case of the three-dimensional linear stability equations. Notice that equation (1.22) is of the same order as the Orr-Sommerfeld equation but it involves higher derivatives of the base flow. The non-Newtonian terms do not increase the order of the stability equation, unlike for the mean flow equation (1.10). Therefore, no extra boundary condition is needed.

In order to study the temporal stability, the wavenumber α is assumed to be real. The phase velocity c appears as the eigenvalue in the modified Orr-Sommerfeld equation (1.22) and ϕ the associated eigenfunction. For the spatial stability, we assume a real frequency ω and equation (1.22) becomes a fifth order eigenvalue problem where α is the eigenvalue.

The modified Orr-Sommerfeld equation is subject to the boundary conditions

$$\phi(y) = \phi'(y) = 0, \qquad \text{at } y = 0,$$
$$\phi(y), \ \phi'(y) \to 0, \qquad \text{as } y \to \infty.$$

The first set of conditions is due to no-slip and no-penetration at the rigid wall $y = 0$. The conditions at infinity emerge from assuming that the disturbances tend to zero far from the surface of the plate.

1.5. Two-dimensional linear stability results

The modified Orr-Sommerfeld equation (1.22) is solved using a Chebyshev collocation method. The semi-infinite domain $y \in [0, \infty)$ is mapped
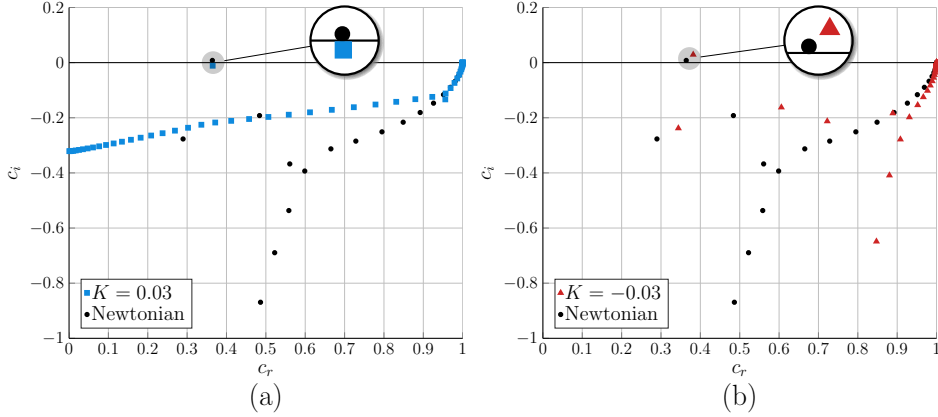
FIGURE 1.6. Comparison between Newtonian and non-Newtonian eigenspectrum for the temporal problem with $\alpha^* = 0.179$, $Re = 580$ and (a) $K = 0.03$, (b) $K = -0.03$. The least damped eigenvalues are those in the grey circle.

onto the finite interval $\xi \in [-1, 1]$ by means of the algebraic transformation

$$\xi = \frac{y - l}{y + l}, \tag{1.23}$$

where l is a stretching parameter. Other mappings are possible, but the numerical tests performed, that can be found in Section 5.3, indicate that a good choice to solve (1.22) is an algebraic mapping with $l = 4$.

All the numerical results are validated in the Newtonian limiting case by comparing with results in the literature (Schmid and Henningson [77] and Criminale, Jackson and Joslin [17]).

In Figure 1.6, the eigenvalues resulting from the linear temporal analysis of the flow over a flat plate ($\beta_H = 0$) are displayed. In Figure 1.6(a), we compare the eigenspectrum for the second grade model with a parameter $K = K_0 C^2 = 0.03$ with eigenvalues obtained in the Newtonian case. The choice of Reynolds number $Re = Re_0/C = 580$ and a wavenumber of $\alpha^* = \alpha/C = 0.179$ (C defined in (1.21)) generates an unstable mode (i.e. $c_i > 0$) in the Newtonian case, known as a *Tollmien-Schlichting wave*. We can see the stabilising effect of elasticity that moves the unstable mode into the lower half plane. Thus, the flow is temporally stable for the second grade model, for this choice of wavenumber and Reynolds number. In Figure 1.6(b) we compare the eigenvalues for the second order model with $K = -0.03$ with the
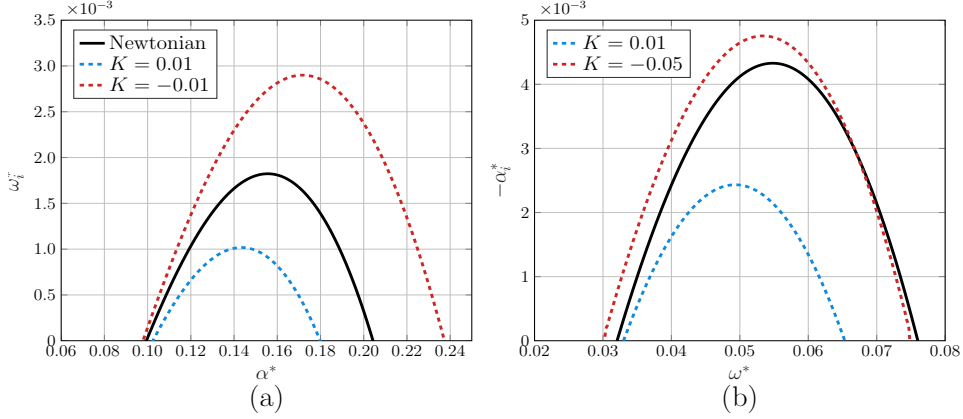
FIGURE 1.7. Temporal (a) and spatial (b) growth rates for a flat plate ($\beta_H = 0$) and $Re = 580$. Newtonian case and non-Newtonian case with: (a) $K = \pm 0.01$; (b) $K = 0.01, -0.05$.

Newtonian eigenvalues for the same values of Reynolds number and wavenumber. We observe that in this case, elasticity is destabilising since it pushes the unstable eigenvalues forward into the positive half plane. We also notice that the structure of the rest of the spectrum is different for the two non-Newtonian models.

1.5.1. Growth rates. Considering the flat plate configuration ($\beta_H = 0$), Figure 1.7(a) shows the temporal growth rate $\omega_i^* = \omega_i/C$ as a function of α^*. We notice that when $K = 0.01$, the maximum growth rate reduces dramatically, from $\omega_i^* \approx 1.8 \times 10^{-3}$ to about 10^{-3}. Instead, when $K = -0.01$ the maximum growth rate increases to almost 3×10^{-3}. In general, decreasing K extends the range of positive rates to shorter waves.

Figure 1.7(b) shows the spatial growth rate $-\alpha_i^*$ as a function of frequency ω^*. Again we observe the marked stabilising effect of elasticity in terms of growth rate reduction for the second grade model ($K = 0.01$). We observe that, for the second order model ($K = -0.05$) the maximum growth rate increases, but not so dramatically. Also, we notice that for some wavenumbers α^* the growth rate is actually smaller in the non-Newtonian case. The non-Newtonian effects in both models move the maximum to longer waves.

$\times 10^{-4}$

- ——— Newtonian
- - - - $K = 3 \times 10^{-4}$
- - - - $K = -3 \times 10^{-4}$

(a)

$\times 10^{-4}$

- ——— Newtonian
- - - - $K = 10^{-4}$
- - - - $K = -10^{-4}$

(b)

$\times 10^{-4}$

- ——— Newtonian
- - - - $K = 10^{-4}$
- - - - $K = -10^{-4}$

(c)

$\times 10^{-2}$

- ——— Newtonian
- - - - $K = 0.05$
- - - - $K = -0.05$

(d)
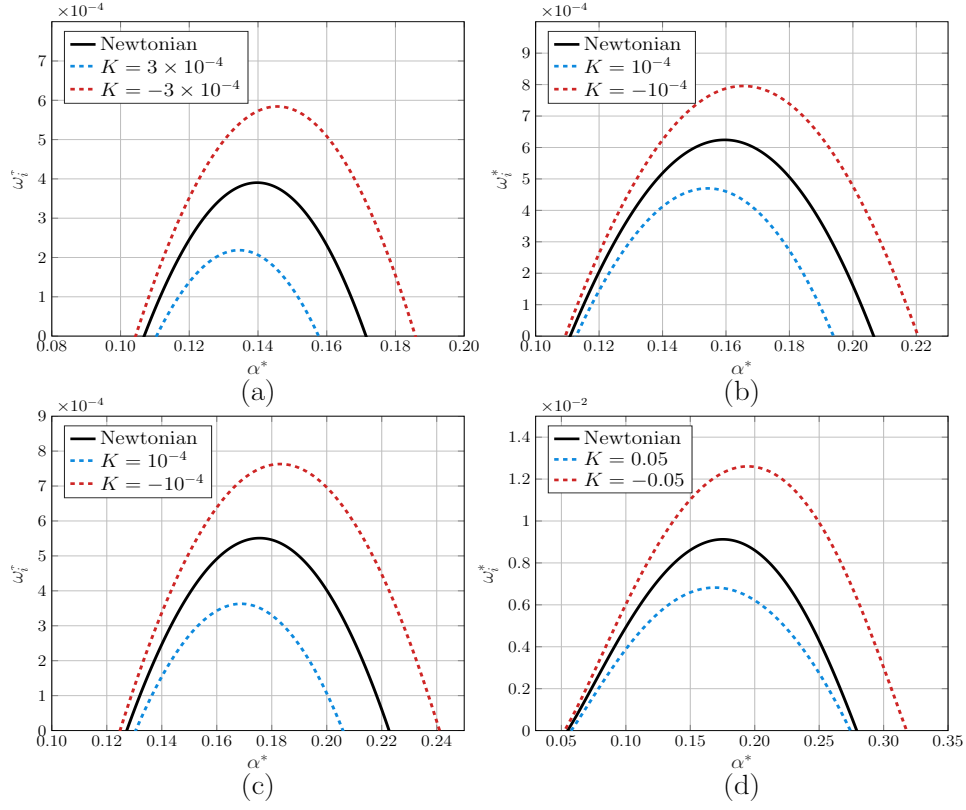
FIGURE 1.8. Temporal growth rates for the flow past a wedge and past a corner, Newtonian case and non-Newtonian case. (a) $\beta_H = 0.5$, $Re = 10000$, $K = \pm 3 \times 10^{-4}$; (b) $\beta_H = 1$ (stagnation flow), $Re = 27000$, $K = \pm 10^{-4}$; (c) $\beta_H = 1.2$, $Re = 27000$, $K = \pm 10^{-4}$; (d) $\beta_H = -0.14$ (flow past a corner), $Re = 300$, $K = \pm 0.05$.

Figure 1.8 shows temporal growth rates in the Newtonian and non-Newtonian cases for different values of β_H. In each case we observe a reduction of temporal growth rate of the Tollmien-Schlichting waves due to elasticity for $K > 0$ and an increase of growth rate for $K < 0$. Observe from Figure 1.8(d) that the growth rates are significantly larger, of order 10^{-2}, when there is an adverse pressure gradient ($\beta_H < 0$).

Notice that we choose Reynolds numbers of different orders of magnitude for different values of β_H, since instability occurs at lower Reynolds numbers when the angle parameter β_H is small (Schmid and Henningson [77]). The choice of K is justified by the fact that, as

remarked in Section 1.3, we need a Weissenberg number ($Wi_0 = K_0 \times Re_0$) of order 1 for the non-Newtonian effects to be significant and the boundary layer theory to hold.

1.5.2. Temporal neutral stability curves.

Temporal neutral stability curves define the region in the Re_0-α plane where exponentially growing modes exist and where they do not. The region inside the curves represents instability while the region outside corresponds to stability.

Notice that in order to plot neutral stability curves we need to take into account that both Re_0 and K_0 depend on the location x_0. If we decide to perform the stability analysis considering a variation of the Reynolds number as a variation of the distance x_0 from the leading edge where the local stability analysis is performed, then we need to write K_0 in terms of the Reynolds number and the base profile needs to be computed for each value of Re_0. In the flat plate case ($\beta_H = 0$), the non-Newtonian parameter based on the displacement thickness can be rewritten as

$$K_0(Re_0) = \frac{\alpha_1}{\rho \delta_0^2} = \frac{\alpha_1 a^2}{\rho \nu^2} \frac{1}{Re_0^2}.$$

Thus, we define the fixed quantity

$$\tilde{K} = \frac{\alpha_1 a^2}{\rho \nu^2},$$

which is independent of x_0, so that $K_0(Re_0) = \tilde{K}/Re_0^2$.

Figure 1.9(a) shows a comparison between the neutral stability curve in the Newtonian case and for $\tilde{K} = \pm 10^3$ for flow over a flat plate. This clearly shows the stabilising effect of elasticity in the second grade model ($\tilde{K} > 0$) in terms of increase of the critical Reynolds number. The non-Newtonian effects in the second order model ($\tilde{K} < 0$) promotes the onset of instabilities. For high Reynolds numbers, the non-Newtonian neutral curves approach the Newtonian neutral curve. This behaviour is expected, since when $Re_0 \to \infty$, we have $K_0 \to 0$.

In the case of a non-zero pressure gradient ($\beta_H \neq 0$), it is not possible to isolate Re_0 to vary the position x_0 only through the Reynolds number
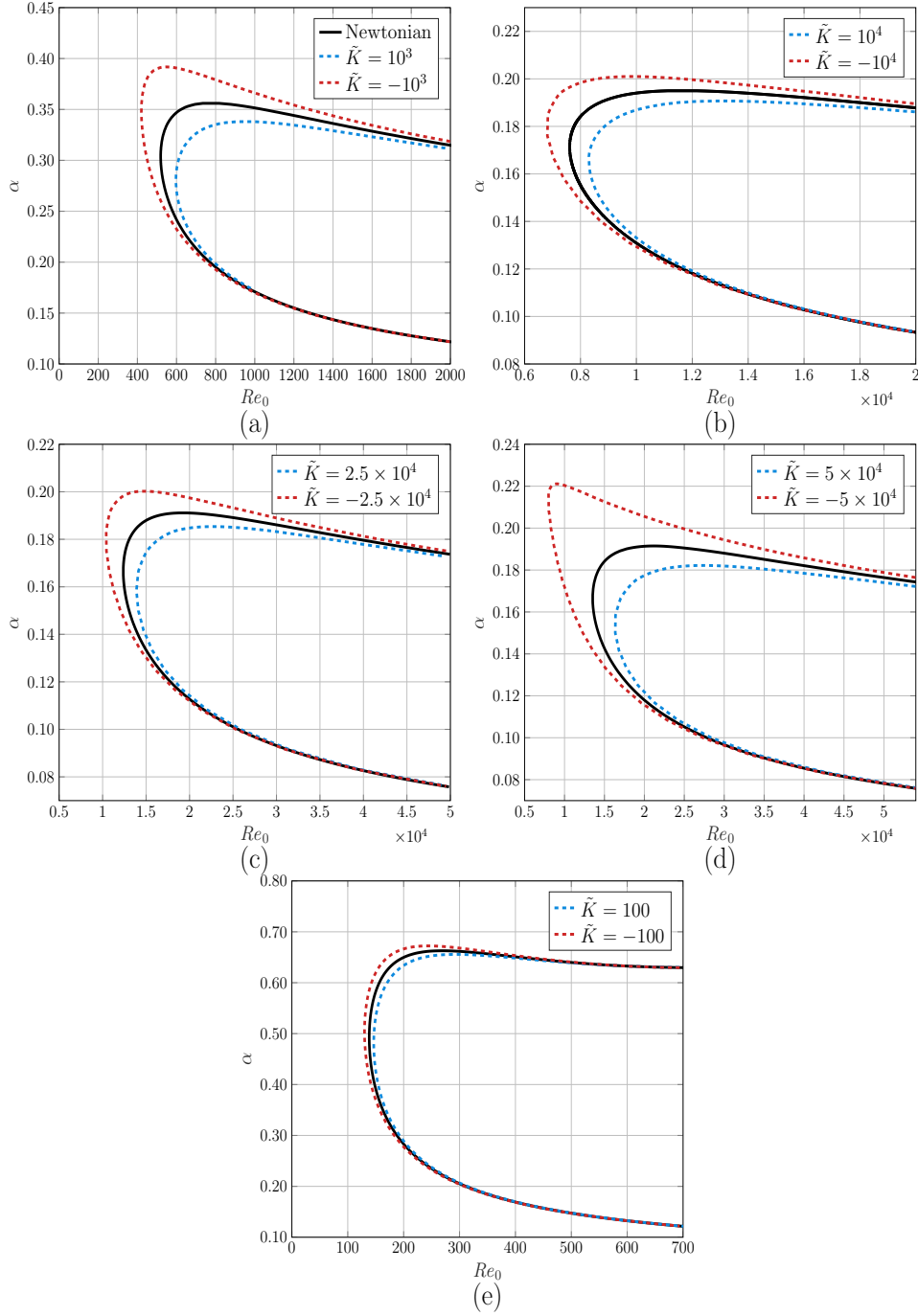
FIGURE 1.9. Temporal neutral curves in the Newtonian and non-Newtonian cases. (a) $\beta_H = 0$ (flat plate), $\tilde{K} = \pm 10^3$; (b) $\beta_H = 0.5$, $\tilde{K} = \pm 10^4$, $x_0 = 1$; (c) $\beta_H = 1$ (stagnation point), $\tilde{K} = \pm 2.5 \times 10^4$, $x_0 = 1$; (d) $\beta_H = 1.2$, $\tilde{K} = \pm 5 \times 10^4$, $x_0 = 1$; (e) $\beta_H = -0.14$ (inflection point), $\tilde{K} = \pm 100$; $x_0 = 1$.

since we have

$$K_0 = \frac{\alpha_1}{\rho \delta_0^2} = \frac{\alpha_1 a^2}{\rho \nu^2} \frac{x_0^{2m}}{Re_0^2}.$$

For this reason, we decided to plot the neutral curves in Figures 1.9(b) -(e) by fixing the streamwise position at $x_0 = 1$. In this case the interpretation must be different, the Reynolds number varies through a variation of the free-stream velocity U. Once again, when $\tilde{K} > 0$, elasticity has the effect of reducing the region of two-dimensional instability as shown in Figure 1.9 for different angle parameters. When $\tilde{K} < 0$, the instability happens at lower Reynolds numbers. Moreover, the neutral curves in the non-Newtonian case approach the Newtonian curves when the Reynolds number increases. It is worth noticing that, for the flow past a corner ($\beta_H = -0.14$), as the Reynolds number increases the non-Newtonian curves overlap the Newtonian curve. This means that the inviscid instability, which arises in the presence of an inflectional velocity profile, does not seem to be affected by non-Newtonian effects.

Note that for different values of β_H different values of $\tilde{K}$ are chosen in order to ensure that the Weissenberg number, Wi_0, is of order 1 when the Reynolds number is close to critical for the onset of instability. This is to ensure that the boundary layer theory is valid, whilst the elasticity effects remain significant (Rajagopal *et al.* [**66**]).

1.5.3. Spatial neutral stability curves. We define a frequency F, as follows

$$F = 10^6 \frac{\omega}{Re_0}.$$

This choice of scalings eliminates the streamwise dependency of the frequency ω. Spatial neutral stability curves are curves in the Re_0-F plane that divide the region where there exists an exponentially growing eigenmode and where it does not exist.

Figure 1.10 includes neutral stability curves for zero, positive and negative pressure gradients. We can see that, as for the temporal problem, when $\tilde{K} > 0$ elasticity has the effect of reducing the region of instability. When $\tilde{K} < 0$ elasticity is destabilising and the instability happens at lower Reynolds numbers.
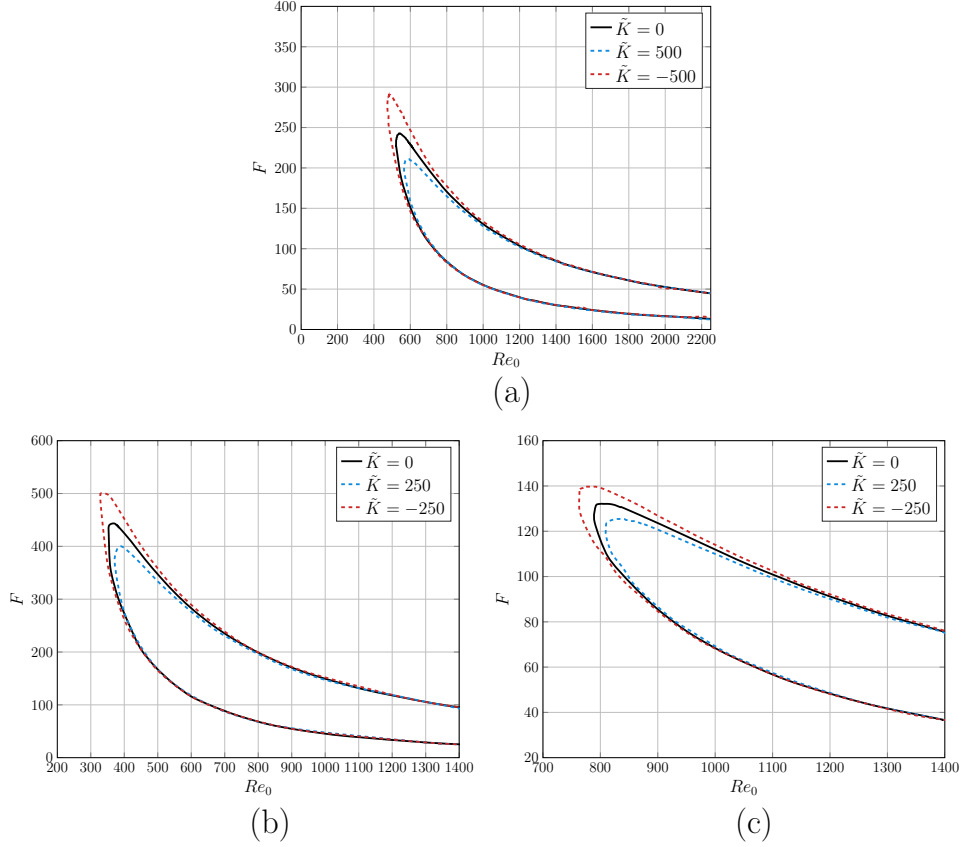
FIGURE 1.10. Spatial neutral curves in the Newtonian and non-Newtonian cases. (a) $\beta_H = 0$ (flat plate), $\tilde{K} = \pm 500$; (b) $\beta_H = 0.04$, $\tilde{K} = \pm 250$, $x_0 = 1$; (e) $\beta_H = -0.04$ (inflection point), $\tilde{K} = \pm 250$; $x_0 = 1$.

1.5.4. Critical Reynolds number. The critical Reynolds number is defined as the smallest Reynolds number for which there exists an exponentially unstable mode. We calculated the critical wavenumbers, α_{cr}, and Reynolds numbers, Re_{cr}, for different values of β_H and the results are displayed in Table 1.1. In order to be able to compare the non-Newtonian effect of elasticity for different values of β_H we choose, as a measure of elasticity, the critical Weissenberg number

$$Wi_{0,\mathrm{cr}} = K_{0,\mathrm{cr}} Re_{0,\mathrm{cr}},$$

defined with reference to the Newtonian critical Reynolds number $Re_{0,\mathrm{cr}}$ and the critical elasticity number $K_{0,\mathrm{cr}} = \tilde{K}/Re_{0,\mathrm{cr}}^2$.

From Table 1.1 we deduce, for the second grade model ($Wi_{0,\mathrm{cr}} > 0$), the stabilising effect in terms of an increase of the critical Reynolds

$Wi_{0,cr}$	non-Newtonian -1	-0.5	Newtonian 0	non-Newtonian 0.5	1
β_H	$Re_{0,cr}$	$Re_{0,cr}$	$Re_{0,cr}$	$Re_{0,cr}$	$Re_{0,cr}$
-0.14	126.68	132.58	138.42	144.07	149.48
0	470.71	495.70	519.06	540.96	561.60
0.5	7005.78	7324.05	7617.06	7890.03	8146.65
1	11483.50	11949.02	12380.61	12784.75	13166.26
1.2	12563.43	13064.70	13529.76	13965.65	14377.28
β_H	α_{cr}	α_{cr}	α_{cr}	α_{cr}	α_{cr}
-0.14	0.5115	0.5025	0.4920	0.4843	0.4774
0	0.3231	0.3130	0.3038	0.2965	0.2902
0.5	0.1776	0.1742	0.1713	0.1687	0.1664
1	0.1722	0.1692	0.1665	0.1642	0.1622
1.2	0.1720	0.1690	0.1665	0.1643	0.1622

TABLE 1.1. Critical Reynolds numbers and critical wavenumbers in the Newtonian and non-Newtonian cases.

number for all values of β_H considered, including the slightly negative value of β_H that represents a profile with an inflection point. The effect is the opposite for the second order model ($Wi_{0,cr} < 0$) where the instability is anticipated for each value of the Hartree parameter β_H.

Note that the magnitude of the critical Reynolds number $Re_{0,cr}$ for the Newtonian case is strongly dependent upon the configuration characterised by β_H. This strong dependence is maintained for the variation found in $Re_{0,cr}$ when the non-Newtonian effects are introduced in the manner that we have described. For example, with a critical Weissenberg number $Wi_{0,cr} = 0.5$, for a flat plate ($\beta_H = 0$) the increase or decrease in critical Reynolds number is of order 10, while for the stagnation point flow ($\beta_H = 1$) it is of order 10^2.

The results in Table 1.1 are summarised in Figure 1.11. In Figure 1.11(a), we show the relative variation of critical Reynolds numbers with respect to the Newtonian critical Reynolds numbers, i.e.

$$\frac{Re_{0,cr} - Re_{0,cr,Newt}}{Re_{0,cr,Newt}},$$

where $Re_{0,cr,Newt}$ is the critical Reynolds number in the Newtonian case, when $Wi_0 = 0$. We can see that, for a Weissenberg number $|Wi_{0,cr}| = 0.5$,
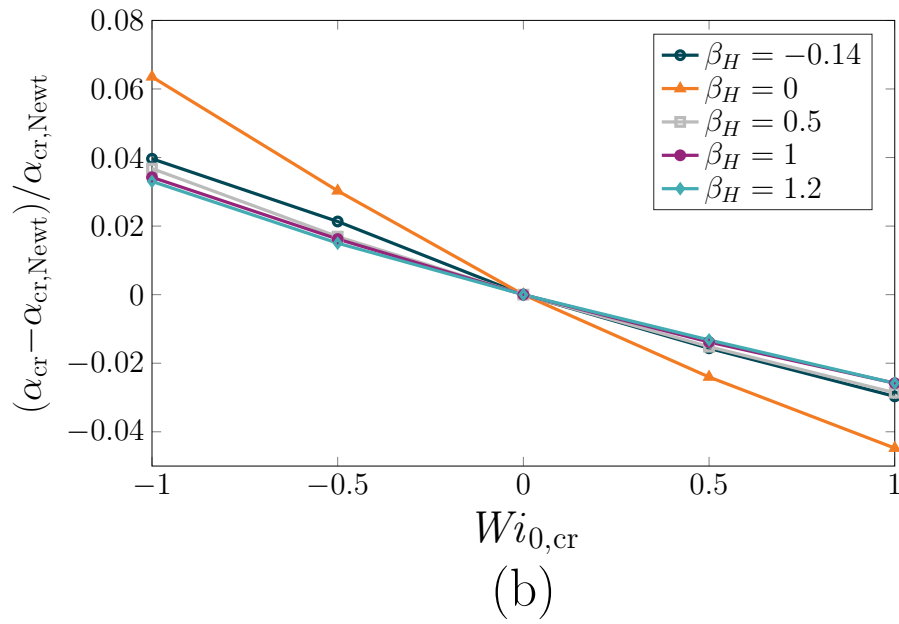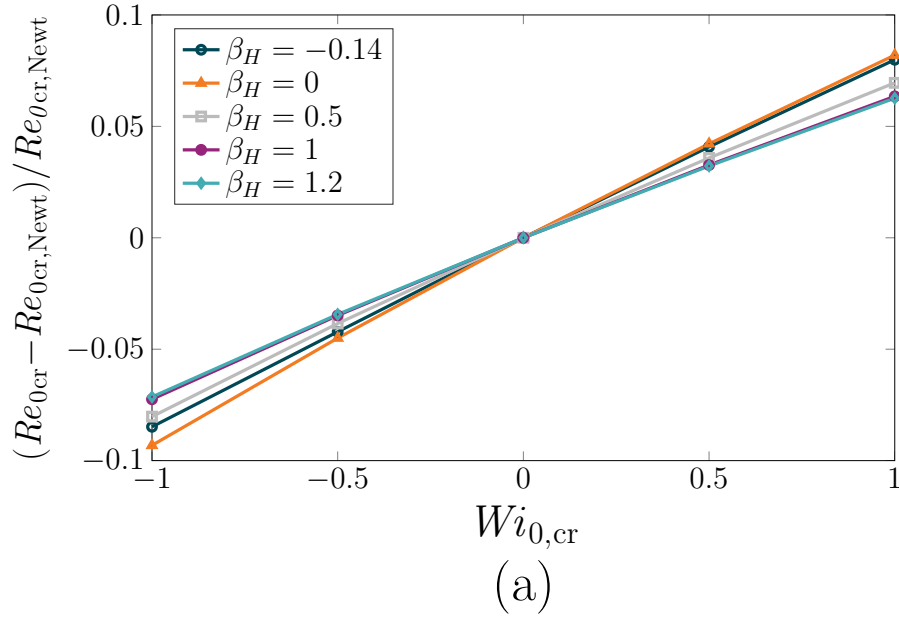
FIGURE 1.11. Non-Newtonian effects on the (a) critical Reynolds numbers; (b) critical spanwise wavenumbers.

the relative variation is around 4%, while for a Weissenberg number $|Wi_{0,\mathrm{cr}}| = 1$, the relative variation is around 8% for every value of the angle parameter β_H. In Figure 1.11(b), we show the relative variation of critical spanwise wavenumbers with respect to the Newtonian critical spanwise wavenumbers. We observe that the non-Newtonian effects affect the flat plate configuration ($\beta_H = 0$) the most.

1.6. Energy theory

In this section we apply energy theory to the non-Newtonian models considered here. We derive an evolution equation for an appropriate choice of disturbance energy in order to study how non-Newtonian effects influence the the energy balance. It is well known that the nonlinear terms of the incompressible Navier-Stokes equations conserve energy. Therefore, in the Newtonian case, the energy balance can be seen as a nonlinear theory, because it applies to disturbances of arbitrary amplitude (Schmid and Henningson [77]). Nonlinear terms play a role in the distribution and transfer of energy but not in its increase.

We showed in Appendix A.5 that nonlinear terms in the incompressible two-dimensional governing equations for the second order models (1.6) conserve energy. Therefore, in order to derive the energy equation we can start from the linearised equations and it will be equivalent to starting from the full nonlinear equations.

In the case of a parallel main flow, the energy balance can be found by multiplying the Orr-Sommerfeld equation by the complex conjugate $\bar{\phi}$ of the stream function ϕ and integrating over the semi-infinite domain in the y-direction (Drazin [23]). The same procedure is applied to the modified Orr-Sommerfeld equation (1.22). After some algebraic manipulation that can be found in Appendix A.6 and defining

$$I_k^2 = \int_0^\infty |\phi^{(k)}|^2 \, dy \qquad \text{for } k = 0, 1, 2,$$

we obtain the following equation

$$-i\alpha c \left(I_1^2 + \alpha^2 I_0^2 \right) = \left(-\frac{1}{Re_0} + i\alpha c K_0 \right) \left(I_2^2 + 2\alpha^2 I_1^2 + \alpha^4 I_0^2 \right)$$

$$- i\alpha \int_0^\infty \left(U_B |\phi'|^2 + \left(U_B'' + \alpha^2 U_B \right) |\phi|^2 + U_B' \phi' \bar\phi \right) \, dy$$

$$- i\alpha K_0 \int_0^\infty \left(U_B'' \phi'' \bar\phi + 2U_B' \left(\phi'' \bar\phi' + \alpha^2 \phi' \bar\phi \right) - U_B^{iv} |\phi|^2 \right) \, dy$$

$$- i\alpha K_0 \int_0^\infty \left(U_B \left(|\phi''|^2 + 2\alpha^2 |\phi'|^2 + \alpha^4 |\phi|^2 \right) \right) \, dy.$$

Taking the real part of this equation we find the following energy balance

$$\alpha c_i = \underbrace{-\frac{1}{Re_0 E} \left(I_2^2 + 2\alpha^2 I_1^2 + \alpha^4 I_0^2 \right)}_{\mathcal{D}} \underbrace{-\frac{i\alpha}{2E} \int_0^\infty \left(U_B' \left(\phi' \bar\phi - \phi \bar\phi' \right) \right) \, dy}_{\mathcal{P}}$$

$$\underbrace{-\frac{i\alpha K_0}{2E} \int_0^\infty \left(\left(2\alpha^2 U_B' - U_B''' \right) \left(\phi' \bar\phi - \phi' \bar\phi \right) \right) \, dy}_{\mathcal{N}_1}$$

$$\underbrace{-\frac{i\alpha K_0}{2E} \int_0^\infty \left(2U_B' (\phi'' \bar\phi' - \phi' \bar\phi'') \right) \, dy}_{\mathcal{N}_2}. \quad (1.24)$$

where we divided every term by a total energy E, defined as follows

$$E = I_1^2 + \alpha^2 I_0^2 + K_0 \left(I_2^2 + 2\alpha^2 I_1^2 + \alpha^4 I_0^2 \right). \quad (1.25)$$

Equation (1.24) is essentially what, for Newtonian fluids, is known as the *Reynolds-Orr equation*. The left-hand side term, αc_i, represents the temporal growth rate. On the right-hand side of the energy balance (1.24), $\mathcal{D}$ represents the rate of dissipation of the perturbation due to the viscosity and is always negative, since for all perturbations viscosity dissipates energy. The term $\mathcal{P}$, also known as the production term, represents the energy transfer from the mean flow to the perturbation by means of the Reynolds stress. The remaining terms $\mathcal{N}_1$ and $\mathcal{N}_2$ are due to non-Newtonian effects.

We can measure the proportion of energy E due to Newtonian and non-Newtonian sources by dividing the definition (1.25) by E. We obtain

$$1 = \underbrace{\frac{I_1^2 + \alpha^2 I_0^2}{E}}_{\mathcal{E}_k} + \underbrace{\frac{K_0 \left(I_2^2 + 2\alpha^2 I_1^2 + \alpha^4 I_0^2 \right)}{E}}_{\mathcal{E}_n}, \quad (1.26)$$

where $\mathcal{E}_k$ represents the Newtonian fraction and $\mathcal{E}_n$ represents the non-Newtonian fraction.

The Reynolds stress mechanism is a phenomenon of energy conversion between the mean and the fluctuating flow (Butler and Farrell [14], Pedlosky [58]). To visualise this mechanism, we express the transfer term, $\mathcal{P}$, in terms of the fluctuation velocities u and v. We can see that energy increases due to the production term $\mathcal{P}$ when

$$-uvU_B'$$

is positive. Hence, energy increases when

$$\frac{\partial \psi}{\partial x}\frac{\partial \psi}{\partial y}U_B' = -\left(\frac{\partial y}{\partial x}\right)_\psi \left(\frac{\partial \psi}{\partial y}\right)^2 U_B'$$

is positive over the integral in the semi-infinite domain $y \in [0, \infty)$, where ψ is the stream function. When the lines of constant ψ slope in the opposite direction of that of the mean flow, $\left(\frac{\partial y}{\partial x}\right)_\psi U_B' < 0$ and the perturbation gains energy. As the perturbation is advected, it becomes orientated in the opposite direction and the energy returns to the mean flow.

1.6.1. Results. We now analyse the results from the energy balance (1.24). First, we consider the case of a zero pressure gradient ($\beta_H = 0$), a wavenumber and a Reynolds number that gives an unstable mode in the Newtonian case, i.e. $\alpha^* = \alpha/C = 0.179$, $Re = Re_0/C = 580$. In Figure 1.12 we can see the role of different terms in equation (1.24) and how they change by introducing non-Newtonian effects. In agreement with the results shown in the previous sections, by increasing the non-Newtonian parameter $K = K_0 C^2$, the temporal growth rate αc_i decreases. We can see from Figure 1.12 that this stabilising effect is principally due to the production term $\mathcal{P}$, the diffusion due to the viscosity $\mathcal{D}$ decreases slightly while the extra terms $\mathcal{N}_1$ and $\mathcal{N}_2$ remain very small. The opposite happens for the second order model ($K < 0$), where the kinetic energy increases due to an increase of $\mathcal{P}$.

In Figure 1.13 we performed the energy balance for a base flow with an inflection point. We choose the angle parameter to be slightly
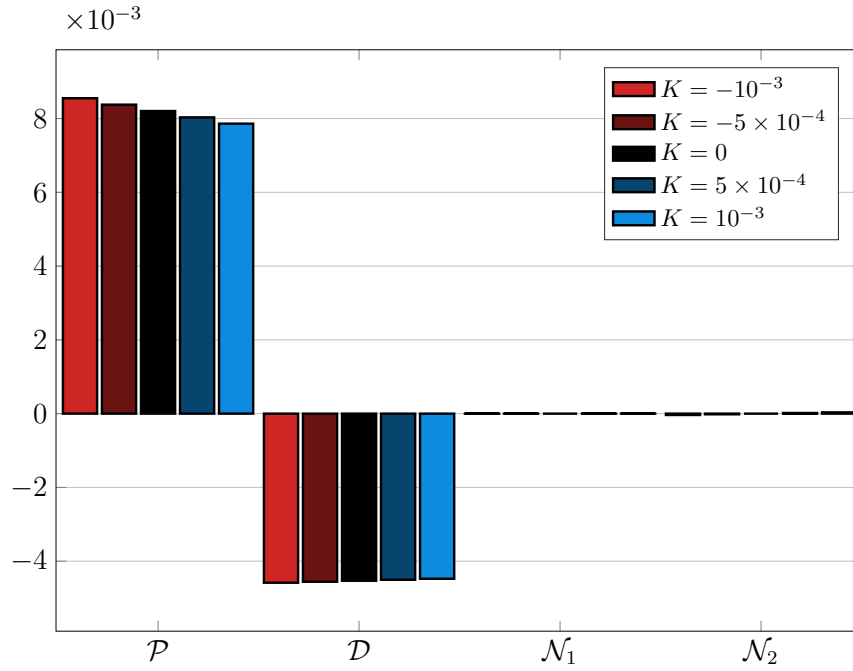
FIGURE 1.12. Energy balance for the flat plate $(\beta_H = 0)$ and $\alpha^* = 0.179$, $Re = 580$ for different values of the parameter K.
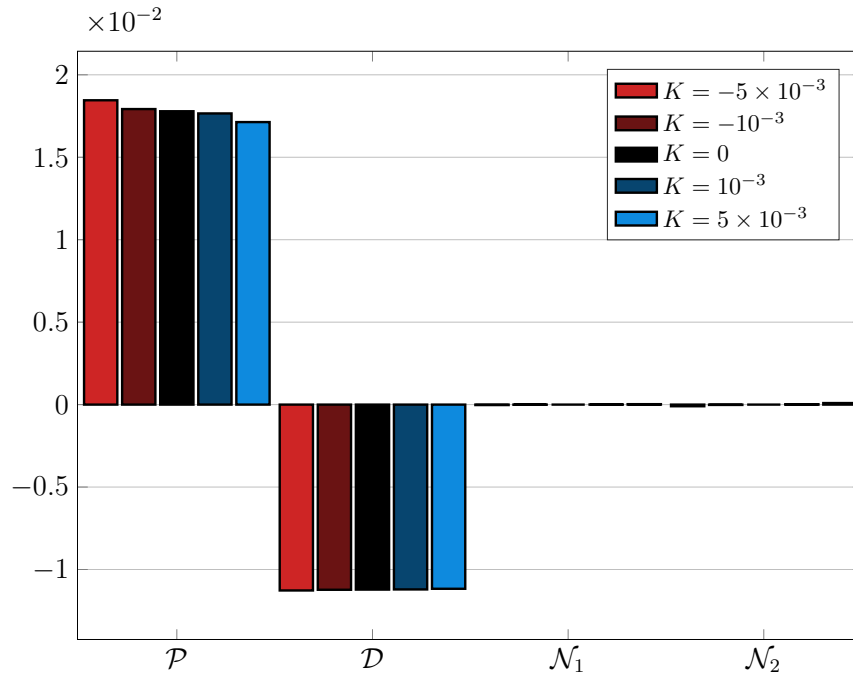
FIGURE 1.13. Energy balance for a profile with an inflection point $(\beta_H = -0.14)$ and $\alpha^* = 0.15$, $Re = 100$ for different values of the parameter K.

negative $\beta_H = -0.14$ in order to have a point of inflection in the velocity profile. We choose a Reynolds number and a wavenumber to have an unstable mode in the Newtonian case. We observe that also in this case the temporal growth rate αc_i decreases when the non-Newtonian parameter K is positive and it increases when K is negative. Once again, this is due to the change in the production term $\mathcal{P}$.

In all the tests performed, we found that the magnitude of the non-Newtonian contribution to the energy, $\mathcal{E}_n$, is very small with respect to the Newtonian fraction, $\mathcal{E}_k$, defined by relation (1.26).

It is clear that, also for the non-Newtonian models considered, the preferential route for instability is the transfer of energy from the mean flow to the perturbations by means of the Reynolds stress. This conclusion is valid for all the geometrical configurations considered. To avoid redundancy, figures representing the energy balance for other values of the Hartree parameter β_H are not reported in this work.

A similar result was obtained by Zhang *et al.* [**96**]. They performed an energy balance for the channel flow of FENE-P fluids and found that the production of perturbation kinetic energy due to the work of the Reynolds stress against the mean shear is responsible for the observed effects on the stability.

In Figure 1.14, we represent S defined by

$$S = \phi_i' \phi_r - \phi_r' \phi_i = \frac{1}{2i} \left(\phi' \bar{\phi} - \bar{\phi}' \phi \right),$$

which is proportional to the Reynolds stress and the mean shear U_B', in the case of a flat plate ($\beta_H = 0$). We can see how the non-Newtonian effects influence S and U_B'. The non-Newtonian effects for the second order model ($K < 0$) increase the Reynolds stress S and slightly decrease the mean shear. Therefore, we can say that an increase of S is causing the destabilisation process. Instead, the non-Newtonian effects for the second grade model ($K > 0$) provoke a decrease in S and stabilise the flow.
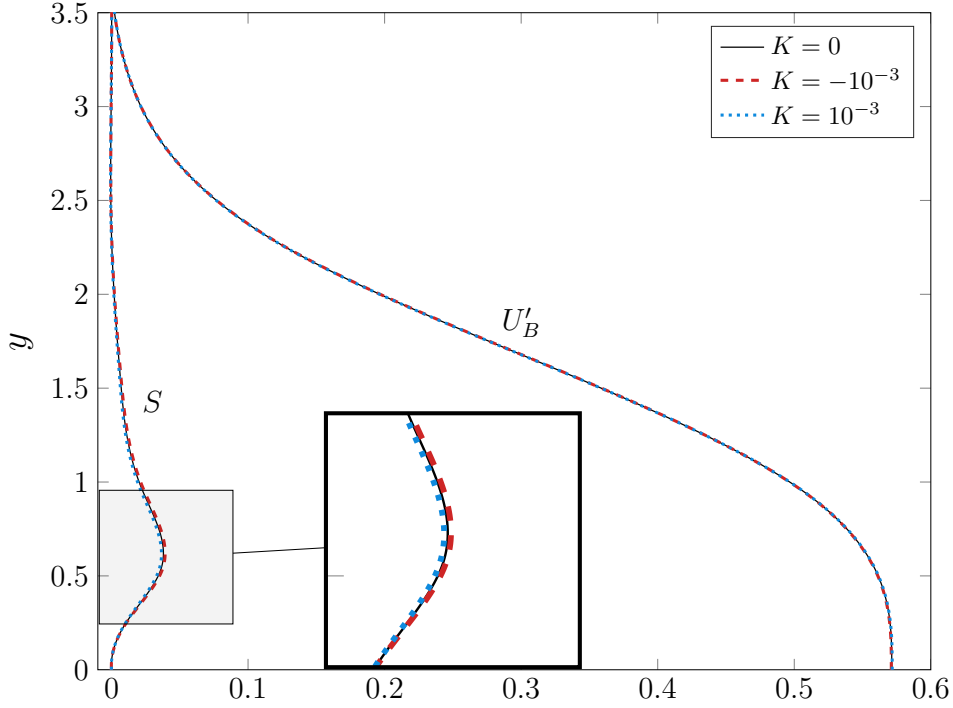
FIGURE 1.14. Mean shear U'_B and $S = \phi'_i \phi_r - \phi'_r \phi_i$ for the flat plate $\beta_H = 0$ with $Re = 580$ and $\alpha^* = 0.179$.

The physical perturbation velocities in the streamwise and spanwise directions, respectively u and v, can be calculated as follows

$$u = (\phi')_r,$$

$$v = (i\alpha\phi)_r.$$

In Figure 1.15 we plot the magnitude of the perturbation velocities u and v, normalised such that the Newtonian velocities have maximum equal to one. We can see that for zero and positive pressure gradients $(\beta_H \geq 0)$ a negative elasticity parameter K decreases the wall-normal perturbation velocity v and increases the streamwise velocity u. A positive elasticity number K provokes an increase in $|v|$ and a decrease in $|u|$. We can see from Figure 1.15(d) that the opposite happens in the case of a negative pressure gradient $\beta_H < 0$.

In order to perform the energy balance, the numerical integration has been performed following the method described in Section 5.4. We find that the eigenfunctions of the Orr-Sommerfeld equation (1.22) are numerically sensitive to a decrease of the elasticity parameter K for the
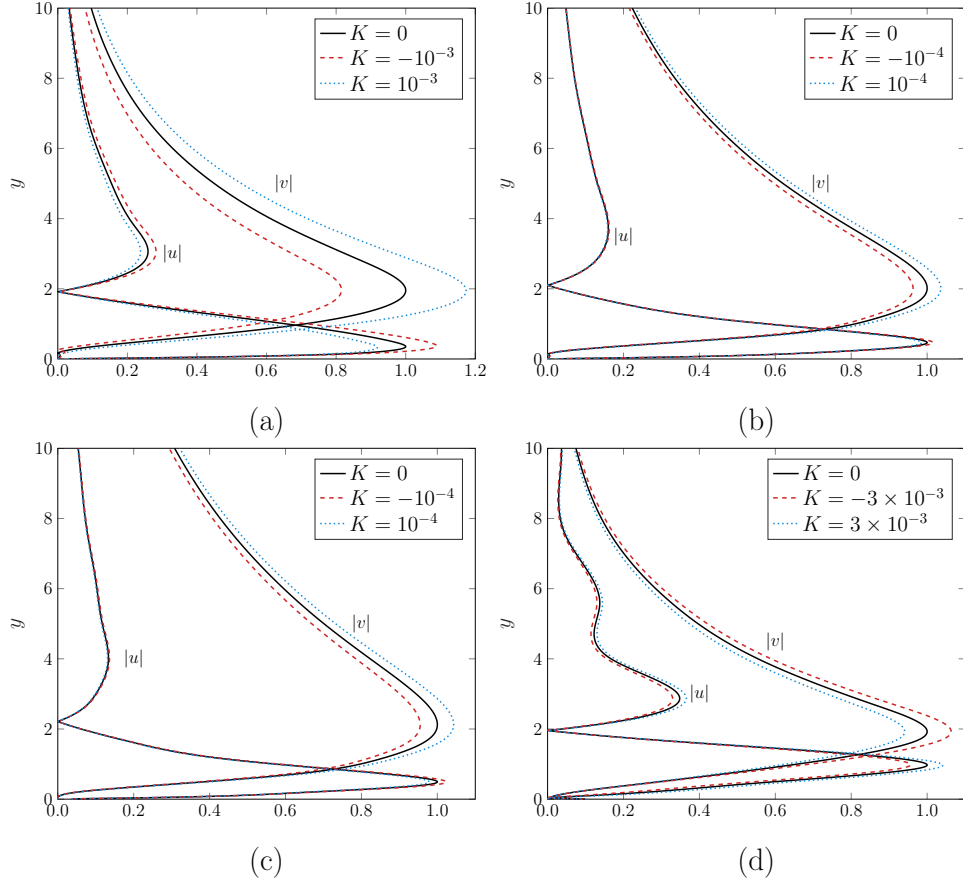
FIGURE 1.15. Disturbance velocities for (a) $\beta_H = 0$ (flat plate), $Re = 580, \alpha^* = 0.179$; (b) $\beta_H = 0.5$ (flow past a wedge), $Re = 1500, \alpha^* = 0.18$; (c) $\beta_H = 1$ (stagnation flow), $Re = 2500, \alpha^* = 0.18$; (d) $\beta_H = -0.14$ (inflectional profile), $Re = 100, \alpha^* = 0.15$.

second order model ($K < 0$). Hence, the mapping parameter l in the transformation (1.23) needs to be adjusted to better approximate the eigenfunctions. We find that, in general, the optimal choice is $l \approx 20$. This stretching parameter is much greater than the one we used to calculate the eigenvalues ($l \approx 4$), and it clusters fewer Chebyshev points in the boundary layer. Therefore, a stretching parameter $l \approx 20$ allows a better resolution of the eigenfunctions for $y \to \infty$.

1.7. Three-dimensional stability analysis

A study of three-dimensional disturbances for fluids of second order is required. For parallel Newtonian flow, Squire's theorem justifies the study of two-dimensional instead of three-dimensional disturbances. Squire's theorem states that each three-dimensional mode corresponds to some two-dimensional mode at a lower Reynolds number. Therefore, to determine the critical Reynolds number, it is sufficient to study two-dimensional disturbances for Newtonian fluids.

An equivalent Squire's theorem was proved for Oldroyd B fluids by Bistagnino *et al.* [**8**]. Zhang *et al.* [**96**] analysed three-dimensional modes for the channel flow of FENE-P fluids and observed that the two-dimensional waves appear to be the first to become unstable. A result similar to the Squire's theorem for a fluid of second grade cannot be proven. Therefore, an extension to the study of three-dimensional disturbances is necessary.

The linear system governing three-dimensional disturbances has been derived in Appendix A.4, after the application of the normal mode form to the wall-normal velocity v and vorticity $\eta = \frac{\partial u}{\partial z} - \frac{\partial w}{\partial x}$ of the perturbation, as follows

$$(v, \eta) = (\hat{v}(y), \hat{\eta}(y)) \, e^{i(\alpha x + \beta z - \omega t)},$$

where α and β are, respectively, the streamwise and spanwise wavenumbers and ω represents the frequency. Defining $\mathbf{q} = (\hat{v}, \hat{\eta})^T$, the problem to be solved is a linear system of the form

$$\mathcal{L}\mathbf{q} = \omega \mathcal{M}\mathbf{q}, \tag{1.27}$$

where $\mathcal{M}$ and $\mathcal{L}$ are linear operators defined as follows

$$\mathcal{M} = \begin{bmatrix} k^2 - \mathcal{D}^2 + K_0 \left(k^2 - \mathcal{D}^2\right)^2 & 0 \\ 0 & 1 + K_0 \left(k^2 - \mathcal{D}^2\right) \end{bmatrix}, \tag{1.28a}$$

$$\mathcal{L} = \begin{bmatrix} \mathcal{L}_{OS} & \mathcal{L}_{CN} \\ \mathcal{L}_C & \mathcal{L}_{SQ} \end{bmatrix}, \tag{1.28b}$$

(a)   (b)
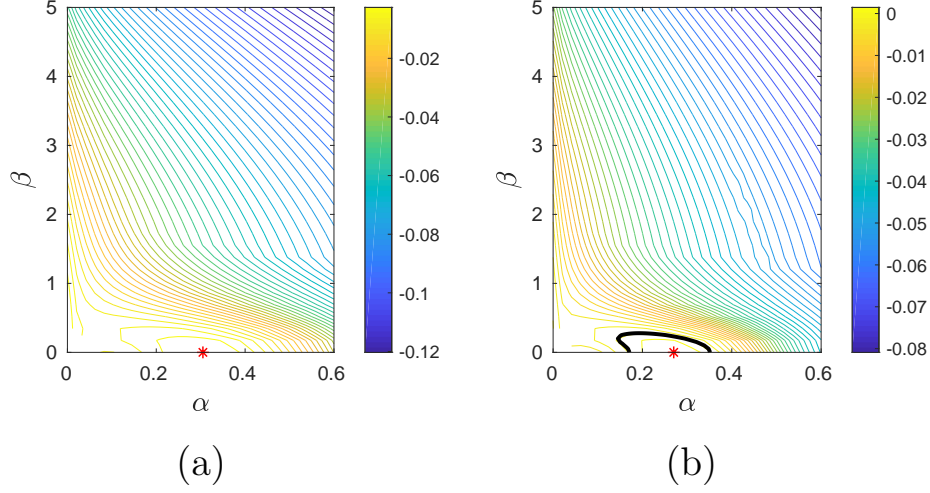
FIGURE 1.16. Contour plot for the temporal growth rate, ω_i, in the Newtonian case ($K = 0$) for the flat plate ($\beta_H = 0$). The red star ($*$) represents $\max_{\alpha,\beta} \omega_i$. The black line represents the neutral curve. (a) $Re_0 = 500$; (b) $Re_0 = 1000$.

with

$$\mathcal{L}_{OS} = \alpha U_B \left(k^2 - \mathcal{D}^2\right) + \alpha U_B'' + \frac{1}{iRe_0} \left(k^2 - \mathcal{D}^2\right)^2$$
$$+ K_0 \left(-\alpha U_B^{iv} + \alpha k^4 U_B - 2\alpha k^2 U_B \mathcal{D}^2 + \alpha U_B \mathcal{D}^4\right),$$
$$\mathcal{L}_{CN} = K_0 \left(-\beta k^2 U_B' - \beta U_B''' + \beta U_B' \mathcal{D}^2\right),$$
$$\mathcal{L}_C = \beta U_B' - K_0 \beta U_B''',$$
$$\mathcal{L}_{SQ} = \alpha U_B + \frac{1}{iRe_0}\left(k^2 - \mathcal{D}^2\right) + \alpha K_0 U_B \left(k^2 - \mathcal{D}^2\right),$$

where $\mathcal{D}$ denotes the derivative with respect to y and $k^2 = \alpha^2 + \beta^2$.

We can see that in the Newtonian case, when $K_0 = 0$, the equation for $\hat{v}$ does not involve the wall-normal vorticity $\hat{\eta}$. Instead, the equation for $\hat{\eta}$, also known as Squire's equation, is driven by solutions to the Orr-Sommerfeld equation through the forcing term $\beta U' \hat{v}$. In the Newtonian case, this term is responsible for an algebraic growth of energy and is referred to as the *vortex tilting term*. Ellingsen and Palm [27] first identified this mechanism by showing that inviscid channel flows are always unstable to perturbations independent of the streamwise coordinate.
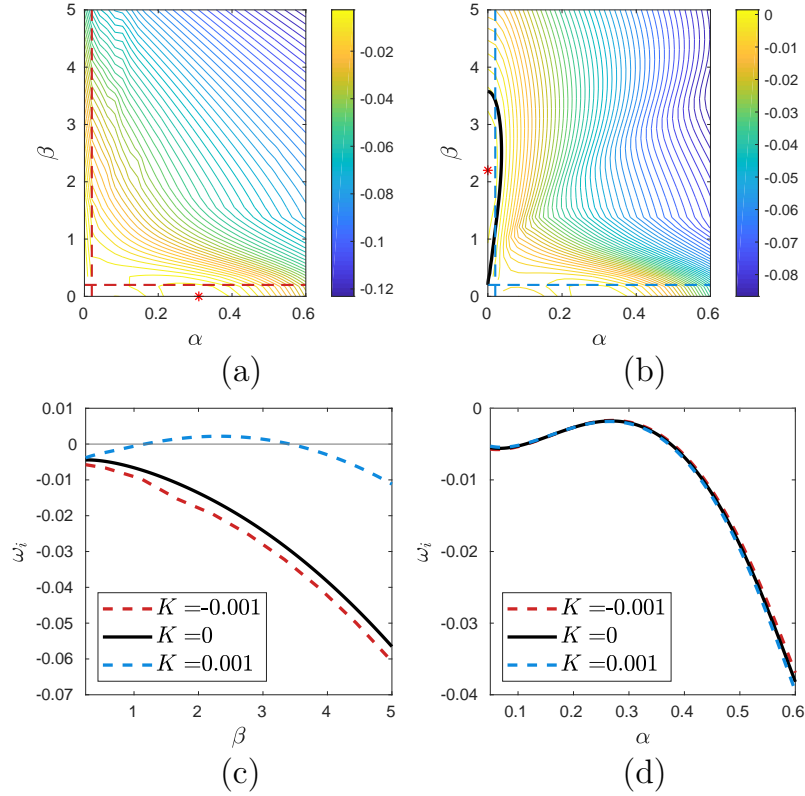
FIGURE 1.17. (a),(b) Contour plots for ω_i in the non-Newtonian cases for the flat plate ($\beta_H = 0$) and $Re_0 = 500$. The red star ($*$) represents $\max_{\alpha,\beta} \omega_i$. The black line represents the neutral curve. (a) $K = -0.001$; (b) $K = 0.001$. (c),(d) Comparison of Newtonian (-) and non-Newtonian (- -) temporal growth rates for (c) $\alpha = 0.02$; (d) $\beta = 0.2$.

We observe that for a non-zero non-Newtonian parameter K_0, the equation for the vorticity $\hat{\eta}$ has an additional forcing term and the equation for the wall-normal velocity $\hat{v}$ is no more homogeneous but is related to the vorticity through some non-Newtonian terms. Therefore, the system we are considering now is fully coupled.

1.7.1. Results. We solved the three-dimensional eigenvalue problem (1.27). The results obtained are summarised by displaying the neutral stability curves in an α-β plane.
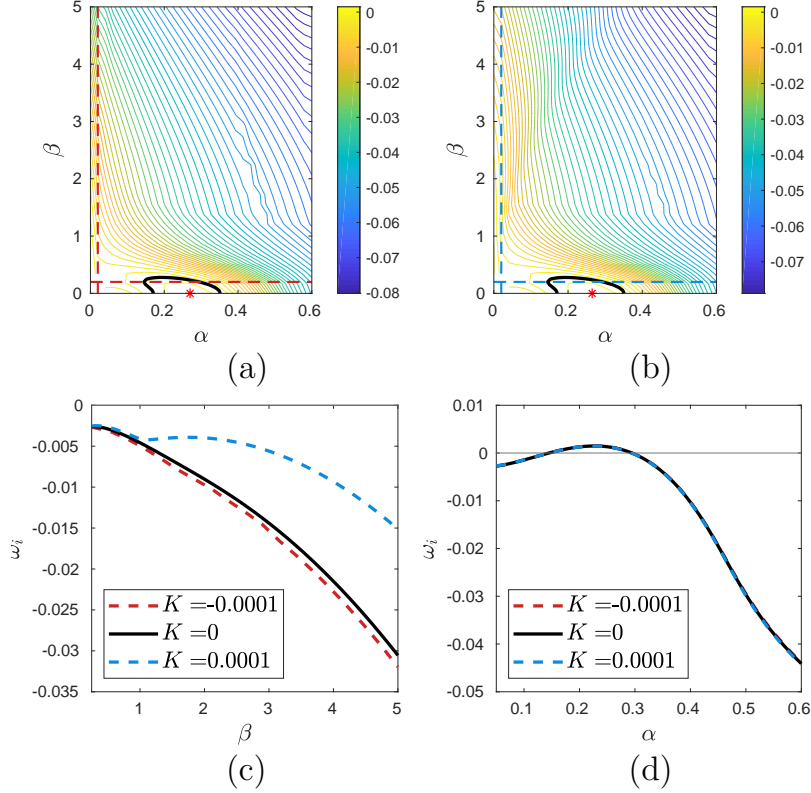
FIGURE 1.18. (a),(b) Contour plots for ω_i in the non-Newtonian cases for the flat plate ($\beta_H = 0$) and $Re_0 = 1000$. The red star ($*$) represents $\max_{\alpha,\beta} \omega_i$. The black lines represent neutral curves. (a) $K = -0.0001$; (b) $K = 0.0001$. (c),(d) Comparison of Newtonian (-) and non-Newtonian (- -) temporal growth rates for (c) $\alpha = 0.02$; (d) $\beta = 0.2$.

Figure 1.16 shows the contour plot of the temporal growth rate ω_i in the Newtonian case for the flat plate ($\beta_H = 0$). Figure 1.16(a) shows that the choice of a subcritical Reynolds number ($Re = 500$) gives a stable flow. In Figure 1.16(b), we increase the Reynolds number to $Re = 1000$ and we can see an exponential instability, for which $\omega_i > 0$, appearing at small spanwise wavenumbers. The red star ($*$) represents the maximum growth rate reached in the α-β plane, i.e. $\max_{\alpha,\beta} \omega_i$. We can see that, in both cases, the maximum is reached for spanwise independent waves. This confirms the Squire's theorem for Newtonian fluids.
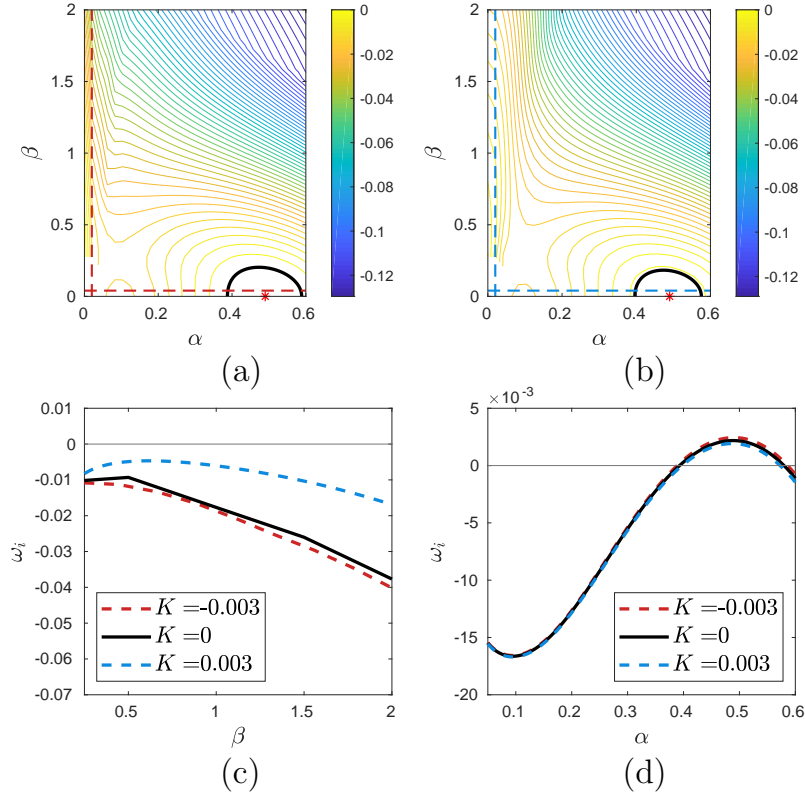
FIGURE 1.19. (a),(b) Contour plots for ω_i in the non-Newtonian cases for the flow past a corner ($\beta_H = -0.14$) and $Re_0 = 150$. The red star ($*$) represents $\max_{\alpha,\beta} \omega_i$. The black lines represent neutral curves. (a) $K = -0.003$; (b) $K = 0.003$. (c),(d) Comparison of Newtonian (-) and non-Newtonian (- -) temporal growth rates for (c) $\alpha = 0.02$; (d) $\beta = 0.04$.

Figures 1.17(a),(b) show the contour plots of the temporal growth rates ω_i, for the second order model ($K < 0$) and for the second grade model ($K > 0$), respectively. We can see that, for the second grade model, there is a region of exponential instability for small streamwise wavenumbers and for a value of the Reynolds number ($Re = 500$) that gives an stable flow in the Newtonian case. In Figure 1.17(c) we displayed the growth rates for a fixed and small α and for a fixed β in Figure 1.17(d). We observe how a positive elasticity number K destabilises spanwise disturbances while it stabilises the Tollmien-Schlichting waves. The opposite happens for a negative K, which decreases the growth rates of mainly streamwise independent waves

($\alpha \approx 0$) and increases the growth rates of mainly spanwise independent waves ($\beta \approx 0$).

Figure 1.18 shows the results for a Reynolds number of $Re = 1000$. The conclusions are the same, for the second grade model the Tollmien-Schlichting wave is slightly stabilised while growth rates near the $\alpha = 0$ axis become larger. The opposite happens for the second order model, where $K < 0$.

Figure 1.19 shows growth rates for the flow past a corner with $\beta = -0.14$. The results are very similar to that of the flat plate. We do not report results for other values of the angle parameter β_H since they are in line with the results we discussed so far.

1.8. Concluding remarks

We applied a boundary layer theory to second order fluids in order to determine the mean flow. As for Newtonian fluids, this approach allowed us to simplify the governing equations. We applied a pseudo-similarity transformation and obtained a local ODE, which was solved numerically for the purpose of the linear stability analysis.

The modified Orr-Sommerfeld equation was solved using a Chebyshev collocation method. We presented the results in terms of temporal and spatial growth rates, neutral stability curves and critical Reynolds numbers. For all the values of the angle parameter β_H, we observe a stabilisation of the Tollmien-Schlichting waves for the second grade model ($K > 0$) and a destabilisation for the second order model ($K < 0$).

Moreover, by means of an energy balance, we showed that the stabilising effect for the second grade model is mainly due to a decrease of the production term, which represents the transfer of energy between the mean flow and the disturbance. For the second order model the increase of energy occurs because of an increase of the production term.

Finally, we expanded the analysis to three-dimensional disturbances. We showed that, for $K > 0$, spanwise disturbances become more unstable. On the contrary, when $K < 0$ the growth rates of mainly streamwise independent waves decrease.

Transient growth of second order fluids

The traditional starting point of hydrodynamic stability is an eigenvalue analysis such as the one performed in Chapter 1. Classical linear stability analysis proceeds to diagonalise the exponential operator by extracting the temporal behaviour of individual modes, while ignoring the effects due to the transformation, which leads to a diagonal operator. For most wall bounded shear flows, it only gives the asymptotic behaviour of the perturbation ($t \to \infty$) and fails to capture the short-time characteristics (Schmid and Henningson [**77**]). Instabilities and transition scenarios are observed in experiments on a shorter timescale than those typical for Tollmien-Schlichting waves (Schmid [**75**]). In fact, the time-asymptotic predictions may be irrelevant to the overall perturbation dynamics, as this limit may never, or only under artificial conditions, be reached. Therefore, it is necessary to describe disturbance behaviour for all times.

The approach we consider in this chapter is called *bypass transition*, because it bypasses the classical route of instability due to the presence of an exponentially growing eigenmode. The basic idea is that there can be short-time growth of energy even if all the eigenvalues decay exponentially. Quoting Schmid and Henningson [**77**], bypass transition can be defined as "the transition emanating from nonmodal growth mechanism". This scenario is related to the nonnormality of the stability operators involved. A linear operator $\mathcal{L}$ is said to be normal if it commutes with its Hermitian adjoint, i.e. if it satisfies the following relation

$$\mathcal{L}\mathcal{L}^H = \mathcal{L}^H \mathcal{L}.$$

Normal operators can be unitarily diagonalisable, i.e. they have orthogonal eigenfunctions (Trefethen and Embree [**89**]). This is, for example, the case for the Rayleigh-Bénard convection (a plane horizontal layer of fluid heated from below) and Taylor-Couette flow (fluid confined in a gap between rotating cylinders). However, in shear flows such as Poiseuille, Couette and Blasius, the stability operators are nonnormal and their eigenfunctions form a non-orthogonal set. It can be seen that the non-orthogonal superposition of exponentially decaying eigenfunctions can lead to transient amplification of energy, before the modal behaviour eventually prevails (Trefethen *et al.* [**90**]).

Moreover, eigenvalue analysis provides a critical Reynolds number, Re_{cr}, above which exponentially growing disturbances exist. Energy stability theory gives the critical Reynolds number Re_{E} below which the energy of arbitrary perturbations decays in time. This critical Reynolds number, based on energy methods, is usually determined using the Reynolds-Orr equation (Drazin [**23**]). For flows dominated by normal systems, like the Rayleigh-Bénard convection, the two critical Reynolds numbers coincide, i.e. $Re_{\mathrm{cr}} = Re_{\mathrm{E}}$. However, for Poiseuille flow, eigenvalue analysis predicts a critical Reynolds number $Re_{\mathrm{cr}} \approx 5772$ while energy methods predict a critical Reynolds number as low as $Re_{\mathrm{E}} \approx 49.6$. The wide gap between Re_{cr} and Re_{E} is a characteristic of many nonnormal systems and, for Reynolds numbers in this gap, transient growth prevails (Reddy and Henningson [**69**], Schmid [**74**]).

A result known as *Squire's theorem* has led to an over-emphasis on two-dimensional studies over three-dimensional studies. Squire's theorem states that every unstable three-dimensional modal disturbance corresponds to a more unstable two-dimensional disturbance at a lower Reynolds number. Therefore, two-dimensional disturbances are the first to become unstable and they determine the critical Reynolds number Re_{cr}. Bypass transition analysis reveals that the variations that mostly exploit the transient growth of energy commonly take the form of streamwise vortices, which are vortices aligned with the flow direction. These structures develop into streamwise streaks, elongated regions of high or low velocity, relative to the mean flow, by means of the so-called *lift-up effect*. The lift-up mechanism for instability is the vertical

displacement of fluid particles by means of cross-stream momentum (Brandt [11]).

Disturbances resulting from nonmodal growth mechanisms and elongated in the streamwise directions are a common feature of many transition processes (Alfredsson and Matsubara [2]). For this reason, it is natural to expand the linear stability analysis of the second order model, performed in Chapter 1, to include bypass transition.

In Section 2.1, we provide a summary of previous work on bypass transition for Newtonian and non-Newtonian fluids, without any claim to completeness. In Section 2.2, we provide an example to illustrate the dramatic effects of nonnormal operators. Section 2.3 is dedicated to the derivation of an initial-value problem which drives the temporal evolution of disturbances for second order fluids. In Section 2.4, we introduce the concept of maximum possible amplification which is used to quantify the tendency of the flow to grow transiently and we present the results obtained for second order fluids. In Section 2.5, the definition of optimal disturbance is given. Section 2.6 is an introduction to other tools useful to study nonnormal operators, such as pseudospectra. In Section 2.7, we present some time-dependent simulations performed to verify the transient growth results obtained in the previous sections. In Section 2.8, we comment briefly on the results obtained in this chapter.

2.1. Previous studies

The phenomenon of transient growth has been known, for Newtonian fluids, since the late 1980s and some work has been done also for non-Newtonian fluids. In this section we summarise the main results.

2.1.1. Newtonian fluids. In 1975, Ellingsen and Palm [27] first identified a linear growth mechanism for inviscid, incompressible and non-stratified channel flows. They showed that, for these flows, streamwise independent disturbances grow linearly with time and this growth is usually referred to as *algebraic instability*. The mechanism which leads to this kind of instability has been explained by Landahl [49] and is referred to as the *lift-up effect*. The lift-up effect is the generation of

horizontal velocity perturbations by the lifting-up of fluid elements in the presence of the mean shear. These particles initially retain their horizontal momentum, while being displaced in the wall-normal direction, leading to the formation of streamwise velocity variations (streaks).

Early work on algebraic growth focused on degeneracies (double eigenvalues) and exact resonances (coincidence of an Orr-Sommerfeld mode and a Squire mode). For example, Gustavsson [37] studied the effect of direct resonances for Poiseuille flow as a possible mechanism for transient growth. The presence of degeneracies and resonances introduces an algebraic growth term into the temporal development of a disturbance. Various results on degeneracies and resonances were obtained, but significant energy growth was not found. Resonances and degeneracies are not necessary for transient growth, which can occur when the linear stability operator is nonnormal.

Butler and Farrell [14] investigated the transient growth of three-dimensional disturbances in Poiseuille, Couette and boundary layer flows. They found a growth of energy of three orders of magnitude at subcritical Reynolds numbers, that is for $Re < Re_{\mathrm{cr}}$. Butler and Farrell showed, using a variational method, that the optimal perturbations are not of modal form and they resemble streamwise vortices.

Reddy and Henningson [69] considered different aspects of transient energy growth at subcritical Reynolds number for two and three-dimensional Poiseuille and Couette flows. They analysed the conditions for no energy growth, the dependence of the growth on the wavenumbers and on time and the effects of degenerate eigenvalues. They showed that the maximum transient growth is of order $O(Re^2)$ and that it occurred at a time proportional to the Reynolds number, Re. Moreover, Reddy and Henningson showed, by applying the Hille-Yosida theorem, that the conditions of no growth based on the numerical range, which will be defined in Section 2.6, are equivalent to those obtained by applying standard energy methods to the full Navier-Stokes equations, which apply to perturbations of finite amplitude. This result has two important implications. First, there cannot be an energy growth of disturbances of arbitrary amplitude unless there is a linear growth

mechanism. Secondly, subcritical transition for Poiseuille and Couette flows can occur because the linear operator is nonnormal.

Corbett and Bottaro [16] proved, using a direct-adjoint technique, that an adverse pressure gradient causes an increase of the resulting growth of energy while a positive pressure gradient has the opposite effect. The disturbance which evokes the greatest response over all time is a streamwise oriented vortex which gives rise to a streamwise streak. Furthermore, they showed that maximum local optima (perturbations that maximise growth at a shorter time) gain significant amplification, tend to be oblique and can compete in terms of energy growth with Tollmien-Schlichting waves for supercritical Reynolds numbers, that is for $Re > Re_{\mathrm{cr}}$.

2.1.2. Experiments and DNS. The lift-up effect turns out to be dominant at moderate and high level of external noise, whereas the so-called Tollmien-Schlichting waves are responsible for transition in low-noise environments (Brandt [11], Schmidt and Henningson [77]). Direct numerical simulations demonstrated the importance of the lift-up mechanism in the case of the laminar-turbulent transition in boundary layers subject to high level of free-stream turbulence (Brandt, Schlatter and Henningson [12]). Streamwise streaks induced by the lift-up effect dominate over the two-dimensional Tollmien-Schlichting waves, even at supercritical Reynolds numbers ($Re > Re_{\mathrm{CR}}$), and are followed by streaks, oscillations and turbulent spots until the flow becomes fully turbulent. Experiments extensively show the role of streaks (Afredsson and Matsubara [2]). After the formation of streaks, the flow is in a more complicated laminar state where nonlinear interactions intervene. The breakdown seems to be associated with a secondary instability which develops due to the highly spanwise inflectional profiles associated with high and low speed regions.

2.1.3. Non-Newtonian fluids. One important motivation for studying the stability behaviour of viscoelastic fluids, and in particular polymer suspensions, can be found in drag reduction in turbulent regime

(White and Godfrey Mungal [94], De Angelis *et al.* [20, 21]). This phenomenon was first observed over 70 years ago. In turbulent boundary layers, dissolving a small quantity of long-chain flexible polymers into solution can reduce turbulent friction by a significant amount.

Brandt [11] reviewed the main results in bypass transition for non-Newtonian fluids. In the context of classical linear stability analysis, for inelastic non-Newtonian fluids shear-thinning is found to be stabilising while shear-thickening is destabilising. When viscosity variations are ignored, plane Poiseuille flow of a shear-thinning fluid shows a slight decrease in transient growth. When viscosity variations are included, transient growth increases with respect to the Newtonian case. In Couette flow, transient growth increased substantially for shear-thinning fluids. Therefore, although shear-thinning damps the exponentially unstable mode, it can promote nonmodal instability.

Zhang *et al.* [96] performed the modal and nonmodal linear analysis of inertia-dominated channel flow of viscoelastic fluids modelled by Oldroyd B and FENE-P closures. The authors observed destabilisation of both modal and nonmodal instability when the polymer relaxation time is shorter than the instability timescale (i.e. for Weissenberg numbers $Wi \lesssim 1$), whereas the flow is more stable in the opposite case. In the subcritical regime, the nonmodal amplification of streamwise elongated structures is still the most dangerous energy growth mechanism and is slightly enhanced by the presence of polymers. The lift-up effect is still the dominant instability mechanism also for viscoelastic fluids.

Hoda *et al.* [42] performed an input-output analysis where the equations are transformed into a state-space representation and external disturbances are expressed in form of body forces. The input is harmonic in the streamwise and spanwise directions, respectively x and z, and random in the wall-normal direction, y, and in time, t. An ensemble-average energy density is used due to the stochastic character of the velocity field. They found that, increasing fluid elasticity through polymer contribution to the viscosity or the elasticity number enhances energy amplification. Once again, the disturbances that are most

amplified are streamwise-elongated, with elasticity acting to reduce spanwise length scale.

Hoda *et al.* [**43**] studied the frequency responses of streamwise-constant perturbations in channel flows of Oldroyd B fluids. An explicit Reynolds number scaling of frequency responses shows the same Re-dependence as in Newtonian fluids. The maximum transient growth, which will be defined in Section 2.4, is proportional to Re^2. Moreover, they analysed the Reynolds-Orr equation (energy-evolution equation) for streamwise-constant perturbations. As in Newtonian fluids, the nonlinear terms do not contribute to the growth of kinetic energy.

2.1.4. Different approaches and extensions. In nonmodal analysis, two general approaches can be distinguished: the response to initial conditions and the response to external forcing (Schmid [**75**], Schmid and Brandt [**76**]). The first approach is adopted in hydrodynamic stability theory and focuses on seeking the most dangerous initial condition, i.e. the initial condition that results in the maximum amplification of energy. The second is central to receptivity analysis. The external forcing may represent free-stream turbulence, wall roughness, body forces or even neglected nonlinear terms. Receptivity analysis focuses on the response to external forces, in terms of disturbance growth, resonance behaviour, and pattern selection. Nonnormal systems can have a large amplitude response to forcing, even though the forcing frequency is far from one of the eigenfrequencies of the system. This phenomenon is called *pseudoresonance*. In this work we focus on the study of the response to initial conditions.

Since bypass transition analysis is not based on eigenvalues, it can apply to stability operators that are explicitly time-dependent for which a normal mode form cannot be applied in the first place (Schmid [**74**]). In this case, the problem of determining the optimal energy growth condition is studied in a variational formulation and iterative optimisation techniques are employed.

Spatial evolution of disturbances can also be studied by writing the stability equations in the form of a spatial evolution problem, or

signalling problem. The spatial framework is preferable in problems where the disturbance is induced by a roughness element, a vibrating ribbon or harmonic point source or response to boundary layer to free-stream turbulence (Schmid [**74**]).

In this chapter, we focus on the temporal problem. The temporal evolution of disturbances is easier to study and will give an idea on how the non-zero normal stress differences in the second order models affect the transient growth.

2.2. Effects of nonnormal operators

We introduce a simple example in order to illustrate the effects of nonnormal operators (Schmid and Henningson [**77**], Schmid and Brandt [**76**]). Consider the following system of equations

$$\frac{d}{dt}\begin{bmatrix} v \\ \eta \end{bmatrix} = \begin{bmatrix} -\frac{1}{M} & 0 \\ \epsilon & -\frac{2}{M} \end{bmatrix}\begin{bmatrix} v \\ \eta \end{bmatrix},$$

where M are ϵ are positive constants. The matrix is nonnormal due to the presence of an element outside the diagonal, ϵ. This system of equations closely resembles the initial-value problem that drives the time evolution of perturbed wall-normal velocity and vorticity, governed by the Navier-Stokes equations. The equivalent system for second order fluids will be derived in Section 2.3.

The solution of the system with initial conditions $v(0) = v_0$ and $\eta(0) = \eta_0$ can be written as follows

$$\begin{bmatrix} v \\ \eta \end{bmatrix} = v_0 e^{-t/M}\begin{bmatrix} 1 \\ \epsilon M \end{bmatrix} + (\eta_0 - \epsilon M v_0)e^{-2t/M}\begin{bmatrix} 0 \\ 1 \end{bmatrix}.$$

The eigenvalues of the matrix that governs the system of equations are negative and this may suggest that the solutions v and η would decay exponentially. This is clearly true for v. However, the solution for η can be written as

$$\eta(t) = \eta_0 e^{-2t/M} + v_0 \epsilon M(e^{-t/M} - e^{-2t/M}).$$

The first term represents the initial condition η_0 which decays exponentially in time. The second term can be analysed for small times
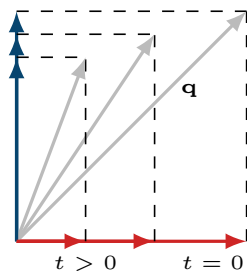
(a) Orthogonal
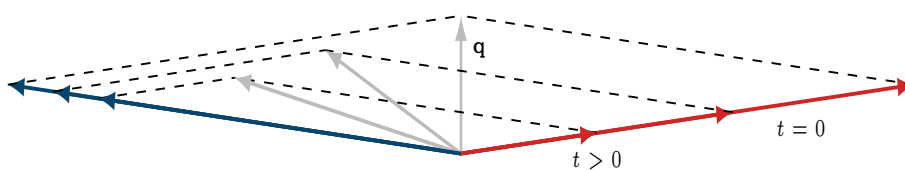
(b) Non-orthogonal

FIGURE 2.1. Illustration of transient growth due to decaying nonorthogonal eigenvectors.

$t/M \ll 1$ by expanding the exponentials in Taylor series as follows

$$v_0 \epsilon M (e^{-t/M} - e^{-2t/M}) = v_0 \epsilon t + O\left(\frac{t^2}{M}\right).$$

Therefore, the term that represents the response of η to the forcing due to v grows algebraically at early times proportionally to the parameter ϵ.

Figure 2.1 shows a geometric interpretation of the algebraic growth due to nonorthogonal eigenvectors that decay exponentially in time at different rates. An initial condition $\mathbf{q}$ represented in an orthogonal eigenvector basis, as in Figure 2.1a, will decay in time if the eigenvectors decay. If the initial condition $\mathbf{q}$ is a superposition of nonorthogonal eigenvectors, as in Figure 2.1b, as time passes it is subject to an increase in length before decaying in the large time limit. It is clear that eigenvalues alone cannot fully represent the dynamics of the solutions and a more complete study must involve eigenvectors.

2.3. Initial-value problem

In this section the initial-value problem that drives the development of disturbances is derived for the second order fluids. We follow, for example, the approach of Schmid and Henningson [**77**]. A formulation based on the initial-value problem enables us to study the behaviour of general solutions, not only of single eigenmodes.

We start with the unsteady three-dimensional motion (1.4) and continuity (1.5) equations and we proceed to linearise them about the parallel base flow $U_B = U_B(y)$. Then, we take the normal mode form for the perturbations, as follows

$$(u, v, w, p) = \big(\hat{u}(t, y), \hat{v}(t, y), \hat{w}(t, y), \hat{p}(t, y)\big)e^{i(\alpha x + \beta z)}, \qquad (2.1)$$

where α and β are, respectively, the streamwise (x-direction) and spanwise (z-direction) wavenumbers (see Figure 1.1). Unlike in Section 1.4, we do not assume an exponential time-dependence. Some algebraic manipulation, which can be found in Appendix A.4, leads to two coupled equations for the disturbance wall-normal velocity $\hat{v}$ and wall-normal vorticity $\hat{\eta} = i\beta\hat{u} - i\alpha\hat{w}$, that are

$$\big(k^2 - \mathcal{D}^2\big)\hat{v}_t + K_0\big(k^2 - \mathcal{D}^2\big)^2\hat{v}_t = -i\alpha U_B\big(k^2 - \mathcal{D}^2\big)\hat{v} \qquad (2.2a)$$

$$- i\alpha U_B''\hat{v} - \frac{1}{Re_0}\big(k^2 - \mathcal{D}^2\big)^2\hat{v} + K_0\Big[-i\alpha U_B\big(\mathcal{D}^2 - k^2\big)^2\hat{v}$$

$$+ i\alpha U_B^{iv}\hat{v} + i\beta k^2 U_B'\hat{\eta} + i\beta U_B'''\hat{\eta} - i\beta U_B'\mathcal{D}^2\hat{\eta}\Big],$$

$$\hat{\eta}_t + K_0\big(k^2 - \mathcal{D}^2\big)\hat{\eta}_t = -i\alpha U_B\hat{\eta} - i\beta U_B'\hat{v} \qquad (2.2b)$$

$$+ \frac{1}{Re_0}\big(\mathcal{D}^2 - k^2\big)\hat{\eta} + K_0\Big[i\alpha U_B\big(\mathcal{D}^2 - k^2\big)\hat{\eta} + i\beta U_B'''\hat{v}\Big],$$

where $k^2 = \alpha^2 + \beta^2$, the subscript t indicates the time-derivative and $\mathcal{D}$ indicates the derivative with respect to y. The mean flow velocity is denoted by U_B and is derived in Section 1.3. The Reynolds number, $Re_0 = U_e(x_0)\delta_0/\nu$, and the elasticity number, $K_0 = \frac{\alpha_1}{\rho\delta_0^2}$, are defined as in Chapter 1 by equations (1.12) and (1.14). The boundary conditions are

$$\hat{v} = \mathcal{D}\hat{v} = \hat{\eta} = 0 \qquad \text{at} \quad y = 0 \quad \text{and} \quad y \to \infty.$$

The horizontal velocities $\hat{u}$ and $\hat{w}$ can be recovered from $\hat{v}$ and $\hat{\eta}$ using the following relations

$$\hat{u} = \frac{i}{k^2} \left(\alpha \mathcal{D} \hat{v} - \beta \hat{\eta} \right), \qquad (2.3)$$

$$\hat{w} = \frac{i}{k^2} \left(\beta \mathcal{D} \hat{v} + \alpha \hat{\eta} \right). \qquad (2.4)$$

It is easy to see that in the Newtonian case, when $K_0 = 0$, equation (2.2a) involves only the wall-normal velocity $\hat{v}$ and can be solved given an initial condition. Squire's equation (2.2b) instead, is driven by solutions to the Orr-Sommerfeld equation through the forcing term $i\beta U'_B \hat{v}$. Therefore, in the Newtonian case, this term is responsible for an algebraic growth of energy and is referred to as the *vortex tilting* term.

Ellingsen and Palm [**27**] first identified this mechanism showing that the streamwise velocity grows linearly with time for a disturbance independent of the streamwise coordinate. Given any base flow in the x-direction, $U(y)$, the linearised momentum equation for the streamwise velocity component u, when there is no variation in the streamwise direction ($\partial/\partial x = 0$), becomes

$$\frac{\partial u}{\partial t} = -U'v.$$

The mean momentum is transported by the perturbation wall-normal velocity, v. The Rayleigh equation, which is equation (2.2a) in the inviscid Newtonian case ($\nu = 0, K_0 = 0$), implies that v is not a function of time when $\alpha = 0$. Therefore, the streamwise velocity increases linearly with time. This linear growth is known as *algebraic instability*.

The vortex tilting, otherwise known as *lift-up* effect, becomes more clear when considering the linearised vorticity equation, which is

$$\frac{\partial \eta}{\partial t} = -U' \frac{\partial v}{\partial z},$$

where $\eta = \frac{\partial w}{\partial x} - \frac{\partial u}{\partial z}$ is the vorticity in the y-direction. This means that the vorticity of the mean flow $-U'$, which is in the cross-stream

direction z, is tilted into the y-direction by the strain rate $\frac{\partial v}{\partial z}$ of the perturbation, generating an increase of y vorticity.

We observe that, for a non-zero non-Newtonian parameter K_0 and a non-zero spanwise wavenumber β, equation (2.2b) has an additional forcing term, $iK_0\beta U_B'''\hat{v}$. Equation (2.2a) is now related to the vorticity through some non-Newtonian terms, when disturbances are not spanwise-independent ($\beta \neq 0$). Therefore, the system we are considering now is fully coupled.

When considering the case of streamwise independent disturbances ($\alpha = 0$) in the inviscid case ($\nu = 0$), the vorticity equation (2.2b) reduces to

$$\hat{\eta}_t + K_0 \left(\beta^2 - \mathcal{D}^2\right) \hat{\eta}_t = -i\beta U_B'\hat{v} + K_0 i\beta U_B'''\hat{v}.$$

There is no immediate interpretation of this equation as in the Newtonian case, when $K_0 = 0$. We cannot conclude that the wall-normal vorticity, and consequently the streamwise velocity $\hat{u}$, experiences a linear growth because $\hat{v}$ is not necessarily time-independent.

Defining $\mathbf{q} = (\hat{v}, \hat{\eta})^T$, equations (2.2) can be written in a compact form as follows

$$\mathcal{M}\frac{\partial \mathbf{q}}{\partial t} = -i\mathcal{L}\mathbf{q} \qquad \text{or} \qquad \frac{\partial \mathbf{q}}{\partial t} = \mathcal{L}_1\mathbf{q}, \tag{2.5}$$

where $\mathcal{L}_1 = -i\mathcal{M}^{-1}\mathcal{L}$. The linear operators $\mathcal{M}$, $\mathcal{L}$ are defined in Section 1.7 by equations (1.28).

2.4. Optimal growth

In this section, we define the maximum possible amplification and other quantities useful to examine the tendency of the flow to transient growth.

2.4.1. Eigenfunction expansion. Seeking solutions of equation (2.5) of the form

$$\mathbf{q}(t, y) = \tilde{\mathbf{q}}(y)e^{-i\omega t},$$

where ω is the frequency, allows us to reduce the initial-value problem (2.5) to the following generalised eigenvalue problem

$$\omega \mathcal{M} \tilde{\mathbf{q}} = \mathcal{L} \tilde{\mathbf{q}}. \qquad (2.6)$$

This eigenvalue problem is entirely equivalent to the problem (1.27), introduced in Section 1.7, which governs three-dimensional disturbances.

General solutions of the initial-value problem (2.5) are assumed to belong to the space $\mathbb{S}^N$ spanned by a sufficient number N of eigenfunctions, that is defined as follows

$$\mathbb{S}^N = \mathrm{span}\{\tilde{\mathbf{q}}_1, \tilde{\mathbf{q}}_2, \ldots, \tilde{\mathbf{q}}_N\},$$

where $\{\tilde{\mathbf{q}}_j\}_j$ are solutions of (2.6). In other words, $\mathbf{q} \in \mathbb{S}^N$ can be expressed as

$$\mathbf{q} = \sum_{j=1}^N k_j(t) \tilde{\mathbf{q}}_j, \qquad (2.7)$$

where $\{k_j\}_j$ are the coefficients of the expansion.

This allows us to express the eigenvalue problem (2.5) as N separated ordinary differential equations for the expansion coefficients, as follows

$$k_j'(t) = -i\omega_j k_j(t), \qquad \text{for } j = 1, \ldots, N,$$

or in a more compact form, i.e.

$$\mathbf{k}'(t) = -i\Omega \mathbf{k}(t), \qquad (2.8)$$

where $\mathbf{k} = (k_1, \ldots, k_N)^T$ and $\Omega = \mathrm{diag}\{\omega_1, \ldots, \omega_N\}$. This simplified formulation (2.8) of the initial-value problem (2.5) is possible provided that the eigenspectrum is a complete set composed of discrete eigenmodes. For Newtonian fluids, it is known that if the domain is bounded then the eigenspectrum is discrete, but for unbounded boundary layers the spectrum is composed of a discrete and a continuous part.

Butler and Farrell [14] successfully employed a discretised approximation of the continuous spectrum. Although the discrete approximation differs from the exact representation, the sum of these eigenmodes correctly describes the solutions to the initial-value problem. An alternative method involves numerical integration in time of the direct and adjoint dynamic equations, as done by Corbett and Bottaro [16],

while studying configurations that excite an optimal growth of energy in Falkner-Skan boundary layers. This method does not involve any modal representation and it is computationally more complex without giving any advantage in terms of accuracy (Schmid and Henningson [**77**]).

For Newtonian fluids, the completeness of the spectrum is proven by Gustavsson [**36**] (see for example the review by Herron [**40**]). To the best of our knowledge, the completeness of the spectrum has not been proven yet for second order fluids or for non-Newtonian fluids in general. We will not research this further in this thesis.

In this thesis, we discretise the continuous spectrum for the second grade models, as done by Butler and Farrell [**14**]. Therefore, particular attention is required to ensure that the results are independent of the discretisation parameter. Numerical tests have been performed and will be explained in detail in Section 5.5.

2.4.2. Choice of perturbation energy. In order to determine the perturbation that grows the most in some sense, we need a way to quantify the growth. In general, for Newtonian fluids the perturbation energy density is used (Gustavsson [**37**]) and it is defined as follows

$$E_{\text{Newt}}(\mathbf{q}) = \frac{1}{k^2} \int_0^\infty \mathbf{q}^H \mathcal{M}_{\text{Newt}} \mathbf{q} \, dy \qquad (2.9)$$

$$= \frac{1}{k^2} \int_0^\infty \left(k^2 |\hat{v}|^2 + |\mathcal{D}\hat{v}|^2 + |\hat{\eta}|^2 \right) \, dy,$$

where $\mathbf{q}^H = (\hat{v}^*, \hat{\eta}^*)$ represents the conjugate transpose of $\mathbf{q}$ and $\mathcal{M}_{\text{Newt}}$ is the Newtonian part of the operator $\mathcal{M}$ defined by (1.28a), i.e.

$$\mathcal{M}_{\text{Newt}} = \begin{bmatrix} k^2 - \mathcal{D}^2 & 0 \\ 0 & 1 \end{bmatrix},$$

The energy E_{Newt} is proportional to the kinetic energy of the perturbation (Farrell and Butler [**14**]). The kinetic energy of a perturbation confined to a single wavenumber in the x and in the z directions is

$$E_{\text{K}} = \frac{\rho}{2} \int_0^\infty \int_0^a \int_0^b \left(\tilde{u}^2 + \tilde{v}^2 + \tilde{w}^2 \right) dx \, dz \, dy,$$

where $a = 2\pi/\alpha$ and $b = 2\pi/\beta$ are the wavelengths. The physical velocities $\tilde{u}$, $\tilde{v}$ and $\tilde{w}$ can be calculated by taking the real part of the

complex variables. For example, using the normal mode form (2.1), $\tilde{u}$ is given by

$$\tilde{u} = \Re\left(\hat{u}(t,y)e^{i(\alpha x + \beta z)}\right) = \frac{1}{2}\left[\hat{u}(t,y)e^{-i(\alpha x + \beta z)} + \bar{\hat{u}}(t,y)e^{i(\alpha x + \beta z)}\right],$$

where $\bar{\hat{u}}$ represents the complex conjugate of $\hat{u}$. Applying relations (2.3) and (2.4) to eliminate $\hat{u}$ and $\hat{w}$, the kinetic energy E_{K} becomes

$$E_{\mathrm{K}} = \frac{\rho ab}{4}\int_0^\infty \left(|\hat{v}|^2 + \frac{1}{k^2}\left(|\mathcal{D}\hat{v}|^2 + |\hat{\eta}|^2\right)\right)dy,$$

which is proportional to E_{Newt} defined by equation (2.9).

The most natural choice for the second order model is to take the full operator $\mathcal{M}$ that appears on the left hand side of the system of equations (2.5). Therefore, the energy norm is taken to be

$$E(\mathbf{q}) = \frac{1}{k^2}\int_0^\infty \mathbf{q}^H \mathcal{M}\mathbf{q}\,dy \tag{2.10}$$

$$= \frac{1}{k^2}\int_0^\infty \left(\hat{v}^*(k^2 - \mathcal{D}^2)\hat{v} + K_0\hat{v}^*(k^2 - \mathcal{D}^2)^2\hat{v}\right)dy$$

$$+ \frac{1}{k^2}\int_0^\infty \left(\hat{\eta}^*\hat{\eta} + K_0\hat{\eta}^*(k^2 - \mathcal{D}^2)\hat{\eta}\right)dy$$

$$= \frac{1}{k^2}\int_0^\infty \left(k^2|\hat{v}|^2 + |\mathcal{D}\hat{v}|^2 + |\hat{\eta}|^2\right)dy$$

$$+ \frac{K_0}{k^2}\int_0^\infty \left(|\mathcal{D}^2\hat{v}|^2 + k^2|\hat{\eta}|^2 + |\mathcal{D}\hat{\eta}|^2 + k^4|\hat{v}|^2 + 2k^2|\mathcal{D}\hat{v}|^2\right)dy.$$

This energy norm does not have an immediate physical interpretation as the kinetic energy norm. It will be seen later that the two choices produce qualitatively the same results.

2.4.3. Inner product and energy norm. The scalar product between two functions $\mathbf{q}_1, \mathbf{q}_2 \in \mathbb{S}^N$ is defined as

$$(\mathbf{q}_1, \mathbf{q}_2)_E = \frac{1}{k^2}\int_0^\infty \mathbf{q}_2^H \mathcal{M}\mathbf{q}_1\,dy = \mathbf{k}_2^H M\mathbf{k}_1,$$

where $M \in \mathbb{C}^{N\times N}$ is the matrix whose components are defined by

$$M_{ij} = (\mathbf{q}_j, \mathbf{q}_i)_E = \frac{1}{k^2}\int_0^\infty \mathbf{q}_i^H \mathcal{M}\mathbf{q}_j\,dy.$$

Since the matrix M is Hermitian $(M = M^H)$ and positive definite, it can be factorised such that $M = F^H F$. Thus, the inner product satisfies

$$
\begin{aligned}
(\mathbf{q}_1, \mathbf{q}_2)_E &= \mathbf{k}_2^H M \mathbf{k}_1 \\
&= \mathbf{k}_2^H F^H F \mathbf{k}_1 \\
&= (F \mathbf{k}_1, F \mathbf{k}_2)_2 \\
&= (\mathbf{k}_1, \mathbf{k}_2)_E,
\end{aligned}
$$

where $(\cdot, \cdot)_2$ is the usual l^2-norm defined as follows

$$
(u, v)_2 = u^H v.
$$

Therefore, the associated norm satisfies

$$
\|\mathbf{q}\|_E = \|F \mathbf{k}\|_2 = \|\mathbf{k}\|_E \qquad \text{for} \quad \mathbf{q} \in \mathbb{S}^N.
$$

For practical purposes the factorisation of M can be performed by calculating a singular value decomposition (SVD) as follows

$$
M = U S V^H,
$$

where S is a diagonal matrix with real entries and $U = V$ because M is Hermitian. Therefore, we can easily calculate the matrix F and its inverse as

$$
F = S^{1/2} U^H, \qquad F^{-1} = U S^{-1/2}.
$$

For a matrix $B \in \mathbb{C}^{N \times N}$, the energy norm is defined as follows

$$
\begin{aligned}
\|B\|_E &= \max_{\mathbf{k} \in \mathbb{C}^N \smallsetminus \{0\}} \frac{\|B \mathbf{k}\|_E}{\|\mathbf{k}\|_E} \\
&= \max_{\mathbf{k} \in \mathbb{C}^N \smallsetminus \{0\}} \frac{\|F B \mathbf{k}\|_2}{\|F \mathbf{k}\|_2} \\
&= \max_{\mathbf{k} \in \mathbb{C}^N \smallsetminus \{0\}} \frac{\|F B F^{-1} F \mathbf{k}\|_2}{\|F \mathbf{k}\|_2} \\
&= \|F B F^{-1}\|_2.
\end{aligned}
$$

2.4.4. Maximum possible amplification. In order to quantify the transient growth, we define the *maximum possible amplification* of

initial energy density, as follows

$$G(t, \alpha, \beta) = \max_{\mathbf{q}_0 \in S^N \smallsetminus \{0\}} \frac{\|\mathbf{q}(t)\|_E^2}{\|\mathbf{q}_0\|_E^2} = \|e^{\mathcal{L}_1 t}\|_E^2, \qquad (2.11)$$

where $\mathcal{L}_1$ is the linear operator given by (2.5). Fixing the wavenumber vector (α, β), the function G represents the envelope of the energy evolution of all the initial perturbations, $\mathbf{q}_0$, with unit energy norm. At each moment in time, we maximise over all possible initial conditions.

In order to compute the exponential norm (2.11), we use the decomposition (2.7) and the identities proved in Section 2.4.3. Thus, G becomes

$$\begin{aligned}
G(t, \alpha, \beta) &= \max_{\mathbf{k}_0 \in \mathbb{C}^N \smallsetminus \{0\}} \frac{\|\mathbf{k}(t)\|_E^2}{\|\mathbf{k}_0\|_E^2} \\
&= \|e^{-i\Omega t}\|_E^2 \\
&= \|F e^{-i\Omega t} F^{-1}\|_2^2 \\
&= \sigma_1^2 \left(F e^{-i\Omega t} F^{-1} \right),
\end{aligned}$$

where σ_1 is the principal singular value of the matrix $B = F e^{-i\Omega t} F^{-1}$. Employing the decomposition (2.7) provides an easy way to compute the maximum possible amplification G, which can be obtained by calculating the SVD of the matrix B.

Notice that, traditional stability analysis focuses attention only on the eigenvalues of $e^{-i\Omega t}$. These do not capture the whole behaviour of G, which is determined also by the eigenvector matrix F and its inverse. Deducing the behaviour of G from the eigenvalue matrix Ω alone is only valid when the similarity transformation given by F does not alter the norm, that is when V is unitary and composed by orthogonal eigenvectors. This is the case when B is normal. If this is not the case, B is nonnormal and short-time growth of perturbation energy is possible even though the matrix has stable eigenvalues. For large times, the energy amplification is governed by the least stable eigenvalue. Therefore, we expect the behaviour of G as $t \to \infty$ to be in accordance with the results of the eigenvalue stability analysis.

We define the *global optimal disturbance* as the initial condition, $\mathbf{q}_0$, that maximises the growth over time, i.e.

$$G_{\max}(\alpha, \beta) = G(t_{\max}, \alpha, \beta) = \max_{t \in [0, \infty)} G(t, \alpha, \beta). \qquad (2.12)$$

Notice that $G_{\max}$ can only be defined when all the eigenvalues are stable. If an unstable mode exists, then $G(t) \to \infty$ as $t \to \infty$.

We can also define the *largest global growth* obtained for any wavenumber vector as follows

$$G_{\Gamma} = G_{\max}(\alpha_{\Gamma}, \beta_{\Gamma}) = \max_{\alpha, \beta} G_{\max}(\alpha, \beta). \qquad (2.13)$$

The latter depends only on the base flow conditions and Reynolds number Re.

2.4.5. Results. The results obtained have been validated by comparing with those found in the literature for Newtonian fluids. For this purpose, we refer to the book by Schmid and Henningson [77] and the work by Corbett and Bottaro [16].

Figure 2.2 shows the maximum possible amplification of initial energy norm defined by (2.11) for fixed values of the wavenumbers ($\alpha = 0.2, \beta = 0.4$) and a Reynolds number $Re_0 = 1000$. This choice of parameters has been made to demonstrate the qualitative effect of the non-Newtonian terms in the second order model on the maximum possible amplification, G. For the Newtonian case, a two-dimensional exponentially unstable mode exists for $Re_0 \approx 520$ and $\alpha \approx 0.3$ as reported in Table 1.1. However, for $\alpha = 0.2, \beta = 0.4$ and $Re_0 = 1000$, the flow is exponentially stable for all the non-Newtonian parameters considered in Figure 2.2 and therefore, G decays as $t \to \infty$.

We compare the results obtained with the two choices of energy norm discussed in Section 2.4.2. In Figure 2.2(a), we use the energy norm defined by (2.10), while in Figure 2.2(b) we use the kinetic energy density defined by (2.9). We can see that qualitatively the results are the same and the two norms can be distinguished only when the non-Newtonian parameter K differs substantially from zero. It can be seen that for the second grade model ($K > 0$) an increase of the
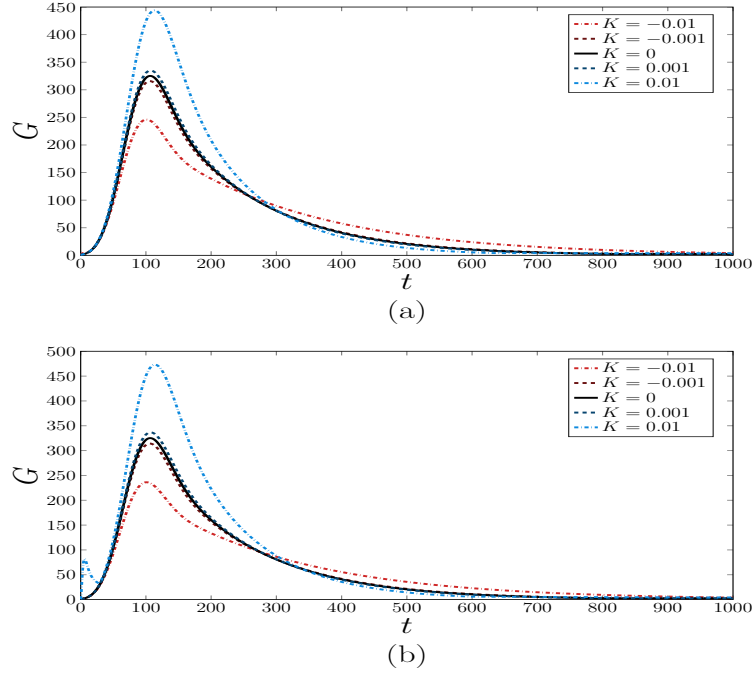
FIGURE 2.2. Maximum possible amplification G for the flat plate $\beta_H = 0$ and $Re_0 = 1000, \alpha = 0.2, \beta = 0.4$. (a) total energy; (b) kinetic energy.
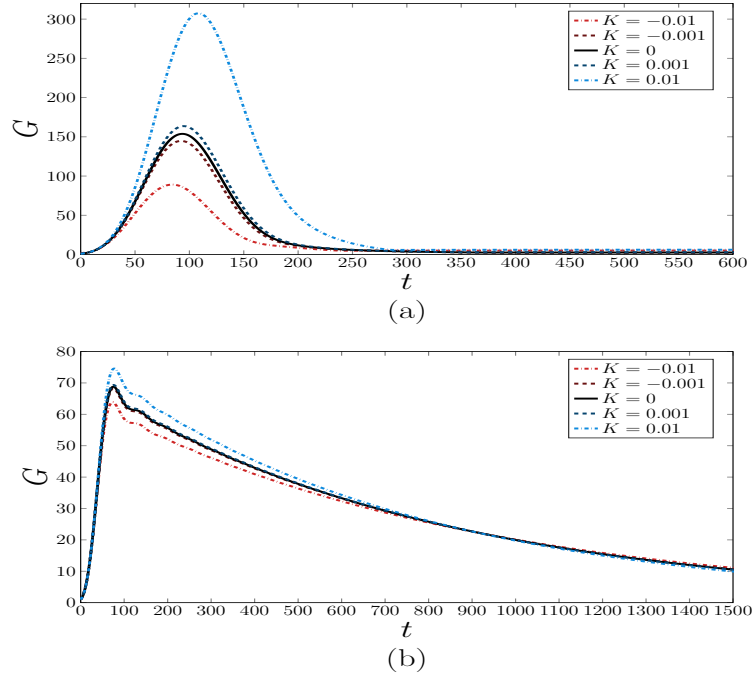
FIGURE 2.3. Maximum possible amplification G for $\alpha = 0.2, \beta = 0.4$. (a) $Re_0 = 1000, \beta_H = 0.5$ (flow past a corner); (b) $Re_0 = 300, \beta_H = -0.14$ (flow past a wedge).

non-Newtonian parameter K provokes an increase of the maximum transient growth while the second order model $(K < 0)$ has the opposite behaviour.

Figures 2.3(a) and 2.3(b) show the maximum possible amplification of initial energy norm for flow past a corner $(\beta_H = 0.5)$ and past a wedge $(\beta_H = -0.14)$, respectively. This choice of parameters gives exponentially stable flows for all the non-Newtonian parameters considered. The non-Newtonian terms have the same effects as for the flat plate.

Figure 2.4 shows the contour plot of $G_{\max}$ defined by (2.12) for the flat plate $(\beta_H = 0)$. The black line represents the neutral stability curve inside which an exponentially growing mode exists and where the maximum possible amplification is not defined or can be thought of as infinite. The Newtonian results in Figure 2.4(a) are in agreement with the literature (Schmid and Henningson [77], Schmid [74]). The largest global optimal growth defined by (2.13) is $G_\Gamma = 1515.6$ reached at time $t = 782$ for $\alpha_\Gamma = 0$, $\beta_\Gamma = 0.65$, as calculated by Corbett and Bottaro [16].

Figures 2.4(b),(c) show the contour plot for the second order models with $K = 10^{-4}$ and $K = -10^{-4}$ respectively. These non-Newtonian parameters have been chosen as an example to show the non-Newtonian effects. We can see that the largest amplification of energy is still reached for streamwise independent disturbances, as in the Newtonian case. However, when $K > 0$, the amplification of energy is generally larger and, when $K < 0$, the amplification of energy is smaller than in the Newtonian case.

Figure 2.5 shows the contour plot of $G_{\max}$ for the flow past a wedge $(\beta_H = 0.5)$. The non-Newtonian effects on the transient growth are qualitatively similar to the flat plate case.

Figure 2.6(a) displays the ratio of non-Newtonian $G_{\max}$ to Newtonian $G_{\max}$ for a fixed spanwise wavenumber $\beta = 0.6$ and varying Weissenberg number Wi_0. We can observe the non-Newtonian terms mostly affect streamwise independent disturbances, i.e. for $\alpha = 0$. In Figure 2.6(b) we can see that for $K > 0$ the global optima happen for larger times
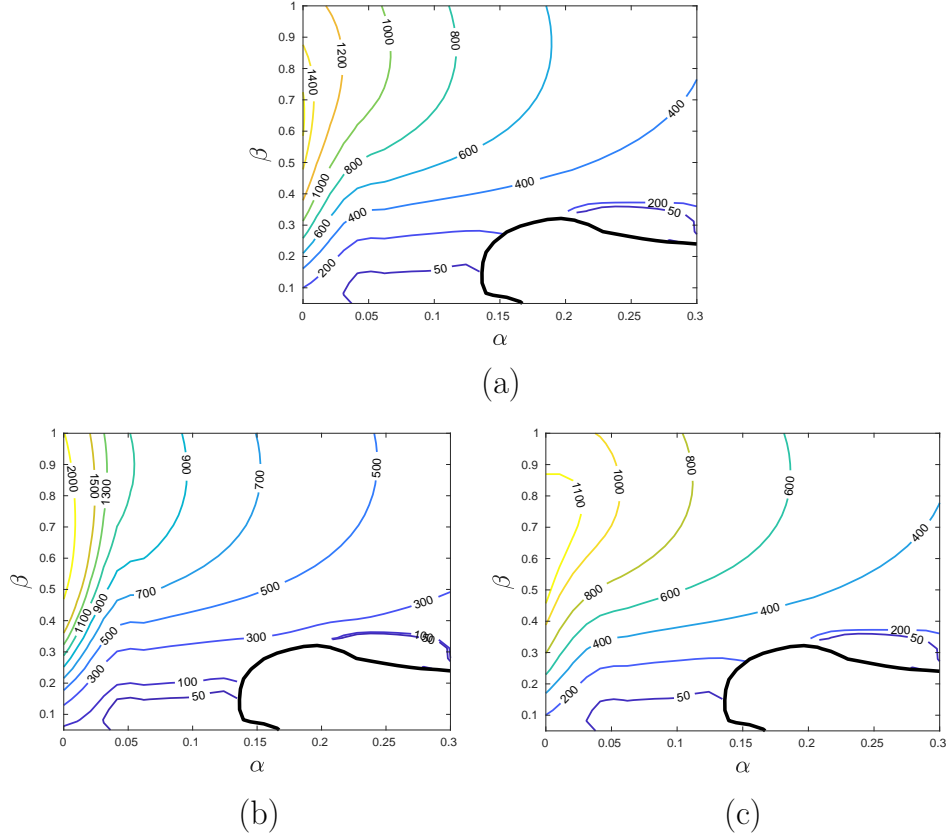
FIGURE 2.4. Contour plot of $G_{\max}$ for $\beta_H = 0$ (flat plate) and $Re_0 = 1000$. The black line indicates where an exponentially unstable mode exists. (a) $K = 0$; (b) $K = 10^{-4}$; (c) $K = -10^{-4}$.

than in the Newtonian case, while for $K < 0$ the global optima happen for shorter times.

This result is confirmed by looking at Figure 2.7, where we plot the quantity

$$\tilde{G}_{\max}(\alpha) = G_{\max}(\alpha, \tilde{\beta}) = \max_{\beta} G_{\max}(\alpha, \beta), \tag{2.14}$$

that represents $G_{\max}$ defined by (2.12) maximised over β.

Figure 2.7(a) shows that the change in maximum transient growth due to non-Newtonian effects happens at small streamwise wavenumbers α. A small non-Newtonian parameter $K = 0.0001$ has a dramatic impact on the largest global optima $G_\Gamma = \tilde{G}_{\max}(0)$, which increases from $G_\Gamma = 1515.6$ in the Newtonian case to $G_\Gamma = 2402.3$. Moreover, the
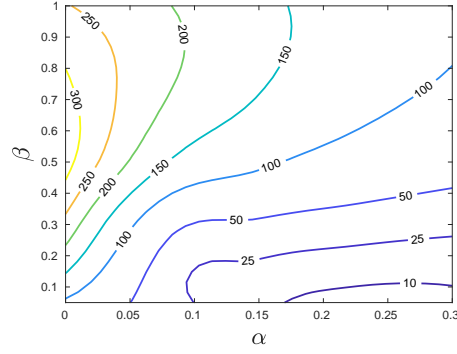
(a)
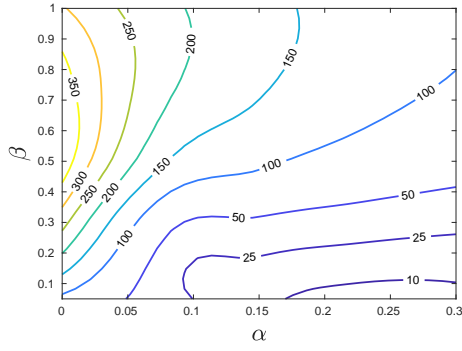
(b)
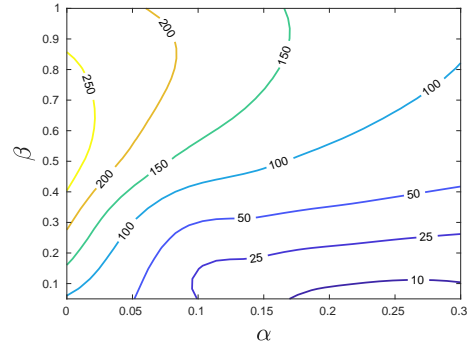
(c)

FIGURE 2.5. Contour plot of $G_{\max}$ for $\beta_H = 0.5$ and $Re_0 = 500$. (a) $K = 0$; (b) $K = 10^{-4}$; (c) $K = -10^{-4}$.
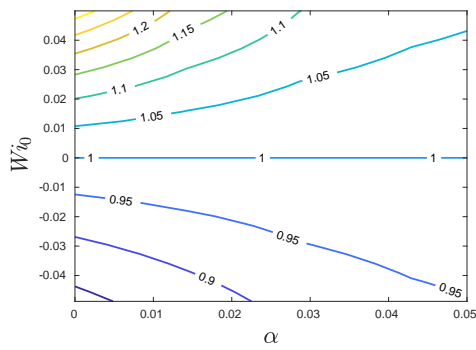
(a)
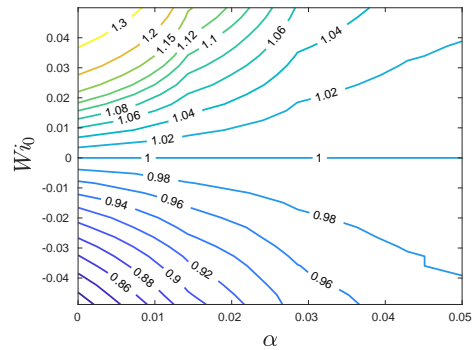
(b)

FIGURE 2.6. Ratio of non-Newtonian to Newtonian maximum possible amplification for the flat plate $\beta_H = 0$ and $Re_0 = 500, \beta = 0.6$. (a) $G_{\max}/G_{\max,\text{Newt}}$; (b) $t_{\max}/t_{\max,\text{Newt}}$.
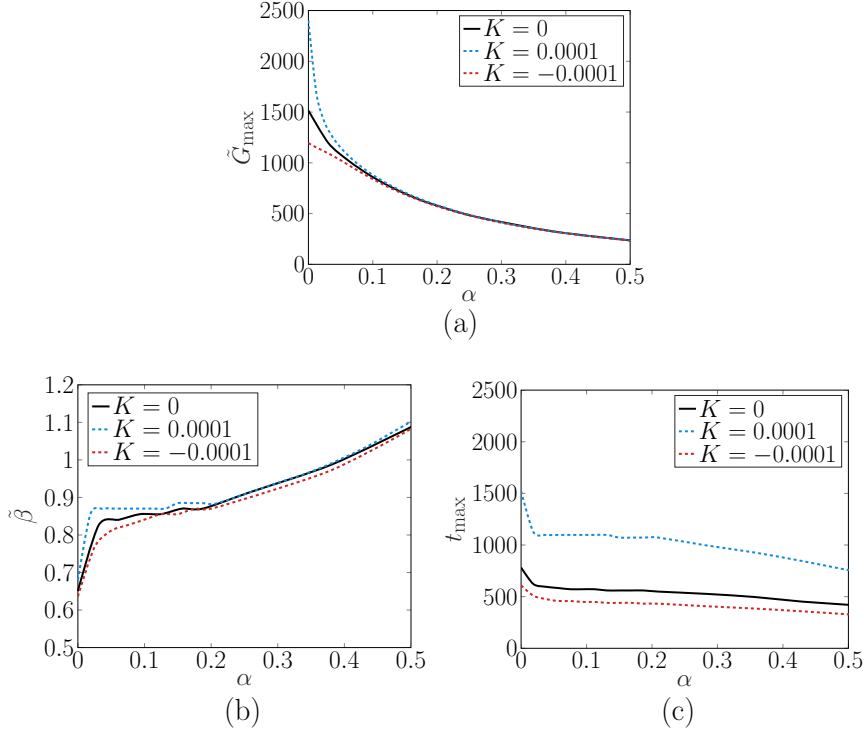
FIGURE 2.7. Maximum transient growth versus the streamwise wavenumber α for $\beta_H = 0$ (flat plate) and $Re_0 = 1000$. (a) $\tilde{G}_{max}$ defined by (2.14); (b) $\tilde{\beta}$ spanwise wavenumber at which the maximum, $\tilde{G}_{max}$, is reached; (c) t_{max} time at which the maximum is reached.

maximum is reached later in time (see Figure 2.7(c)), i.e. t_{max} increases from the Newtonian $t_{max} = 782$ to $t_{max} = 1522$ and for shorter waves (see Figure 2.7(b)), i.e. β_Γ increases from the Newtonian $\beta_\Gamma = 0.65$ to $\beta_\Gamma = 0.68$. A negative $K = -0.0001$ produces the opposite effects. The largest global optima is $G_\Gamma = 1193.7$ and it is reached for a shorter time $t_{max} = 609$ and longer waves with $\beta_\Gamma = 0.64$, when compared to the Newtonian case.

Figure 2.8 shows the results for the flow past a wedge with $\beta_H = 0.5$ and a Reynolds number $Re_0 = 500$. We can see that the results are qualitatively similar to the flat plate case and do not need further comment.

In Table 2.1 we report the largest global optima G_Γ defined in (2.13). For these calculations, we choose the momentum thickness scaling,
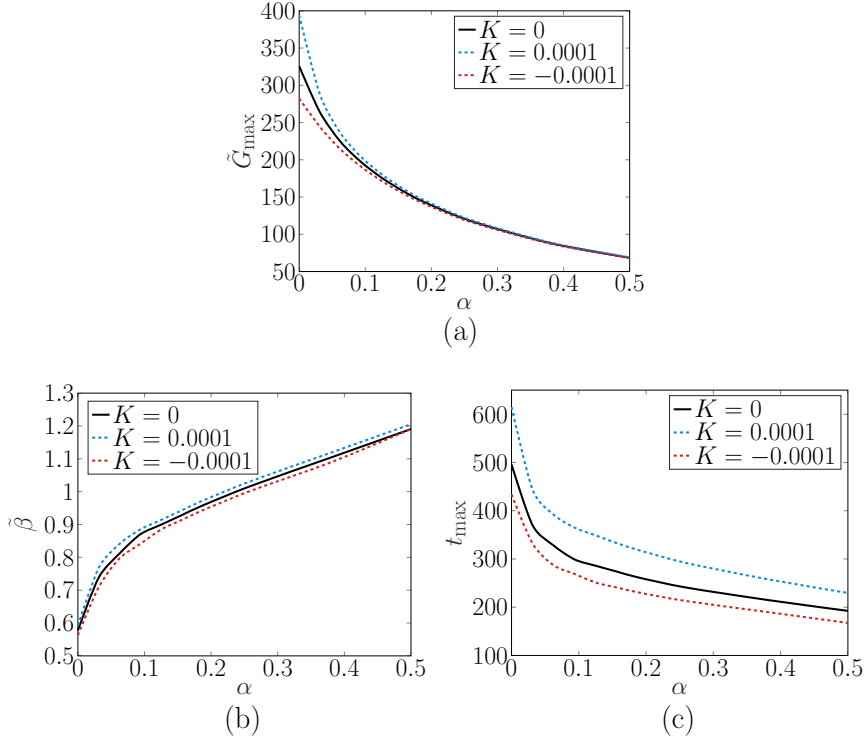
FIGURE 2.8. Maximum transient growth versus the streamwise wavenumber α for $\beta_H = 0.5$ (flow past a wedge) and $Re_0 = 500$. (a) $\tilde{G}_{\max}$ defined by (2.14); (b) $\tilde{\beta}$ spanwise wavenumber; (c) $t_{\max}$ time at which the maximum is reached.

following Corbett and Bottaro [16]. The reason is that, when scaled using the momentum thickness, the spanwise wavenumber at which the largest global optima is reached is independent of the mean flow conditions. Moreover, momentum thickness scaling accounts for the variation in t_Γ (the time in which the optimal disturbance reaches its maximum) resulting from differences in the base flow.

The momentum thickness is defined by equation (1.18). We choose to scale the lengths with the momentum thickness θ_0 relative to the fixed streamwise location x_0 which is defined as follows

$$\theta_0 = \theta_{\text{Newt},1}\delta(x_0),$$

where δ is defined by equation (1.16) and $\theta_{\text{Newt},1}$ is the constant

$$\theta_{\text{Newt},1} = \int_0^\infty \left(f'_{\text{Newt}} \left(1 - f'_{\text{Newt}} \right) \right) d\eta,$$

calculated in the Newtonian case. We introduce Reynolds and Weissenberg numbers based on θ_0, as follows

$$Re_\theta = \frac{U_e(x_0)\theta_0}{\nu}, \quad Wi_\theta = \frac{\alpha_1 U_e(x_0)}{\mu\theta_0}.$$

Notice that the following relations hold

$$Re_0 = H Re_\theta, \quad Wi_0 = \frac{Wi_\theta}{H},$$

where $H = C/\theta_{\mathrm{Newt},1}$ is the shape factor defined as the ratio between displacement and momentum thickness, calculated in the Newtonian case. For the flat plate case, $H \approx 2.59$ as we can see from Figure 1.5 in Section 1.3.

In Table 2.1, we represent the results obtained for Reynolds numbers $Re_\theta = 166$ and $Re_\theta = 385$. These Reynolds numbers have been chosen to compare the results with the ones obtained by Corbett and Bottaro [16]. Specifically, $Re_\theta = 385$ corresponds to the Reynolds number based on the displacement thickness $Re_0 \approx 1000$ for the flat plate case.

For all the flows considered, the largest global optimum is reached for streamwise-independent waves, i.e. $\alpha_\Gamma = 0$. We can see that, in the Newtonian case, when scaled with θ_0, the spanwise wavenumber for G_Γ appears to be independent of the mean flow condition characterised by β_H and $\beta_\theta \approx 1/4$. Notice that, in the Newtonian case, the moment in time at which the largest global optimum is reached is about the same for all the positive angle parameters considered, $t_\theta \approx 880$.

For flow past a corner ($\beta_H = -0.14$), the maximum is reached at a larger time $t_\theta \approx 927$. We observe how, for all the angle parameters considered the spanwise wavenumber β_θ, the time t_θ and the largest possible amplification G_Γ decreases when the second order model is selected, with $Wi_\theta < 0$, and decreases when the second grade model is selected, with $Wi_\theta > 0$. Moreover, β_θ appears to change approximately linearly with the Weissenberg number based on the momentum thickness. A Weissenberg number $Wi_0 = \pm 0.05$ produces a change in β_θ of about 1% and $Wi_0 = \pm 0.1$ produces a change of about 2%. This linear dependence on the Weissenberg number manifests also on the time t_θ and on the largest transient growth G_Γ.

		$Re_\theta = 166$			$Re_\theta = 385$		
β_H	Wi_θ	β_θ	t_θ	G_Γ	β_θ	t_θ	G_Γ
	-0.10	0.2390	802.03	357.49*	0.2347	1629.56	1674.25*
	-0.05	0.2410	856.30	380.72*	0.2386	1827.99	1888.35*
-0.14	0	0.2432	926.30	408.82*	0.2432	2151.88	2202.45*
	0.05	0.2457	1021.51	444.12*	0.2494	2856.03	2749.60*
	0.10	0.2485	1165.67	491.16*	-	-	-
	-0.10	0.2452	768.81	283.86*	0.2414	1562.67	1332.59*
	-0.05	0.2470	819.99	301.87*	0.2448	1750.79	1498.67*
-0.07	0	0.2489	885.33	323.59*	0.2489	2057.06	1742.94*
	0.05	0.2510	973.27	350.59*	0.2542	2693.02	2157.79*
	0.10	0.2533	1100.95	385.74*	-	-	-
	-0.10	0.2475	758.86	247.29	0.2438	1544.18	1162.12*
	-0.05	0.2491	808.67	262.74	0.2470	1730.97	1307.12*
0	0	0.2508	872.23	281.42	0.2509	2026.73	1515.60*
	0.05	0.2528	956.55	304.52	0.2557	2617.47	1862.12*
	0.10	0.2550	1075.89	334.05	0.2649	5467.14	2771.06*
	-0.10	0.2479	765.91	168.13	0.2446	1568.41	792.59
	-0.05	0.2495	812.86	178.30	0.2476	1750.22	889.17
0.5	0	0.2512	871.08	190.36	0.2513	2024.78	1024.65
	0.05	0.2531	945.42	204.99	0.2561	2520.51	1238.61
	0.10	0.2552	1045.30	223.25	0.2650	3948.30	1688.11
	-0.10	0.2471	774.23	147.29	0.2436	1590.90	694.91
	-0.05	0.2487	820.22	156.10	0.2467	1769.96	778.84
1	0	0.2504	876.65	166.49	0.2505	2037.67	895.93
	0.05	0.2524	947.52	179.00	0.2556	2504.65	1078.00
	0.10	0.2547	1041.05	194.51	0.2651	3701.44	1440.19
	-0.10	0.2469	775.71	142.60	0.2434	1594.62	672.67
	-0.05	0.2485	821.55	151.13	0.2465	1773.57	753.97
1.2	0	0.2503	877.53	161.17	0.2504	2040.22	867.26
	0.05	0.2523	947.83	173.25	0.2556	2501.90	1043.04
	0.10	0.2547	1039.94	188.21	0.2654	3662.17	1390.06

TABLE 2.1. Largest global optima for $Re_\theta = 166$ and $Re_\theta = 385$. The asterisk (*) indicates where an exponentially unstable mode exists and G_Γ is calculated excluding the TS wave. The missing values indicate where an exponential unstable mode exists also as $\beta \to 0$.

2.5. Optimal disturbances

We can determine the initial condition that reaches the maximum possible amplification at a given time t_0 by using the singular value decomposition (SVD) of the matrix $B = F e^{-i t_0 \Omega} F^{-1}$. The initial condition that reaches the global optima $G_{\max}$ at $t = t_{\max}$ defined by (2.12) is referred to as *optimal disturbance.*

Using identities proven in Section 2.4.3, the maximum possible amplification G at a certain time $t = t_0$ can be written as follows

$$G(t_0, \alpha, \beta) = \max_{\|F \mathbf{k}_0\|_2 = 1} \|F \mathbf{k}(t_0)\|_2^2 = \sigma_1^2(B).$$

We define $\mathbf{k}_{0,\max}$ as the vector of coefficients of the initial perturbation with unitary energy norm that reaches the maximum at t_0. We define $\mathbf{k}_{\max} = e^{-i t_0 \Omega} \mathbf{k}_{0,\max}$ as the vector of coefficients at the time t_0. Then, we can write

$$\begin{aligned} G(t_0, \alpha, \beta) &= (F \mathbf{k}_{\max}, F \mathbf{k}_{\max})_2 \\ &= (F \mathbf{k}_{\max})^H F e^{-i t_0 \Omega} \mathbf{k}_{0,\max} \\ &= (F \mathbf{k}_{\max})^H F e^{-i t_0 \Omega} F^{-1} F \mathbf{k}_{0,\max} \\ &= (F \mathbf{k}_{\max})^H B F \mathbf{k}_{0,\max}. \end{aligned}$$

Therefore, defining

$$v_1 = F \mathbf{k}_{0,\max},$$
$$u_1 = F \mathbf{k}_{\max} / \|F \mathbf{k}_{\max}\|_2,$$

and remembering that

$$\|F \mathbf{k}_{\max}\|_2 = \|F e^{-i t_0 \Omega} F^{-1} F k_{0,\max}\|_2 = \|F e^{-i t_0 \Omega} F^{-1}\|_2 = \sigma_1(B),$$

we obtain the following equation

$$B v_1 = \sigma_1 u_1. \tag{2.15}$$

Equation (2.15) can be interpreted as the singular value decomposition (SVD) of the matrix B, where σ_1 is the largest singular value, v_1 and u_1 are the principal right and left singular vectors, respectively, corresponding to σ_1. The vector v_1 represents the input of the system

from which we can easily compute the initial perturbation $\mathbf{q}_0$ using the eigenmode decomposition (2.7) and u_1 represents the output from which we can compute $\mathbf{q}(t_0)$, as follows

$$\mathbf{q}_0 = \sum_{j=1}^{N} (k_{0,\max})_j \, \tilde{\mathbf{q}}_j, \qquad \mathbf{k}_{0,\max} = F^{-1} v_1,$$

$$\mathbf{q}(t_0) = \sum_{j=1}^{N} (k_{\max})_j \, \tilde{\mathbf{q}}_j, \qquad \mathbf{k}_{\max} = F^{-1} u_1.$$

In order to solve this problem we calculate the SVD of the matrix B, that is

$$BV = \Sigma U,$$

where $\Sigma = \operatorname{diag}\{\sigma_1, \ldots, \sigma_N\}$ is the diagonal matrix consisting of the singular values of B in descending order, V and U are unitary matrices.

2.5.1. Results. Figure 2.9 shows a comparison between optimal disturbances in the Newtonian and non-Newtonian cases for the stagnation point flow ($\beta_H = 1$) and a Reynolds number $Re_0 = 500$. We choose a wavenumber vector $(\alpha, \beta) = (0, 0.6)$ which is close to the global optima. In Figures 2.9(a),(c), $\mathbf{u}$ has been scaled such that $\max(v_{0,\text{Newt}}) = 1$ and in Figures 2.9(b),(d), $\mathbf{u}$ has been scaled such that $\max(v_{\max,\text{Newt}}) = 1$.

We see that the optimal disturbances, in the non-Newtonian cases, have the same structure of streamwise-oriented vortices as in the Newtonian case. From Figures 2.9(a),(c), we observe that the initial streamwise velocity u_0 is always two orders of magnitude less than the cross-flow components. Figures 2.9(b),(d) show the evolved state of the optimal disturbances at $t = t_{\max}$. The shape of the initial vortex is still present although it has diffused outwards away from the wall.

At $t = t_{\max}$, the streamwise velocity $u_{\max}$ is one order of magnitude larger than the cross-flow velocities, which indicates the presence of streaks. From Figures 2.9(a),(b) we see that, when $K > 0$ the vortices are more diffused away from the wall, whereas, when $K < 0$ the vortices are closer to the wall. Figures 2.9(c),(d) shows that, for the non-Newtonian fluid with $K = -0.0001$, the initial optimal streamwise velocity is larger than in the Newtonian case and at $t_{\max}$ it grows
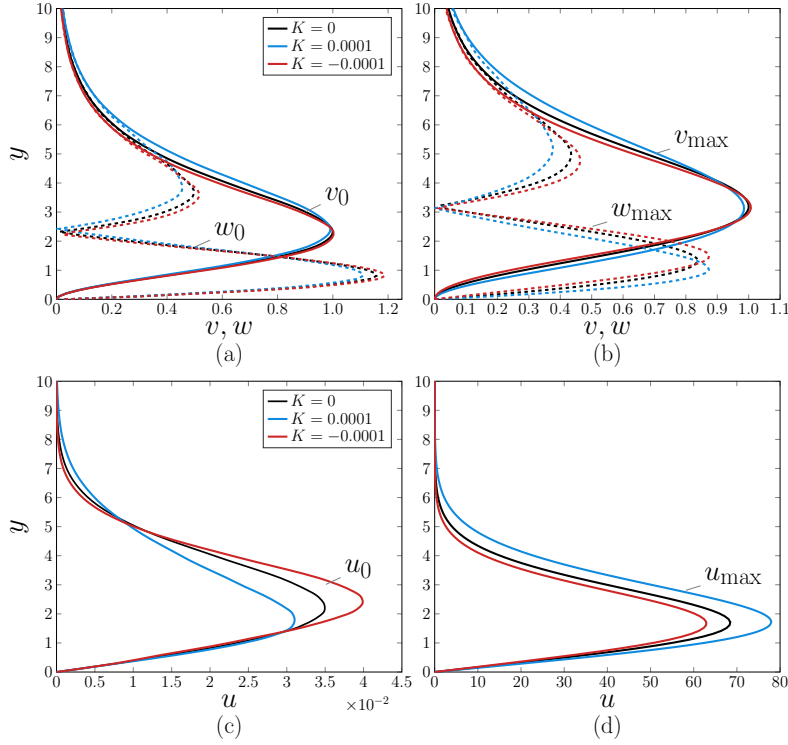
FIGURE 2.9. Comparison between Newtonian and non-Newtonian optimal disturbances for the stagnation point flow with $\beta_H = 1, Re_0 = 1000, \alpha = 0.6, \beta = 0$. (a) wall-normal, v_0, and spanwise, w_0, initial velocities; (b) wall-normal, v_{max}, and spanwise, w_{max}, velocities at $t = t_{max}$; (c) streamwise, u_0, initial velocities; (d) streamwise, u_{max}, streamwise velocity at $t = t_{max}$.

more than in the Newtonian case. The behaviour is the opposite when $K = 0.0001$. This is in agreement the results obtained in the previous sections.

In Figure 2.10 we plotted the streamwise vortices for the second order fluid with $K = -0.0001$ and $Re_0 = 1000$. The solutions plotted are such that $\|\mathbf{q}_0\|_E = 1$ and $\|\mathbf{q}(t_{max})\|_E = G_{max}$. In Figures 2.10(a) and (c) we can see the streamwise vortices at $t = 0$ and at $t = t_{max}$, respectively. From Figures 2.10(b) and (d), we can see the lift-up effect in action, which transforms streamwise vortices into streamwise streaks.
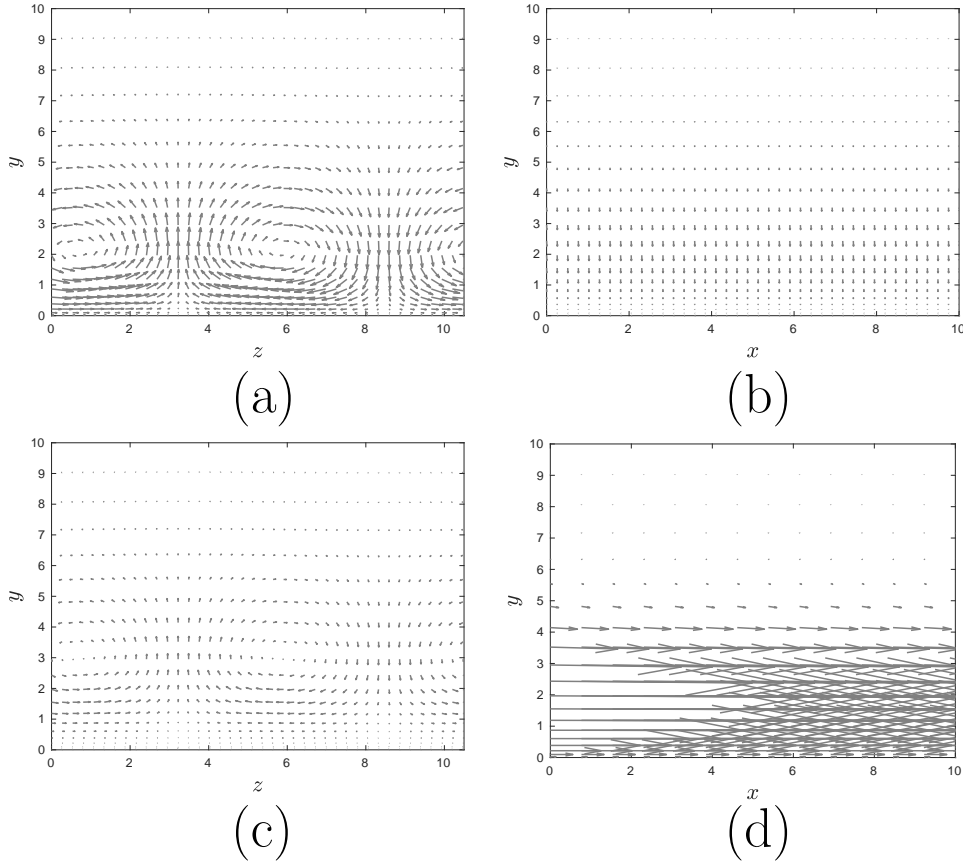
FIGURE 2.10. Optimal disturbance for the stagnation point flow with $\beta_H = 1, Re_0 = 500, \alpha = 0.6, \beta = 0$ and a non-Newtonian parameter $K = -0.0001$. (a),(b) disturbance at $t = 0$; (c),(d) disturbance at $t = t_{\max}$.

2.6. Pseudospectra, numerical range and applications to energy growth

Another way to study nonnormal operators is through their pseudospectra and numerical range (Trefethen and Embree [89]). In many applications, not only in hydrodynamic stability, eigenvalue analysis proves to be misleading. In many physical situations, dominated by non-normal systems, eigenvalues do not describe correctly the whole dynamics.

2.6.1. Pseudospectra. Pseudospectra are mathematical tools, introduced by Trefethen [85], which extend the definition of eigenvalues.

For the sake of brevity, we present only the definition for matrices. However, it can be extended to linear operators in Banach spaces (Trefethen and Embree [**89**]).

Let A denote a matrix in $\mathbb{C}^{N \times N}$. An eigenvalue $z \in \mathbb{C}$ and an eigenvector $\mathbf{v} \in \mathbb{C}^N$ satisfy

$$A\mathbf{v} = z\mathbf{v}.$$

Therefore, an equivalent condition for z to be an eigenvalue is to require $z\mathbb{I} - A$ to be a singular matrix. Pseudoeigenvalues are defined such that, for an appropriate choice of norm $\| \cdot \|$,

$$\|(z\mathbb{I} - A)^{-1}\|$$

is arbitrarily large. The matrix $R(z) = (z\mathbb{I} - A)^{-1}$ is known as the *resolvent* of A at z.

More precisely, the ϵ-*pseudospectra* of A are regions of the complex plane defined for each $\epsilon \geq 0$, as follows

$$\Lambda_\epsilon(A) = \{z \in \mathbb{C} : \|(z\mathbb{I} - A)^{-1}\| \geq \epsilon^{-1}\}.$$

When z is an eigenvalue of A, the resolvent $R(z)$ is not defined and $\|(z\mathbb{I} - A)^{-1}\|$ is thought of as infinite, by convention. Therefore, the ϵ-pseudospectra are closed nested sets containing $\Lambda(A) = \Lambda_0(A)$, which is the spectrum of A.

Restricting our attention to the case in which $\| \cdot \| = \| \cdot \|_2$, if A is normal, then

$$\|R(z)\|_2 = \|(z\mathbb{I} - A)^{-1}\|_2 = \frac{1}{\text{dist}\,(z, \Lambda(A))},$$

where $\text{dist}(z, \Lambda(A))$ denotes the usual distance from a point to a set in the complex plane. Thus, $\Lambda_\epsilon(A)$ is the union of the closed disks of radius ϵ centred at the eigenvalues of A. For nonnormal matrices, the norm of the resolvent, $\|R(z)\|_2$, can be much larger even if z is far from the spectrum.

An equivalent definition is based on the connection between resolvent norm and eigenvalue perturbation theory. The ϵ-pseudospectra of the

matrix A is defined as follows

$$\Lambda_\epsilon(A) = \{z \in \mathbb{C} : z \in \Lambda(A + E) \text{ for some } E \text{ with } \|E\| \le \epsilon\}.$$

In other words, z is a ϵ-eigenvalue if it is an exact eigenvalue of A perturbed by a random matrix E with norm less than or equal to ϵ.

The two definitions are equivalent. Pseudospectra give approximate information about the maximum transient growth. Roughly speaking, the maximum transient growth $G_{\max}$ depends on how far the pseudospectra extend into the upper half-plane. A rigorous connection between pseudospectra and transient growth is given by Reddy and Henningson [**69**].

2.6.2. Numerical range. The energy growth rate at any time t is defined as the *numerical range*. Using the discrete eigenfunction expansion formulation (2.7), we obtain

$$\frac{1}{E}\frac{dE}{dt} = \frac{1}{\|k\|_E^2}\frac{d\|k\|_E^2}{dt} = \frac{1}{\|k\|_E^2}\left[\left(\frac{dk}{dt}, k\right)_E + \left(k, \frac{dk}{dt}\right)_E\right]$$

$$= \frac{1}{\|k\|_E^2}\left[(-i\Omega k, k)_E + (k, -i\Omega k)_E\right]$$

$$= \frac{1}{\|k\|_E^2}\left[i\left(\Omega k, k\right)_E - i\left(k, \Omega k\right)_E\right]$$

$$= \frac{1}{\|k\|_E^2}\left[\frac{(k, \Omega k)_E - \overline{(k, \Omega k)}_E}{i}\right] = 2\Im\left(\frac{(k, \Omega k)_E}{(k, k)_E}\right).$$

The numerical range determines the potential for energy growth and it is defined as the set in the complex plane of all Rayleigh quotients of the matrix Ω defined by equation (2.8). Therefore, the numeric al range of Ω is given by

$$\mathcal{F}(\Omega) = \{z \in \mathbb{C} : z = (k, \Omega k)_E \text{ with } \|k\|_E = 1\}$$
$$= \left\{z \in \mathbb{C} : z = \left(v, F\Omega F^{-1}v\right)_2 \text{ with } \|v\|_2 = 1\right\}.$$

When the operator Ω is normal, the numerical range is the convex hull of its eigenspectrum. Therefore, there is no energy growth if all the eigenvalues lie in the lower half plane. This explains why the critical Reynolds numbers based on energy theory and based on eigenvalue analysis coincide for the Rayleigh-Bénard convection (Schmid [**74**]).

The numerical range for nonnormal operators is larger than the convex hull of the spectrum. Thus, it can protrude in the unstable half plane even if the spectrum is confined in the stable half plane.

2.6.3. Numerical abscissa. To capture the short-time dynamic we can define the *numerical abscissa* that is the slope of the curve $G(t)$ at $t = 0^+$. Using the Taylor-series expansion of the matrix exponential around $t = 0^+$, i.e. $e^{-i\Omega t} \approx 1 - i\Omega t$ yields the following result

$$
\begin{aligned}
\frac{dG}{dt}\Big|_{t=0^+} &= \max_{\|k_0\|_E=1} \frac{d}{dt}\|k\|_E^2\Big|_{t=0^+} = \max_{\|Fk_0\|_2=1} \frac{d}{dt}\|Fe^{-i\Omega t}k_0\|_2^2\Big|_{t=0^+} \\
&= \max_{\|Fk_0\|_2=1} \frac{d}{dt}\Big(F(1-i\Omega t)k_0, F(1-i\Omega t)k_0\Big)_2\Big|_{t=0^+} \\
&= \max_{\|Fk_0\|_2=1} \Big(Fk_0, F(-i\Omega)k_0\Big)_2 + \Big(F(-i\Omega)k_0, Fk_0\Big)_2 \\
&= \max_{\|Fk_0\|_2=1} \Big(Fk_0, \big(F(-i\Omega)F^{-1} + (F(-i\Omega)F^{-1})^H\big)Fk_0\Big)_2 \\
&= \lambda_1\Big(-iF\Omega F^{-1} + (-iF\Omega F^{-1})^H\Big).
\end{aligned}
$$

The numerical abscissa is calculated as the maximum Rayleigh quotient of the Hermitian matrix $-iF\Omega F^{-1} + (-iF\Omega F^{-1})^H$ that is given by its largest eigenvalue. The maximum protrusion of the numerical range into the unstable half plane is equivalent to the numerical abscissa and determines the maximum energy growth at $t = 0^+$.

2.6.4. Results. In Figure 2.11, we show the contour plot of the logarithm of the resolvent norm, i.e.

$$
\log\left(\|R(z)\|_E\right) = \log\left(\|z\mathbb{I} - \Omega\|_E\right).
$$

As an example, we choose the case of a flat plate with $\beta_H = 0$, Reynolds number $Re_0 = 500$, wavenumbers $\alpha = 0.3, \beta = 0.2$ and non-Newtonian parameter $K = -0.01$. These parameters have been chosen to illustrate the concept of numerical range and pseudospectra.

From Figure 2.11, we can see how the contour plot of the resolvent norm does not consist in the union of balls centred on the eigenvalues and this indicates that the system is nonnormal. Moreover, the numerical range, represented by the red dashed line, reaches into the unstable
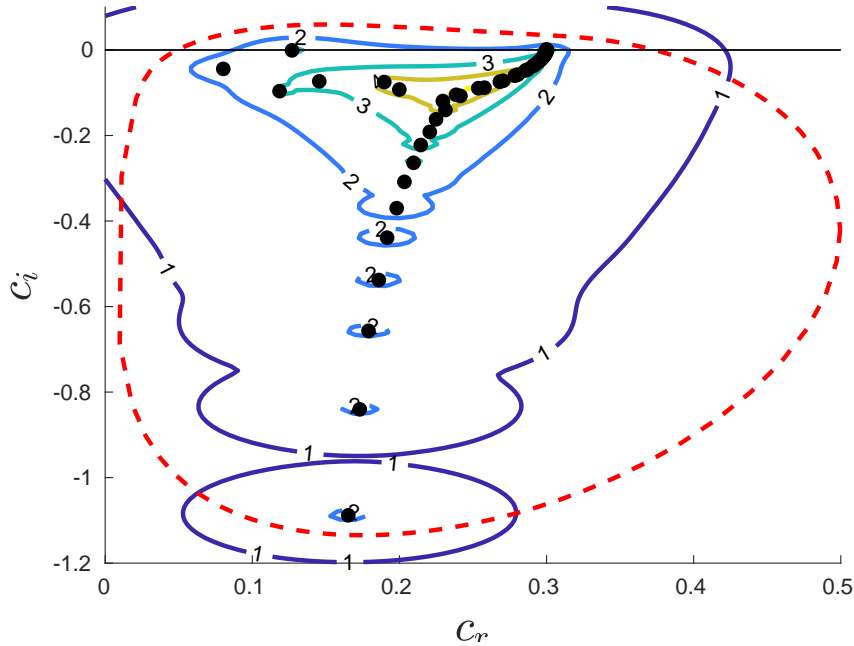
FIGURE 2.11. Contour plot for the logarithm of the resolvent norm and spectrum for the flat plate case with $\beta_H = 0, Re_0 = 500, \alpha = 0.3, \beta = 0.2$ and $K = -0.01$. The red dashed line represents the numerical range, the black dashed line represents the numerical range in the Newtonian case.

half plane. This means that there exists positive energy growth rates, despite all the eigenvalues being confined to the stable half plane.

In Figure 2.12, we compare the numerical range with the Newtonian numerical range. We can see that, for $K = -0.01$ the numerical range changes slightly with respect to the Newtonian case and extends less into the positive half plane, while the least stable eigenvalue becomes more unstable. For $K = 0.01$, the least stable eigenvalue moves away from the positive half plane but the numerical range is larger than in the Newtonian case.

2.7. Time-dependent simulations

In order to verify the transient growth results obtained in the previous sections, we solved the initial-value problem (2.5) marching in time
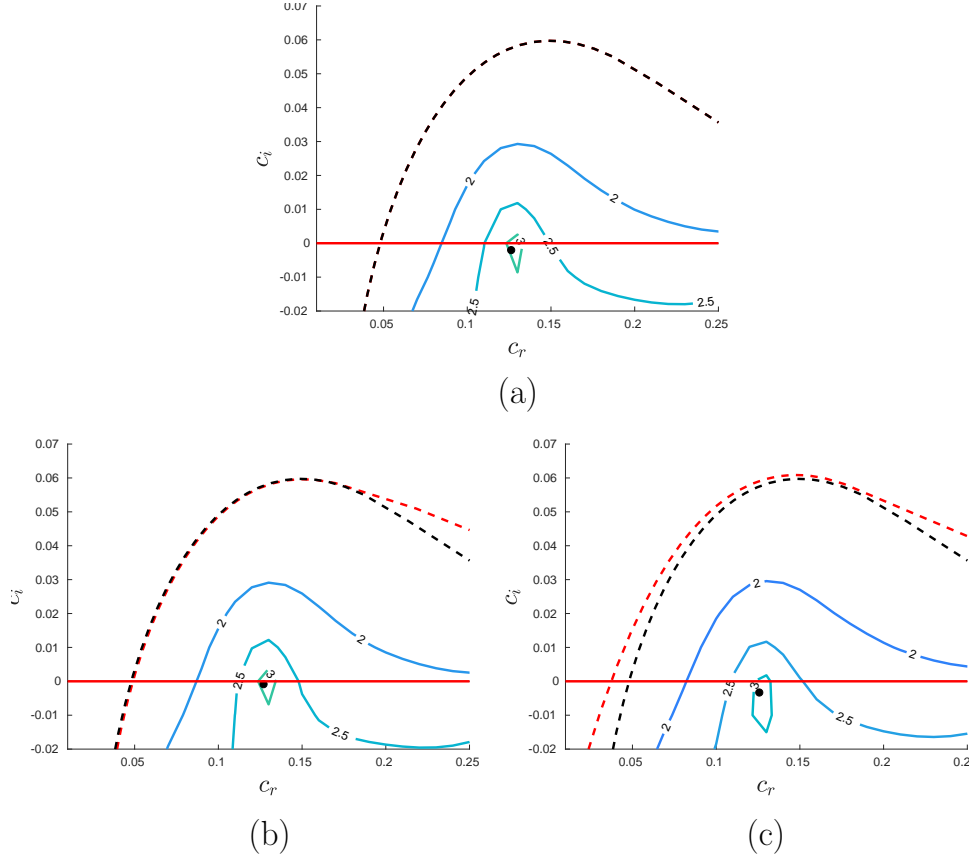
FIGURE 2.12. Numerical range for the flat plate case with $\beta_H = 0, Re_0 = 500, \alpha = 0.3, \beta = 0.2$. (a) Newtonian ($K = 0$); (b) non-Newtonian ($K = -0.01$); (c) non-Newtonian ($K = 0.01$). The black dashed line (- -) represents the numerical range in the Newtonian case.

with a numerical scheme. Thus, the problem to solve numerically is

$$\begin{cases} \mathcal{M}\dfrac{\partial \mathbf{q}}{\partial t} = -i\mathcal{L}\mathbf{q}, \\ \mathbf{q}(t = 0) = \mathbf{q}_0, \end{cases}$$

where $\mathbf{q} = (\hat{v}, \hat{\eta})^T$ and $\mathbf{q}_0$ is a given initial disturbance. The linear operators $\mathcal{M}$ and $\mathcal{L}$ are defined by equations (1.28).

Discretisation in the wall-normal direction y is performed by applying a mapping to the semi-infinite domain and using a Chebyshev collocation method, as described in Section 5.1. Therefore, the semi-discretised

system becomes

$$\begin{cases} M\dfrac{d\mathbf{q}}{dt} = -iL\mathbf{q}, \\ \mathbf{q}(t=0) = \mathbf{q}_0, \end{cases}$$

where $\mathbf{q}$ is a vector of length N, equal to the chosen number of Chebyshev collocation points and M, L are $N \times N$ matrices.

For the time discretisation, we choose an implicit second order numerical scheme known as the Crank-Nicolson method. We define a number $\tilde{N}$ of points in the interval of time $[0, t_{\text{fin}}]$, such that

$$t_n = hn \quad \text{for} \quad n = 0, \ldots, \tilde{N},$$

where $h = t_{\text{fin}}/\tilde{N}$ is a small discretisation parameter. The fully discretised system becomes

$$\begin{cases} \left(M + i\dfrac{h}{2}L\right)\mathbf{q}_{n+1} = \left(M - i\dfrac{h}{2}L\right)\mathbf{q}_n, \\ \mathbf{q}_0 = \mathbf{q}(t=0), \end{cases}$$

where $\mathbf{q}_n$ is the approximated solution at the time t_n.

The solution of the numerical simulation at $t_{\text{fin}} = h\tilde{N}$, $\mathbf{q}_{\text{fin}}$, is then compared with the solution given by the eigenmode decomposition (2.7), that is

$$\mathbf{q}_{\mathrm{D}} = \sum_{j=1}^{N} k_j(t_{\text{fin}})\tilde{\mathbf{q}}_j,$$

where the coefficients of the expansion $k_j(t_{\text{fin}})$ are the components of the following vector

$$\mathbf{k}(t_{\text{fin}}) = e^{-i\Omega t_{\text{fin}}}\mathbf{k}_0.$$

This solution is given by solving the system of equations (2.8) for the coefficients of the expansion and $\mathbf{k}_0$ is the vector which contains the coefficients of the expansion of the initial disturbance, $\mathbf{q}_0$.

2.7.1. Results. Several numerical tests have been performed. We choose different types of initial disturbance and we observed that, in each case, the solution of the simulation, $\mathbf{q}_D$, agrees with the solution obtained with the eigenmode decomposition, $\mathbf{q}_{\text{fin}}$. In this work, we present four tests that have been performed.
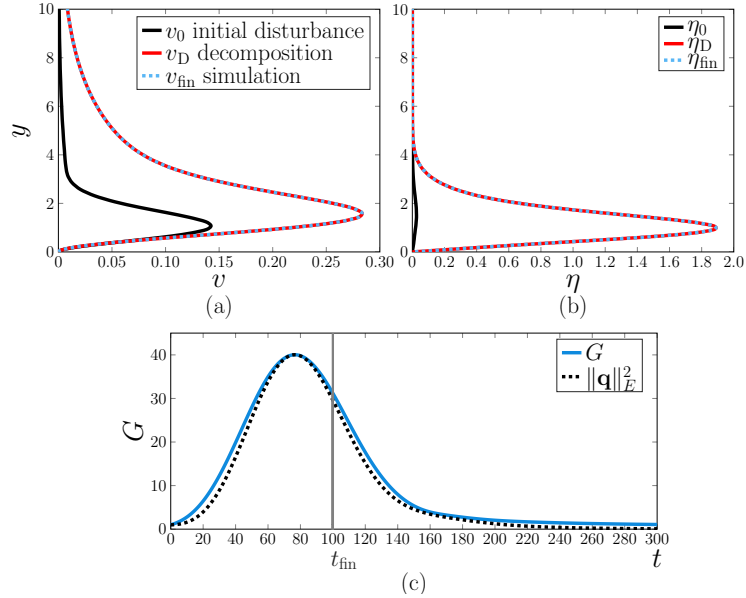
FIGURE 2.13. Evolution of the optimal disturbance for the flow past a wedge with $\beta_H = 0.5, Re_0 = 500, K = 0.001, \alpha = 0.3, \beta = 0.2$. (a) wall-normal velocity; (b) vorticity; (c) amplification of disturbance energy.
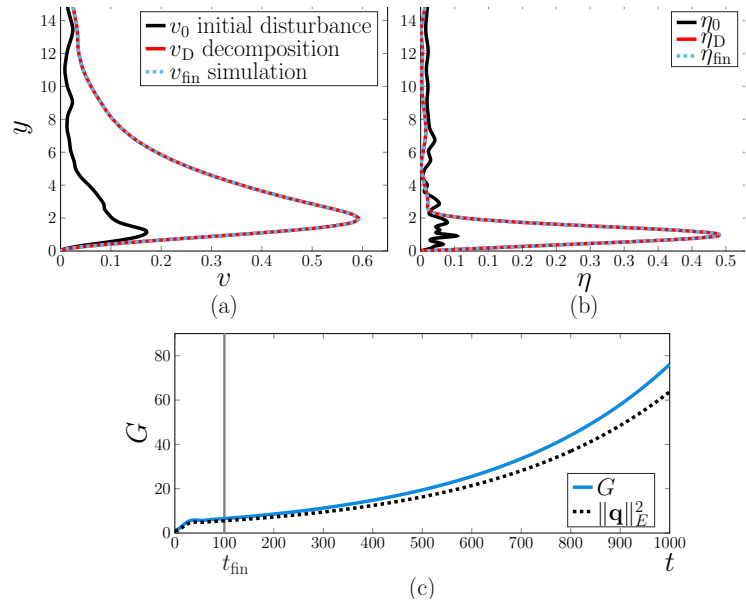
FIGURE 2.14. Evolution of a randomly perturbed two-dimensional optimal disturbance for the flow past a corner with $\beta_H = -0.14, Re_0 = 200, K = -10^{-5}, \alpha = 0.3, \beta = 0.1$. (a) wall-normal velocity; (b) vorticity; (c) amplification of disturbance energy.

2.7.1.1. *Test 1.* The initial disturbance is chosen to be the global optimum, defined in Section 2.5, with unit energy norm. This is the initial configuration which maximises the growth over all time, i.e. it reaches the maximum $G_{\max}$ at a time $t_{\max}$ as defined by (2.12).

Figure 2.13 shows the results for the flow past a wedge with $\beta_H = 0.5$, $Re_0 = 500$ and $K = 0.001$. The wavenumbers in the x- and z-directions are chosen to be $\alpha = 0.3$ and $\beta = 0.2$, respectively. From Figure 2.13(c) we see that $G_{\max} \approx 40$ is reached at $t_{\max} \approx 80$. The evolution of the optimal disturbance energy norm, $\|\mathbf{q}\|_E^2$, is plotted along with the maximum possible amplification G, defined by (2.11). By definition, the energy norm of the disturbance touches the curve G exactly at $t = t_{\max}$.

Figures 2.13(a),(b) show the initial configuration, $\mathbf{q}_0$, and the comparison at $t_{\text{fin}} = 100$ between the solution given by the eigenmode decomposition, $\mathbf{q}_D$, and the solution obtained by marching in time, $\mathbf{q}_{\text{fin}}$. Figure 2.13(a) shows the wall-normal velocity v, while Figure 2.13(b) shows the vorticity η. We see good agreement between the solutions.

2.7.1.2. *Test 2.* The initial disturbance is chosen to be the configuration which reaches the maximum possible amplification in the interval of time $[0, 1000]$ which is randomly perturbed. In other words, the initial disturbance is taken to be

$$\mathbf{q}_0 = \sum_{j=1}^{N} (\mathbf{k}_0)_j \, \tilde{\mathbf{q}}_j,$$

where $\mathbf{k}_0$ is a random perturbation of the optimal solution $\mathbf{k}_{0,\max}$ defined in Section 2.5.

Figure 2.14 shows the results for flow past a corner with $\beta_H = -0.14$, $Re_0 = 200$ and $K = -10^{-5}$. The wavenumbers in the x- and z-directions are chosen to be $\alpha = 0.3$ and $\beta = 0.1$, respectively. From Figure 2.14(c), we see that G does not decay as time increases. This is due to the presence of an exponentially unstable eigenvalue.
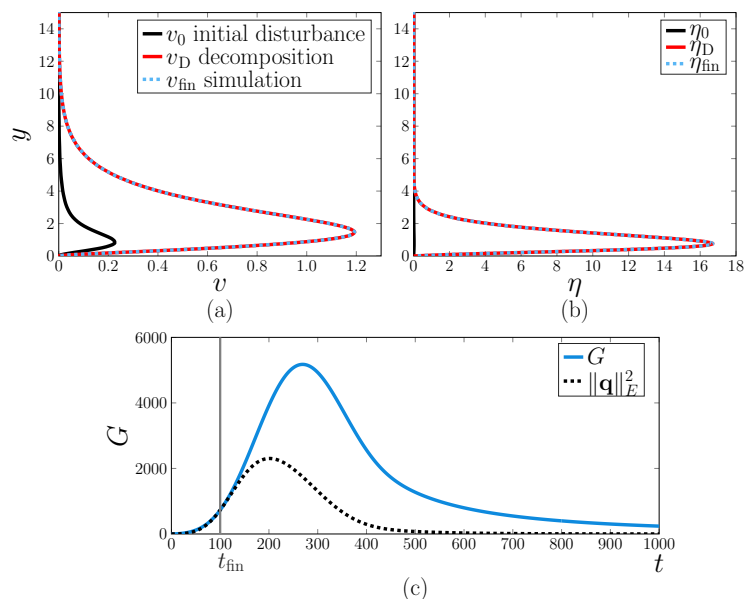
FIGURE 2.15. Evolution of the disturbance which reaches the maximum possible amplification at $T = 100$ for a stagnation point flow with $\beta_H = 1, Re_0 = 10000, K = 10^{-5}, \alpha = 0.1, \beta = 0.6$. (a) wall-normal velocity; (b) vorticity; (c) amplification of disturbance energy.
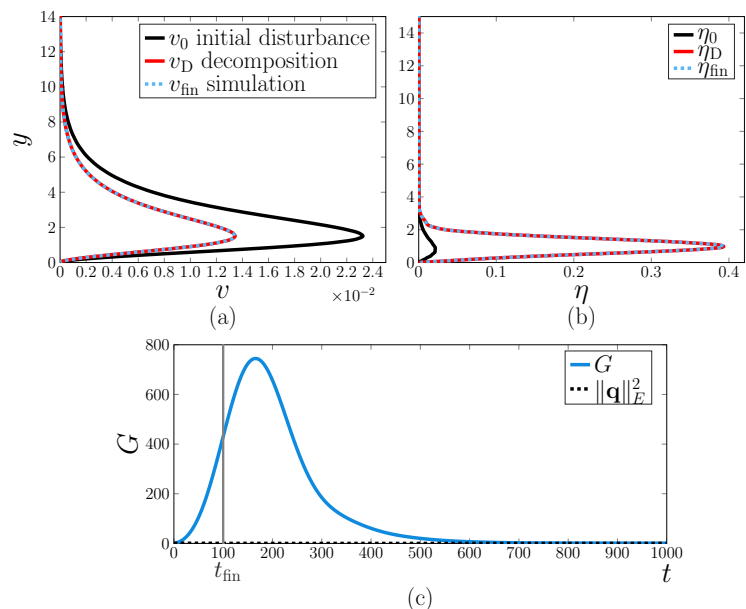
FIGURE 2.16. Evolution of the least stable mode for the flow over a flat plate with $\beta_H = 0, Re_0 = 1000, K = -10^{-5}, \alpha = 0.1, \beta = 0.6$. (a) wall-normal velocity; (b) vorticity; (c) amplification of disturbance energy.

We observe from Figures 2.14(a),(b) that the solution computed using the Crank-Nicolson method, $\mathbf{q}_{\mathrm{fin}}$ at $t_{\mathrm{fin}} = 100$ coincides with the solution given by the eigenmode decomposition, $\mathbf{q}_{\mathrm{D}}$.

2.7.1.3. *Test 3.* In this case, we choose as initial configuration a disturbance that reaches the maximum possible amplification of energy at time $T = 100$ as defined in Section 2.5.

The test is run for the stagnation point flow with $\beta_H = 1$, $Re_0 = 10000$ and $K = 10^{-5}$ and the results are reported in Figure 2.15. The choice of wavenumbers ($\alpha = 0.1$, $\beta = 0.6$) gives a very high maximum possible amplification, as can be seen in Figure 2.15(c). By definition, the evolution of the optimal disturbance energy norm, $\|\mathbf{q}\|_E^2$, touches the curve G exactly at $T = 100$. Figures 2.15(a),(b) show a good agreement between the simulation and the solution calculated using the decomposition.

2.7.1.4. *Test 4.* For this test, the eigenfunction corresponding to the least stable eigenvalue is selected as initial perturbation.

We run the test for the flow past a flat plate with $\beta_H = 0$, $Re_0 = 1000$ and $K = -10^{-5}$. The results, shown in Figure 2.16, show once again that there is good agreement between the solutions obtained with the two methods. Moreover, we can see from Figure 2.16(c) that the least stable eigenmode does not experience energy growth, that is $\|\mathbf{q}\|_E \leq 1$ throughout the whole time period considered.

2.8. Concluding remarks

In this chapter, we extended the linear stability analysis to include the bypass transition scenario. The initial-value problem, which governs the development of disturbances, was derived for second order fluids. We found that, for second grade fluids ($K > 0$) the maximum transient growth increases, while for second order fluids ($K < 0$) the maximum transient growth decreases. Streamwise independent waves still reach the largest amplification of energy, as in the Newtonian case. Hence, the lift-up effect is still responsible for the transient growth of energy.

Moreover, we observed that non-Newtonian terms mostly affect streamwise independent waves. When $K > 0$, the global optimum is reached for larger times and larger spanwise wavenumbers. When $K < 0$, the global optimum occurs for shorter times and smaller spanwise wavenumbers.

CHAPTER 3

Monochromatic DNS

The aim of this chapter is to introduce the velocity-vorticity formulation and to use it in order to verify the linear stability results obtained in Chapter 1. Throughout this chapter, we refer to the contributions of Davies and Carpenter [19], Davies [18] and Morgan [51].

The main idea of velocity-vorticity methods is to rewrite the equations in the form of a vorticity transport equation. This formulation is remarkably simpler than the primitive-variable formulation, which involves the velocity field $\mathbf{v}$ and the pressure $\mathbf{p}$. The pressure does not appear explicitly in velocity-vorticity formulations which involve only the velocity $\mathbf{v}$ and the vorticity $\boldsymbol{\omega}$. For more details on the advantages of velocity-vorticity methods we refer to Speziale [79].

The approach followed by Davies and Carpenter [19] relies on a compact formulation where the number of variables in the system is reduced. There are only three equations to be solved in terms of three dependent variables, the so-called *primary variables*. The novelty of their formulation is that the no-slip condition is applied in a mathematically consistent way through integral constraints for the primary vorticity components to be associated with the corresponding transport equations.

The three primary variables are the two perturbation vorticity components in the plane of the solid surface, x and z, and the perturbation velocity in the wall-normal direction, y. These are governed by two transport equations for the vorticity components and a Poisson equation for the velocity. The remaining dependent variables are called *secondary variables* and can be determined explicitly from the primary variables.

In Section 3.1, we introduce the velocity-vorticity formulation of the Navier-Stokes equations without going into details of the derivation. Section 3.2 is dedicated to the derivation the velocity-vorticity formulation for the second order fluids introduced in Chapter 1. In Section 3.3 we describe the numerical methods and in Section 3.4 we present the results of the simulations.

3.1. Velocity-Vorticity Formulation of the Navier-Stokes equations

In this section, we present an overview of the velocity-vorticity formulation for Newtonian fluids. We follow the approach of Davies and Carpenter [19] and Davies [18].

Let $\mathbf{U}_{\mathrm{B}} = (U_{\mathrm{B}}, V_{\mathrm{B}}, W_{\mathrm{B}})^T$ denote a general mean flow and $\boldsymbol{\Omega}_{\mathrm{B}} = \nabla \times \mathbf{U}_{\mathrm{B}} = (\Omega_x, \Omega_y, \Omega_z)^T$ the mean flow vorticity. Consider the vector $\mathbf{v} = (u, v, w)^T$ to be the disturbance velocity field and $\boldsymbol{\omega} = \nabla \times \mathbf{v} = (\omega_x, \omega_y, \omega_z)^T$ its vorticity. Henceforth, we consider all variables to be dimensionless and the Reynolds number, Re, is defined in the usual manner, using appropriate characteristic length and velocity.

The Navier-Stokes equations will be written in terms of the so-called primary dependent variables, $\{\omega_x, \omega_z, v\}$. The secondary dependent variables, which can be determined explicitly from the primary variables, are $\{\omega_y, u, w\}$. Therefore, the secondary variables can be ignored for the purposes of the numerical simulations.

The Navier-Stokes equations written in terms of the primary variables are

$$\frac{\partial \omega_x}{\partial t} + \frac{\partial N_z}{\partial y} - \frac{\partial N_y}{\partial z} = \frac{1}{Re}\Delta\omega_x, \tag{3.1a}$$

$$\frac{\partial \omega_z}{\partial t} + \frac{\partial N_y}{\partial x} - \frac{\partial N_x}{\partial y} = \frac{1}{Re}\Delta\omega_z, \tag{3.1b}$$

$$\Delta v = \frac{\partial \omega_z}{\partial x} - \frac{\partial \omega_x}{\partial z}, \tag{3.1c}$$

where $\mathbf{N} = (N_x, N_y, N_z)^T$ is defined as

$$\mathbf{N} = \boldsymbol{\Omega}_{\mathrm{B}} \times \mathbf{v} + \boldsymbol{\omega} \times \mathbf{U}_B + \boldsymbol{\omega} \times \mathbf{v}.$$

Linearisation can be performed by neglecting the non-linear term, $\boldsymbol{\omega} \times \mathbf{v}$. In order to obtain the velocity-vorticity formulation (3.1), we take the curl of the three-dimensional Navier-Stokes equations, subtract the equations for the base flow vorticity $\boldsymbol{\Omega}_B$ and consider the transport equations for the streamwise and spanwise vorticity only, ω_x and ω_z. The last equation (3.1c) for the wall-normal disturbance velocity v is derived by taking the curl of the definition of vorticity and making use of the continuity equation, i.e.

$$\nabla \times \boldsymbol{\omega} = -\Delta \mathbf{u}.$$

In this section, we omit the details of the derivation for the Newtonian case. We will follow all the steps of the derivation for the second order model in the next section.

Note that equations (3.1a) and (3.1b) still depend on the secondary variables through the convective quantity $\mathbf{N}$. Therefore, we define the secondary variables in terms of the primary variables as follows

$$u = \int_y^\infty \left(\omega_z - \frac{\partial v}{\partial x} \right) d\tilde{y}, \tag{3.2a}$$

$$w = -\int_y^\infty \left(\omega_x + \frac{\partial v}{\partial z} \right) d\tilde{y}, \tag{3.2b}$$

$$\omega_y = \int_y^\infty \left(\frac{\partial \omega_x}{\partial x} + \frac{\partial \omega_z}{\partial z} \right) d\tilde{y}. \tag{3.2c}$$

The definitions of u and w are derived by integrating the definition of vorticity with respect to y and assuming implicitly that u and w vanish at infinity. The last definition (3.2c) is derived by integrating the following equation

$$\nabla \cdot \boldsymbol{\omega} = 0,$$

assuming that ω_y tends to 0 as $y \to \infty$. The vorticity is solenoidal since the divergence of a curl is always zero.

3.1.1. Equivalence to the full Navier-Stokes equations. It
is possible to recover the full Navier-Stokes equations provided that two further conditions for the behaviour of the perturbations at infinity are satisfied. Further details can be found in Davies and Carpenter [19].

The two conditions are

$$\lim_{y \to \infty} \frac{\partial v}{\partial y} = 0, \tag{3.3}$$

and

$$\lim_{y \to \infty} \left(\frac{\partial \omega_y}{\partial t} + \frac{\partial N_x}{\partial z} - \frac{\partial N_z}{\partial x} - \frac{1}{Re} \Delta \omega_y \right) = 0.$$

Assuming that $v \to 0$ and V_B tends to a constant as $y \to \infty$, and remembering that the secondary variables u, w, ω_y are all defined so as to vanish at infinity, the latter condition may be simplified to

$$\lim_{y \to \infty} \left[\left(-V_B + \frac{1}{Re} \frac{\partial}{\partial y} \right) \left(\frac{\partial \omega_x}{\partial x} + \frac{\partial \omega_z}{\partial z} \right) \right] = 0. \tag{3.4}$$

It may seem that these two conditions need to be imposed directly in this formulation. However, they will be automatically satisfied by making a convenient choice of mapping.

Notice that equivalent conditions need to be derived for the non-Newtonian case. More details are given in the next section.

3.1.2. Boundary conditions at the wall. Assuming a wall placed at $y = \eta(x, z, t)$, the no-slip and no-penetration conditions at the wall read

$$u(x, \eta, z, t) = u_{\text{wall}}(x, z, t),$$
$$v(x, \eta, z, t) = v_{\text{wall}}(x, z, t),$$
$$w(x, \eta, z, t) = w_{\text{wall}}(x, z, t),$$

where $u_{\text{wall}}, v_{\text{wall}}, w_{\text{wall}}$ are functions determined by the wall motion. In the presence of a rigid wall, $u_{\text{wall}}, v_{\text{wall}}, w_{\text{wall}}$ are all set to zero.

The boundary condition on v can be imposed easily on the Poisson equation (3.1c). The boundary conditions at the wall for u and w are imposed indirectly by deriving integral constraints for the primary vorticity components, ω_x and ω_z. Rewriting the definitions (3.2a) and (3.2b) and making use of the conditions on u and w, we obtain

$$\int_\eta^\infty \omega_x \, dy = -w_{\text{wall}} - \int_\eta^\infty \frac{\partial v}{\partial z} \, dy,$$
$$\int_\eta^\infty \omega_z \, dy = u_{\text{wall}} + \int_\eta^\infty \frac{\partial v}{\partial x} \, dy.$$

These can be viewed as constraints on the primary vorticity components, ω_x and ω_z, and can be applied on the associated transport equations (3.1a) and (3.1b).

3.1.3. Conditions at infinity.

There is no problem in applying the condition $v \to 0$ as $y \to \infty$, since it can be easily associated with the Poisson equation (3.1c). However, there is no natural way to constrain ω_x and ω_y at infinity and conditions (3.3) and (3.4) are not straightforward to implement and apply. They are replaced by the stronger conditions that both ω_x and ω_z vanish at infinity.

The consistency requirements (3.3) and (3.4) are clearly met if the y-derivatives of all the primary variables ω_x, ω_z and v at infinity. Making use of an algebraic mapping from the semi-infinite domain $y \in [0, \infty)$ to $\xi \in (0, 1]$, it is easy to check the validity of (3.3) and (3.4). The mapping is defined as follows

$$\xi = \frac{l}{l+y}, \tag{3.5}$$

where l is a stretching parameter. Notice that this mapping is very similar to the one defined by equation (1.23) in Section 1.5. The derivative of a function f with respect to the physical variable y can be written with respect to the transformed variable ξ as follows

$$\frac{\partial f}{\partial y} = -\frac{\xi^2}{l}\frac{\partial f}{\partial \xi}.$$

The limit as $y \to \infty$ in the physical domain corresponds to the limit as $\xi \to 0$ in the computational domain. Therefore, the derivative of a function with respect to y goes to zero as $y \to \infty$ if the derivative with respect to ξ remains bounded as $\xi \to 0$. The compatibility conditions (3.3) and (3.4) are satisfied provided that the ξ-derivatives of the primary variables remain bounded as $\xi \to 0$.

3.2. Velocity-vorticity formulation for the second order model

In this section, we derive the velocity-vorticity formulation for the second order model (1.1) defined in Chapter 1.

Let $\tilde{\mathbf{v}}$ denote the velocity field and $\tilde{\boldsymbol{\omega}}$ its vorticity. The dimensionless governing equations for the second order model with constitutive equation (1.1) are

$$\frac{\partial \tilde{\mathbf{v}}}{\partial t} + (\tilde{\mathbf{v}} \cdot \nabla)\tilde{\mathbf{v}} = -\nabla \tilde{p} + \nabla \cdot \tilde{\boldsymbol{\tau}}, \tag{3.6}$$

$$\nabla \cdot \tilde{\mathbf{v}} = 0.$$

The dimensional governing equations can be found in Section 1.2. The non-dimensional extra-stress tensor $\tilde{\boldsymbol{\tau}}$ is defined as follows

$$\tilde{\boldsymbol{\tau}} = \frac{1}{Re}\tilde{\mathbf{A}}_1 + K(\tilde{\mathbf{A}}_2 - \tilde{\mathbf{A}}_1^2),$$

where Re and K are, respectively, the Reynolds and elasticity numbers defined in the same way as in the previous chapters, i.e.

$$Re = \frac{\rho U L}{\mu}, \qquad K = \frac{\alpha_1}{\rho L^2},$$

based on an appropriate choice of characteristic length L and velocity U which will be specified later. The Rivlin-Ericksen tensors $\tilde{\mathbf{A}}_1$ and $\tilde{\mathbf{A}}_2$ are defined as follows

$$\tilde{\mathbf{A}}_1 = \nabla \tilde{\mathbf{v}} + \nabla \tilde{\mathbf{v}}^T,$$

$$\tilde{\mathbf{A}}_2 = \frac{\partial \tilde{\mathbf{A}}_1}{\partial t} + (\tilde{\mathbf{v}} \cdot \nabla)\tilde{\mathbf{A}}_1 + \nabla \tilde{\mathbf{v}}\tilde{\mathbf{A}}_1 + \tilde{\mathbf{A}}_1 \nabla \tilde{\mathbf{v}}^T.$$

By taking the curl of the equation of motion in vectorial form (3.6), we obtain a transport equation for the vorticity $\tilde{\boldsymbol{\omega}}$, i.e.

$$\frac{\partial \tilde{\boldsymbol{\omega}}}{\partial t} + \nabla \times \tilde{\mathbf{N}} = \frac{1}{Re}\Delta \tilde{\boldsymbol{\omega}} + K\Delta \left(\frac{\partial \tilde{\boldsymbol{\omega}}}{\partial t}\right), \tag{3.7}$$

where $\tilde{\mathbf{N}}$ is the convective quantity

$$\tilde{\mathbf{N}} = \tilde{\boldsymbol{\omega}} \times \tilde{\mathbf{v}} - K\left[\nabla \cdot \left((\tilde{\mathbf{v}} \cdot \nabla)\tilde{\mathbf{A}}_1\right) + \nabla \cdot \left(\nabla \tilde{\mathbf{v}}\nabla \tilde{\mathbf{v}}^T - \nabla \tilde{\mathbf{v}}^T \nabla \tilde{\mathbf{v}}\right)\right],$$

Notice the additional terms due to non-Newtonian effects are those multiplied by the non-Newtonian parameter K. When $K = 0$ we recover the Newtonian case.

Consider now the usual decomposition of the velocity and vorticity fields into base flow and disturbances, as follows

$$\tilde{\mathbf{v}} = \mathbf{U}_B + \mathbf{v}, \qquad \tilde{\boldsymbol{\omega}} = \boldsymbol{\Omega}_B + \boldsymbol{\omega}.$$

Subtracting the transport equation for the base flow vorticity $\boldsymbol{\Omega}_B$ from equation (3.7) leads to the following equation for the disturbance vorticity $\boldsymbol{\omega}$, i.e.

$$\frac{\partial \boldsymbol{\omega}}{\partial t} + \nabla \times \mathbf{N} = \frac{1}{Re}\Delta\boldsymbol{\omega} + K\Delta\left(\frac{\partial \boldsymbol{\omega}}{\partial t}\right),$$

where $\mathbf{N}$ takes the form

$$\begin{aligned}
\mathbf{N} = {}& \boldsymbol{\omega} \times \mathbf{U}_B + \boldsymbol{\Omega}_B \times \mathbf{v} + \boldsymbol{\omega} \times \mathbf{v} \\
& - K\left[\nabla \cdot \left((\mathbf{U}_B \cdot \nabla)\,\mathbf{A}_1 + (\mathbf{u} \cdot \nabla)\,\mathbf{A}_{B,1} + (\mathbf{u} \cdot \nabla)\,\mathbf{A}_1\right)\right] \\
& - K\left[\nabla \cdot \left(\nabla\mathbf{U}_B\nabla\mathbf{v}^T + \nabla\mathbf{v}\nabla\mathbf{U}_B^T + \nabla\mathbf{v}\nabla\mathbf{v}^T\right)\right] \\
& + K\left[\nabla \cdot \left(\nabla\mathbf{U}_B^T\nabla\mathbf{v} + \nabla\mathbf{v}^T\nabla\mathbf{U}_B + \nabla\mathbf{v}^T\nabla\mathbf{v}\right)\right],
\end{aligned}$$

with $\mathbf{A}_1 = \nabla\mathbf{v} + \nabla\mathbf{v}^T$ and $\mathbf{A}_{B,1} = \nabla\mathbf{U}_B + \nabla\mathbf{U}_B^T$. Neglecting nonlinear terms, $\mathbf{N}$ simplifies considerably to

$$\begin{aligned}
\mathbf{N} = {}& \boldsymbol{\omega} \times \mathbf{U}_B + \boldsymbol{\Omega}_B \times \mathbf{v} - K\left[\nabla \cdot \left((\mathbf{U}_B \cdot \nabla)\,\mathbf{A}_1 + (\mathbf{u} \cdot \nabla)\,\mathbf{A}_{B,1}\right)\right] \\
& - K\left[\nabla \cdot \left(\nabla\mathbf{U}_B\nabla\mathbf{v}^T + \nabla\mathbf{v}\nabla\mathbf{U}_B^T - \nabla\mathbf{U}_B^T\nabla\mathbf{v} - \nabla\mathbf{v}^T\nabla\mathbf{U}_B\right)\right]. \quad (3.8)
\end{aligned}$$

Therefore, the velocity-vorticity formulation written in terms of the primary variables ω_x, ω_z, v reads

$$\frac{\partial \omega_x}{\partial t} + \frac{\partial N_z}{\partial y} - \frac{\partial N_y}{\partial z} = \frac{1}{Re}\Delta\omega_x + K\frac{\partial(\Delta\omega_x)}{\partial t} \qquad (3.9a)$$

$$\frac{\partial \omega_z}{\partial t} + \frac{\partial N_y}{\partial x} - \frac{\partial N_x}{\partial y} = \frac{1}{Re}\Delta\omega_z + K\frac{\partial(\Delta\omega_z)}{\partial t} \qquad (3.9b)$$

$$\Delta v = \frac{\partial \omega_z}{\partial x} - \frac{\partial \omega_x}{\partial z}, \qquad (3.9c)$$

where the Poisson equation for the wall-normal velocity v is derived as for the Newtonian case, described in Section 3.1. The convective terms N_x, N_y, N_z involve secondary variables which are defined, as for the Newtonian case, in terms of the primary variables only by relations (3.2). The system of equations (3.9) is associated with the same boundary conditions at the wall and at infinity described in Section 3.1 for the Newtonian case.

3.2.1. Equivalence to the original formulation. The velocity-vorticity formulation (3.9) is equivalent to the governing equations for the second order model provided that two conditions for the behaviour

of the disturbances far from the wall are satisfied. The first condition is required to ensure that the incompressibility condition ($\nabla \cdot \mathbf{v} = 0$) holds. By differentiating definitions (3.2a),(3.2b) for the secondary variables u and w with respect to x and z, respectively, and then summing, we obtain

$$\frac{\partial u}{\partial x} + \frac{\partial w}{\partial z} = \int_y^\infty \left(\frac{\partial \omega_z}{\partial x} - \frac{\partial \omega_x}{\partial z} - \frac{\partial^2 v}{\partial x^2} - \frac{\partial^2 v}{\partial z^2} \right) d\tilde{y}.$$

By applying the Poisson equation (3.9c) for v, this becomes

$$\frac{\partial u}{\partial x} + \frac{\partial w}{\partial z} = \int_y^\infty \left(\frac{\partial^2 v}{\partial y^2} \right) d\tilde{y}.$$

Thus, the incompressibility condition is satisfied if

$$\lim_{y \to \infty} \frac{\partial v}{\partial y} = 0. \tag{3.10}$$

This is the same condition obtained in the Newtonian case.

The second condition is needed in order to obtain the transport equation for the secondary component of the vorticity ω_y. It is obtained by differentiating the vorticity transport equations (3.9a),(3.9b) with respect to x and z, respectively, summing the results and using $\nabla \cdot \boldsymbol{\omega} = 0$. We can recover the transport equation for ω_y, that is

$$\frac{\partial \omega_y}{\partial t} + \frac{\partial N_x}{\partial z} - \frac{\partial N_z}{\partial x} = \frac{1}{Re} \Delta \omega_y + K \frac{\partial (\Delta \omega_y)}{\partial t},$$

provided that it holds in the limit as $y \to \infty$, i.e.

$$\lim_{y \to \infty} \left(\frac{\partial \omega_y}{\partial t} - K \frac{\partial (\Delta \omega_y)}{\partial t} + \frac{\partial N_x}{\partial z} - \frac{\partial N_z}{\partial x} - \frac{1}{Re} \Delta \omega_y \right) = 0. \tag{3.11}$$

For simplicity, we restrict our attention to the case of a parallel mean flow, $\mathbf{U}_B = (U_B(y), 0, 0)$. The secondary variables $\{u, w, \omega_y\}$ are defined to vanish at infinity. We also assume that $v \to 0$ as $y \to \infty$ and take into account that $U_B' \to 0$ as $y \to \infty$. Therefore, condition (3.11) simplifies to

$$\lim_{y \to \infty} \left\{ \left(\frac{1}{Re} + K \frac{\partial}{\partial t} \right) \left[\frac{\partial}{\partial y} \left(\frac{\partial \omega_x}{\partial x} + \frac{\partial \omega_z}{\partial z} \right) \right] + KF \right\} = 0, \tag{3.12}$$

where F is defined by

$$F = U_B \left(\frac{\partial g_3}{\partial y} + \frac{\partial^2 g_2}{\partial y^2} \right) + g_0 \left(\frac{\partial g_2}{\partial y} + \frac{\partial^2 g_1}{\partial y^2} + \frac{\partial^3 g_0}{\partial y^3} \right)$$

$$+ g_1 \left(\frac{\partial g_1}{\partial y} + \frac{\partial^2 g_0}{\partial y^2} \right) + \frac{\partial g_0}{\partial y} \left(g_2 + \frac{\partial g_1}{\partial y} + \frac{\partial^2 g_0}{\partial y^2} \right),$$

and the functions g_j are linear combinations of derivatives of order j with respect to x and z of the velocity field components, i.e.

$$g_j \in \mathrm{span} \left(\left\{ \frac{\partial^j v_l}{\partial x^k \partial z^{j-k}} \right\}_{l,k} \right).$$

The condition (3.12) that must be satisfied in order to obtain the transport equation for the secondary vorticity component ω_y, appears to be much more complicated than in the Newtonian case. The first term of condition (3.12) goes to zero if the y-derivatives of ω_x and ω_z tend to zero at infinity. As in the Newtonian case, this is achieved by a convenient choice of mapping, as explained in Section 3.1. The second term in the condition (3.12), KF, cannot easily be written in terms of the primary variables only. However, the term KF tends to zero if all the y-derivatives up to the 3rd of u, v, w tend to zero at infinity, i.e.

$$\frac{\partial^j v_k}{\partial y^j} \to 0 \quad \text{as } y \to \infty, \qquad \text{for } j = 1, 2, 3.$$

Applying the mapping (3.5) from the physical domain to the computational one, as in the previous section, we have

$$\frac{\partial f}{\partial y} = -\frac{\xi^2}{l} \frac{\partial f}{\partial \xi},$$

$$\frac{\partial^2 f}{\partial y^2} = 2 \frac{\xi^3}{l^2} \frac{\partial f}{\partial \xi} + \frac{\xi^4}{l^2} \frac{\partial^2 f}{\partial \xi^2},$$

$$\frac{\partial^3 f}{\partial y^3} = -6 \frac{\xi^4}{l^3} \frac{\partial f}{\partial \xi} - 6 \frac{\xi^5}{l^3} \frac{\partial^2 f}{\partial \xi^2} - \frac{\xi^6}{l^3} \frac{\partial^3 f}{\partial \xi^3}.$$

Therefore, it is only necessary to check that the computed ξ-derivatives up to the third order of u, v, w remain bounded as $\xi \to 0$.

3.2.2. Parallel mean flow.
Assuming a steady and parallel mean flow, $\mathbf{U}_B$ becomes

$$\mathbf{U}_B = (U_B(y), 0, 0)^T,$$

with vorticity

$$\mathbf{\Omega}_B = (0, 0, -U_B'(y))^T,$$

where $'$ indicates the derivative with respect to the wall-normal direction y. Notice that, for the non-Newtonian case, the mean flow profile is

found by solving a local ODE. The derivation of the base flow is explained extensively in Section 1.3. Therefore, U_B depends also on the streamwise position x through the non-Newtonian parameter K. In order to simplify our analysis, we perform a "local-flow" approximation.

Similarly to what was done for the linear stability analysis in Section 1.4, we linearise the equations around a mean flow which is taken at a fixed dimensional streamwise location x_0. The lengths are scaled using the displacement thickness δ_0 at location x_0, defined by equation (1.11), and the velocities are scaled using the free-stream velocity $U_e(x_0)$. Detailed definitions are given in Section 1.4. The Reynolds and elasticity numbers are thus defined locally and based on the displacement thickness by equations (1.12) and (1.14), i.e.

$$Re = Re_0 = \frac{\rho U_e(x_0)\delta_0}{\mu}, \qquad K = K_0 = \frac{\alpha_1}{\rho \delta_0^2}.$$

By applying the parallel flow approximation, the components of the convective quantity $\mathbf{N}$, defined by (3.8), simplify to

$$N_x = U_B' v + K_0 \hat{N}_x,$$
$$N_y = U_B \omega_z - U_B' u + K_0 \hat{N}_y,$$
$$N_z = -U_B \omega_y + K_0 \hat{N}_z,$$

where $\hat{N}_x, \hat{N}_y, \hat{N}_z$ are the non-Newtonian terms given by

$$\hat{N}_x = -\left(2\frac{\partial^3 u}{\partial x^3} + \frac{\partial^3 v}{\partial y \partial x^2} + \frac{\partial^3 u}{\partial y^2 \partial x} + \frac{\partial^3 w}{\partial z \partial x^2} + \frac{\partial^3 u}{\partial z^2 \partial x} \right) U_B$$
$$+ \left(\frac{\partial^2 v}{\partial y^2} - \frac{\partial^2 v}{\partial x^2} + \frac{\partial^2 w}{\partial z \partial y} \right) U_B' - \frac{\partial u}{\partial x} U_B'' - v U_B''',$$

$$\hat{N}_y = -\left(\frac{\partial^3 u}{\partial y \partial x^2} + \frac{\partial^3 v}{\partial x^3} + 2\frac{\partial^3 v}{\partial y^2 \partial x} + \frac{\partial^3 v}{\partial z^2 \partial x} + \frac{\partial^3 w}{\partial z \partial y \partial x} \right) U_B$$
$$- \left(\frac{\partial^2 u}{\partial x^2} + 2\frac{\partial^2 u}{\partial y^2} + \frac{\partial^2 u}{\partial z^2} + \frac{\partial^2 v}{\partial y \partial x} \right) U_B' - \left(2\frac{\partial u}{\partial y} + \frac{\partial v}{\partial x} \right) U_B'',$$

$$\hat{N}_z = -\left(\frac{\partial^3 w}{\partial x^3} + \frac{\partial^3 u}{\partial z \partial x^2} + \frac{\partial^3 w}{\partial y^2 \partial x} + \frac{\partial^3 v}{\partial z \partial y \partial x} + 2\frac{\partial^3 w}{\partial z^2 \partial x} \right) U_B$$
$$- \left(\frac{\partial^2 u}{\partial z \partial y} + \frac{\partial^2 v}{\partial z \partial x} \right) U_B' - \frac{\partial u}{\partial z} U_B''.$$

Using the continuity equation ($\nabla \cdot \mathbf{v} = 0$), these terms can be simplified as follows

$$\hat{N}_x = - \left(\frac{\partial^3 u}{\partial x^3} + \frac{\partial^3 u}{\partial y^2 \partial x} + \frac{\partial^3 u}{\partial z^2 \partial x} \right) U_B$$
$$- \left(\frac{\partial^2 u}{\partial x \partial y} + \frac{\partial^2 v}{\partial x^2} \right) U_B' - \frac{\partial u}{\partial x} U_B'' - v U_B''',$$

$$\hat{N}_y = - \left(\frac{\partial^3 v}{\partial x^3} + \frac{\partial^3 v}{\partial y^2 \partial x} + \frac{\partial^3 v}{\partial z^2 \partial x} \right) U_B$$
$$- \left(\frac{\partial^2 u}{\partial x^2} + 2 \frac{\partial^2 u}{\partial y^2} + \frac{\partial^2 u}{\partial z^2} + \frac{\partial^2 v}{\partial y \partial x} \right) U_B' - \left(2 \frac{\partial u}{\partial y} + \frac{\partial v}{\partial x} \right) U_B'',$$

$$\hat{N}_z = - \left(\frac{\partial^3 w}{\partial x^3} + \frac{\partial^3 w}{\partial y^2 \partial x} + \frac{\partial^3 w}{\partial z^2 \partial x} \right) U_B$$
$$- \left(\frac{\partial^2 u}{\partial z \partial y} + \frac{\partial^2 v}{\partial z \partial x} \right) U_B' - \frac{\partial u}{\partial z} U_B''.$$

We rewrite these using the definition of disturbance vorticity $\boldsymbol{\omega}$ in order to isolate derivatives with respect to the wall-normal component y for computational reasons, which gives

$$\hat{N}_x = - \left(\frac{\partial^3 u}{\partial x^3} + \frac{\partial^3 u}{\partial z^2 \partial x} \right) U_B - \frac{\partial^2 v}{\partial x^2} U_B' - \frac{\partial u}{\partial x} U_B'' - v U_B'''$$
$$- \frac{\partial}{\partial y} \left(\left(\frac{\partial^2 v}{\partial x^2} - \frac{\partial \omega_z}{\partial x} \right) U_B \right),$$

$$\hat{N}_y = - \left(\frac{\partial^3 v}{\partial x^3} + \frac{\partial^3 v}{\partial z^2 \partial x} \right) U_B - \left(\frac{\partial^2 u}{\partial x^2} + \frac{\partial^2 u}{\partial z^2} \right) U_B' - \frac{\partial v}{\partial x} U_B''$$
$$- \frac{\partial^2}{\partial y^2} \left(\frac{\partial v}{\partial x} U_B + 2u U_B' \right) + \frac{\partial}{\partial y} \left(\frac{\partial v}{\partial x} U_B' + 2u U_B'' \right),$$

$$\hat{N}_z = - \left(\frac{\partial^3 w}{\partial x^3} + \frac{\partial^3 w}{\partial z^2 \partial x} \right) U_B + \left(\frac{\partial \omega_x}{\partial x} + \frac{\partial \omega_z}{\partial z} - \frac{\partial^2 v}{\partial z \partial x} \right) U_B'$$
$$- \frac{\partial u}{\partial z} U_B'' - \frac{\partial}{\partial y} \left(\left(\frac{\partial \omega_x}{\partial x} + \frac{\partial^2 v}{\partial x \partial z} \right) U_B \right).$$

3.2.3. Normal mode form. We assume a normal mode form for the disturbances in a similar fashion as in Section 2.3, as follows

$$\mathbf{u}(x, y, z, t) = \tilde{\mathbf{u}}(y, t) e^{i(\alpha x + \beta z)}, \quad \boldsymbol{\omega}(x, y, z, t) = \tilde{\boldsymbol{\omega}}(y, t) e^{i(\alpha x + \beta z)},$$

where α and β are the streamwise and spanwise wavenumbers. The equations (3.9), omitting the tilde for a simpler notation, become

$$\frac{\partial \omega_x}{\partial t} + K_0 \left(k^2 - \mathcal{D}^2\right) \frac{\partial \omega_x}{\partial t} = -\frac{1}{Re_0} \left(k^2 - \mathcal{D}^2\right) \omega_x - \mathcal{D}N_z + i\beta N_y, \tag{3.13a}$$

$$\frac{\partial \omega_z}{\partial t} + K_0 \left(k^2 - \mathcal{D}^2\right) \frac{\partial \omega_z}{\partial t} = -\frac{1}{Re_0} \left(k^2 - \mathcal{D}^2\right) \omega_z - i\alpha N_y + \mathcal{D}N_x, \tag{3.13b}$$

$$\left(k^2 - \mathcal{D}^2\right) v = i\beta \omega_x - i\alpha \omega_z, \tag{3.13c}$$

where $k^2 = \alpha^2 + \beta^2$ and $\mathcal{D} = \partial/\partial y$. The vector $\mathbf{N}$ is decomposed into a Newtonian, $\hat{\mathbf{N}}^0$, and non-Newtonian part, $\hat{\mathbf{N}}$, i.e.

$$\mathbf{N} = \hat{\mathbf{N}}^0 + K_0 \hat{\mathbf{N}}.$$

The Newtonian term $\hat{\mathbf{N}}^0$ has components

$$\begin{aligned}
\hat{N}_x^0 &= U_B' v, \\
\hat{N}_y^0 &= U_B \omega_z - U_B' u, \\
\hat{N}_z^0 &= -U_B \omega_y,
\end{aligned} \tag{3.14}$$

while the non-Newtonian term $\hat{\mathbf{N}}$ has components

$$\begin{aligned}
\hat{N}_x &= \hat{N}_x^1 + \mathcal{D}\hat{N}_x^2 = i\alpha k^2 u U_B + \alpha^2 v U_B' - i\alpha u U_B'' - v U_B''' \\
&\quad + \mathcal{D}\left(\left(\alpha^2 v + i\alpha \omega_z\right) U_B\right), \\
\hat{N}_y &= \hat{N}_y^1 + \mathcal{D}\hat{N}_y^2 + \mathcal{D}^2 \hat{N}_y^3 = i\alpha k^2 v U_B + k^2 u U_B' - i\alpha v U_B'' \\
&\quad + \mathcal{D}\left(i\alpha v U_B' + 2u U_B''\right) \\
&\quad - \mathcal{D}^2 \left(i\alpha v U_B + 2u U_B'\right), \\
\hat{N}_z &= \hat{N}_z^1 + \mathcal{D}\hat{N}_z^2 = i\alpha k^2 w U_B + \left(i\alpha \omega_x + i\beta \omega_z + \alpha\beta v\right) U_B' \\
&\quad - i\beta u U_B'' - \mathcal{D}\left(\left(i\alpha \omega_x - \alpha\beta v\right) U_B\right).
\end{aligned} \tag{3.15}$$

Notice that we separated terms in order to facilitate the application of the numerical scheme, which will be explained in detail in the next section.
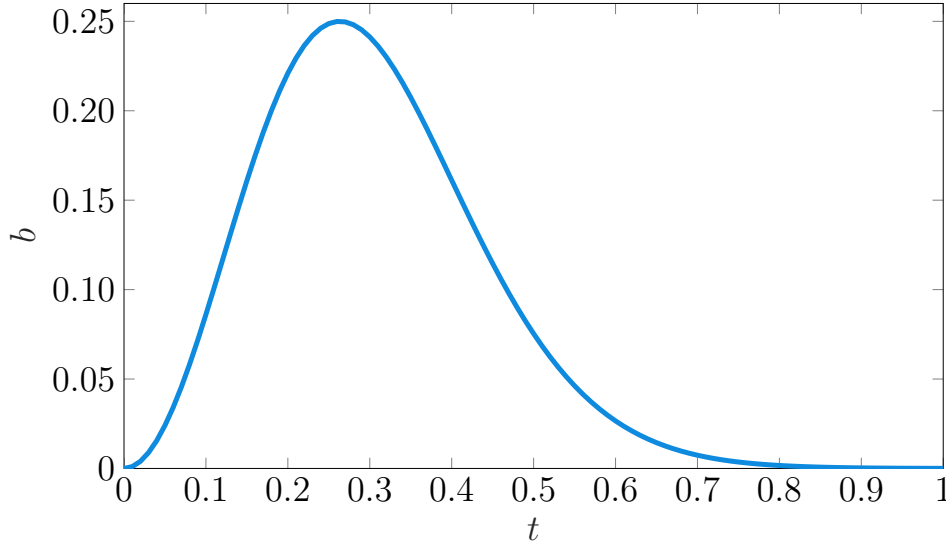
FIGURE 3.1. Temporal evolution of the impulse for $\sigma = 10$.

3.3. Numerical methods

In this section, we give an overview of the numerical techniques employed to solve the system of time-dependent PDEs (3.13). The flow is disturbed by a temporally localised forced impulse of the form

$$\eta(t) = b(t)e^{i(\alpha x + \beta z)}, \tag{3.16}$$

where η represents the height of the wall at a given time and b represents a time-dependent amplitude, given by

$$b(t) = (1 - e^{-\sigma t^2})e^{-\sigma t^2},$$

and σ is the parameter which characterises the timescale of the impulse. Figure 3.1 shows the temporal evolution of the impulse $b(t)$ for $\sigma = 10$.

The wall is only allowed to move in the wall-normal direction. Therefore, the boundary conditions for the disturbance velocities, after linearisation about the undisturbed wall at $y = 0$, become

$$u(0) = -b(t)U_B'(0), \quad v(0) = b'(t), \quad w(0) = 0. \tag{3.17}$$

The primary perturbation variables are expanded in terms of odd Chebyshev polynomials and mapping the physical wall-normal coordinate $y \in [0, \infty)$ to the computational coordinate $\xi \in (0, 1]$ by means

of the transformation (3.5). An even representation is chosen for the secondary variables and the base flow profile U_B. The equations are then integrated twice with respect to ξ. We apply a predictor-corrector method for the convective quantity $\mathbf{N}$ and for some other terms. The system is then solved by marching in time with a second order two-step scheme.

As a first step, to facilitate the application of the numerical scheme, we can rewrite the system (3.13) as follows

$$\frac{\partial \omega_x}{\partial t} + K_0 \left(k^2 - \mathcal{D}^2\right) \frac{\partial \omega_x}{\partial t} = \frac{1}{Re_0} \frac{\partial^2 \omega_x}{\partial y^2} + A_x + \mathcal{D}B_x + \mathcal{D}^2 C_x,$$

$$\frac{\partial \omega_z}{\partial t} + K_0 \left(k^2 - \mathcal{D}^2\right) \frac{\partial \omega_z}{\partial t} = \frac{1}{Re_0} \frac{\partial^2 \omega_z}{\partial y^2} + A_z + \mathcal{D}B_z + \mathcal{D}^2 C_z, \quad \text{(3.18)}$$

$$\left(k^2 - \mathcal{D}^2\right) v = i\beta \omega_x - i\alpha \omega_z,$$

where

$$A_x = -\frac{k^2}{Re_0} \omega_x + i\beta \left(\hat{N}_y^0 + K_0 \hat{N}_y^1\right),$$

$$B_x = -\hat{N}_z^0 - K_0 \hat{N}_z^1 + i\beta K_0 \hat{N}_y^2,$$

$$C_x = -K_0 \hat{N}_z^2 + i\beta K_0 \hat{N}_y^3,$$

$$A_z = -\frac{k^2}{Re_0} \omega_z - i\alpha \left(\hat{N}_y^0 + K_0 \hat{N}_y^1\right),$$

$$B_z = \hat{N}_x^0 + K_0 \hat{N}_x^1 - i\alpha K_0 \hat{N}_y^2,$$

$$C_z = K_0 \hat{N}_x^2 - i\alpha K_0 \hat{N}_y^3,$$

where terms of the form $\hat{N}_m^k$ are defined by equations (3.14) and (3.15). Dividing the system (3.18) by ξ^2, integrating twice with respect to ξ between 0 and 1 and applying integration by parts, we obtain

$$\frac{\partial I_2 \tilde{\omega}_x}{\partial t} + K_0 \left(k^2 \frac{\partial I_2 \tilde{\omega}_x}{\partial t} - \frac{1}{l^2} \frac{\partial J_2 \tilde{\omega}_x}{\partial t}\right) = \frac{1}{l^2 Re_0} J_2 \tilde{\omega}_x \quad \text{(3.19a)}$$

$$+ I_2 \tilde{A}_x - \frac{1}{l} I_1 B_x + \frac{1}{l^2} J_2 \tilde{C}_x,$$

$$\frac{\partial I_2 \tilde{\omega}_z}{\partial t} + K_0 \left(k^2 \frac{\partial I_2 \tilde{\omega}_z}{\partial t} - \frac{1}{l^2} \frac{\partial J_2 \tilde{\omega}_z}{\partial t}\right) = \frac{1}{l^2 Re_0} J_2 \tilde{\omega}_z \quad \text{(3.19b)}$$

$$+ I_2 \tilde{A}_z - \frac{1}{l} I_1 B_z + \frac{1}{l^2} J_2 \tilde{C}_z,$$

$$\left(-k^2 I_2 + \frac{1}{l^2} J_2\right) \tilde{v} = i\alpha I_2 \tilde{\omega}_z - i\beta I_2 \tilde{\omega}_x, \quad \text{(3.19c)}$$

where the tilde indicates quantities divided by ξ^2. The operators I_1, I_2, J_2 are integral operators, defined as follows

$$I_1 f = \int f \, d\xi,$$

$$I_2 f = \iint f \, d\xi,$$

$$J_2 f = \xi^4 f - 2 \int \left(\xi^3 f \right) \, d\xi.$$

3.3.1. Temporal discretisation. The two ODEs (3.19a) (3.19b) for the vorticity components $\tilde{\omega}_x$, $\tilde{\omega}_z$ can be written on the form

$$y'(t) = f(t, y), \quad y(t = 0) = y_0.$$

For the purpose of this work, we consider $y_0 = 0$. A disturbance in the flow is induced by imposing a temporally localised forced impulse, as described at the beginning of this section.

In order to solve this system starting from an initial condition y_0, we employ an Adams predictor-corrector scheme which is of second order in time and consists of two steps:

(1) Predictor step: we apply the two-step Adams-Bashforth method, as follows

$$y_{n+1}^P = y_n + \frac{\Delta t}{2} \left[3f\left(t_n, y_n\right) - f\left(t_{n-1}, y_{n-1}\right) \right],$$

where y_n approximates the solution y at the time $t_n = n\Delta t$, Δt is the time discretisation parameter and y_{n+1}^P is the predicted solution.

(2) Corrector step: we apply the two-step Adams-Moulton method, as follows

$$y_{n+1} = y_n + \frac{\Delta t}{2} \left[f\left(t_{n+1}, y_{n+1}^P\right) + f\left(t_n, y_n\right) \right].$$

Notice that the Poisson equation (3.19c) can be solved directly at each time-step, given $\tilde{\omega}_x$, $\tilde{\omega}_z$, to obtain the wall-normal velocity $\tilde{v}$. More details regarding the implementation of the numerical scheme can be found in Section 5.6.

3.4. Results

We validate the results of the simulations by comparing them against the solutions obtained by solving the eigenvalue problem. We compare the temporal growth rate, ω_i, obtained from the eigenvalue analysis, as described in Section 1.7, with the final growth rate calculated through the simulations, when it settles to a constant value.

The temporal growth rate can be determined from the simulations using the following formula

$$\omega_S = \frac{i}{A} \frac{\partial A}{\partial t},$$

where A is the amplitude of a computed variable. The variable chosen for the simulations is the spanwise vorticity at the wall, $\omega_z(0)$.

We chose to run the simulations for $t \in [0, T]$, where T is sufficiently large for all the transient behaviour to pass and the growth rates to settle to a constant value. Then, the temporal growth rate ω_i is compared with the imaginary part of

$$\omega_S(T) \approx \lim_{t \to \infty} \omega_S.$$

For the purpose of the simulations in this chapter we use a time discretisation parameter $\Delta t \approx 0.01$.

Figure 3.2(a) shows the temporal evolution of the temporal growth rate calculated with the simulations $\omega_{S,i}$ for the flat plate case, where $\beta_H = 0$. We can see that, for sufficiently large values of t/T, the growth rate $\omega_{S,i}$ settles to a constant value which coincides with the solution to the eigenvalue problem, ω_i. The error between the two computed growth rates at $t/T = 1$ is $O(10^{-5})$. In Figure 3.2(b), we plotted the temporal evolution of the wall-normal vorticity at the wall, i.e. $\omega_z(0)$. Since the choice of parameters ($Re_0 = 500, \alpha = 0.3, \beta = 0.2, K = -10^{-5}$) gives an exponentially stable mode, after an initial oscillation caused by the wall-normal impulse, $\omega_z(0)$ tends to zero as time increases. Figure 3.2(c) shows the temporal evolution of the wall vorticity, $\omega_z(0)$, in a logarithmic scale compared with the temporal evolution as predicted by the eigenvalue problem.
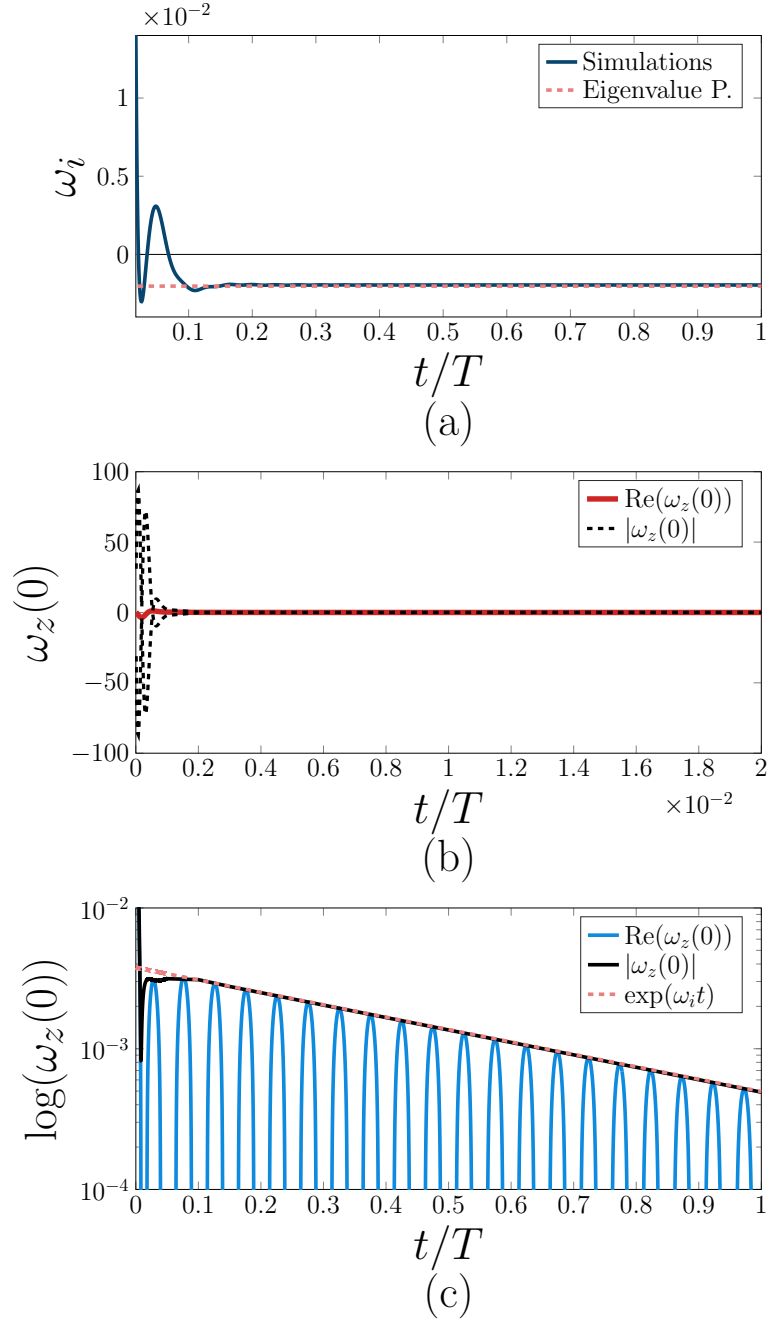
FIGURE 3.2. Numerical simulation for the flat plate case with $\beta_H = 0, Re_0 = 500, \alpha = 0.3, \beta = 0.2, K = -10^{-5}$ and $T = 1000$. (a) Comparison between the simulated temporal growth rates (–) and solution to the eigenvalue problem (--); (b) Evolution of $\omega_z(0)$, the wavepacket envelope $\pm|\omega_z(0)|$ is also shown (--); (c) Evolution of $\omega_z(0)$ in a logarithmic scale and its approximated evolution given by the eigenvalue problem (--).
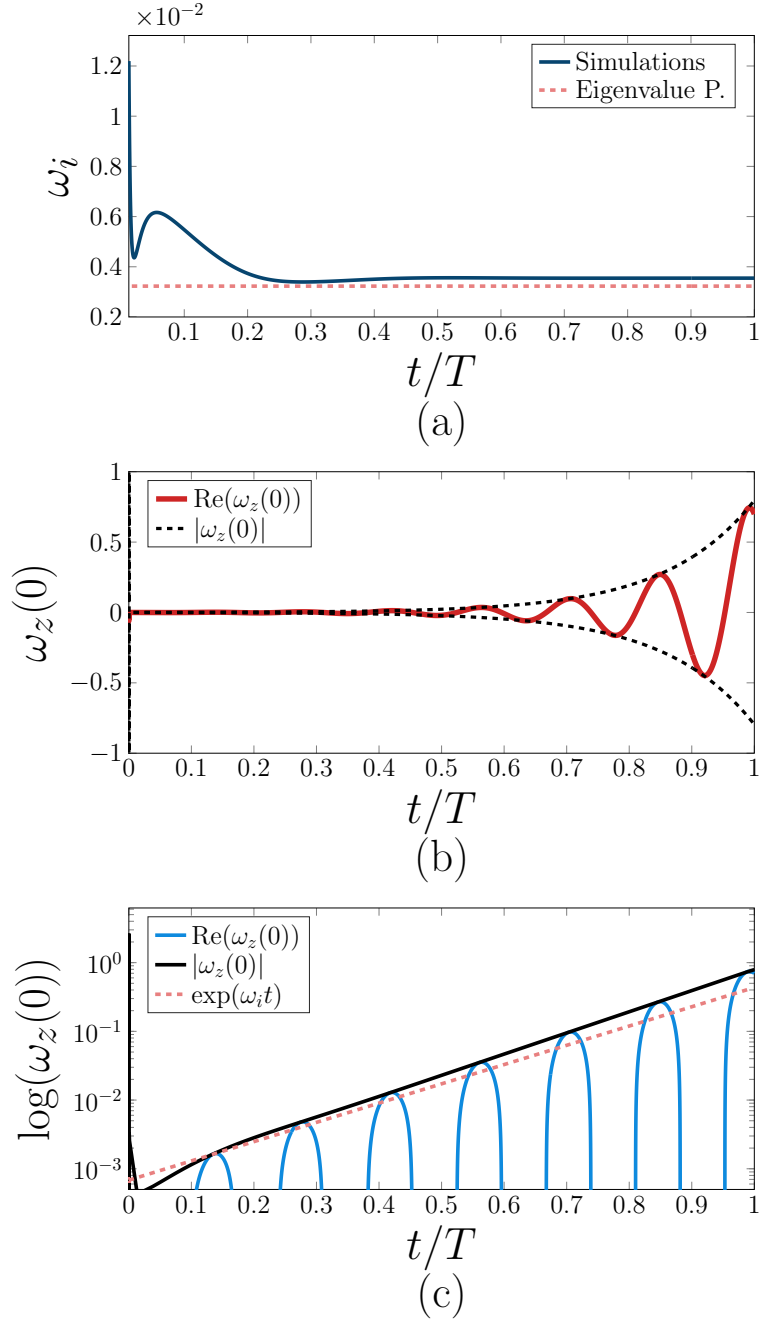
FIGURE 3.3. Numerical simulation for the flat plate case with $\beta_H = 0, Re_0 = 1000, \alpha = 0.05, \beta = 0.5, K = 0.01$ and $T = 2000$. (a) Comparison between the simulated temporal growth rates $(-)$ and solution to the eigenvalue problem $(--)$; (b) Evolution of $\omega_z(0)$, the wavepacket envelope $\pm|\omega_z(0)|$ is also shown $(--)$; (c) Evolution of $\omega_z(0)$ in a logarithmic scale and its approximated evolution given by the eigenvalue problem $(--)$.
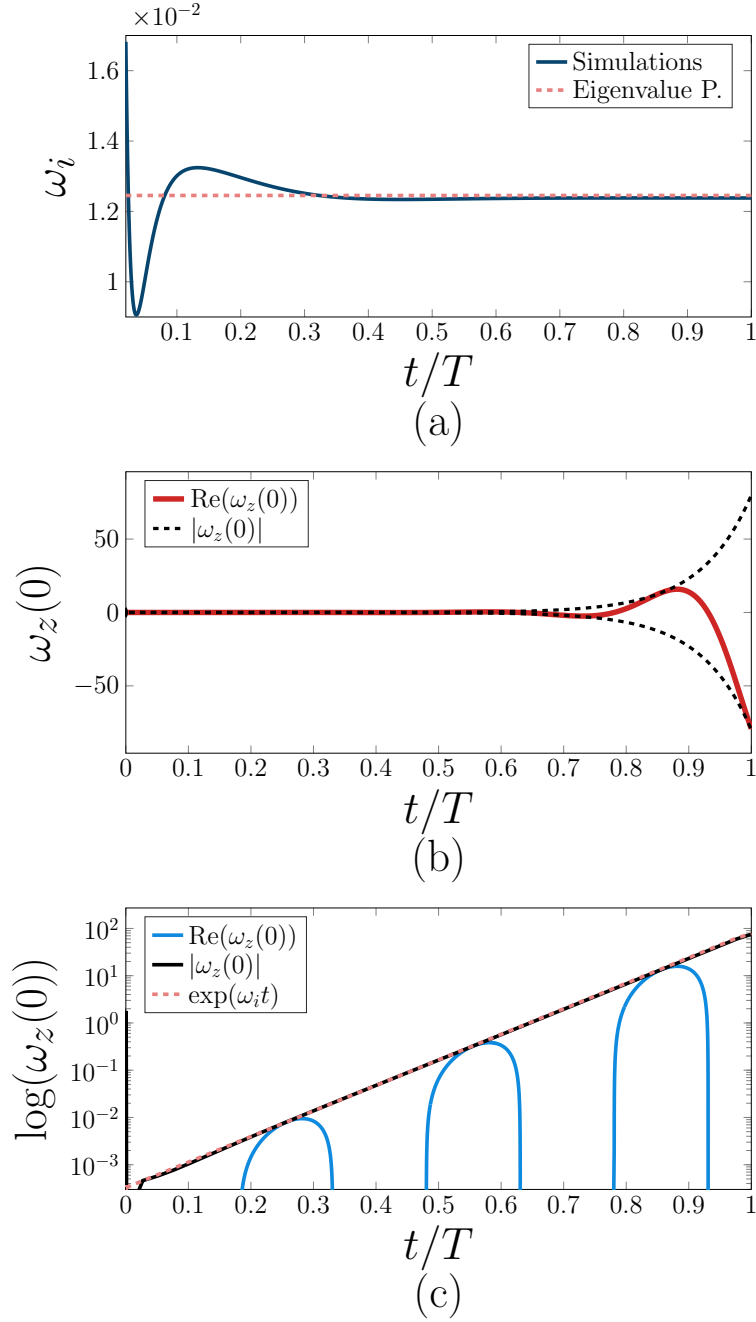
FIGURE 3.4. Numerical simulation for the flow past a wedge with $\beta_H = 0.5$, $Re_0 = 1000$, $\alpha = 0.05$, $\beta = 0.5$, $K = 0.01$ and $T = 1000$. (a) Comparison between the simulated temporal growth rates (–) and solution to the eigenvalue problem (- -); (b) Evolution of $\omega_z(0)$, the wavepacket envelope $\pm|\omega_z(0)|$ is also shown (- -); (c) Evolution of $\omega_z(0)$ in a logarithmic scale and its approximated evolution given by the eigenvalue problem (- -).
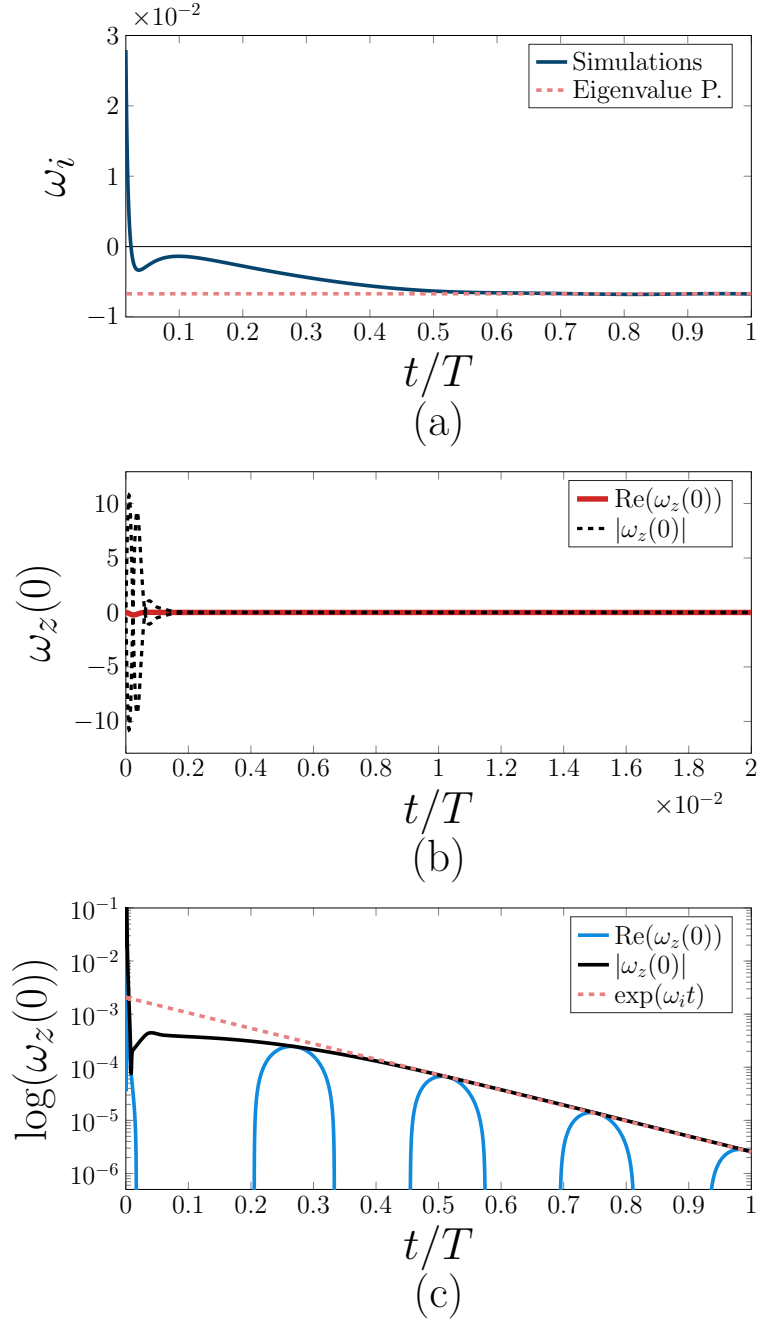
FIGURE 3.5. Numerical simulation for the flat plate case with $\beta_H = 1, Re_0 = 1000, \alpha = 0.05, \beta = 0.5, K = 0.0001$ and $T = 1000$. (a) Comparison between the simulated temporal growth rates (–) and solution to the eigenvalue problem (- -); (b) Evolution of $\omega_z(0)$, the wavepacket envelope $\pm|\omega_z(0)|$ is also shown (- -); (c) Evolution of $\omega_z(0)$ in a logarithmic scale and its approximated evolution given by the eigenvalue problem (- -).

In Figure 3.3 we show the results for the case of the flat plate ($\beta_H = 0$). The wavenumber vector $(\alpha, \beta) = (0.05, 0.5)$ represents disturbances mostly directed in the spanwise direction z. We observed in Section 1.7 that these waves can become exponentially unstable for certain positive values of the parameter K. In order to confirm this result, we run the simulation for $Re_0 = 1000$ and $K = 0.01$. As expected, the vorticity at the wall $\omega_z(0)$, does not decay asymptotically, as shown in Figure 3.3(b). Therefore, the simulations confirm the presence of an exponentially unstable mode for small streamwise wavenumbers α and positive K. Figure 3.3(a) shows that, when the growth rate given by the simulation, $\omega_{S,i}$, settles to a constant, it converges to the one given by the eigenvalue problem, ω_i. The error between the two computed growth rates at $t = T$ is $O(10^{-4})$.

In Figures 3.4 and 3.5, we show the results for the flow past a wedge, where $\beta_H = 0.5$, and for the stagnation point flow, where $\beta_H = 1$. In general, we see how the results of the simulations confirm the solutions to the eigenvalue problem. In both cases, the error between the growth rate given by the simulation, $\omega_{S,i}$, and the one given by the eigenvalue problem, ω_i, is $O(10^{-5})$ for large t.

We performed several tests of this type, varying the angle parameter β_H and the non-Newtonian parameter K. We observe that the simulated temporal growth rate agrees very well with the one calculated by solving the eigenvalue problem as described in Section 1.7. However, we notice an increased numerical sensitivity of the numerical scheme when the parameter K is negative. More specifically, it was not possible to report any result for values of K smaller than -10^{-5}. The reason is that the numerical scheme diverges when K is negative and larger than $O(10^{-5})$ in modulus. One possible explanation is the presence of a diffusive term in the non-Newtonian part $\hat{\mathbf{N}}$, given by equation (3.15), which would need to be treated implicitly. This is not straightforward to implement since $\hat{\mathbf{N}}$ involves the mean flow profile. An attempt, without success, to solve this problem was to repeat the corrector step a few times to achieve convergence. However, for all the positive values of the non-Newtonian parameter K we observed a good agreement, for large t,

between the growth rates calculated with the DNS and the ones given by the solution to the eigenvalue problem.

CHAPTER 4

Other viscoelastic models

In this chapter, we consider the flow of more complex viscoelastic fluids. As mentioned in Chapter 1, the second order model is suitable to study the effects of non-zero normal stress differences. This model predicts a constant shear viscosity and it is not used in practice. However, the second order model has been chosen as a "toy problem" for its simplicity and the possibility of applying a boundary layer approximation similarly to Newtonian fluids.

Viscoelastic fluids can be said to lie in between viscous fluids and elastic solids (Phan-Thien [59]). Viscous fluids resist forces exerted upon them through internal friction and they instantaneously forget the shape they are in. For these fluids, the stress is directly proportional to the rate of strain (Newtonian law). Elastic solids always remember the shape they start from and, when the stress is removed, they relax back to their original shape. The stress experienced by the solid is directly proportional to the strain. Instead, viscoelastic fluids remember the shape until its molecules have the time to relax. The stress is neither directly proportional to the strain nor the rate of strain, but the relationship is more complicated.

In particular, polymeric fluids are characterised by the presence of long chain molecules which are made from joining together small molecules (Barnes *et al.* [4]). The polymers affect the flow by the way they align to the motion of the fluid, they are stretched and they retract back to their unstressed configuration. Polymeric fluids can be said to have a memory of their previous flow history.

We can distinguish two approaches that are widely used in order to model the behaviour of materials: one is based on continuum mechanics and one on microstructural theories (Tanner [82], Sibley [78]). The

123

derivation of models such as the Upper-Convected Maxwell (UCM) and the Oldroyd B models is based on continuum mechanics. These are examples of models of differential type that are suitable to describe only dilute solutions of polymer molecules. The UCM and Oldroyd-B models are the simplest nonlinear viscoelastic models and cannot represent any shear-thinning behaviour. Moreover, they predict zero second normal stress difference and the extensional viscosity is not bounded.

Models such as the Phan-Thien Tanner and Giesekus models can be considered to be extensions of the Oldroyd B constitutive equation for the polymeric stress that include additional terms so as to provide a model with shear-thinning behaviour, bounded extensional viscosity and a non-zero second normal stress difference.

There are broadly three approaches to deriving constitutive equations from miscrostructural theories (Barnes *et al.* [**4**]):

- Dilute solution theories: each particle interacts only with the solvent and not with other suspended particles. The polymer molecules are treated individually and modelled as a chain of beads and springs or beads and rods. Both the UCM and the Oldroyd B models can be derived in that way.
- Network theories: for concentrated solutions and melts there are particle-particle interactions. A polymer is considered as a network of springs linked at junction points. The Phan-Thien Tanner model was originally derived using these network theories.
- Reptation theories: the motion of each molecule is reduced by the surrounding polymers, which are assumed to form a tube around the polymer.

There is a vast and increasing number of constitutive models available. The models we focus on in this chapter were chosen because they can represent some non-Newtonian features while remaining relatively simple. We take into consideration four different viscoelastic models (UCM, Oldroyd B, Phan-Thien Tanner and Giesekus models) and use a single constitutive equation to represent them all.

The purpose is to study the stability characteristics. We start by considering the asymptotic suction boundary layer (ASBL) theory to determine the mean flow. We show that, similarly to the Newtonian case, for the UCM and the Oldroyd B models, it is possible to obtain an analytical solution which results in an exponential profile. For the Phan-Thien Tanner and the Giesekus models, the equations simplify considerably and can be solved numerically.

Section 4.1 provides an overview of the main literature regarding viscoelastic fluids in boundary layers and their stability properties. In Section 4.2, we introduce the viscoelastic models and derive the governing equations. In Section 4.3, the mean flow is derived by applying an asymptotic suction boundary layer. In Section 4.4, we perform the first steps to study the linear stability.

4.1. Literature review

In this section, we summarise some of the results obtained regarding boundary layers of viscoelastic fluids and stability results without any claim to completeness.

4.1.1. Boundary layers. Beard and Walters [6] considered flow of liquid B' (designed by Walters) near a stagnation point, using boundary layer approximations. The Oldroyd B model is a special case of liquid B'. For mathematical convenience, Beard and Walters restricted the analysis to liquids with short memories (i.e. short relaxation times). This approximation is reasonable because boundary layers are thought to develop in viscoelastic fluids that are not highly elastic. If the flow is regarded as a perturbation of the Newtonian viscous flow, the concept of a boundary layer can be expected to apply. A self-similar solution is only possible for the stagnation point flow.

Bhatnagar *et al.* [7] considered the flow of an Oldroyd B fluid due to a stretching sheet in the presence of a constant free-stream velocity. The governing equations are reduced by introducing a similarity transformation for the velocity field and for the components of the stress tensor. The problem is solved by applying a regular perturbation

analysis in terms of the Weissenberg number. This solution is in agreement with the numerical solution found by adding a physically acceptable boundary condition.

Sajid *et al.* [**72**] derived boundary layer equations for an Oldroyd B fluid in the region of a stagnation point over a stretching sheet. They followed the approach described by Harris [**38**] for an upper-convected Maxwell fluid and obtained a similarity solution. The equations derived by Sajid *et al.* [**72**] differ from the ones derived by Beard and Walters [**6**]. The approach described by Harris [**38**] consists of applying the Oldroyd derivative operator to the momentum equations and inter-exchanging the operators of divergence and Oldroyd derivative for the extra-stress tensor. In principle, this is not consistent.

Later, several authors utilised the same approach as Sajid *et al.* [**72**]. Hayat *et al.* [**39**] studied the stagnation flow subject to convective boundary conditions of an Oldroyd B fluid. The boundary layer equations used are the same as Sajid *et al.* [**72**]. Abbasbandy *et al.* [**1**] investigated the Falkner-Skan flow of MHD Oldroyd B fluid using the same boundary layer equations as in Sajid *et al.* [**72**].

4.1.2. Flow in the far field. All the papers related to the mean flow determination summarised in the previous section assume a potential flow at infinity. In general this is not obvious because irrotational flow is not, in general, compatible with the non-Newtonian equations. As remarked in Section 1.3, Joseph and Liao [**47**] provided a condition for the extra-stress tensor for an irrotational flow to satisfy the equations. Not many constitutive equations are compatible with irrotational solutions. This condition is satisfied by inviscid and viscous Newtonian fluids, linear viscoelastic fluids and for second order fluids.

Therefore, by assuming an irrotational flow at infinity there is an implicit assumption that elastic effects affect only the boundary layer region.

4.1.3. Stability of viscoelastic fluids. Porteous and Denn [**61**] studied the linear stability analysis of plane Poiseuille flow for the

second order and Maxwell fluids. They showed that the second order model, for which $\alpha_1 < 0$ (see Section 1.1), is a consistent approximation to the Maxwell model in the limit of small elasticity (i.e. elasticity number $K \ll 1$ and Weissenberg number $Wi = KRe \ll 1$) and when the disturbance time scale is large compared to the characteristic time scale of the fluid. The results shows a destabilisation process due to elasticity. At high values of K the stability is qualitatively different than that for Newtonian fluids because it results from the second mode of the Orr-Sommerfeld equation.

Ho and Denn [41] also examined the stability of Poiseuille flow of a Maxwell fluid focusing on providing an explanation for a phenomenon called "melt fracture", a low Reynolds number extrusion instability. They showed that at low Reynolds numbers the flow is stable and at higher Reynolds numbers elasticity has a destabilising effect. They commented on experimental results on melt fracture in high density polyethylene. The growth of infinitesimal disturbances cannot be the mechanism for melt fracture.

Sureshkumar and Beris [80] used an Arnoldi-based orthogonalization algorithm to investigate the linear stability of Poiseuille flow. The models investigated are UCM, Oldroyd B and Chilcott-Rallison fluids. The results show that the destabilisation caused by elasticity for the UCM fluid is reduced when effects of solvent viscosity and finite extensibility are taken into account.

Palmer and Phillips [57] studied the spectra of linear Phan-Thien Tanner liquids for plane Poiseuille flow. The base flow was solved numerically using a Chebyshev-tau method. The linear stability equations are also discretised using Chebyshev approximations. The spectrum includes a continuous and a discrete part. The results are validated for the UCM and Oldroyd B models, which are special cases of the PPT model, by comparing with results in the literature. The linear PPT fluid is stable for the range of parameters considered.

4.2. Governing equations

In this section we present four different constitutive equations for viscoelastic fluids. These are all derived using a microstructural approach, which takes into account the polymer molecule behaviour. We derive a single constitutive equation to represent the four models considered and facilitate the application of the asymptotic suction boundary layer.

4.2.1. Upper-Convected Maxwell model.

The Upper-Convected Maxwell (UCM) model can be derived by representing a viscoelastic fluid by dumbbells immersed in a Newtonian solvent. This can be represented using a mechanical model consisting of a spring and a dashpot in series (Palmer [56], Owen and Phillips [54]). An element composed of a spring and a dashpot in series is known as *Maxwell element*. The spring obeys Hooke's law for perfectly elastic solids and the dashpot follows the Newtonian law for purely viscous fluids. The UCM model is one of the most important viscoelastic models, because more complicated models are based on modifications of this one.

For this model, the stress tensor follows the constitutive equation given by

$$\mathbf{T} + \lambda_1 \overset{\triangledown}{\mathbf{T}} = \eta_0 \dot{\boldsymbol{\gamma}},$$

where λ_1 is the *relaxation time* and η_0 is the viscosity of the viscous element constituting the dumbbell. The tensor $\dot{\boldsymbol{\gamma}} = \nabla\mathbf{v} + \nabla\mathbf{v}^T$ is the rate of strain and $\overset{\triangledown}{\mathbf{T}}$ represents the upper-convected derivative, which is defined as follows

$$\overset{\triangledown}{\mathbf{T}} = \frac{\mathrm{D}\mathbf{T}}{\mathrm{D}t} - (\nabla\mathbf{v})^T\mathbf{T} - \mathbf{T}(\nabla\mathbf{v}),$$

or, component-wise, as follows

$$\overset{\triangledown}{T}_{ij} = \frac{\partial T_{ij}}{\partial t} + v_k\frac{\partial T_{ij}}{\partial x_k} - \frac{\partial v_i}{\partial x_k}T_{kj} - T_{ik}\frac{\partial v_j}{\partial x_k}.$$

In the UCM model, the relaxation time, λ_1, is given by the ratio of the viscosity, η_0, to the spring constant, k, which is defined as the ratio of force acting on the spring to the displacement of the spring. The relaxation time is the time taken for the molecules to relax after

experiencing an instantaneous stretch due to a step strain being applied on the fluid. Notice that, when $\lambda_1 = 0$, we retrieve the Newtonian constitutive equation.

A constitutive equation must be independent of changes of reference frame, such as its translation, rotation or acceleration. This property is called *material frame-indifference*. The upper-convected derivative, also known as co-deformational derivative, is the rate of change as observed while deforming and translating with the fluid. This is only one of the possible adjustments to obtain frame-indifference which give rise to various Maxwell models. However, the UCM is preferred to the other Maxwell models since it gives the closest match to experimental data for N_2/N_1, the ratio of the second normal stress differences to the first normal stress differences. The definitions of first and second normal stress differences can be found in Section 1.2.1. Experimental data broadly suggests N_2/N_1 to be small in magnitude and negative for polymer melts and solutions (Tanner [**82**]). The UCM model predicts positive first normal stress difference and zero second normal difference.

This constitutive equation is very popular thanks to its simplicity, but it is not very realistic for the description of many polymers. The UCM model predicts a viscosity which is constant in steady simple shear flow (Figure 1.2) and equal to η_0. In steady extensional flow, the extensional viscosity is not bounded. For the definition of steady simple shear and extensional flow, we refer to Section 1.2.1.

The UCM model may also be derived from dilute solution theory. This is achieved by modelling the polymer molecules individually as a linear elastic dumbbell, which consists of two beads connected by a spring.

4.2.2. Oldroyd B model. The UCM model only considers the polymer contribution to the stress. The Oldroyd B model comes from the linear superposition of the UCM model stress with the Newtonian contribution of the solvent. The constitutive equation includes an extra term for the Newtonian part of the fluid and an extra constant, referred

to as the *retardation time*. Thus, the Oldroyd B model can be seen as an extension of the UCM model (Owen and Phillips [**54**]).

The Oldroyd B model was derived by Oldroyd [**52**] in 1950. It can be obtained from a molecular model which consists of a suspension of Hookean dumbbells immersed in a Newtonian solvent, the dumbbells simulating the dynamics of polymer chains.

The equation for the stress tensor is as follows

$$\mathbf{T} + \lambda_1 \overset{\triangledown}{\mathbf{T}} = \eta_0 \left(\dot{\boldsymbol{\gamma}} + \lambda_2 \overset{\triangledown}{\dot{\boldsymbol{\gamma}}} \right),$$

where $\eta_0 = \eta_s + \eta_p$ is the total viscosity, which is the sum of the polymeric viscosity, η_p, and the solvent viscosity, η_s. The constant λ_2 is the retardation time of the solvent part of the liquid. Roughly, the retardation time is the delay in the strain response after imposition of a stress. The following relation between viscosities and characteristic times holds

$$\frac{\lambda_2}{\lambda_1} = \frac{\eta_s}{\eta_s + \eta_p}.$$

By separating the solvent and the polymeric contributions to the stress, as follows

$$\mathbf{T} = \eta_s \dot{\boldsymbol{\gamma}} + \boldsymbol{\tau},$$

we can write an equation for the elastic stress, $\boldsymbol{\tau}$, that is

$$\boldsymbol{\tau} + \lambda_1 \overset{\triangledown}{\boldsymbol{\tau}} = \eta_p \dot{\boldsymbol{\gamma}}.$$

The Oldroyd B model reduces to the UCM model when $\eta_s = 0$.

In steady simple shear flow the model predicts a quadratic first normal stress difference, a zero second normal stress difference and a constant viscosity. The Oldroyd B model has been found to qualitatively describe many of the features of Boger fluids, which are dilute solutions of polymers in highly viscous solvents (James [**44**]). Boger fluids are so dilute that the variation of viscosity with shear rate can be ignored. Moreover, they present a quadratic first normal stress difference like the second order fluids, as seen in Section 1.2.1. However, Boger fluids are not very common and the use of the Oldroyd B model in industry is limited.

Another major limitation is that the infinite extensibility of the Hookean spring leads to an extensional viscosity which blows up at a finite extensional rate. Various models have been proposed to overcome this flaw by constraining the length of the dumbbell to a maximum allowable length. One example is the Giesekus model which will be described later in this section.

4.2.3. Phan-Thien Tanner model. The Phan-Thien Tanner (P-TT) model was proposed by Phan-Thien and Tanner [**83**] in 1977. Unlike UCM and Oldroyd B models, it is derived from a non-dilute situation, assuming the polymer chains form a network. The PPT model is based on the Lodge-Yamamoto network theory, which states that the polymer liquid forms a network of molecules with temporary junctions. The junctions are supposed to appear and disappear so that the network configuration keeps changing. The strands connecting the junctions are able to transmit force. More details about the derivation of this model can be found, for example, in Tanner [**82**].

The stress tensor is given by the sum of the solvent and the polymeric contributions to the stress, i.e.

$$\mathbf{T} = \eta_s \dot{\boldsymbol{\gamma}} + \boldsymbol{\tau},$$

where $\boldsymbol{\tau}$ is the elastic stress which satisfies the following relation

$$\boldsymbol{\tau} + \lambda_1 \overset{\triangledown}{\boldsymbol{\tau}} + \xi \frac{\lambda_1}{2} \left(\dot{\boldsymbol{\gamma}} \boldsymbol{\tau} + \boldsymbol{\tau} \dot{\boldsymbol{\gamma}} \right) + f(\boldsymbol{\tau}) \boldsymbol{\tau} = \eta_p \dot{\boldsymbol{\gamma}}.$$

The PTT model is called exponential when

$$f(\boldsymbol{\tau}) = \exp \left(\epsilon \frac{\lambda_1}{\eta_p} \mathrm{tr}(\boldsymbol{\tau}) \right) - 1,$$

and it is called linear when

$$f(\boldsymbol{\tau}) = \epsilon \frac{\lambda_1}{\eta_p} \mathrm{tr}(\boldsymbol{\tau}).$$

The linear PTT model could be considered to be a linearisation of its exponential equivalent.

The parameters in this model are the relaxation time λ_1, the solvent and the polymer viscosities, η_s and η_p, respectively. The parameters $\xi \in [0, 2]$ and $\epsilon \in [0, 1]$ are known as the *extensional* and *shear-thinning*

parameters, respectively. They are specific to the PTT model and determined experimentally by fitting the model to data for elongational and shearing flows. Typical values for ξ are $O(10^{-2})$ and for ϵ are $O(10^{-1})$ (Tanner [**82**]).

Notice that by choosing $\xi = \epsilon = 0$, we recover the Oldroyd B model and, when $\xi = \epsilon = \eta_p = 0$, we recover the UCM model. PTT can be seen as an improvement on the Oldroyd B model, since it incorporates shear-thinning behaviour and it gives a bounded extensional viscosity. However, it does not give a non-zero second normal stress difference.

4.2.4. Giesekus model. The Giesekus model was derived in 1982 by Giesekus [**33**], who introduced the idea of a non-isotropic drag on the beads. The derivation is based on kinetic theory of dilute solutions.

The elastic part of the stress tensor is modelled by

$$\boldsymbol{\tau} + \lambda_1 \overset{\triangledown}{\boldsymbol{\tau}} + \alpha \frac{\lambda_1}{\eta_p} \boldsymbol{\tau}^2 = \eta_p \dot{\boldsymbol{\gamma}}.$$

In this model α is the so-called *mobility parameter* with $\alpha \in [0, 1]$. When $\alpha = 0$, we recover the UCM model. With this model, the second normal stress difference is non-zero (negative) in shearing and the elongational viscosity is bounded.

4.2.5. A single constitutive equation. We write a single constitutive equation to represent all the viscoelastic models introduced in the previous sections in order to facilitate the study. The governing equations are

$$\begin{cases} \nabla \cdot \mathbf{v} = 0, \\ \rho \dfrac{\mathrm{D}\mathbf{v}}{\mathrm{D}t} = -\nabla p + \nabla \cdot \boldsymbol{\tau} + \eta_s \Delta \mathbf{v}, \end{cases} \tag{4.1}$$

where the elastic stress tensor $\boldsymbol{\tau}$ satisfies the constitutive equation

$$\boldsymbol{\tau} + \lambda_1 \overset{\triangledown}{\boldsymbol{\tau}} + g(\boldsymbol{\tau}, \dot{\boldsymbol{\gamma}}) = \eta_p \dot{\boldsymbol{\gamma}}. \tag{4.2}$$

The function g is defined as follows

$$g(\boldsymbol{\tau}, \dot{\boldsymbol{\gamma}}) = \xi \frac{\lambda_1}{2} \left(\dot{\boldsymbol{\gamma}} \boldsymbol{\tau} + \boldsymbol{\tau} \dot{\boldsymbol{\gamma}} \right) + \delta_{\mathrm{L}} \epsilon \frac{\lambda_1}{\eta_p} \mathrm{tr}(\boldsymbol{\tau}) \boldsymbol{\tau} \tag{4.3}$$

$$+ \delta_{\mathrm{E}} \left[\exp \left(\epsilon \frac{\lambda_1}{\eta_p} \mathrm{tr}(\boldsymbol{\tau}) \right) - 1 \right] \boldsymbol{\tau} + \alpha \frac{\lambda_1}{\eta_p} \boldsymbol{\tau}^2,$$

where the additional parameters $\delta_{\mathrm{L}}, \delta_{\mathrm{E}}$ are included to select the linear and the exponential PTT models, respectively. The various models can be retrieved by appropriate choices of the parameters:

- Newtonian for $\eta_s = \lambda_1 = \xi = \epsilon = \alpha = 0$;
- Upper-Convected Maxwell model for $\eta_s = \xi = \epsilon = \alpha = 0$;
- Oldroyd B model for $\xi = \epsilon = \alpha = 0$;
- Linear PTT model for $\delta_{\mathrm{L}} = 1, \delta_{\mathrm{E}} = 0, \alpha = 0$;
- Exponential PTT model for $\delta_{\mathrm{L}} = 0, \delta_{\mathrm{E}} = 1, \alpha = 0$;
- Giesekus model for $\xi = \epsilon = 0$.

4.3. Mean flow

In this section, we describe how we approximate the mean flow, which is the starting point to perform a linear stability analysis.

4.3.1. Two-dimensional governing equations.
The mean flow is assumed to be two-dimensional, therefore we can write the governing equations (4.1) as follows

$$\begin{cases} \dfrac{\partial u}{\partial x} + \dfrac{\partial v}{\partial y} = 0, \\[2mm] \rho \dfrac{\mathrm{D}u}{\mathrm{D}t} = -\dfrac{\partial p}{\partial x} + \dfrac{\partial \tau_{xx}}{\partial x} + \dfrac{\partial \tau_{xy}}{\partial y} + \eta_s \Delta u, \\[2mm] \rho \dfrac{\mathrm{D}v}{\mathrm{D}t} = -\dfrac{\partial p}{\partial y} + \dfrac{\partial \tau_{xy}}{\partial x} + \dfrac{\partial \tau_{yy}}{\partial y} + \eta_s \Delta v, \end{cases} \tag{4.4}$$

where $\mathbf{v} = (u, v)^T$, x is the streamwise direction and y is the wall-normal direction (see Figure 1.1). The equation for the elastic part of the stress tensor (4.2), written component by component, gives

$$\tau_{xx} + \lambda_1 \left[\frac{\partial \tau_{xx}}{\partial t} + u \frac{\partial \tau_{xx}}{\partial x} + v \frac{\partial \tau_{xx}}{\partial y} - 2 \left(\frac{\partial u}{\partial x} \tau_{xx} + \frac{\partial u}{\partial y} \tau_{xy} \right) \right]$$

$$+ \xi\lambda_1 \left[2\frac{\partial u}{\partial x}\tau_{xx} + \left(\frac{\partial u}{\partial y} + \frac{\partial v}{\partial x}\right)\tau_{xy} \right] + \delta_{\mathrm{L}}\epsilon\frac{\lambda_1}{\eta_p}(\tau_{xx} + \tau_{yy})\tau_{xx}$$

$$+ \delta_{\mathrm{E}} \left[\exp\left(\epsilon\frac{\lambda_1}{\eta_p}(\tau_{xx} + \tau_{yy})\right) - 1 \right]\tau_{xx} + \alpha\frac{\lambda_1}{\eta_p}(\tau_{xx}^2 + \tau_{xy}^2) = 2\eta_p\frac{\partial u}{\partial x},$$

$$\tau_{xy} + \lambda_1 \left[\frac{\partial \tau_{xy}}{\partial t} + u\frac{\partial \tau_{xy}}{\partial x} + v\frac{\partial \tau_{xy}}{\partial y} - \left(\frac{\partial u}{\partial y}\tau_{yy} + \frac{\partial v}{\partial x}\tau_{xx}\right) \right]$$

$$+ \xi\frac{\lambda_1}{2}\left(\frac{\partial u}{\partial y} + \frac{\partial v}{\partial x}\right)(\tau_{xx} + \tau_{yy}) + \delta_{\mathrm{E}} \left[\exp\left(\epsilon\frac{\lambda_1}{\eta_p}(\tau_{xx} + \tau_{yy})\right) - 1 \right]\tau_{xy}$$

$$+ \delta_{\mathrm{L}}\epsilon\frac{\lambda_1}{\eta_p}(\tau_{xx} + \tau_{yy})\tau_{xy} + \alpha\frac{\lambda_1}{\eta_p}(\tau_{xx}\tau_{xy} + \tau_{xy}\tau_{yy}) = \eta_p\left(\frac{\partial u}{\partial y} + \frac{\partial v}{\partial x}\right),$$

$$\tau_{yy} + \lambda_1 \left[\frac{\partial \tau_{yy}}{\partial t} + u\frac{\partial \tau_{yy}}{\partial x} + v\frac{\partial \tau_{yy}}{\partial y} - 2\left(\frac{\partial v}{\partial x}\tau_{xy} + \frac{\partial v}{\partial y}\tau_{yy}\right) \right]$$

$$+ \xi\lambda_1 \left[2\frac{\partial v}{\partial y}\tau_{yy} + \left(\frac{\partial u}{\partial y} + \frac{\partial v}{\partial x}\right)\tau_{xy} \right] + \delta_{\mathrm{L}}\epsilon\frac{\lambda_1}{\eta_p}(\tau_{xx} + \tau_{yy})\tau_{yy}$$

$$+ \delta_{\mathrm{E}} \left[\exp\left(\epsilon\frac{\lambda_1}{\eta_p}(\tau_{xx} + \tau_{yy})\right) - 1 \right]\tau_{yy} + \alpha\frac{\lambda_1}{\eta_p}(\tau_{xy}^2 + \tau_{yy}^2) = 2\eta_p\frac{\partial v}{\partial y}.$$

These equations were derived with MAPLE [**50**].

4.3.2. Difficulties in applying a boundary layer approximation. Unlike Newtonian and second order fluids (Rajagopal [**66**]), an irrotational flow does not satisfy the governing equations. This was the first step in order to apply a boundary layer approximation to the wedge flow configuration (Figure 1.1), as done in Section 1.3 for second order fluids. The outer layer was assumed to be irrotational and the velocity varied as a power law with the distance from the leading edge.

In Section 1.3.1, we pointed out a condition given by Joseph and Liao [**47**] for a constitutive equation to be compatible with irrotational solutions. This condition is satisfied by inviscid and viscous Newtonian fluids, linear viscoelastic fluids and for second order fluids. However, it is not straightforward to prove for the more complicated viscoelastic models that we study in this chapter.

Flows of the type $\mathbf{v} = (ax^m, 0)$ do not satisfy the irrotational governing equations. Alternatively, a linear stability analysis which

assumes a Newtonian base flow as a starting point for a linear stability analysis gives a zero mean polymeric stress. In this way, the only contribution of the function $g(\boldsymbol{\tau}, \sigma)$, which is defined by equation (4.3), to the linear stability equations is given by the term multiplied by ξ, because all the other terms are non-linear in $\boldsymbol{\tau}$.

For this chapter, we decided to focus our attention on the flat plate case. The mean flow is determined by applying an asymptotic suction boundary layer theory. For this purpose, we assume a constant free-stream velocity.

4.3.3. Asymptotic suction boundary layers. Applying a uniform suction is one of the techniques used in laminar flow control, which is a method to delay the laminar-turbulent transition. An asymptotic suction boundary layer (ASBL) profile develops in porous boundary layers, at some distance downstream of the leading edge, when uniform suction is applied over a large area through the surface (Schlichting [**73**], Fransson [**30**]). ASBL is one of the analytical solutions of the incompressible Navier-Stokes equations. An interesting feature of this theory is that an analytical solution can be easily obtained resulting in an exponential profile. The suction has a similar effect as a favourable pressure gradient in that it makes the Blasius profile more stable.

Another advantage of the ASBL is that it lacks the complications associated with spatially growing boundary layer flows. The boundary layer growth is counteracted by the constant homogeneous suction and the displacement thickness is a constant. The transition to turbulence for this flow has been widely studied for Newtonian fluids, both experimentally and numerically (Fransson [**30**], Khapko [**48**]).

The assumptions that are made in order to obtain an asymptotic suction profile are:

- steadiness, $\frac{\partial}{\partial t} = 0$;
- all variables depend only on y;
- constant suction at the wall $v(0) = -V_0$, where $V_0 > 0$ is the suction rate.

Notice that, in order to apply ASBL to the viscoelastic models considered, we also have to assume that the elastic stress tensor $\boldsymbol{\tau}$ depends only on y.

To obtain the stability characteristics, we need to derive a modified Orr-Sommerfeld equation to take into account the effects of the cross-flow velocity. When deriving the Orr-Sommerfeld and Squire's equations the assumption of parallel flow is made. This assumption may be argued to hold for a continuous suction case where the mean wall-normal velocity component is constant. In order to neglect the v-component the suction rate has to be small. However, the cross-flow term can easily be considered and the parallel flow assumption is not needed.

4.3.4. Derivation of the mean flow. With the ASBL assumptions already outlined and assuming that the polymeric stress depends on the wall-normal direction y only, i.e. $\boldsymbol{\tau} = \boldsymbol{\tau}(y)$, the continuity and motion equations (4.4) simplify to

$$
\begin{cases}
\dfrac{dv}{dy} = 0, \\[2mm]
\rho v \dfrac{du}{dy} = \dfrac{d\tau_{xy}}{dy} + \eta_s \dfrac{d^2 u}{dy^2}, \\[2mm]
\rho v \dfrac{dv}{dy} = -\dfrac{dp}{dy} + \dfrac{d\tau_{yy}}{dy} + \eta_s \dfrac{d^2 v}{dy^2}.
\end{cases}
\tag{4.5}
$$

These are subject to the following boundary conditions

$$u(0) = 0, \qquad u(\infty) = U_e,$$

$$v(0) = 0, \qquad v(\infty) = -V_0,$$

where U_e, V_0 are positive constants. The continuity equation implies that v must be a constant. By applying constant suction boundary conditions at the wall, i.e. $v(y = 0) = -V_0$, we obtain

$$v(y) = -V_0,$$

where V_0 is the suction rate. Thus, the equations of motion become

$$-\rho V_0 \frac{du}{dy} = \frac{d\tau_{xy}}{dy} + \eta_s \frac{d^2 u}{dy^2},$$

$$0 = -\frac{dp}{dy} + \frac{d\tau_{yy}}{dy}.$$

With the same assumptions, the equations for the polymeric stress become

$$\tau_{xx} - \lambda_1 \left(V_0 \frac{d\tau_{xx}}{dy} + 2\frac{du}{dy}\tau_{xy} \right) + \xi\lambda_1 \frac{du}{dy}\tau_{xy} + \delta_{\mathrm{L}}\epsilon\frac{\lambda_1}{\eta_p}(\tau_{xx} + \tau_{yy})\tau_{xx}$$

$$+ \delta_{\mathrm{E}} \left[\exp\left(\epsilon\frac{\lambda_1}{\eta_p}(\tau_{xx} + \tau_{yy}) \right) - 1 \right] \tau_{xx} + \alpha\frac{\lambda_1}{\eta_p}\left(\tau_{xx}^2 + \tau_{xy}^2 \right) = 0,$$

$$\tau_{xy} - \lambda_1 \left(V_0 \frac{d\tau_{xy}}{dy} + \frac{du}{dy}\tau_{yy} \right) + \xi\frac{\lambda_1}{2}\frac{du}{dy}(\tau_{xx} + \tau_{yy})$$

$$+ \delta_{\mathrm{L}}\epsilon\frac{\lambda_1}{\eta_p}(\tau_{xx} + \tau_{yy})\tau_{xy} + \delta_{\mathrm{E}} \left[\exp\left(\epsilon\frac{\lambda_1}{\eta_p}(\tau_{xx} + \tau_{yy}) \right) - 1 \right] \tau_{xy}$$

$$+ \alpha\frac{\lambda_1}{\eta_p}(\tau_{xx}\tau_{xy} + \tau_{xy}\tau_{yy}) = \eta_p\frac{du}{dy},$$

$$\tau_{yy} - \lambda_1 V_0 \frac{d\tau_{yy}}{dy} + \xi\lambda_1 \frac{du}{dy}\tau_{xy} + \delta_{\mathrm{L}}\epsilon\frac{\lambda_1}{\eta_p}(\tau_{xx} + \tau_{yy})\tau_{yy}$$

$$+ \delta_{\mathrm{E}} \left[\exp\left(\epsilon\frac{\lambda_1}{\eta_p}(\tau_{xx} + \tau_{yy}) \right) - 1 \right] \tau_{yy} + \alpha\frac{\lambda_1}{\eta_p}\left(\tau_{xy}^2 + \tau_{yy}^2 \right) = 0.$$

4.3.5. Newtonian results. For Newtonian fluids, $\lambda_1 = \eta_p = \xi = \alpha = \epsilon = 0$. The ASBL equations (4.5) become

$$-\rho V_0 \frac{du}{dy} = \eta_0 \frac{d^2 u}{dy^2},$$

$$0 = -\frac{dp}{dy}.$$

We apply the following boundary conditions

$$u(0) = 0, \quad u(\infty) = U_e,$$

where U_e is the constant velocity in the free stream. As reported for example by Fransson [30], the solution is of the following exponential form

$$u = U_e \left[1 - \exp\left(-\frac{\rho V_0 y}{\eta_0} \right) \right].$$

The displacement and momentum thickness, defined in Section 1.3 by equations (1.16) and (1.18), are easily calculated, and are given by

$$\delta_* = \frac{\eta_0}{\rho V_0}, \quad \theta_* = \frac{1}{2}\frac{\eta_0}{\rho V_0}. \tag{4.6}$$

The Newtonian displacement thickness will be used as characteristic length for the stability analysis. Thus, the Reynolds number based on

δ_* becomes the ratio between the free-stream and suction velocities, i.e.

$$Re = \frac{\rho U_e \delta_*}{\eta_0} = \frac{U_e}{V_0}.$$

4.3.6. UCM. For the Upper Convected Maxwell model, $\eta_s = \xi = \epsilon = \alpha = 0$. In this case, the ASBL governing equations (4.5) become

$$\rho V_0 \frac{du}{dy} + \frac{d\tau_{xy}}{dy} = 0, \tag{4.7a}$$

$$-\frac{\partial p}{\partial y} + \frac{d\tau_{yy}}{dy} = 0, \tag{4.7b}$$

$$\tau_{xx} - \lambda_1 V_0 \frac{d\tau_{xx}}{dy} - 2\lambda_1 \frac{du}{dy}\tau_{xy} = 0, \tag{4.7c}$$

$$\tau_{xy} - \lambda_1 V_0 \frac{d\tau_{xy}}{dy} - \lambda_1 \frac{du}{dy}\tau_{yy} - \eta_0 \frac{du}{dy} = 0, \tag{4.7d}$$

$$\tau_{yy} - \lambda_1 V_0 \frac{\partial \tau_{yy}}{\partial y} = 0. \tag{4.7e}$$

The last equation (4.7e) only involves τ_{yy} and can be easily solved, giving

$$\tau_{yy} = D \exp\left(\frac{y}{\lambda_1 V_0}\right),$$

for some constant D. In this case D must be zero, since τ_{yy} cannot be infinitely large as $y \to \infty$. Hence, equations (4.7a) and (4.7d) become a system of coupled equations, that is

$$\rho V_0 \frac{du}{dy} + \frac{d\tau_{xy}}{dy} = 0,$$

$$\tau_{xy} - \lambda_1 V_0 \frac{d\tau_{xy}}{dy} - \eta_0 \frac{du}{dy} = 0.$$

These can be solved analytically by imposing $u(0) = 0$ and $u(\infty) = U_e$. The analytical solution is

$$u = U_e \left[1 - \exp\left(\frac{\rho V_0 y}{\rho V_0{}^2 \lambda_1 - \eta_0}\right)\right],$$

$$\tau_{xy} = \rho U_e V_0 \exp\left(\frac{V_0 \rho y}{\rho V_0{}^2 \lambda_1 - \eta_0}\right).$$

These solutions can also be written as follows

$$u = U_e \left[1 - \exp\left(\frac{y}{\delta_* (K - 1)}\right)\right],$$

$$\tau_{xy} = \rho U_e V_0 \exp\left(\frac{y}{\delta_*(K-1)}\right),$$

where $K = \frac{Wi}{Re}$ and Wi is the Weissenberg number based on the displacement thickness $\delta_* = \frac{\eta_0}{\rho V_0}$, which is given by

$$Wi = \frac{\lambda_1 U_e}{\delta_*} = \frac{\rho \lambda_1 U_e V_0}{\eta_0}.$$

These solutions do not diverge as $y \to \infty$, since we consider $K < 1$. The component τ_{xx} of the elastic stress can be calculated by solving equation (4.7c), in which we substitute the solutions for u, τ_{xy}, which gives

$$\tau_{xx} = 2\frac{\lambda_1 \rho^2 V_0^2 U_e^2}{\rho V_0^2 \lambda_1 + \eta_p} \exp\left(\frac{2\rho V_0 y}{\rho V_0^2 \lambda_1 - \eta_p}\right) + C \exp\left(\frac{y}{\lambda_1 V_0}\right).$$

The constant C must be zero to have a solution bounded at infinity. It can also be written as

$$\tau_{xx} = 2\rho U_e V_0 \frac{Wi}{K+1} \exp\left(\frac{2y}{\delta_*(K-1)}\right).$$

Notice that the displacement thickness for the UCM model is easily calculated and can be written in terms of the Newtonian displacement thickness, δ_*, as follows

$$\delta_*^{\mathrm{UCM}} = (1-K)\delta_*.$$

4.3.7. Oldroyd B. For Oldroyd B fluids, $\xi = \epsilon = \alpha = 0$. Hence, the ASBL equations (4.5) become

$$\rho V_0 \frac{du}{dy} + \frac{d\tau_{xy}}{dy} + \eta_s \frac{d^2 u}{dy^2} = 0,$$

$$-\frac{\partial p}{\partial y} + \frac{d\tau_{yy}}{dy} = 0,$$

$$\tau_{xx} - \lambda_1 V_0 \frac{d\tau_{xx}}{dy} - 2\lambda_1 \frac{du}{dy}\tau_{xy} = 0,$$

$$\tau_{xy} - \lambda_1 V_0 \frac{d\tau_{xy}}{dy} - \lambda_1 \frac{du}{dy}\tau_{yy} - \eta_p \frac{du}{dy} = 0,$$

$$\tau_{yy} - \lambda_1 V_0 \frac{\partial \tau_{yy}}{\partial y} = 0.$$

Notice that only the equation of motion in the x-direction has changed from the UCM model. Making the same considerations as for the

UCM model, we deduce that $\tau_{yy} = 0$ and we can solve analytically the following system

$$\rho V_0 \frac{du}{dy} + \frac{d\tau_{xy}}{dy} + \eta_s \frac{d^2u}{dy^2} = 0,$$

$$\tau_{xy} - \lambda_1 V_0 \frac{d\tau_{xy}}{dy} - \eta_p \frac{du}{dy} = 0.$$

The solution obtained by imposing zero velocity at the wall, i.e. $u(0) = 0$, is given by

$$u = -C - D + C \exp\left(-k_1 \frac{y}{\delta_*}\right) + D \exp\left(-k_2 \frac{y}{\delta_*}\right),$$

where C, D are some constants and

$$k_1 = \frac{K - 1 + \sqrt{1 + K(K + 4\beta - 2)}}{2\beta K},$$

$$k_2 = \frac{K - 1 - \sqrt{1 + K(K + 4\beta - 2)}}{2\beta K},$$

where $\beta = \eta_s/\eta_0$ is known as the *viscosity ratio*. Clearly, $k_2 < 0$. Therefore, we impose $D = 0$ in order to not have the solution tending to infinity as $y \to \infty$. Imposing the condition at infinity, $u(\infty) = U_e$, we obtain $C = -U_e$. The solutions for u and τ_{xy} are

$$u = U_e \left[1 - \exp\left(-k_1 \frac{y}{\delta_*}\right)\right],$$

$$\tau_{xy} = \rho V_0 U_e a \exp\left(-k_1 \frac{y}{\delta_*}\right),$$

where a is a constant defined by

$$a = \frac{K + 1 - \sqrt{1 + K(K + 4\beta - 2)}}{2K}.$$

The equation for the elastic stress component τ_{xx} can also be solved analytically and gives

$$\tau_{xx} = \rho V_0 U_e b \exp\left(-2k_1 \frac{y}{\delta_*}\right),$$

where b is the constant defined by

$$b = \frac{Wi k_1 \left(K + 1 - \sqrt{1 + K(K + 4\beta - 2)}\right)}{2K^2 k_1 + K},$$

or else written as

$$b = \frac{Wi\left(K - 1 - 2K\beta + \sqrt{1 + K^2 + (-2 + 4\beta)K}\right)}{K^2\left(K - 1 + \beta + \sqrt{1 + K(K + 4\beta - 2)}\right)}.$$

The displacement thickness is a constant which can be easily calculated and written in terms of the Newtonian displacement thickness, δ_*, as follows

$$\delta_*^{\mathrm{OB}} = \frac{\delta_*}{k_1}.$$

4.3.8. Linear PTT. For the linear PTT model, $\delta_{\mathrm{L}} = 1$ and $\delta_{\mathrm{E}} = \alpha = 0$. Therefore, the ASBL equations become

$$\rho V_0 \frac{du}{dy} + \frac{d\tau_{xy}}{dy} + \eta_s \frac{d^2 u}{dy^2} = 0,$$

$$-\frac{\partial p}{\partial y} + \frac{d\tau_{yy}}{dy} = 0.$$

The equations for the polymeric stress tensor become

$$\tau_{xx} - \lambda_1 V_0 \frac{d\tau_{xx}}{dy} - 2\lambda_1 \frac{du}{dy}\tau_{xy} + \xi\lambda_1 \frac{du}{dy}\tau_{xy} + \epsilon\frac{\lambda_1}{\eta_p}\tau_{xx}\left(\tau_{xx} + \tau_{yy}\right) = 0,$$

$$\tau_{xy} - \lambda_1 V_0 \frac{d\tau_{xy}}{dy} - \lambda_1 \frac{du}{dy}\tau_{yy} + \xi\frac{\lambda_1}{2}\frac{du}{dy}\left(\tau_{xx} + \tau_{yy}\right)$$

$$+ \epsilon\frac{\lambda_1}{\eta_p}\tau_{xy}\left(\tau_{xx} + \tau_{yy}\right) - \eta_p\frac{du}{dy} = 0,$$

$$\tau_{yy} - \lambda_1 V_0 \frac{d\tau_{yy}}{dy} + \xi\lambda_1 \frac{du}{dy}\tau_{xy} + \epsilon\frac{\lambda_1}{\eta_p}\tau_{yy}\left(\tau_{xx} + \tau_{yy}\right) = 0.$$

For this model there is no straightforward way to find an analytical solution. We cannot conclude that $\tau_{yy} = 0$. Therefore, these equations will be solved numerically.

4.3.9. Exponential PTT. For the exponential PTT model, $\delta_{\mathrm{E}} = 1$ and $\delta_{\mathrm{L}} = \alpha = 0$. Therefore, the ASBL equations become

$$\rho V_0 \frac{du}{dy} + \frac{d\tau_{xy}}{dy} + \eta_s \frac{d^2 u}{dy^2} = 0,$$

$$-\frac{\partial p}{\partial y} + \frac{d\tau_{yy}}{dy} = 0.$$

The elastic stress components satisfy the following equations

$$\tau_{xx} - \lambda_1 V_0 \frac{d\tau_{xx}}{dy} - 2\lambda_1 \frac{du}{dy}\tau_{xy} + \xi\lambda_1 \frac{du}{dy}\tau_{xy}$$
$$+ \left[\exp\left(\epsilon\frac{\lambda_1}{\eta_p}(\tau_{xx}+\tau_{yy})\right) - 1\right]\tau_{xx} = 0,$$

$$\tau_{xy} - \lambda_1 V_0 \frac{d\tau_{xy}}{dy} - \lambda_1 \frac{du}{dy}\tau_{yy} + \xi\frac{\lambda_1}{2}\frac{du}{dy}\left(\tau_{xx}+\tau_{yy}\right)$$
$$+ \left[\exp\left(\epsilon\frac{\lambda_1}{\eta_p}(\tau_{xx}+\tau_{yy})\right) - 1\right]\tau_{xy} - \eta_p\frac{du}{dy} = 0,$$

$$\tau_{yy} - \lambda_1 V_0 \frac{d\tau_{yy}}{dy} + \xi\lambda_1 \frac{du}{dy}\tau_{xy} + \left[\exp\left(\epsilon\frac{\lambda_1}{\eta_p}(\tau_{xx}+\tau_{yy})\right) - 1\right]\tau_{yy} = 0.$$

As for the linear PTT fluids, the mean flow equations will be solved numerically.

4.3.10. Giesekus. For the Giesekus model, $\epsilon = \xi = 0$. Therefore, the ASBL equations become

$$\rho V_0 \frac{du}{dy} + \frac{d\tau_{xy}}{dy} + \eta_s \frac{d^2 u}{dy^2} = 0,$$

$$-\frac{\partial p}{\partial y} + \frac{d\tau_{yy}}{dy} = 0,$$

The equations for the elastic stress become

$$\tau_{xx} - \lambda_1 V_0 \frac{d\tau_{xx}}{dy} - 2\lambda_1 \frac{du}{dy}\tau_{xy} + \alpha\frac{\lambda_1}{\eta_p}\left(\tau_{xx}^2 + \tau_{xy}^2\right) = 0,$$

$$\tau_{xy} - \lambda_1 V_0 \frac{d\tau_{xy}}{dy} - \lambda_1 \frac{du}{dy}\tau_{yy} + \alpha\frac{\lambda_1}{\eta_p}\tau_{xy}\left(\tau_{xx}+\tau_{yy}\right) - \eta_p\frac{du}{dy} = 0,$$

$$\tau_{yy} - \lambda_1 V_0 \frac{d\tau_{yy}}{dy} + \alpha\frac{\lambda_1}{\eta_p}\left(\tau_{xy}^2 + \tau_{yy}^2\right) = 0.$$

As for the PTT models, these equations will be solved numerically. Notice that when $\alpha = 0$, the Giesekus model reduces to the Oldroyd B model and, when $\eta_s = \alpha = 0$, it reduces to the UCM model.

4.4. Linear Stability equations

As a characteristic length, we chose the Newtonian displacement thickness derived in Section 4.3.5, which is defined by equation (4.6). The velocity vector field is non-dimensionalised using the velocity in the far

field, U_e. The new dimensionless variables are as follows

$$\mathbf{v} = \frac{\mathbf{v}_*}{U_e}, \quad \mathbf{x} = \frac{\rho V_0 \mathbf{x}_*}{\eta_0}, \quad t = \frac{\rho V_0 U_e t_*}{\eta_0}, \quad \boldsymbol{\tau} = \frac{\boldsymbol{\tau}_*}{\rho V_0 U_e}, \quad p = \frac{p_*}{\rho U_e^2},$$

$$(4.8)$$

where starred variables indicate dimensional variables. We omitted the asterisk $*$ in the previous sections for the sake of notational simplicity.

Thus, the equation of motion (4.1) in dimensionless form becomes

$$\begin{cases} \nabla \cdot \mathbf{v} = 0 \\ \dfrac{\mathrm{D}\mathbf{v}}{\mathrm{D}t} = -\nabla p + \dfrac{1}{Re} \nabla \cdot \boldsymbol{\tau} + \dfrac{\beta}{Re} \Delta \mathbf{v}, \end{cases} \tag{4.9}$$

where $\beta = \eta_s/\eta_0$ is the viscosity ratio and $Re = U_e/V_0$ is the Reynolds number. The equation (4.2) for the elastic contribution to the stress becomes

$$\boldsymbol{\tau} + Wi \overset{\triangledown}{\boldsymbol{\tau}} + g(\boldsymbol{\tau}, \boldsymbol{\gamma}) = (1 - \beta) \dot{\boldsymbol{\gamma}}, \tag{4.10}$$

where

$$g(\boldsymbol{\tau}, \boldsymbol{\gamma}) = \xi \frac{Wi}{2} (\dot{\boldsymbol{\gamma}} \boldsymbol{\tau} + \boldsymbol{\tau} \dot{\boldsymbol{\gamma}}) + \delta_{\mathrm{L}} \epsilon \frac{Wi}{1 - \beta} \mathrm{tr}(\boldsymbol{\tau}) \boldsymbol{\tau}$$

$$+ \delta_{\mathrm{E}} \left[\exp\left(\epsilon \frac{Wi}{1 - \beta} \mathrm{tr}(\boldsymbol{\tau}) \right) - 1 \right] \boldsymbol{\tau} + \alpha \frac{Wi}{1 - \beta} \boldsymbol{\tau}^2,$$

where $Wi = \lambda_1 U_e/\delta_*$ is the Weissenberg number based on the displacement thickness, δ_*.

4.4.1. Linear stability equations. In order to perform a linear stability analysis, we decompose the velocity field, pressure and elastic stress into mean flow and infinitesimal disturbances as follows

$$\mathbf{v}(x, y, z, t) = \mathbf{V}(y) + \tilde{\mathbf{v}}(x, y, z, t),$$

$$p(x, y, z, t) = P(y) + \tilde{p}(x, y, z, t),$$

$$\boldsymbol{\tau}(x, y, z, t) = \mathbf{T}(y) + \tilde{\boldsymbol{\tau}}(x, y, z, t).$$

where $\mathbf{V} = (U_B(y), V_B, 0)^T$ is the mean flow velocity field, P the mean pressure and $\mathbf{T}$ is the undisturbed elastic stress that reads

$$\mathbf{T}(y) = \begin{bmatrix} T_{xx}(y) & T_{xy}(y) & 0 \\ T_{xy}(y) & T_{yy}(y) & 0 \\ 0 & 0 & 0 \end{bmatrix}.$$
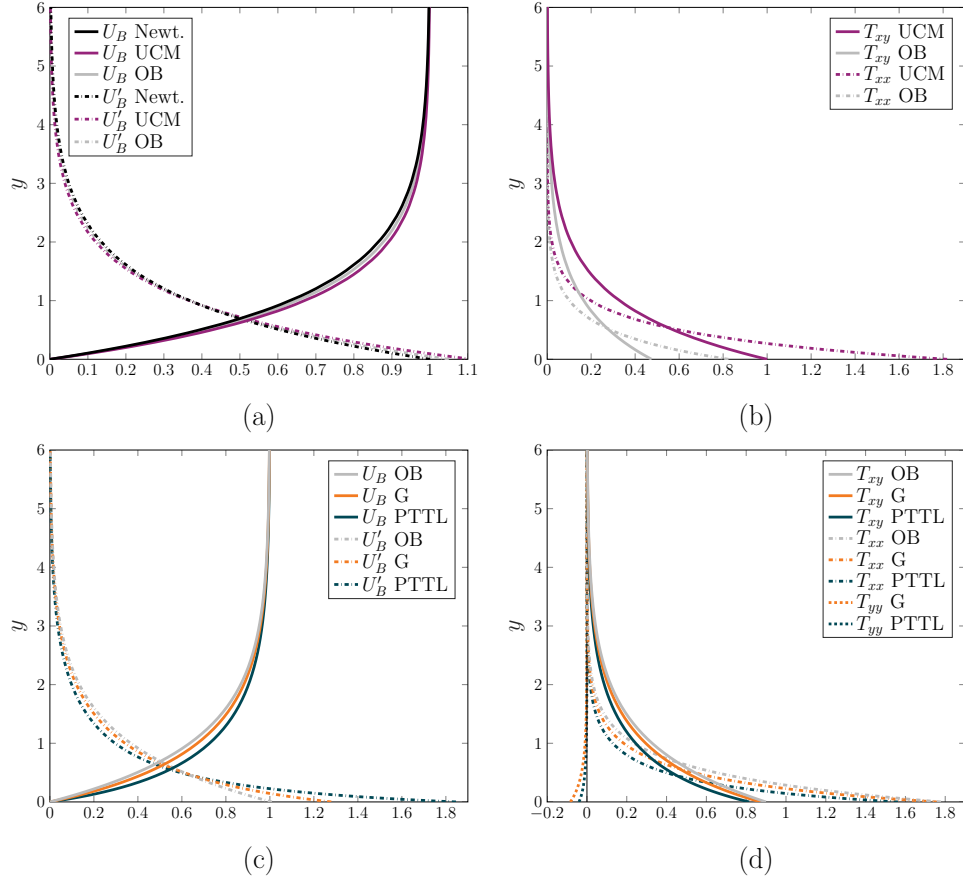
FIGURE 4.1. ASBL velocity profiles and solutions for the elastic stress for the Newtonian, UCM, Oldroyd B (OB), linear Phan-Thien Tanner (PTTL) and Giesekus (G) models. (a),(b) Newtonian solution, UCM solution with $Wi = 1, K = 0.1$ and Oldroyd B solution with $Wi = 1, K = 0.1, \beta = 0.5$; (c),(d) Oldroyd B solution with $K = 0.01, Wi = 1$, linear Phan-Thien Tanner solution with $K = 0.01, Wi = 1, \beta = 0.1, \xi = 0.05, \epsilon = 0.5$ and Giesekus solution with $K = 0.01, Wi = 1, \beta = 0.1, \alpha = 0.1$.

In Figure 4.1, we show the mean flow velocity profiles and the mean elastic stress obtained applying the asymptotic suction boundary layer, as described in the previous section. The solutions have been non-dimensionalised according to the transformations (4.8). The parameters have been chosen merely to give qualitatively appreciable results. In Appendix A.7, we report the non-dimensionalised equations for the Linear and Exponential PTT and the Giesekus models. These have been solved numerically using the Chebyshev collocation method, described in

Section 5.1, to approximate derivatives in the wall-normal component. The system of equations have been solved using MATLAB routine, `fsolve`.

From Figure 4.1(a), we notice that the UCM and the Oldroyd B models make the velocity at all points in the boundary layer larger than the Newtonian velocity. This is as expected since the displacement thickness for the UCM and the Oldroyd B models reduces with respect to the Newtonian case. In Figure 4.1(b), we report the components of the elastic stress tensor, τ_{xx} and τ_{xy}, which are zero in the Newtonian case. For the UCM and the Oldroyd B models, we have shown that $\tau_{yy} = 0$.

In Figure 4.1(c), we plot the velocity profiles for the Linear PTT and the Giesekus models compared with the Oldroyd B model, which is a special case of the former two. Notice that, for these two models the τ_{yy} component of the polymeric stress tensor is non-zero.

We assume a normal mode form for the disturbances in the streamwise and spanwise directions, x and z, as follows

$$\tilde{\mathbf{v}}(x, y, z, t) = \hat{\mathbf{v}}(y, t)e^{i(k_x x + k_z z)},$$

$$\tilde{\boldsymbol{\tau}}(x, y, z, t) = \hat{\boldsymbol{\tau}}(y, t)e^{i(k_x x + k_z z)},$$

$$\tilde{p}(x, y, z, t) = \hat{p}(y, t)e^{i(k_x x + k_z z)},$$

where k_x, k_z are streamwise and spanwise wavenumbers, respectively.

For the sake of brevity, we present here only the two-dimensional governing equations for the Oldroyd B model. The linear stability equations become

$$\frac{\partial u}{\partial t} + V_B \mathcal{D}u + U_B' v + ik_x U_B u + ik_x p$$

$$+ \frac{\beta}{Re}\left(k^2 - \mathcal{D}^2\right)u - \frac{1}{Re}\left(ik_x \tau_{xx} + \mathcal{D}\tau_{xy}\right) = 0,$$

$$\frac{\partial v}{\partial t} + V_B \mathcal{D}v + ik_x U_B v + \mathcal{D}p$$

$$+ \frac{\beta}{Re}\left(k^2 - \mathcal{D}^2\right)v - \frac{1}{Re}\left(ik_x \tau_{xy} + \mathcal{D}\tau_{yy}\right) = 0,$$

where $\mathcal{D}$ indicates derivative with respect to y. The equations for the elastic stress become

$$\tau_{xx} - 2i\left(1 - \beta\right)k_x u + Wi\left(\frac{\partial \tau_{xx}}{\partial t} - 2\tau_{xy}U_B'\right.$$

$$\left. + V\frac{\partial \tau_{xx}}{\partial y} + i\tau_{xx}U_B k_x - 2iT_{xx}k_x u + vT_{xx}' - 2T_{xy}\frac{\partial u}{\partial y}\right) = 0,$$

$$\tau_{xy} + \left(\beta - 1\right)\frac{\partial u}{\partial y} - i\left(1 - \beta\right)k_x v + Wi\left(\frac{\partial \tau_{xy}}{\partial t} - \tau_{yy}U_B' - T_{yy}\frac{\partial u}{\partial y}\right.$$

$$\left. + V_B\frac{\partial \tau_{xy}}{\partial y} - ik_x uT_{xy} - iT_{xx}k_x v + iU_B k_x \tau_{xy} + vT_{xy}' - T_{xy}\frac{\partial v}{\partial y}\right) = 0,$$

$$\tau_{yy} + 2\left(\beta - 1\right)\frac{\partial v}{\partial y} + Wi\left(\frac{\partial \tau_{yy}}{\partial t} - 2T_{yy}\frac{\partial v}{\partial y}\right.$$

$$\left. + V_B\frac{\partial \tau_{yy}}{\partial y} - 2ik_x T_{xy}v + iU k_x \tau_{yy} + vT_{yy}'\right) = 0.$$

4.4.2. Conclusive comments. The natural continuation of this work is to proceed studying the linear stability analysis of the viscoelastic models here considered, following the approach outlined for second order fluids in Chapters 1 and 2. Then, the results can be compared with those available in the literature for the same models obtained for channel flows.

CHAPTER 5

Numerical methods

In this chapter, we describe some of the numerical techniques employed to obtained the results in the previous chapters.

5.1. Chebyshev differentiation matrices

In this section, we describe briefly how we approximate the derivatives in the wall-normal direction, y, for the purpose of finding the mean flow and solving the stability equations introduced in Chapter 1. We use a Chebyshev spectral collocation method and refer mostly to Trefethen [86, 87]. The main idea of spectral collocation methods, also called *pseudospectral* methods, is to interpolate the data globally on a grid, then evaluate the derivative of the interpolant on the grid. Spectral methods allow remarkably high accuracy to be reached. They typically converge faster than algebraically for functions that are smooth.

In order to approximate the derivatives involved in the mean flow and stability equations, we use Chebyshev differentiation matrices. Firstly, we restrict our attention to the interval $[-1, 1]$ and we introduce the *Chebyshev extreme points*, also known as *Gauss-Lobatto-Chebyshev points*, defined by

$$x_j = \cos\left(\frac{j\pi}{N}\right), \qquad j = 0, \dots, N. \tag{5.1}$$

From a geometric point of view, Chebyshev extreme points are projections of equispaced points on the unit circle onto the interval $[-1, 1]$, as represented in Figure 5.1. They are closely related to the Chebyshev polynomials since the Chebyshev extreme points are the extrema of the N-th Chebyshev polynomial. The latter will be introduced in Section 5.6.
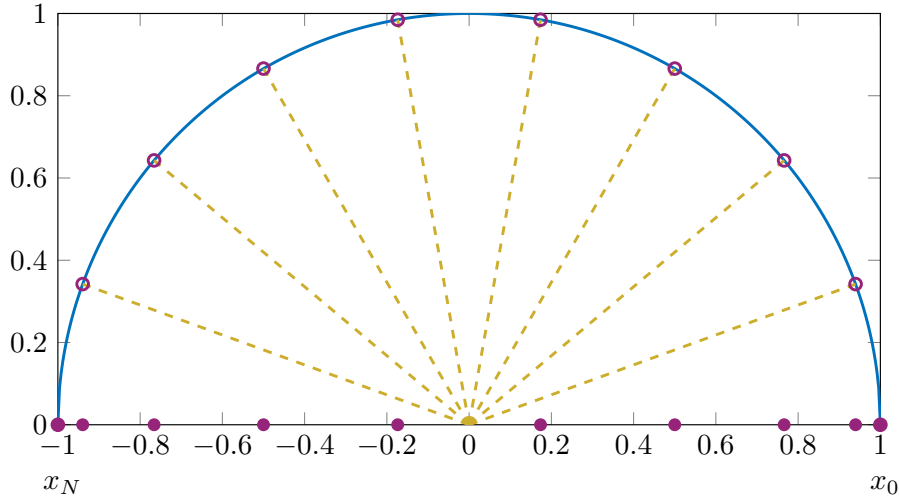
FIGURE 5.1. Chebyshev extreme points, $N = 10$.

Notice that the points (5.1) are numbered in the reverse order, starting from 1, following the convention of Trefethen's book [**87**]. The Chebyshev extrema are naturally clustered at the boundaries -1 and 1. This property is particularly suitable for problems where more points are required near the wall to resolve the rapid changes happening inside the boundary layer. Moreover, spectral methods based on polynomials must cluster at boundaries to avoid the numerically catastrophic problem of oscillations, known as the *Runge phenomenon*. Various choices of grid points are possible but they are all distributed with the density that tends to $N/\left(\pi\sqrt{1-x^2}\right)$ as $N \to \infty$. This allows a spacing between grid points that is $O(N^{-2})$ to be achieved near the boundaries -1 and 1, and $O(N^{-1})$ in the interior of the domain.

Given a function v, defined on the Chebyshev extreme points (5.1), the method can be summarised in two steps:

(1) Interpolate v by a polynomial $p_N(x)$ of degree $\leq N$, such that

$$v(x_j) = p_N(x_j), \qquad j = 0, \ldots, N.$$

(2) Using the Lagrange form of the interpolation polynomial, differentiate the interpolant at the grid points, that is

$$w_j = p'_N(x_j), \qquad j = 0, \ldots, N.$$

Therefore, the discrete derivative of the function v is obtained by a matrix multiplication of the form

$$\mathbf{w} = D\mathbf{v} \approx \mathbf{v}',$$

where $\mathbf{v} = (v_0, \ldots, v_N)$ is the vector containing the values of the function v at the grid points (5.1), $\mathbf{w}$ represents the approximated derivative of v at the grid points and D is a square matrix of order $N+1$.

Formulas for the entries of the matrix D can be found in Trefethen [**87**] and details are not discussed here. During the numerical tests, for practical reasons, we used the MATLAB function `cheb.m` provided in the same book and reported in the Listing 5.1. We observe that, unlike finite difference matrices, Chebyshev differentiation matrices are, in general, dense. Furthermore, higher-order derivatives can be easily approximated by calculating powers of the Chebyshev differentiation matrix D. For example, the second derivative of the function v at the grid points $\{x_j\}_{j=0}^N$ can be approximated by the vector $\mathbf{z}$ defined as follows

$$\mathbf{z} = D^2\mathbf{v} \approx \mathbf{v}''.$$

5.2. Mean flow

In this section, we describe how we approximate the mean flow profile for the purpose of the linear stability analysis. Consider the base flow equation (1.13), derived in Section 1.3, which reads

$$2(m+1)f''' + (m+1)ff'' + 2m\left(1 - f'^2\right) =$$
$$K\Big[(m+1)\,f^{iv}f + 2(1-3m)f'f''' + (3m-1)(f'')^2\Big], \quad (5.2)$$

where $K = K_0 C^2$, and C is defined by (1.21). The boundary conditions are

$$f(\eta) = f'(\eta) = 0 \qquad \text{at } \eta = 0,$$
$$f'(\eta) \to 1, f''(\eta) \to 0 \qquad \text{as } \eta \to \infty.$$

We define a new function $z(\eta) = f(\eta) - \eta$. The reason for this choice will become clear later. We can write f and its derivatives in terms of

LISTING 5.1. MATLAB code for the
Chebyshev differentiation matrix.

```
function [D, x] = cheb(N)

x = cos(pi*(0:N)/N)';
c = [2; ones(N-1, 1); 2].*(-1).^(0:N)';
X = repmat(x, 1, N+1);
dX = X - X';
D = (c*(1./c)')./(dX+(eye(N+1)));
D = D - diag(sum(D'));

end
```

z as follows

$$f(\eta) = \eta + z(\eta),$$
$$f'(\eta) = 1 + z'(\eta),$$
$$f''(\eta) = z''(\eta), \ f'''(\eta) = z'''(\eta), \ f^{iv}(\eta) = z^{iv}(\eta).$$

Equation (5.2), written in terms of the new function z, becomes

$$2(m+1)z''' + (m+1)(z+\eta)z'' + 2m\left(1 - (1+z')^2\right) =$$
$$K\left[(m+1)z^{iv}(z+\eta) + 2(1-3m)(1+z')z''' + (3m-1)(z'')^2\right],$$
$$(5.3)$$

with boundary conditions

$$z(\eta) = 0, z'(\eta) = -1 \qquad \text{at } \eta = 0,$$
$$z'(\eta), z''(\eta) \to 0 \qquad \text{as } \eta \to \infty.$$

In order to apply the Chebyshev collocation method described in Section 5.1, we apply the algebraic mapping from the physical domain $\eta \in [0, \infty)$ to the computational domain $\xi \in [-1, 1)$, as follows

$$\xi = \frac{\eta - l}{\eta + l},$$

where l is the stretching parameter. Thus, the extreme of the physical interval $\eta = 0$ corresponds to $\xi = -1$, and the limit $\eta \to +\infty$ corresponds to $\xi \to 1$. Therefore, the transformed boundary conditions

(a)

(b)
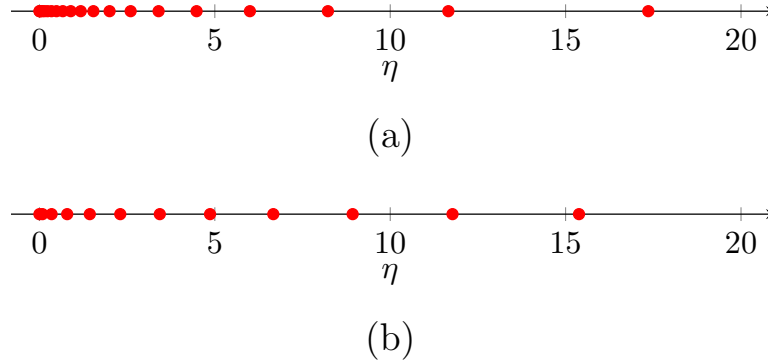
FIGURE 5.2. Chebyshev collocation points mapped into the physical domain using the algebraic mapping with $N = 25$. Only points ≤ 20 are shown. (a) $l = 2, |\{\eta_n : \eta_n \leq 6\}| = 16$; (b) $l = 20, |\{\eta_n : \eta_n \leq 6\}| = 8$.

become

$$z(\eta = 0) = 0 \implies z(\xi = -1) = 0,$$

$$z'(\eta = 0) = -1 \implies \left. \frac{dz}{d\xi} \right|_{\xi=-1} = -\frac{l}{2}.$$

The conditions $z'(\infty) = 0$ and $z''(\infty) = 0$ are automatically satisfied thanks to the specific choice of mapping, provided that $\frac{dz}{d\xi}, \frac{d^2z}{d\xi^2}$ remain bounded as $\xi \to 1$. In fact, the function z has been introduced in order to have z' vanishing at infinity and make it possible to apply the algebraic mapping.

Note that the constant δ_1 defined by equation (1.17) in Section 1.3.3 and shown in Figure 1.5 can be now easily calculated as follows

$$\delta_1 = \int_0^\infty (1 - f') \, d\eta = z(\xi = 1).$$

It is straightforward to transform all the η-derivatives of z in equation (5.3) and write them in terms of derivatives with respect to ξ. Then, discretisation in the computational domain $\xi \in [-1, 1]$ is performed by means of the Chebychev collocation method described in Section 5.1.

The discretised equations are written as a system of four first order equations and then solved using the MATLAB routine `fsolve`.

In Figure 5.3, we show the residual error increasing the number of Chebyshev points, N. Let us denote with $\mathbf{N}$ a vector of increasing N, the residual error is calculated as follows

$$R_j = \|g_j - g_{j-1}\|_\infty,$$

where g_j is the solution calculated with $N = \mathbf{N}(j)$ collocation points. We plot the residual errors for the solution f of equation (5.2) and its derivatives for the flat plate case ($\beta_H = 0$) and a non-Newtonian parameter $K = -0.2$. We can clearly see that the convergence is much faster with a stretching parameter $l = 15$ than it is for $l = 4$. A higher value of l clusters fewer points inside the boundary layer and resolves better the outer layer, as can be seen in Figure 5.2.

Various numerical tests have been performed, varying the non-Newtonian parameter, K, and the angle parameter, β_H. The results indicate that the case where K is negative is numerically more difficult. While for $K \geq 0$, the choice of l does not seem to influence the convergence of the scheme, the case where $K < 0$ needs extra care. From extensive numerical tests, we can conclude that a good choice for the stretching parameter is $l \approx 15$ and for the number of collocation points is $N \approx 65$. In Figure 5.4 we show the residual errors for different values of the angle parameter, β_H, and non-Newtonian parameter, K. We can see that when $N = 65$ the residual error is $O(10^{-5})$.

For the purpose of the stability analysis, we chose the number of collocation points $N = 65$ and the stretching parameter $l = 15$. The mean flow is then interpolated in order to perform the stability analysis.

Other methods have been explored for the solution of the mean flow equation (5.2), such as the Chebfun package [24] in MATLAB. Chebfun is an open-source package which implements the ideas described by Trefethen [88]. The implementation is based on the fact that every smooth function can be efficiently represented by a polynomial interpolation in Chebyshev points. However, for our problem this method is found to not converge for negative values of the non-Newtonian parameter K.
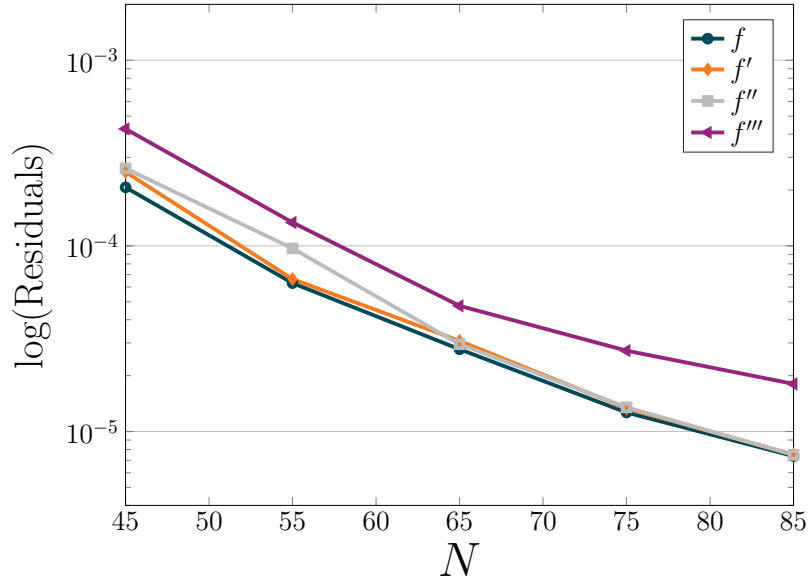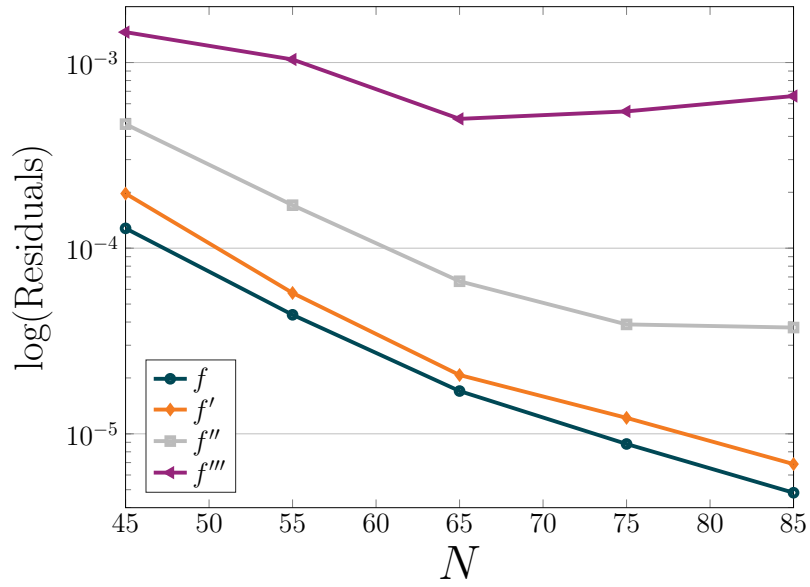
FIGURE 5.3. Convergence of the numerical scheme used to calculate the mean flow with $\beta_H = 0$ and $K = -0.2$. Stretching parameter: (a) $l = 15$; (b) $l = 4$.
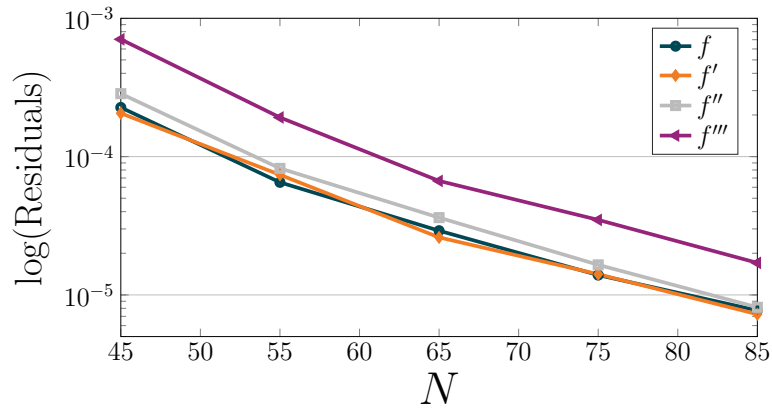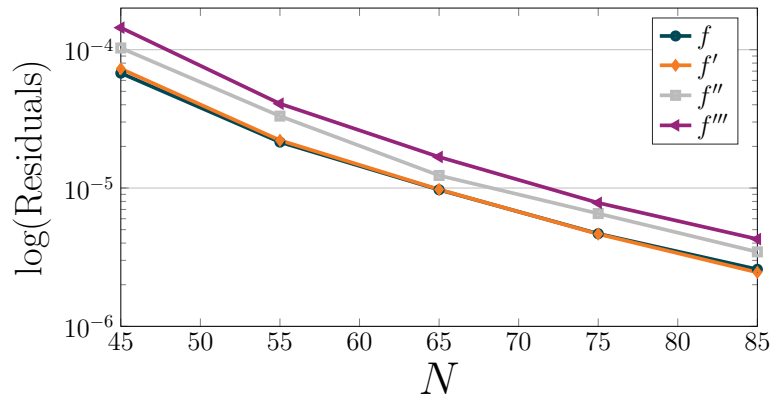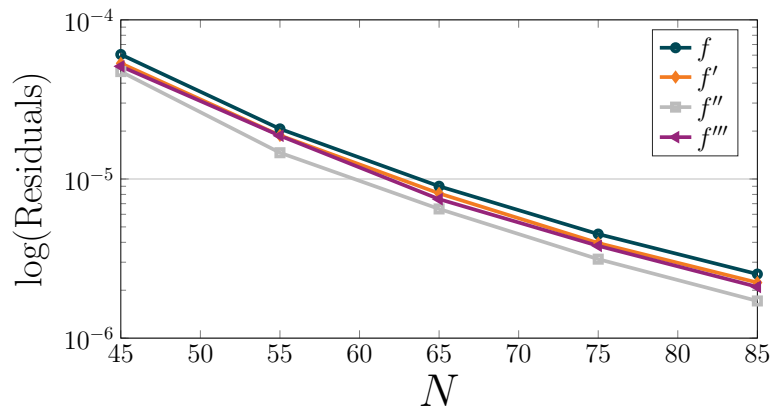
FIGURE 5.4. Convergence of the numerical scheme used to calculate the mean flow with stretching parameter $l = 15$. (a) $\beta_H = -0.14, K = 0.05$; (b) $\beta_H = 0.5, K = -0.05$; (c) $\beta_H = 1, K = 0.1$.

5.3. Linear stability analysis

In this section, we describe the numerical methods used to perform the linear stability analysis described in Section 1.4 and Section 1.7. The modified Orr-Sommerfeld equation (1.22) is an eigenvalue problem where the solution, c, represents the phase velocity of the disturbance.

In 1971, Orszag [53] demonstrated the efficiency and accuracy of Chebyshev spectral methods for solving linear eigenvalue problems by solving the Orr-Sommerfeld equation for plane Poiseuille flow. Chebyshev spectral methods naturally cluster grid points near the boundaries.

Different approaches are possible, such as the one proposed by Bridges and Morris [13] in which the equations are integrated. This method will be used later for the Direct Numerical Simulations and explained in Section 5.6. For this work, we chose the Chebyshev collocation matrix approach because it is easier to formulate. Furthermore, the integration method requires major modifications for each new mean velocity profile.

In this section, the modified Orr-Sommerfeld equation (1.22) is solved by approximating derivatives using the Chebyshev collocation method described in Section 5.1. The eigenvalue problem is then solved using the MATLAB routines `eig` and `polyeig`. We are interested in comparing two different types of mapping from the semi-infinite domain $y \in [0, \infty)$ to the computational domain $\xi \in [-1, 1]$ and in finding the optimal choice of stretching parameter.

5.3.1. Mapping the semi-infinite domain. In order to apply the Chebyshev collocation method, the semi-infinite domain $y \in [0, \infty)$ is mapped onto the finite interval $\xi \in [-1, 1]$ by means of the transformation (1.23), i.e.

$$\xi = \frac{y - l}{y + l},$$ (5.4)

or

$$\xi = 2e^{-\frac{y}{l}} - 1.$$ (5.5)

The mapping (5.4) is referred to as the *algebraic mapping* and the mapping (5.5) is called the *exponential mapping*. As shown in Figure 5.2

the Chebyshev extreme points (5.1) mapped into the physical domain $y \in [0, \infty)$ through the algebraic mapping (5.4) are naturally clustered near the origin. Moreover, an increase of the stretching parameter l translates to fewer points inside the boundary layer. This is true also for the exponential mapping (5.5).

The derivatives of a function ϕ with respect to y can be written in terms of derivatives with respect to ξ as follows

$$\frac{d\phi}{dy} = M\frac{d\phi}{d\xi},$$

$$\frac{d^2\phi}{dy^2} = MM'\frac{d\phi}{d\xi} + M^2\frac{d^2\phi}{d\xi^2},$$

$$\frac{d^3\phi}{dy^3} = \left(MM'^2 + M^2M''\right)\frac{d\phi}{d\xi} + 3M^2M'\frac{d^2\phi}{d\xi^2} + M^3\frac{d^3\phi}{d\xi^3},$$

$$\frac{d^4\phi}{dy^4} = \left(MM'^3 + 4M^2M'M'' + M^3M'''\right)\frac{d\phi}{d\xi}$$
$$+ \left(7M^2M'^2 + 4M^3M''\right)\frac{d^2\phi}{d^2\xi} + 6M^3M'\frac{d^3\phi}{d^3\xi} + M^4\frac{d^4\phi}{d^4\xi}.$$

The metric $M = M(\xi)$ is defined as $M = \frac{d\xi}{dy}$. For the algebraic mapping (5.4), M and its derivatives become

$$M = \frac{1}{2}\frac{(\xi - 1)^2}{l}, \ M' = \frac{\xi - 1}{l}, \ M'' = \frac{1}{l}, \ M''' = 0,$$

while for the exponential mapping (5.5) M and its derivatives become

$$M = -\frac{1}{l}(\xi + 1), \ M' = -\frac{1}{l}, \ M'' = M''' = 0.$$

Grosch and Orszag [35] did some comparisons between these two different kinds of mapping and the truncation method for six different problems, including the Orr-Sommerfeld eigenvalue problem for the Blasius boundary layer flow and the Falkner-Skan equation. They conclude that the algebraic mapping gives better results for the model problems they considered.

5.3.2. Temporal and spatial eigenvalue problems. When considering the temporal stability, the modified Orr-Sommerfeld equation (1.22) needs to be solved for the phase velocity c, for a fixed and real streamwise wavenumber α. The temporal problem can be written

as a generalised eigenvalue problem of the form

$$\mathcal{A}\phi = c\mathcal{B}\phi,$$

where ϕ is the eigenfunction and $\mathcal{A}$, $\mathcal{B}$ are linear operators defined by

$$\mathcal{A} = -U_B'' - \alpha^2 U_B + \frac{i\alpha^3}{Re_0} + K_0 U_B^{iv} - \alpha^4 K_0 U_B$$
$$+ \left[U_B - \frac{2i\alpha}{Re_0} + 2\alpha^2 K_0 U_B \right] \mathcal{D}^2$$
$$+ \left[\frac{i}{\alpha Re_0} - K_0 U_B \right] \mathcal{D}^4,$$
$$\mathcal{B} = -\alpha^2 - \alpha^4 K_0 + \left[1 + 2\alpha^2 K_0 \right] \mathcal{D}^2 - K_0 \mathcal{D}^4,$$

where $\mathcal{D}$ represents differentiation with respect to y, and U_B, U_B'', U_B^{iv} represent the base flow and its derivatives. The derivatives with respect to y are transformed into derivatives with respect to ξ using relations described in Section 5.3.1. The problem is discretised by means of the Chebyshev collocation matrices introduced in Section 5.1. Then, the eigenvalue problem is solved using the MATLAB routine `eig`.

When considering the evolution of disturbances in space, the modified Orr-Sommerfeld equation (1.22) is solved for the streamwise wavenumber α, by fixing a real value for the frequency ω. Therefore, the spatial problem can be written in the form of a polynomial eigenvalue problem as follows

$$\left(\mathcal{C}_0 + \alpha \mathcal{C}_1 + \alpha^2 \mathcal{C}_2 + \alpha^3 \mathcal{C}_3 + \alpha^4 \mathcal{C}_4 + \alpha^5 \mathcal{C}_5 \right) \phi = 0,$$

where

$$\mathcal{C}_0 = i\omega \mathcal{D}^2 + \left[\frac{1}{Re_0} - i\omega K_0 \right] \mathcal{D}^4,$$
$$\mathcal{C}_1 = iU_B'' - iK_0 U_B^{iv} - iU_B \mathcal{D}^2 + iK_0 U_B \mathcal{D}^4,$$
$$\mathcal{C}_2 = -i\omega + \left[-\frac{2}{Re_0} + 2i\omega K_0 \right] \mathcal{D}^2,$$
$$\mathcal{C}_3 = iU_B - 2iK_0 U_B \mathcal{D}^2,$$
$$\mathcal{C}_4 = \frac{1}{Re_0} - i\omega K_0,$$
$$\mathcal{C}_5 = iK_0 U_B.$$

Notice that this is a polynomial eigenvalue problem of order 4 in the Newtonian case, where $K_0 = 0$, and of order 5 in the non-Newtonian case, where $K_0 \neq 0$. Similarly to the temporal case, this polynomial eigenvalue problem is transformed by using one of the mappings introduced in Section 5.3.1, discretised and solved using the MATLAB routine `polyeig`.

5.3.3. Imposing boundary conditions. For both the temporal and spatial problems, the eigenfunctions need to satisfy the boundary conditions, i.e.

$$\phi(y) = \phi'(y) = 0, \qquad \text{at } y = 0,$$
$$\phi(y), \ \phi'(y) \to 0, \qquad \text{as } y \to \infty.$$

After application of the mapping, these boundary conditions mean that ϕ and its y-derivative need to be zero at $\xi = \pm 1$. The condition that $\phi'(y) \to 0$ as $y \to \infty$ is automatically satisfied by applying any of the two mappings, provided that $\frac{d\phi}{d\xi}$ remains bounded in this limit. In fact, we have

$$\frac{d\phi}{dy} = M \frac{d\phi}{d\xi},$$

and $M \to 0$ as $y \to \infty$, that is when $\xi \to 1$ for the algebraic mapping and when $\xi \to -1$ for the exponential mapping. Although one of the boundary conditions is automatically satisfied thanks to the mapping, for simplicity, we impose the following more restrictive boundary conditions

$$\phi(\xi) = \phi'(\xi) = 0, \qquad \text{at } \xi = \pm 1, \tag{5.6}$$

where now the prime $'$ indicates derivatives with respect to ξ. Trefethen [87] provides a handy way to deal with this type of boundary condition, briefly described below.

Let us denote by p the polynomial that approximates ϕ. In order to satisfy the conditions (5.6), we introduce an auxiliary polynomial $q(\xi)$ such that

$$p(\xi) = (1 - \xi^2)q(\xi),$$

and $q(\pm 1) = 0$. Differentiating, we obtain the following relations

$$p' = (1 - \xi^2)q'(\xi) - 2\xi q(\xi),$$
$$p'' = (1 - \xi^2)q''(\xi) - 4\xi q'(\xi) - 2q(\xi),$$
$$p''' = (1 - \xi^2)q'''(\xi) - 6\xi q''(\xi) - 6q'(\xi),$$
$$p^{iv} = (1 - \xi^2)q^{iv}(\xi) - 8\xi q'''(\xi) - 12\xi q''(\xi).$$

Note that, by construction, p now satisfies the conditions (5.6). It is straightforward to apply these transformations to the derivatives appearing in the stability eigenvalue problem.

5.3.4. Numerical tests. In this section, we focus on the temporal problem. We compare the two mappings in the solution of the modified Orr-Sommerfeld equation (1.22). In particular, we study the least stable eigenvalue, c, which is the one with largest imaginary part. The aim is to show that, by increasing the number of Chebyshev collocation points, N, the least stable eigenvalue converges. Let us denote by $\mathbf{N}$ the array containing different values of the number of grid points, N, in an increasing order. The residual errors are defined as

$$R_j = |c_j - c_{j-1}|,$$

where c_j is the least damped eigenvalue calculated with $N = \mathbf{N}(j)$ Chebyshev collocation points.

In Figure 5.5, we show the convergence of the numerical scheme with the algebraic mapping (5.4). We plot the residual errors of the imaginary part and the absolute value of the solution. We choose, as an example, the case of a flat plate with $\beta_H = 0$, $Re_0 = 1000$, $\alpha = 0.3$ and $K = -0.001$. We can see from Figure 5.5, that a stretching parameter $l = 4$ gives a slightly more rapid convergence than $l = 20$. In Figure 5.6, we show the convergence of the numerical scheme with the exponential mapping (5.5). We can see that the convergence with $l = 2$ is very slow. A stretching parameter $l = 5$ works much better.

We performed various numerical tests varying all the parameters. The results indicate that both the algebraic and the exponential mappings work well. The best choice of stretching parameter is $l \approx 4$ for
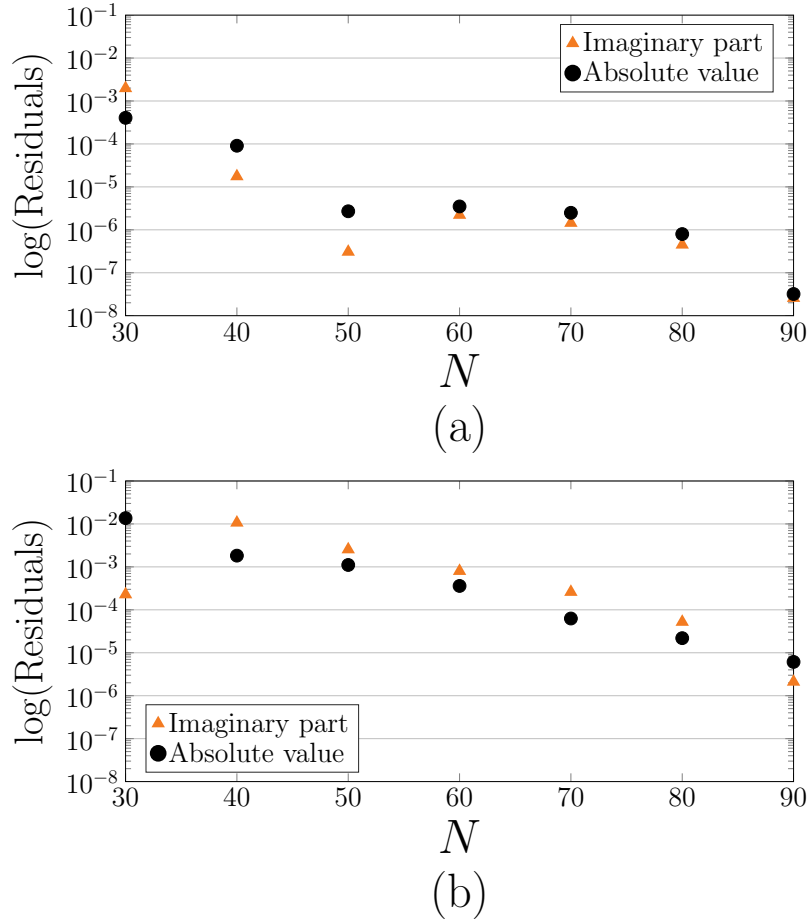
Figure 5.5. Convergence of the numerical scheme used to calculate the least stable eigenmode with the algebraic mapping for $\beta_H = 0$, $Re_0 = 1000$, $\alpha = 0.3$ and $K = -0.001$. Stretching parameter: (a) $l = 4$; (b) $l = 20$.

the algebraic mapping, and $l \approx 10$ for the exponential mapping. For the linear stability results in Section 1.5 and Section 1.7 we chose the algebraic mapping with $l = 4$ and $N = 65$.

5.4. Integration

In order to perform the energy balance, described in Section 1.6, we need a method to approximate the integrals. We follow the method used by Trefethen [87]. Let us consider the integral of a function g, that is

$$I = \int_0^\infty g(y)\, dy.$$
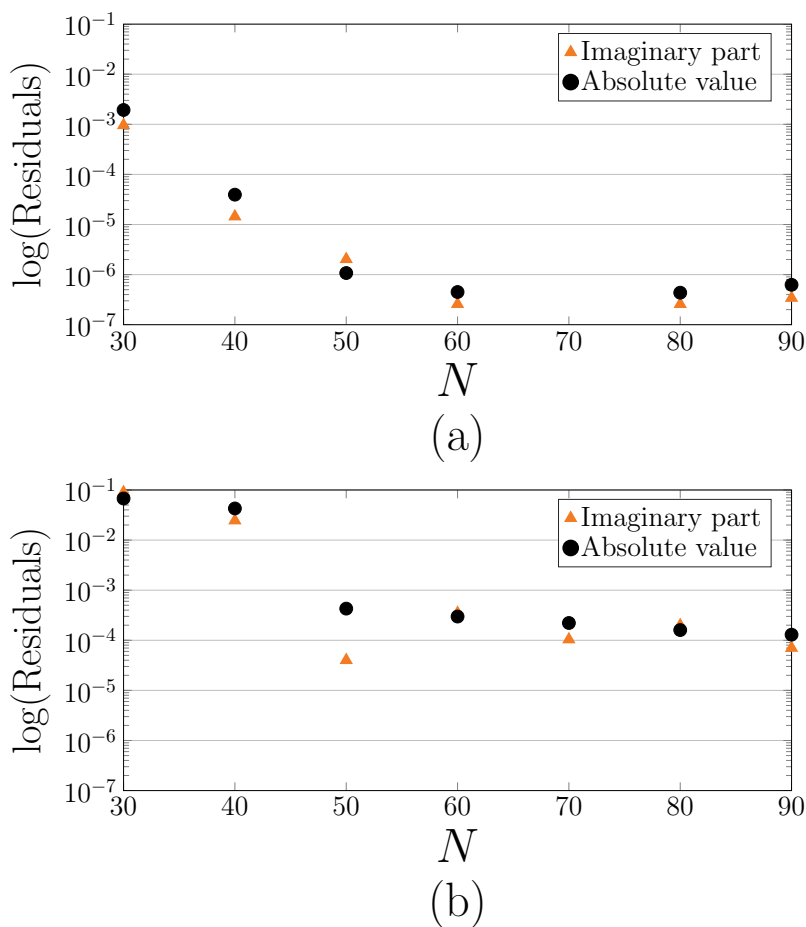
FIGURE 5.6. Convergence of the numerical scheme used to calculate the least stable eigenmode with the exponential mapping for $\beta_H = 0$, $Re_0 = 1000$, $\alpha = 0.3$ and $K = -0.001$. Stretching parameter: (a) $l = 5$; (b) $l = 2$.

We first apply a mapping so that I becomes an integral in the computational domain $[-1, 1]$, as follows

$$I = \int_{-1}^{+1} f(\xi)\, d\xi, \tag{5.7}$$

If the algebraic mapping (5.4) is employed

$$f(\xi) = \frac{dy}{d\xi} g(\xi) = \frac{4}{(1-\xi)^2} g(\xi),$$

and, if the exponential mapping (5.5) is used, then

$$f(\xi) = -\frac{dy}{d\xi} g(\xi) = \frac{l}{1+\xi} g(\xi).$$

We can rewrite the integral in (5.7) as $I = u(1)$, where u satisfies

$$u'(y) = f(y), \qquad u(-1) = 0. \tag{5.8}$$

We can now discretise (5.8) as explained in Section 5.1 using the Chebyshev discretisation matrix D. Therefore, we can approximate the function u at the grid points as follows

$$D\mathbf{u} = \mathbf{f},$$

where the last row and column of D have been removed to impose the boundary condition and $\mathbf{u}, \mathbf{f}$ are vectors containing collocation values of u and f, respectively. Then we can easily approximate $I = u(1)$ by inverting the matrix D. Let $\mathbf{w}^T$ be the first row of D^{-1}, then we approximate the integral I as follows

$$I \approx \mathbf{w}^T \mathbf{f}.$$

5.5. Transient growth

In this section, we perform some numerical tests for the maximum possible amplification of energy density defined in Section 2.4. The numerical techniques are the same used for the eigenvalue problems described in Section 5.3. The main difference is that, in order to calculate the maximum transient growth, the whole spectrum is required.

We study how the two different kind of mappings (5.4) and (5.5) perform in approximating the global optima, $G_{\max}$, defined by (2.12). Given an array, $\mathbf{N}$, containing increasing values of the number of grid points, N, we define the residual error as follows

$$R_j = |G_{\max,j} - G_{\max,j-1}|,$$

where $G_{\max,j}$ is the global optima obtained with $N = \mathbf{N}(j)$ grid points.

In Figure 5.7, we show the convergence of the numerical scheme with the algebraic mapping (5.4). We choose, as an example, the case of a flat plate ($\beta_H = 0$) and $Re_0 = 1000$, wavenumber vector $(\alpha, \beta) = (0.1, 0.6)$ and $K = 0.001$. We plot the residual errors of the global optima $G_{\max}$. From Figure 5.7, we deduce that a stretching parameter $l = 4$ is preferable to $l = 10$.
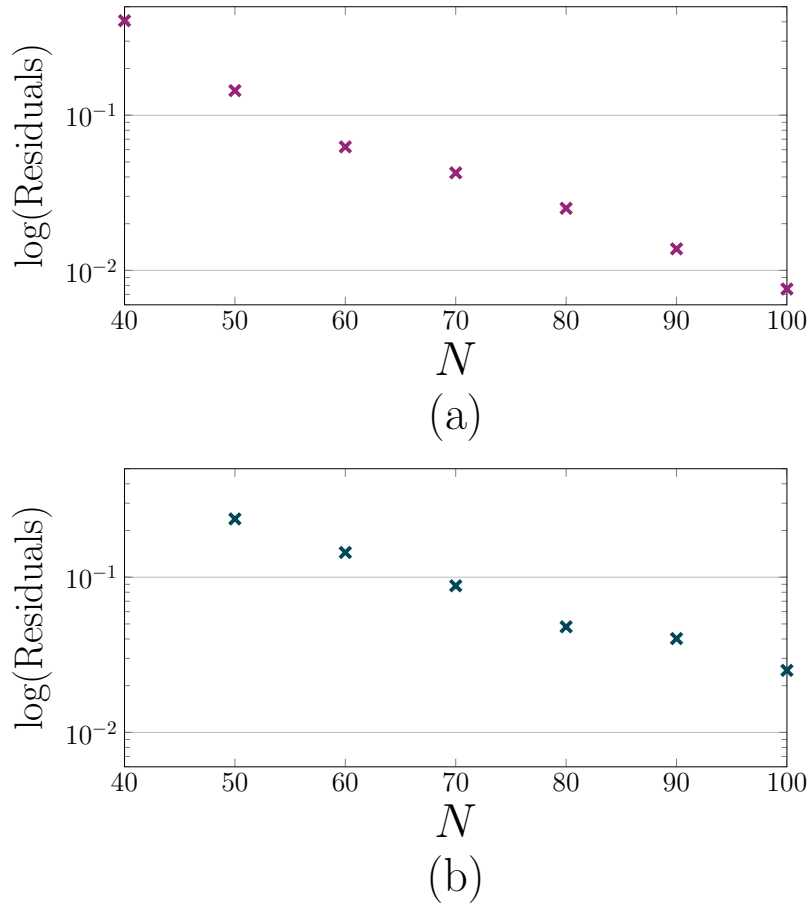
FIGURE 5.7. Convergence of the numerical scheme used to calculate the global optima, $G_{\max}$, with the algebraic mapping for $\beta_H = 0$, $Re_0 = 1000$, $\alpha = 0.1$, $\beta = 0.6$ and $K = 0.001$. Stretching parameter: (a) $l = 4$; (b) $l = 10$.

In Figure 5.8, we show the convergence of the scheme with the exponential mapping (5.5). We can see that a stretching parameter $l = 5$ gives a more rapid convergence than $l = 20$.

We performed several numerical tests varying all the parameters involved. The results, which are not reported in this work for brevity, suggest that the algebraic mapping works slightly better and a good choice for the stretching parameter is $l = 4$.

Notice that in order to calculate $G_{\max}$, we need to find the maximum of G over all time, defined by equation (2.11). Since, when the flow is exponentially stable and no unstable mode exists, G decays at infinity, it is sufficient to calculate the maximum in a interval of time which is
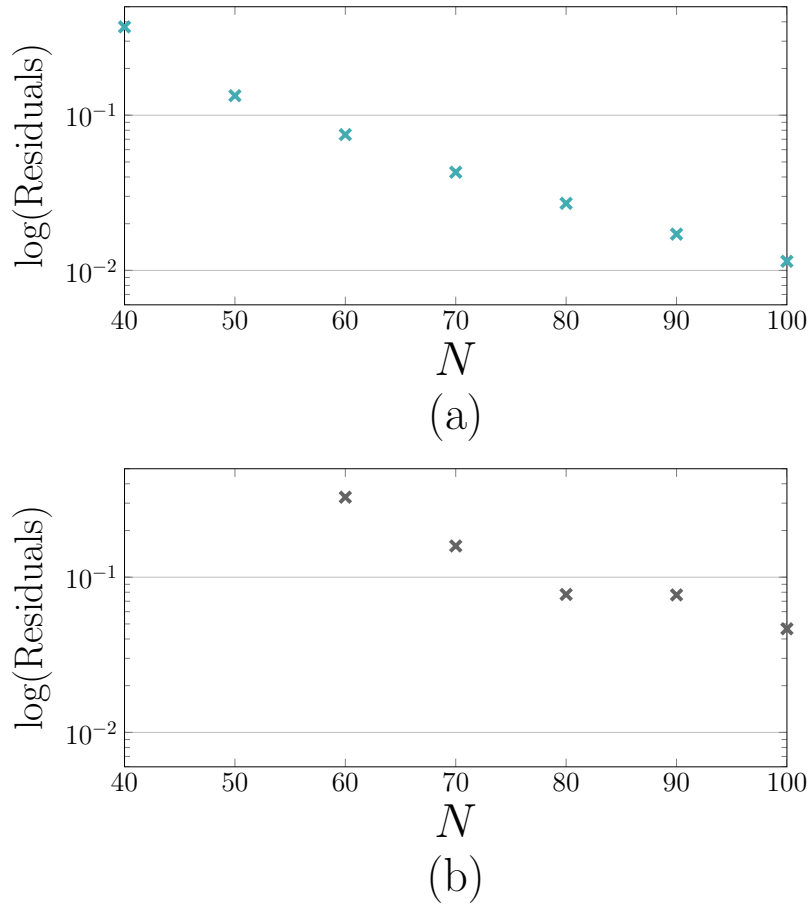
FIGURE 5.8. Convergence of the numerical scheme used to calculate the global optima, $G_{\max}$, with the exponential mapping for $\beta_H = 0$, $Re_0 = 1000$, $\alpha = 0.1$, $\beta = 0.6$ and $K = 0.001$. Stretching parameter: (a) $l = 5$; (b) $l = 20$.

sufficiently large. Hence, the accuracy of the numerical scheme used to calculate $G_{\max}$ also depends on the time discretisation parameter Δt, which we have chosen to be $\Delta t = 0.1$ for the numerical tests reported here.

5.6. Monochromatic DNS

In this section, we describe some of the ideas underlying the monochromatic DNS described in Chapter 3. The numerical scheme adopted is very similar to the one used by Morgan [51] to simulate the evolution of disturbances on periodic modulated rotating disk boundary layers.

A pseudo-spectral method is used, in which some operations are performed in physical space and others in Chebyshev space. We make extensive use of the Fast Fourier Transform (FFT), exploiting the relations between Chebyshev series and Fourier series. The polynomial interpolation in Chebyshev points is equivalent to trigonometric interpolation in equally spaced points and hence can be carried out by the FFT. In this thesis, we do not go into the details of the FFT and its relation to Chebyshev series and we refer to Trefethen [**87**].

We use only even and odd expansions in order to facilitate the imposition of the boundary conditions. Therefore, we only need the Chebyshev extreme collocation points in the interval $(0, 1]$, which are given by

$$x_j = \cos\left(\frac{j\pi}{2N}\right), \qquad j = 0, \ldots, N - 1.$$

The even representation for a function f which is symmetric about 0, is

$$f = \frac{f_0}{2} + \sum_{n=1}^{\infty} f_n T_{2n}(x), \quad x \in (0, 1].$$

The odd representation for a function f which is anti-symmetric about 0 is given by

$$f = \sum_{n=1}^{\infty} f_n T_{2n-1}(x), \quad x \in (0, 1]. \tag{5.9}$$

We use an even Chebyshev representation for the base flow, U_B. Using an odd representation would imply that the base flow decays at $\xi = 0$, but $U_B \to 1$ as $y \to \infty$. The Chebyshev coefficients of the base flow and its derivatives can be calculated by means of the FFT method (Trefethen [**87**]). We use an odd representation for the primary variables and an even representation for the secondary variables. This means that the condition that the primary variables decay as $\xi \to 0$, i.e. $y \to \infty$, is automatically satisfied. As mentioned in Section 3.1.3 these are reasonable restrictions at infinity.

As opposed to what was done for the linear stability analysis described in Section 5.3, we choose the integrated form of the stability equations following for example Bridges and Morris [**13**]. The advantage is that the integral operators can be expressed as n-diagonal banded

matrices and, therefore, easier to invert. This makes the integrated form more suitable for time-dependent simulations.

To build the integration matrices, the following relation for the integration of the Chebyshev polynomials is used

$$\int T_n(x) \ dx = \begin{cases} T_1(x) & n = 1, \\ \dfrac{1}{4} \left[T_0(x) + T_2(x) \right] & n = 1, \\ \dfrac{T_{n+1}(x)}{2\,(n+1)} + \dfrac{T_{n-1}(x)}{2\,(n-1)} & n \geq 2. \end{cases} \tag{5.10}$$

The system of equations to solve for the primary variables $\{\tilde{\omega}_x, \tilde{\omega}_z, \tilde{v}\}$ has been derived in Section 3.2 and are as follows

$$\frac{\partial I_2 \tilde{\omega}_x}{\partial t} + K_0 \left(k^2 \frac{\partial I_2 \tilde{\omega}_x}{\partial t} - \frac{1}{l^2} \frac{\partial J_2 \tilde{\omega}_x}{\partial t} \right) = \frac{1}{l^2 Re_0} J_2 \tilde{\omega}_x$$
$$+ I_2 \tilde{A}_x - \frac{1}{l} I_1 B_x + \frac{1}{l^2} J_2 \tilde{C}_x,$$

$$\frac{\partial I_2 \tilde{\omega}_z}{\partial t} + K_0 \left(k^2 \frac{\partial I_2 \tilde{\omega}_z}{\partial t} - \frac{1}{l^2} \frac{\partial J_2 \tilde{\omega}_z}{\partial t} \right) = \frac{1}{l^2 Re_0} J_2 \tilde{\omega}_z$$
$$+ I_2 \tilde{A}_z - \frac{1}{l} I_1 B_z + \frac{1}{l^2} J_2 \tilde{C}_z,$$

$$\left(-k^2 I_2 + \frac{1}{l^2} J_2 \right) \tilde{v} = i\alpha I_2 \tilde{\omega}_z - i\beta I_2 \tilde{\omega}_x,$$
$$\tag{5.11}$$

where

$$A_x = -\frac{k^2}{Re_0} \omega_x + i\beta \left(\hat{N}_y^0 + K_0 \hat{N}_y^1 \right),$$
$$B_x = -N_z^0 - K_0 \hat{N}_z^1 + i\beta K_0 \hat{N}_y^2,$$
$$C_x = -K_0 \hat{N}_z^2 + i\beta K_0 \hat{N}_y^3,$$
$$A_z = -\frac{k^2}{Re_0} \omega_z - i\alpha \left(\hat{N}_y^0 + K_0 \hat{N}_y^1 \right), \tag{5.12}$$
$$B_z = N_x^0 + K_0 \hat{N}_x^1 - i\alpha K_0 \hat{N}_y^2,$$
$$C_z = K_0 \hat{N}_x^2 - i\alpha K_0 \hat{N}_y^3.$$

The tilde indicates quantities divided by ξ^2 and the $\hat{N}_m^k$ terms are defined by relations (3.14) and (3.15). The integral boundary conditions to impose on the vorticity transport equations, after application of the

mapping, become

$$\int_0^\infty \omega_x \, dy = -w_{\text{wall}} - i\beta l \int_0^1 \tilde{v} \, d\xi,$$

$$\int_0^\infty \omega_z \, dy = u_{\text{wall}} + i\alpha l \int_0^1 \tilde{v} \, dy.$$

The condition that $v = v_{\text{wall}}$ at $y = 0$ can be easily applied to the Poisson equation.

We can now expand the primary variables $\{\tilde{\omega}_x, \tilde{\omega}_z, \tilde{v}\}$ using the odd expansion (5.9). We run the simulation for a time interval $[0, T]$, where T is sufficiently large for all the transient behaviour to pass and the growth rates to settle to a constant value. Then, we divide the interval $[0, T]$ into $M = T/\Delta t$ equal subintervals, where Δt is a step size sufficiently small for the numerical scheme to converge. Let us denote with ω_x^m, ω_z^m and v^m the vectors which contains the Chebyshev coefficients at the time $t_m = m\Delta t$ of $\tilde{\omega}_x, \tilde{\omega}_z$ and $\tilde{v}$, respectively.

Let us denote with $\mathbf{I}_1, \mathbf{I}_2, \mathbf{J}_2$ the matrix representations of the integral operators I_1, I_2, J_2, which are defined as follows

$$I_1 f = \int f \, d\xi, \quad I_2 f = \iint f \, d\xi, \quad J_2 f = \xi^4 f - 2 \int (\xi^3 f) \, d\xi.$$

We do not go into the details of the derivation of these matrices. The main idea is to use the relation (5.10).

Equations (5.11) are solved marching in time with an Adams predictor-corrector method, which is described in Section 3.3, starting from a zero initial disturbance. Disturbances on the flow are excited by means of the wall-normal impulse (3.16) and through application of appropriate boundary conditions. The steps of the numerical scheme can be summarised as follows:

(1) Set up the initial conditions, $\omega_x^0 = \omega_z^0 = v^0 = 0$.
(2) Calculate the mean flow, U_B, its derivatives and their Chebyshev representations.
(3) Compute the inverse of the left-hand side for the predictor and the corrector steps, which is given by

$$\mathbf{L} = \frac{\mathbf{I}_2}{\Delta t} + \frac{K_0}{\Delta t} \left(k^2 \mathbf{I}_2 - \frac{\mathbf{J}_2}{l^2} \right) - \frac{\mathbf{J}_2}{2Re_0 l^2}.$$

(4) Start the temporal march.

(5) Apply the predictor step:

$$\mathbf{L}\omega_x^{P,m+1} = \frac{\mathbf{I}_2\omega_x^m}{\Delta t} + \frac{\mathbf{J}_2\omega_x^m}{2Re_0 l^2} + \frac{1}{2}\left[3R_x^m - R_x^{m-1}\right],$$

$$\mathbf{L}\omega_z^{P,m+1} = \frac{\mathbf{I}_2\omega_z^m}{\Delta t} + \frac{\mathbf{J}_2\omega_z^m}{2Re_0 l^2} + \frac{1}{2}\left[3R_z^m - R_z^{m-1}\right],$$

(5.13)

where

$$R_x^m = \mathbf{I}_2\tilde{A}_x^m - \frac{1}{l}\mathbf{I}_1 B_x^m + \frac{1}{l^2}\mathbf{J}_2\tilde{C}_x^m,$$

$$R_z^m = \mathbf{I}_2\tilde{A}_z^m - \frac{1}{l}\mathbf{I}_1 B_z^m + \frac{1}{l^2}\mathbf{J}_2\tilde{C}_z^m,$$

where $\tilde{A}_k^m, B_k^m, \tilde{C}_k^m$ are the Chebyshev representations of the terms defined by (5.12). Notice that the viscous term is treated using the Crank-Nicolson scheme.

Set the predicted integral boundary conditions in the first rows of the transport equations (5.13):

$$\int_0^\infty \omega_x^{P,m+1}\,dy = -w_{\text{wall}}^{m+1} - i\beta l\int_0^1 \left(2v^m - v^{m-1}\right)\,d\xi,$$

$$\int_0^\infty \omega_z^{P,m+1}\,dy = u_{\text{wall}}^{m+1} + i\alpha l\int_0^1 \left(2v^m - v^{m-1}\right)\,d\xi.$$

(6) Solve the Poisson equation for v^{m+1}.

$$\left(-k^2\mathbf{I}_2 + \frac{1}{l^2}\mathbf{J}_2\right)v^{m+1} = i\alpha\mathbf{I}_2\omega_z^{P,m+1} - i\beta\mathbf{I}_2\omega_x^{P,m+1},$$

applying the boundary condition $v^m = v_{\text{wall}}$ at $\xi = 0$.

(7) Apply the corrector step:

$$\mathbf{L}\omega_x^{m+1} = \frac{\mathbf{I}_2\omega_x^m}{\Delta t} + \frac{\mathbf{J}_2\omega_x^m}{2Re_0 l^2} + \frac{1}{2}\left[R_x^{P,m+1} + R_x^m\right],$$

$$\mathbf{L}\omega_z^{m+1} = \frac{\mathbf{I}_2\omega_z^m}{\Delta t} + \frac{\mathbf{J}_2\omega_z^m}{2Re_0 l^2} + \frac{1}{2}\left[R_z^{P,m+1} + R_z^m\right].$$

Set the corrected integral boundary conditions:

$$\int_0^\infty \omega_x^{m+1}\,dy = -w_{\text{wall}}^{m+1} - i\beta l\int_0^1 v^{m+1}\,d\xi,$$

$$\int_0^\infty \omega_z^{m+1}\,dy = u_{\text{wall}}^{m+1} + i\alpha l\int_0^1 v^{m+1}\,d\xi.$$

(8) Go back to (5) and repeat until $t_m = T$.

Conclusions

The linear stability analysis of the boundary layer flow of a viscoelastic fluid has been investigated. The model chosen as a starting point to study the stability behaviour of viscoelastic fluids in boundary layers is the second order model. This model was introduced in 1955 by Rivlin and Ericksen [**70**] and it belongs to a wider class of fluids called *order models*. This class of constitutive equations is one of the first proposed in order to model departures from non-Newtonian behaviour. These models can represent non-zero normal stress differences which is an important feature of viscoelastic fluids.

The sign of the material parameters in this model has been a source of some controversy, as discussed by Dunn and Rajagopal [**26**] in their critical review. For the purpose of this work, we considered both signs of the material parameter α_1. The reason being that the model with a positive material parameter α_1, which is referred to as *second grade model*, is compatible with the laws of thermodynamics. However, the constitutive equation with a negative material parameter α_1, which is referred to as *second order model*, predicts the correct sign of normal stress differences. Moreover, Porteous and Denn [**61**] showed that the second order model is a consistent approximation to the Maxwell model in terms of linear stability. In this discussion and throughout the whole thesis, we talk about *second order models* to indicate both cases whenever it is clear from the context.

In this thesis, both classical linear stability analysis and bypass transition have been taken into consideration. The main result of classical linear stability analysis is that the second grade model, where $\alpha_1 > 0$, is stabilising with respect to the Newtonian case when considering two-dimensional disturbances, namely disturbances which vary only in the streamwise and wall-normal directions. Instead, the second order model,

169

where $\alpha_1 < 0$, destabilises the flow with respect to the Newtonian case. When extending the analysis to three-dimensional disturbances, which can vary also in the spanwise direction, the non-Newtonian effects prove to be different. For mostly streamwise independent waves the second grade model is destabilising while the second order model is stabilising.

In the bypass transition scenario, the second grade model appears to increase the tendency of the disturbances to grow transiently while the second order model reduces the transient growth.

In Chapter 1, the first step to apply the linear stability analysis was to determine the mean flow profile for second order fluids. It is possible to apply Prandtl's boundary layer theory to the case of a non-Newtonian fluid of second grade (Rajagopal *et al.* [**66**]). We investigated the case where the wall is placed symmetrically with respect to the flow direction and forms a wedge. The geometric configuration is characterised by an angle parameter, β_H. Therefore, the free-stream velocity varies with distance to the leading edge according to potential flow theory as a power law.

As for Newtonian fluids, after suitable assumptions, the boundary layer approximation allows the governing equations to be simplified. We applied a pseudo-similarity transformation (Garg and Rajagopal [**32**]) and obtained a local ODE. This ODE retains the dependency on the streamwise component and reduces to the well-known Falkner-Skan equation for Newtonian fluids when the material parameter $\alpha_1 = 0$. For the stability analysis, the equations were non-dimensionalised using the displacement thickness and the dependency on the streamwise position was included in the elasticity parameter K. This non-Newtonian parameter K is proportional to the material parameter α_1 and is a dimensionless quantity representing the ratio of non-Newtonian normal stress forces to inertial forces.

We solved the ODE numerically using a Chebyshev collocation method combined with a mapping from the semi-infinite domain to the computational domain. The non-Newtonian effects in the second grade ($K > 0$) and the second order model ($K < 0$) have almost opposite effects on the mean flow. In particular, we showed that a

positive K has the effect of decreasing the shape factor H, which is the ratio between displacement thickness and momentum thickness, and a negative K provokes an increase of the shape factor with respect to the Newtonian case. This is true for all the values of the angle parameter, β_H, considered. The results agree with the ones found in the literature for Newtonian fluids (Schlichting [**73**]) and second order fluids (Garg and Rajagopal [**32**]).

We solved numerically, using a Chebyshev collocation method, the modified Orr-Sommerfeld equation which governs the evolution of two-dimensional disturbances (Chun and Schwarz [**15**]). The results were presented in terms of temporal and spatial growth rates and neutral curves. The results indicate that, for all the values of the angle parameter β_H, the non-Newtonian terms in the second grade model stabilise the flow with respect to the Newtonian case, while they have an opposite effect for the second order model. This is consistent with the results already known for Poiseuille flows (Chun and Schwarz [**15**], Sadeghy *et al.* [**71**]). Moreover, we determined the critical Reynolds number, which is the smallest Reynolds number for which there exists an exponentially unstable mode. For the second grade model ($K > 0$), there is a stabilising effect in terms of an increase of the critical Reynolds. The effect is the opposite for the second order model ($K < 0$), where the instability is enhanced. The linear stability results for the second order model, which is the one that predicts the correct sign of the non-zero normal stress differences, are in qualitative agreement with those obtained by Sureshkumar and Beris [**80**] and Zhang [**96**] for the Poiseuille flow of other viscoelastic fluids.

In Chapter 1, we performed an energy balance. It is well known that the non-linear terms of the incompressible Navier-Stokes equations conserve energy. Therefore, in the Newtonian case, the energy balance can be seen as a nonlinear theory, because it applies to disturbances of arbitrary amplitude (Schmid and Henningson [**77**]). We showed that nonlinear terms in the incompressible two-dimensional governing equations for the second order models conserve energy.

For the second grade model ($K > 0$), the stabilising effect is principally due to the production term which represents the energy transfer from the mean flow to the perturbation. The opposite happens for the second order model ($K < 0$), where the kinetic energy increases due to an increase of the production term.

It is necessary not to ignore three-dimensional disturbances. For Newtonian fluids, Squire's theorem justifies the study of two-dimensional instead of three-dimensional disturbances. However, this result for second order fluids cannot be proven. We showed that a positive elasticity number K destabilises spanwise disturbances while it stabilises the two-dimensional Tollmien-Schlichting waves. The opposite happens for a negative K, which decreases the growth rates of mainly streamwise independent waves and increases the growth rates of mainly spanwise independent waves.

In Chapter 2, we extended the linear stability analysis to include the bypass transition scenario. A feature of nonnormal systems, which are governed by nonnormal operators, is that the eigenspectrum does not fully describe the whole dynamics. For flows dominated by shear forces, such as the Blasius flow, there can be transient amplification of energy due to non-orthogonal eigenfunctions (Trefethen *et al.* [**90**]).

In order to give a complete idea of the linear stability characteristics, the potential transient growth of energy cannot be ignored. Over the last few decades, a lot of work has been done for Newtonian fluids. To the best of our knowledge, the transient growth of viscoelastic fluids in boundary layers has not been investigated in the past.

In this work, the initial-value problem that drives the development of disturbances is derived for second order fluids following, for example, Schmid and Henningson [**77**]. This formulation permits the study of the behaviour of general solutions, not only single eigenmodes. The resulting system of equations, unlike in the Newtonian case, is now fully coupled. In order to quantify the tendency of the flow to transient growth, we defined the maximum possible amplification of energy density, G, and the global optimum, $G_{\max}$, which is the maximum amplification over all time.

Once again, the numerical techniques used for the results in Chapter 2 rely heavily on the Chebyshev collocation method. In the Newtonian case, our results agree with those obtained by Schmid [74] for Blasius flow and by Corbett and Bottaro [16] for Falkner-Skan flows. We showed that for the second grade model ($K > 0$) an increase of the non-Newtonian parameter K provokes an increase of the maximum transient growth, G, while the second order model ($K < 0$) has the opposite behaviour. The results are qualitatively similar for all values of the angle parameter, β_H. The largest amplification of energy is still reached for streamwise independent disturbances (zero streamwise wavenumber), as in the Newtonian case.

Non-Newtonian terms mostly affect streamwise independent disturbances. For $K > 0$ the global optimum, $G_{\max}$, is reached for larger times and for shorter waves (larger spanwise wavenumber) than in the Newtonian case. On the contrary, for $K < 0$ the global optimum is reached for shorter times and for longer waves (smaller spanwise wavenumber).

Chapter 3 is dedicated to the verification of the linear stability results obtained in Chapter 1 by means of Direct Numerical Simulations (DNS). Following Davies and Carpenter [19], the disturbance equations for second order fluids are rewritten in a compact velocity-vorticity formulation, where the number of variables in the system is reduced. The resulting formulation consists of three equations involving only two vorticity components and one velocity component. We made sure that, as for Newtonian fluids, this formulation is equivalent to the full governing equations.

The flow is disturbed by a temporally localised forced impulse. After the assumption of a normal mode form for the disturbances in the streamwise and spanwise directions, the variables are expanded in terms of Chebyshev polynomials. We employ a mapping from the physical wall-normal coordinate to the computational coordinate and integrate the equations twice. A comparison between the temporal growth rates obtained with the DNS and the ones given by the eigenvalue analysis was presented. We performed several tests of this type, varying the

angle parameter, β_H, and the non-Newtonian parameter, K. All the results show a remarkable agreement with those obtained from the eigenvalue analysis performed in Chapter 1.

The flow of more complex viscoelastic fluids have been considered in Chapter 4. The second order model has been chosen as a "toy problem" for its simplicity and the possibility of applying a boundary layer approximation similarly to Newtonian fluids. Although this model gives an idea of the effects of non-zero normal stress differences on the stability of boundary layers, it is not used in practice.

As rheologically more complex viscoelastic fluids, we chose the UCM, Oldroyd B, PTT and Giesekus models. The first step was to write a single constitutive equation to represent them all. The application of a boundary layer theory to these models presents some difficulties that we pointed out in Chapter 4. We chose, as a starting point, to consider the case of a porous boundary layer. When uniform suction is applied over a large area through the surface an asymptotic suction boundary layer (ASBL) develops at some distance from the leading edge. For Newtonian fluids, the ASBL equations has an analytical solution.

We showed that, by applying a similar theory to the viscoelastic models considered, an exponential analytical solution can be obtained for the UCM and Oldroyd B models. For the remaining and more complicated models, the equations simplify considerably and were solved numerically.

The natural progression of this work is the investigation of the linear stability properties of the UCM, Oldroyd B, PTT and Giesekus models in boundary layers. A linear stability analysis can be carried out starting from the mean flow profiles obtained by applying the ASBL theory. In particular, it will be interesting to study how the different non-Newtonian features represented by these models can affect the modal and nonmodal linear stability.

Some algebraic manipulation

In this appendix, we derive some of the equations used throughout this thesis.

A.1. Steady two-dimensional equations of motion

In this section, we derive the two-dimensional steady governing equations, starting from the general balance of linear momentum (1.4) and continuity equation (1.5) and making use of the constitutive equation for a second order model (1.1). In the steady case, the left-hand side of the balance of linear momentum (1.4) written component-wise is

$$\left(\rho\frac{\mathrm{D}\mathbf{v}}{\mathrm{D}t}\right)_1 = \rho\left((\mathbf{v}\cdot\nabla)\,\mathbf{v}\right)_1 = \rho\left(u\frac{\partial u}{\partial x} + v\frac{\partial u}{\partial y}\right),$$

$$\left(\rho\frac{\mathrm{D}\mathbf{v}}{\mathrm{D}t}\right)_2 = \rho\left((\mathbf{v}\cdot\nabla)\,\mathbf{v}\right)_2 = \rho\left(u\frac{\partial v}{\partial x} + v\frac{\partial v}{\partial y}\right).$$

By substituting the expression for the stress tensor (1.1) and using the relation $\alpha_1 + \alpha_2 = 0$, the right-hand side of equation (1.4) becomes

$$\nabla\cdot\boldsymbol{\sigma} = -\nabla p + \mu\nabla\cdot A_1 + \alpha_1\nabla\cdot\left(A_2 - A_1^2\right).$$

Since $\mathbf{v}$ is divergence free, we obtain

$$\nabla\cdot A_1 = \Delta\mathbf{v} = \left[\begin{array}{c} \Delta u \\ \Delta v \end{array}\right],$$

where Δ is the Laplacian operator, and

$$\nabla\cdot\left(A_2 - A_1^2\right) = \nabla\cdot\left((\mathbf{v}\cdot\nabla)\,A_1 + \nabla\mathbf{v}\nabla\mathbf{v}^T - \nabla\mathbf{v}^T\nabla\mathbf{v}\right). \qquad (A.1)$$

We have the following identities:

$$(\mathbf{v}\cdot\nabla)\,\nabla\mathbf{v}^T = \left[\begin{array}{cc} u\frac{\partial^2 u}{\partial x^2} + v\frac{\partial^2 u}{\partial x\partial y} & u\frac{\partial^2 u}{\partial x\partial y} + v\frac{\partial^2 u}{\partial y^2} \\ u\frac{\partial^2 v}{\partial x^2} + v\frac{\partial^2 v}{\partial y\partial x} & u\frac{\partial^2 v}{\partial x\partial y} + v\frac{\partial^2 v}{\partial y^2} \end{array}\right],$$

$$\left(\mathbf{v}\cdot\nabla\right)\nabla\mathbf{v} = \begin{bmatrix} u\frac{\partial^2 u}{\partial x^2} + v\frac{\partial^2 u}{\partial x\partial y} & u\frac{\partial^2 v}{\partial x^2} + v\frac{\partial^2 v}{\partial x\partial y} \\ u\frac{\partial^2 u}{\partial x\partial y} + v\frac{\partial^2 u}{\partial y^2} & u\frac{\partial^2 v}{\partial x\partial y} + v\frac{\partial^2 v}{\partial y^2} \end{bmatrix},$$

$$\nabla\mathbf{v}\nabla\mathbf{v}^T = \begin{bmatrix} \left(\frac{\partial u}{\partial x}\right)^2 + \left(\frac{\partial v}{\partial x}\right)^2 & \frac{\partial u}{\partial x}\frac{\partial u}{\partial y} + \frac{\partial v}{\partial x}\frac{\partial v}{\partial y} \\ \frac{\partial u}{\partial x}\frac{\partial u}{\partial y} + \frac{\partial v}{\partial x}\frac{\partial v}{\partial y} & \left(\frac{\partial u}{\partial y}\right)^2 + \left(\frac{\partial v}{\partial y}\right)^2 \end{bmatrix},$$

$$\nabla\mathbf{v}^T\nabla\mathbf{v} = \begin{bmatrix} \left(\frac{\partial u}{\partial x}\right)^2 + \left(\frac{\partial u}{\partial y}\right)^2 & \frac{\partial u}{\partial x}\frac{\partial v}{\partial x} + \frac{\partial u}{\partial y}\frac{\partial v}{\partial y} \\ \frac{\partial u}{\partial x}\frac{\partial v}{\partial x} + \frac{\partial u}{\partial y}\frac{\partial v}{\partial y} & \left(\frac{\partial v}{\partial x}\right)^2 + \left(\frac{\partial v}{\partial y}\right)^2 \end{bmatrix}.$$

Then, the first component of equation (A.1) is

$$\left(\nabla\cdot\left(A_2 - A_1^2\right)\right)_1 = \frac{\partial}{\partial x}\left(2u\frac{\partial^2 u}{\partial x^2} + 2v\frac{\partial^2 u}{\partial x\partial y} + \left(\frac{\partial v}{\partial x}\right)^2 - \left(\frac{\partial u}{\partial y}\right)^2\right)$$

$$+ \frac{\partial}{\partial y}\left(u\frac{\partial^2 u}{\partial x\partial y} + v\frac{\partial^2 u}{\partial y^2} + u\frac{\partial^2 v}{\partial x^2}\right)$$

$$+ \frac{\partial}{\partial y}\left(v\frac{\partial^2 v}{\partial x\partial y} + 2\frac{\partial u}{\partial x}\frac{\partial u}{\partial y} + 2\frac{\partial v}{\partial x}\frac{\partial v}{\partial y}\right)$$

$$= 2\frac{\partial^2}{\partial x^2}\left(u\frac{\partial u}{\partial x} + v\frac{\partial u}{\partial y}\right) + \frac{\partial^2}{\partial y^2}\left(u\frac{\partial u}{\partial x} + v\frac{\partial u}{\partial y}\right)$$

$$+ \frac{\partial^2}{\partial x\partial y}\left(u\frac{\partial v}{\partial x} + v\frac{\partial v}{\partial y}\right) + 2\frac{\partial}{\partial y}\left(\frac{\partial u}{\partial x}\frac{\partial u}{\partial y} + \frac{\partial v}{\partial x}\frac{\partial v}{\partial y}\right)$$

$$+ \frac{\partial}{\partial x}\left(\left(\frac{\partial v}{\partial x}\right)^2 - \left(\frac{\partial u}{\partial y}\right)^2 - 2\left(\frac{\partial u}{\partial x}\right)^2 - 2\frac{\partial v}{\partial x}\frac{\partial u}{\partial y}\right).$$

The second component of (A.1) is

$$\left(\nabla\cdot\left(A_2 - A_1^2\right)\right)_2 = \frac{\partial}{\partial y}\left(2v\frac{\partial^2 v}{\partial y^2} + 2u\frac{\partial^2 v}{\partial x\partial y} + \left(\frac{\partial u}{\partial y}\right)^2 - \left(\frac{\partial v}{\partial x}\right)^2\right)$$

$$+ \frac{\partial}{\partial x}\left(u\frac{\partial^2 u}{\partial x\partial y} + v\frac{\partial^2 u}{\partial y^2} + u\frac{\partial^2 v}{\partial x^2}\right)$$

$$+ \frac{\partial}{\partial x}\left(v\frac{\partial^2 v}{\partial x\partial y} + 2\frac{\partial u}{\partial x}\frac{\partial u}{\partial y} + 2\frac{\partial v}{\partial x}\frac{\partial v}{\partial y}\right)$$

$$= 2\frac{\partial^2}{\partial y^2}\left(u\frac{\partial v}{\partial x} + v\frac{\partial v}{\partial y}\right) + \frac{\partial^2}{\partial x^2}\left(u\frac{\partial v}{\partial x} + v\frac{\partial v}{\partial y}\right)$$

$$+ \frac{\partial^2}{\partial x\partial y}\left(u\frac{\partial u}{\partial x} + v\frac{\partial u}{\partial y}\right) + 2\frac{\partial}{\partial x}\left(\frac{\partial u}{\partial x}\frac{\partial u}{\partial y} + \frac{\partial v}{\partial x}\frac{\partial v}{\partial y}\right)$$

$$+ \frac{\partial}{\partial y}\left(\left(\frac{\partial u}{\partial y}\right)^2 - \left(\frac{\partial v}{\partial x}\right)^2 - 2\left(\frac{\partial v}{\partial y}\right)^2 - 2\frac{\partial v}{\partial x}\frac{\partial u}{\partial y}\right).$$

Therefore, governing equations (1.6) are obtained:

$$\frac{\partial u}{\partial x} + \frac{\partial v}{\partial y} = 0$$

$$u\frac{\partial u}{\partial x} + v\frac{\partial u}{\partial y} = -\frac{1}{\rho}\frac{\partial p}{\partial x} + \frac{\mu}{\rho}\left(\frac{\partial^2 u}{\partial x^2} + \frac{\partial^2 u}{\partial y^2}\right)$$
$$+ \frac{\alpha_1}{\rho}\left[2\frac{\partial^2}{\partial x^2}\left(u\frac{\partial u}{\partial x} + v\frac{\partial u}{\partial y}\right) + \frac{\partial^2}{\partial y^2}\left(u\frac{\partial u}{\partial x} + v\frac{\partial u}{\partial y}\right)\right.$$
$$+ \frac{\partial^2}{\partial x \partial y}\left(u\frac{\partial v}{\partial x} + v\frac{\partial v}{\partial y}\right) + 2\frac{\partial}{\partial y}\left(\frac{\partial u}{\partial x}\frac{\partial u}{\partial y} + \frac{\partial v}{\partial x}\frac{\partial v}{\partial y}\right)$$
$$\left. + \frac{\partial}{\partial x}\left(\left(\frac{\partial v}{\partial x}\right)^2 - \left(\frac{\partial u}{\partial y}\right)^2 - 2\left(\frac{\partial u}{\partial x}\right)^2 - 2\frac{\partial v}{\partial x}\frac{\partial u}{\partial y}\right)\right],$$

$$u\frac{\partial v}{\partial x} + v\frac{\partial v}{\partial y} = -\frac{1}{\rho}\frac{\partial p}{\partial y} + \frac{\mu}{\rho}\left(\frac{\partial^2 v}{\partial x^2} + \frac{\partial^2 v}{\partial y^2}\right)$$
$$+ \frac{\alpha_1}{\rho}\left[2\frac{\partial^2}{\partial y^2}\left(u\frac{\partial v}{\partial x} + v\frac{\partial v}{\partial y}\right) + \frac{\partial^2}{\partial x^2}\left(u\frac{\partial v}{\partial x} + v\frac{\partial v}{\partial y}\right)\right.$$
$$+ \frac{\partial^2}{\partial x \partial y}\left(u\frac{\partial u}{\partial x} + v\frac{\partial u}{\partial y}\right) + 2\frac{\partial}{\partial x}\left(\frac{\partial u}{\partial x}\frac{\partial u}{\partial y} + \frac{\partial v}{\partial x}\frac{\partial v}{\partial y}\right)$$
$$\left. + \frac{\partial}{\partial y}\left(\left(\frac{\partial u}{\partial y}\right)^2 - \left(\frac{\partial v}{\partial x}\right)^2 - 2\left(\frac{\partial v}{\partial y}\right)^2 - 2\frac{\partial v}{\partial x}\frac{\partial u}{\partial y}\right)\right].$$

All the calculations in this section have been checked with MAPLE [**50**].

A.2. Boundary layer approximation

We derive the boundary layer equations for a second order model. We denote L as the x-scale of variation and δ to be the characteristic length in the y-direction. From the continuity equation (1.6a), we deduce that the wall-normal velocity v is of order $\delta U/L$. Taking U and L to be of order 1, we write the orders of magnitude of the various terms underneath each equation. The momentum equation in the x-direction (1.6b) is

$$u\frac{\partial u}{\partial x} + v\frac{\partial u}{\partial y} = -\frac{1}{\rho}\frac{\partial p}{\partial x} + \frac{\mu}{\rho}\left(\frac{\partial^2 u}{\partial x^2} + \frac{\partial^2 u}{\partial y^2}\right) \qquad (A.3)$$

$$\quad 1 \qquad\quad 1 \qquad\qquad\qquad \delta^2 \quad\; 1 \quad\; \frac{1}{\delta^2}$$

$$+ \frac{\alpha_1}{\rho} \left[2\frac{\partial^2}{\partial x^2}\left(u\frac{\partial u}{\partial x} + v\frac{\partial u}{\partial y} \right) + \frac{\partial^2}{\partial y^2}\left(u\frac{\partial u}{\partial x} + v\frac{\partial u}{\partial y} \right) \right.$$

$$\delta^2 \qquad\qquad 1 \qquad 1 \qquad\qquad \frac{1}{\delta^2} \qquad \frac{1}{\delta^2}$$

$$+ \frac{\partial^2}{\partial x \partial y}\left(u\frac{\partial v}{\partial x} + v\frac{\partial v}{\partial y} \right) + 2\frac{\partial}{\partial y}\left(\frac{\partial u}{\partial x}\frac{\partial u}{\partial y} + \frac{\partial v}{\partial x}\frac{\partial v}{\partial y} \right)$$

$$1 \qquad 1 \qquad\qquad \frac{1}{\delta^2} \qquad 1$$

$$+ \frac{\partial}{\partial x}\left(\left(\frac{\partial v}{\partial x}\right)^2 - \left(\frac{\partial u}{\partial y}\right)^2 - 2\left(\frac{\partial u}{\partial x}\right)^2 - 2\frac{\partial v}{\partial x}\frac{\partial u}{\partial y} \right) \right].$$

$$\delta^2 \qquad \frac{1}{\delta^2} \qquad\qquad 1 \qquad\qquad 1$$

The momentum equation in the y-direction (1.6c) is

$$u\frac{\partial v}{\partial x} + v\frac{\partial v}{\partial y} = -\frac{1}{\rho}\frac{\partial p}{\partial y} + \frac{\mu}{\rho}\left(\frac{\partial^2 v}{\partial x^2} + \frac{\partial^2 v}{\partial y^2} \right) \tag{A.4}$$

$$\delta \qquad \delta \qquad\qquad\qquad \delta^2 \quad \delta \quad \frac{1}{\delta}$$

$$+ \frac{\alpha_1}{\rho}\left[2\frac{\partial^2}{\partial y^2}\left(u\frac{\partial v}{\partial x} + v\frac{\partial v}{\partial y} \right) + \frac{\partial^2}{\partial x^2}\left(u\frac{\partial v}{\partial x} + v\frac{\partial v}{\partial y} \right) \right.$$

$$\delta^2 \qquad\qquad \frac{1}{\delta} \qquad \frac{1}{\delta} \qquad\qquad \delta \qquad \delta$$

$$+ \frac{\partial^2}{\partial x \partial y}\left(u\frac{\partial u}{\partial x} + v\frac{\partial u}{\partial y} \right) + 2\frac{\partial}{\partial x}\left(\frac{\partial u}{\partial x}\frac{\partial u}{\partial y} + \frac{\partial v}{\partial x}\frac{\partial v}{\partial y} \right)$$

$$\frac{1}{\delta} \qquad \frac{1}{\delta} \qquad\qquad \frac{1}{\delta} \qquad \delta$$

$$+ \frac{\partial}{\partial y}\left(\left(\frac{\partial u}{\partial y}\right)^2 - \left(\frac{\partial v}{\partial x}\right)^2 - 2\left(\frac{\partial v}{\partial y}\right)^2 - 2\frac{\partial v}{\partial x}\frac{\partial u}{\partial y} \right) \right].$$

$$\frac{1}{\delta^3} \qquad \delta \qquad\qquad \frac{1}{\delta} \qquad\qquad \frac{1}{\delta}$$

Retaining the terms of order 1 from the first equation (A.3), we obtain the following

$$u\frac{\partial u}{\partial x} + v\frac{\partial u}{\partial y} = -\frac{1}{\rho}\frac{\partial p}{\partial x} + \frac{\mu}{\rho}\left(\frac{\partial^2 u}{\partial y^2} \right) + \frac{\alpha_1}{\rho}\left[\frac{\partial^2}{\partial y^2}\left(u\frac{\partial u}{\partial x} + v\frac{\partial u}{\partial y} \right) \right. \tag{A.5}$$

$$\left. + 2\frac{\partial}{\partial y}\left(\frac{\partial u}{\partial x}\frac{\partial u}{\partial y} \right) - \frac{\partial}{\partial x}\left(\left(\frac{\partial u}{\partial y}\right)^2 \right) \right].$$

At leading order, the equation (A.4) gives

$$0 = -\frac{1}{\rho}\frac{\partial p}{\partial y} + \frac{\alpha_1}{\rho}\frac{\partial}{\partial y}\left(\left(\frac{\partial u}{\partial y}\right)^2\right).$$

Defining

$$p_1 = p - \frac{\alpha_1}{\rho}\left(\frac{\partial u}{\partial y}\right)^2,$$

we have that p_1 depends only on x. We take the limit of Equation (A.5) as $y \to \infty$, and we get

$$-\frac{1}{\rho}\frac{\partial p_1}{\partial x} = U_e\frac{dU_e}{dx}.$$

where U_e is the free-stream velocity.

Combining equation (A.5) with the equation for $\tilde{p}$, we obtain the boundary layer approximation (1.8):

$$u\frac{\partial u}{\partial x} + v\frac{\partial u}{\partial y} = -\frac{1}{\rho}\frac{\partial p}{\partial x} + \frac{\mu}{\rho}\frac{\partial^2 u}{\partial y^2}$$
$$+ \frac{\alpha_1}{\rho}\left[v\frac{\partial^3 u}{\partial y^3} + \frac{\partial}{\partial x}\left(u\frac{\partial^2 u}{\partial y^2}\right) + \frac{\partial u}{\partial y}\frac{\partial^2 v}{\partial y^2}\right].$$

A.3. Useful identities in 3D

In this section we derive some identities useful to derive the stability equations for three-dimensional disturbances, which will be done in Section A.4. The left-hand side of the balance of linear momentum (1.4) can be written component-wise as follows

$$\left(\rho\frac{D\mathbf{v}}{Dt}\right)_1 = \rho\left(\frac{\partial \mathbf{v}}{\partial t} + (\mathbf{v}\cdot\nabla)\mathbf{v}\right)_1 = \rho\left(\frac{\partial u}{\partial t} + u\frac{\partial u}{\partial x} + v\frac{\partial u}{\partial y} + w\frac{\partial u}{\partial z}\right),$$

$$\left(\rho\frac{D\mathbf{v}}{Dt}\right)_2 = \rho\left(\frac{\partial \mathbf{v}}{\partial t} + (\mathbf{v}\cdot\nabla)\mathbf{v}\right)_2 = \rho\left(\frac{\partial v}{\partial t} + u\frac{\partial v}{\partial x} + v\frac{\partial v}{\partial y} + w\frac{\partial v}{\partial z}\right),$$

$$\left(\rho\frac{D\mathbf{v}}{Dt}\right)_3 = \rho\left(\frac{\partial \mathbf{v}}{\partial t} + (\mathbf{v}\cdot\nabla)\mathbf{v}\right)_3 = \rho\left(\frac{\partial w}{\partial t} + u\frac{\partial w}{\partial x} + v\frac{\partial w}{\partial y} + w\frac{\partial w}{\partial z}\right).$$

Substituting the expression for the stress tensor (1.1) and making use of relation (1.3), the right-hand side of equation (1.4) becomes

$$\nabla\cdot\boldsymbol{\sigma} = -\nabla p + \mu\nabla\cdot A_1 + \alpha_1\nabla\cdot\left(A_2 - A_1^2\right).$$

Since $\mathbf{v}$ is divergence free, the viscous term becomes

$$\nabla \cdot A_1 = \Delta\mathbf{v} = \begin{bmatrix} \Delta u \\ \Delta v \\ \Delta w \end{bmatrix},$$

where Δ is the Laplacian operator. The non-Newtonian term multiplied by α_1 becomes

$$\nabla \cdot \left(A_2 - A_1^2\right) = \nabla \cdot \left(\frac{\partial \mathbf{A}_1}{\partial t} + (\mathbf{v} \cdot \nabla)\,A_1 + \nabla\mathbf{v}\nabla\mathbf{v}^T - \nabla\mathbf{v}^T\nabla\mathbf{v}\right).$$

The gradient of the velocity field is a tensor that can be written as follows

$$\nabla\mathbf{v} = \begin{bmatrix} \frac{\partial u}{\partial x} & \frac{\partial v}{\partial x} & \frac{\partial w}{\partial x} \\ \frac{\partial u}{\partial y} & \frac{\partial v}{\partial y} & \frac{\partial w}{\partial y} \\ \frac{\partial u}{\partial z} & \frac{\partial v}{\partial z} & \frac{\partial w}{\partial z} \end{bmatrix},$$

Therefore, we obtain the following identities:

$$(\mathbf{v} \cdot \nabla)\,\nabla\mathbf{v}^T = \begin{bmatrix} u\frac{\partial^2 u}{\partial x^2} + v\frac{\partial^2 u}{\partial x\partial y} + w\frac{\partial^2 u}{\partial x\partial z} & u\frac{\partial^2 u}{\partial x\partial y} + v\frac{\partial^2 u}{\partial y^2} + w\frac{\partial^2 u}{\partial y\partial z} & u\frac{\partial^2 u}{\partial x\partial z} + v\frac{\partial^2 u}{\partial y\partial z} + w\frac{\partial^2 u}{\partial z^2} \\ u\frac{\partial^2 v}{\partial x^2} + v\frac{\partial^2 v}{\partial y\partial x} + w\frac{\partial^2 v}{\partial z\partial x} & u\frac{\partial^2 v}{\partial x\partial y} + v\frac{\partial^2 v}{\partial y^2} + w\frac{\partial^2 v}{\partial y\partial z} & u\frac{\partial^2 v}{\partial x\partial z} + v\frac{\partial^2 v}{\partial y\partial z} + w\frac{\partial^2 v}{\partial z^2} \\ u\frac{\partial^2 w}{\partial x^2} + v\frac{\partial^2 w}{\partial y\partial x} + w\frac{\partial^2 w}{\partial z\partial x} & u\frac{\partial^2 w}{\partial x\partial y} + v\frac{\partial^2 w}{\partial y^2} + w\frac{\partial^2 w}{\partial y\partial z} & u\frac{\partial^2 w}{\partial x\partial z} + v\frac{\partial^2 w}{\partial y\partial z} + w\frac{\partial^2 w}{\partial z^2} \end{bmatrix},$$

$$(\mathbf{v} \cdot \nabla)\,\nabla\mathbf{v} = \begin{bmatrix} u\frac{\partial^2 u}{\partial x^2} + v\frac{\partial^2 u}{\partial x\partial y} + w\frac{\partial^2 u}{\partial x\partial z} & u\frac{\partial^2 v}{\partial x^2} + v\frac{\partial^2 v}{\partial y\partial x} + w\frac{\partial^2 v}{\partial x\partial z} & u\frac{\partial^2 w}{\partial x^2} + v\frac{\partial^2 w}{\partial y\partial x} + w\frac{\partial^2 w}{\partial z\partial x} \\ u\frac{\partial^2 u}{\partial x\partial y} + v\frac{\partial^2 u}{\partial y^2} + w\frac{\partial^2 u}{\partial z\partial y} & u\frac{\partial^2 v}{\partial x\partial y} + v\frac{\partial^2 v}{\partial y^2} + w\frac{\partial^2 v}{\partial y\partial z} & u\frac{\partial^2 w}{\partial x\partial y} + v\frac{\partial^2 w}{\partial y^2} + w\frac{\partial^2 w}{\partial z\partial y} \\ u\frac{\partial^2 u}{\partial x\partial z} + v\frac{\partial^2 u}{\partial y\partial z} + w\frac{\partial^2 u}{\partial z^2} & u\frac{\partial^2 v}{\partial x\partial z} + v\frac{\partial^2 v}{\partial y\partial z} + w\frac{\partial^2 v}{\partial z^2} & u\frac{\partial^2 w}{\partial x\partial z} + v\frac{\partial^2 w}{\partial y\partial z} + w\frac{\partial^2 w}{\partial z^2} \end{bmatrix},$$

$$\nabla\mathbf{v}\nabla\mathbf{v}^T = \begin{bmatrix} \left(\frac{\partial u}{\partial x}\right)^2 + \left(\frac{\partial v}{\partial x}\right)^2 + \left(\frac{\partial w}{\partial x}\right)^2 & \frac{\partial u}{\partial x}\frac{\partial u}{\partial y} + \frac{\partial v}{\partial x}\frac{\partial v}{\partial y} + \frac{\partial w}{\partial x}\frac{\partial w}{\partial y} & \frac{\partial u}{\partial x}\frac{\partial u}{\partial z} + \frac{\partial v}{\partial x}\frac{\partial v}{\partial z} + \frac{\partial w}{\partial x}\frac{\partial w}{\partial z} \\ \frac{\partial u}{\partial x}\frac{\partial u}{\partial y} + \frac{\partial v}{\partial x}\frac{\partial v}{\partial y} + \frac{\partial w}{\partial x}\frac{\partial w}{\partial y} & \left(\frac{\partial u}{\partial y}\right)^2 + \left(\frac{\partial v}{\partial y}\right)^2 + \left(\frac{\partial w}{\partial y}\right)^2 & \frac{\partial u}{\partial y}\frac{\partial u}{\partial z} + \frac{\partial v}{\partial z}\frac{\partial v}{\partial y} + \frac{\partial w}{\partial z}\frac{\partial w}{\partial y} \\ \frac{\partial u}{\partial x}\frac{\partial u}{\partial z} + \frac{\partial v}{\partial x}\frac{\partial v}{\partial z} + \frac{\partial w}{\partial x}\frac{\partial w}{\partial z} & \frac{\partial u}{\partial y}\frac{\partial u}{\partial z} + \frac{\partial v}{\partial z}\frac{\partial v}{\partial y} + \frac{\partial w}{\partial z}\frac{\partial w}{\partial y} & \left(\frac{\partial u}{\partial z}\right)^2 + \left(\frac{\partial v}{\partial z}\right)^2 + \left(\frac{\partial w}{\partial z}\right)^2 \end{bmatrix},$$

$$\nabla\mathbf{v}^T\nabla\mathbf{v} = \begin{bmatrix} \left(\frac{\partial u}{\partial x}\right)^2 + \left(\frac{\partial u}{\partial y}\right)^2 + \left(\frac{\partial u}{\partial z}\right)^2 & \frac{\partial u}{\partial x}\frac{\partial v}{\partial x} + \frac{\partial u}{\partial y}\frac{\partial v}{\partial y} + \frac{\partial u}{\partial z}\frac{\partial v}{\partial z} & \frac{\partial u}{\partial x}\frac{\partial w}{\partial x} + \frac{\partial u}{\partial y}\frac{\partial w}{\partial y} + \frac{\partial u}{\partial z}\frac{\partial w}{\partial z} \\ \frac{\partial u}{\partial x}\frac{\partial v}{\partial x} + \frac{\partial u}{\partial y}\frac{\partial v}{\partial y} + \frac{\partial u}{\partial z}\frac{\partial v}{\partial z} & \left(\frac{\partial v}{\partial x}\right)^2 + \left(\frac{\partial v}{\partial y}\right)^2 + \left(\frac{\partial v}{\partial z}\right)^2 & \frac{\partial w}{\partial x}\frac{\partial v}{\partial x} + \frac{\partial w}{\partial y}\frac{\partial v}{\partial y} + \frac{\partial w}{\partial z}\frac{\partial v}{\partial z} \\ \frac{\partial u}{\partial x}\frac{\partial w}{\partial x} + \frac{\partial u}{\partial y}\frac{\partial w}{\partial y} + \frac{\partial u}{\partial z}\frac{\partial w}{\partial z} & \frac{\partial w}{\partial x}\frac{\partial v}{\partial x} + \frac{\partial w}{\partial y}\frac{\partial v}{\partial y} + \frac{\partial w}{\partial z}\frac{\partial v}{\partial z} & \left(\frac{\partial w}{\partial x}\right)^2 + \left(\frac{\partial w}{\partial y}\right)^2 + \left(\frac{\partial w}{\partial z}\right)^2 \end{bmatrix}.$$

A.4. Three-dimensional stability equations

In this section, we derive the three-dimensional stability equations, in the form of an eigenvalue problem (1.27) and in the form of an initial-value problem (2.2). The modified Orr-Sommerfeld equation (1.22) can be obtained as a particular case.

The unsteady and three-dimensional equation of motions for a second grade fluid derived from equations (1.4), (1.5) and Definition (1.1), after applying the non-dimensionalisation (1.20), can be written as follows

$$\begin{cases} \dfrac{\partial u}{\partial x} + \dfrac{\partial v}{\partial y} + \dfrac{\partial w}{\partial z} = 0, \\[2mm] \dfrac{Du}{Dt} = -\dfrac{\partial p}{\partial x} + \dfrac{\partial \tau_{xx}}{\partial x} + \dfrac{\partial \tau_{xy}}{\partial y} + \dfrac{\partial \tau_{xz}}{\partial z}, \\[2mm] \dfrac{Dv}{Dt} = -\dfrac{\partial p}{\partial y} + \dfrac{\partial \tau_{xy}}{\partial x} + \dfrac{\partial \tau_{yy}}{\partial y} + \dfrac{\partial \tau_{yz}}{\partial z}, \\[2mm] \dfrac{Dw}{Dt} = -\dfrac{\partial p}{\partial z} + \dfrac{\partial \tau_{xz}}{\partial x} + \dfrac{\partial \tau_{yz}}{\partial y} + \dfrac{\partial \tau_{zz}}{\partial z}, \end{cases} \tag{A.6}$$

where T_{ij} are components of the extra-stress tensor $\mathbf{T} = \boldsymbol{\sigma} + p\mathbf{I}$, with $\boldsymbol{\sigma}$ stress tensor defined by Equation (1.1). Therefore, the normalised extra-stress tensor $\mathbf{T}$ can be written as

$$\mathbf{T} = \frac{1}{Re_0}\mathbf{A}_1 + K_0\left(\mathbf{A}_2 - \mathbf{A}_1^2\right),$$

where $\mathbf{A}_1$ and $\mathbf{A}_2$ are given by definitions (1.2). Then, using identities that can be found in Appendix A.3, we have

$$\begin{aligned} T_{xx} = {} & \frac{2}{Re_0}\frac{\partial u}{\partial x} + K_0\left[2\frac{\partial^2 u}{\partial t\partial x} + 2u\frac{\partial^2 u}{\partial x^2} + 2v\frac{\partial^2 u}{\partial x\partial y} + 2w\frac{\partial^2 u}{\partial x\partial z}\right. \\[2mm] & \left. + \left(\frac{\partial v}{\partial x}\right)^2 - \left(\frac{\partial u}{\partial y}\right)^2 + \left(\frac{\partial w}{\partial x}\right)^2 - \left(\frac{\partial u}{\partial z}\right)^2\right], \end{aligned}$$

$$\begin{aligned} T_{xy} = {} & \frac{1}{Re_0}\left(\frac{\partial u}{\partial y} + \frac{\partial v}{\partial x}\right) + K_0\left[\frac{\partial^2 u}{\partial t\partial y} + \frac{\partial^2 v}{\partial t\partial x} + u\frac{\partial^2 u}{\partial x\partial y} + v\frac{\partial^2 u}{\partial y^2}\right. \\[2mm] & + w\frac{\partial^2 u}{\partial y\partial z} + u\frac{\partial^2 v}{\partial x^2} + v\frac{\partial^2 v}{\partial x\partial y} + w\frac{\partial^2 v}{\partial x\partial z} + \frac{\partial u}{\partial x}\frac{\partial u}{\partial y} + \frac{\partial v}{\partial x}\frac{\partial v}{\partial y} \\[2mm] & \left. + \frac{\partial w}{\partial x}\frac{\partial w}{\partial y} - \frac{\partial u}{\partial x}\frac{\partial v}{\partial x} - \frac{\partial u}{\partial y}\frac{\partial v}{\partial y} - \frac{\partial u}{\partial z}\frac{\partial v}{\partial z}\right], \end{aligned}$$

$$T_{xz} = \frac{1}{Re_0}\left(\frac{\partial w}{\partial x} + \frac{\partial u}{\partial z}\right) + K_0\left[\frac{\partial^2 w}{\partial t \partial x} + \frac{\partial^2 u}{\partial t \partial z} + u\frac{\partial^2 u}{\partial x \partial z} + v\frac{\partial^2 u}{\partial y \partial z}\right.$$

$$+ w\frac{\partial^2 u}{\partial z^2} + u\frac{\partial^2 w}{\partial x^2} + v\frac{\partial^2 w}{\partial y \partial x} + w\frac{\partial^2 w}{\partial z \partial x} + \frac{\partial u}{\partial x}\frac{\partial u}{\partial z} + \frac{\partial v}{\partial x}\frac{\partial v}{\partial z}$$

$$\left.+ \frac{\partial w}{\partial x}\frac{\partial w}{\partial z} - \frac{\partial u}{\partial x}\frac{\partial w}{\partial x} - \frac{\partial u}{\partial y}\frac{\partial w}{\partial y} - \frac{\partial u}{\partial z}\frac{\partial w}{\partial z}\right],$$

$$T_{yy} = \frac{2}{Re_0}\frac{\partial v}{\partial y} + K_0\left[2\frac{\partial^2 v}{\partial t \partial y} + 2v\frac{\partial^2 v}{\partial y^2} + 2u\frac{\partial^2 v}{\partial x \partial y} + 2w\frac{\partial^2 v}{\partial y \partial z}\right.$$

$$\left.+ \left(\frac{\partial u}{\partial y}\right)^2 - \left(\frac{\partial v}{\partial x}\right)^2 + \left(\frac{\partial w}{\partial y}\right)^2 - \left(\frac{\partial v}{\partial z}\right)^2\right],$$

$$T_{yz} = \frac{1}{Re_0}\left(\frac{\partial w}{\partial y} + \frac{\partial v}{\partial z}\right) + K_0\left[\frac{\partial^2 w}{\partial t \partial y} + \frac{\partial^2 v}{\partial t \partial z} + u\frac{\partial^2 v}{\partial x \partial z} + v\frac{\partial^2 v}{\partial y \partial z}\right.$$

$$+ w\frac{\partial^2 v}{\partial z^2} + u\frac{\partial^2 w}{\partial x \partial y} + v\frac{\partial^2 w}{\partial y^2} + w\frac{\partial^2 w}{\partial z \partial y} + \frac{\partial u}{\partial y}\frac{\partial u}{\partial z} + \frac{\partial v}{\partial z}\frac{\partial v}{\partial y}$$

$$\left.+ \frac{\partial w}{\partial z}\frac{\partial w}{\partial y} - \frac{\partial w}{\partial x}\frac{\partial v}{\partial x} - \frac{\partial w}{\partial y}\frac{\partial v}{\partial y} - \frac{\partial w}{\partial z}\frac{\partial v}{\partial z}\right],$$

$$T_{zz} = \frac{2}{Re_0}\frac{\partial w}{\partial z} + K_0\left[2\frac{\partial^2 w}{\partial t \partial z} + 2u\frac{\partial^2 w}{\partial x \partial z} + 2v\frac{\partial^2 w}{\partial y \partial z} + 2w\frac{\partial^2 w}{\partial z^2}\right.$$

$$\left.+ \left(\frac{\partial u}{\partial z}\right)^2 + \left(\frac{\partial v}{\partial z}\right)^2 - \left(\frac{\partial w}{\partial x}\right)^2 - \left(\frac{\partial w}{\partial y}\right)^2\right].$$

We assume a parallel and steady base flow and we decompose the velocity components and the pressure into base field and small disturbances as follows

$$u = U_B(y) + \epsilon\tilde{u}(x, y, z, t),$$
$$v = \epsilon\tilde{v}(x, y, z, t),$$
$$w = \epsilon\tilde{w}(x, y, z, t),$$
$$p = P_B(x) + \epsilon\tilde{p}(x, y, z, t),$$

where ϵ is a small positive parameter and U_B, P_B represent mean streamwise velocity and pressure, respectively. By substituting these decompositions and retaining terms of order $O(\epsilon)$ in the system (A.6), we obtain

the equations for the disturbance velocities $\tilde{u}, \tilde{v}, \tilde{w}$ and pressure $\tilde{p}$

$$\begin{cases} \dfrac{\partial \tilde{u}}{\partial x} + \dfrac{\partial \tilde{v}}{\partial y} + \dfrac{\partial \tilde{w}}{\partial z} = 0, \\[2mm] \dfrac{\partial \tilde{u}}{\partial t} + U_B \dfrac{\partial \tilde{u}}{\partial x} + U_B' \tilde{v} = -\dfrac{\partial \tilde{p}}{\partial x} + \dfrac{\partial \tilde{T}_{xx}}{\partial x} + \dfrac{\partial \tilde{T}_{xy}}{\partial y} + \dfrac{\partial \tilde{T}_{xz}}{\partial z}, \\[2mm] \dfrac{\partial \tilde{v}}{\partial t} + U_B \dfrac{\partial \tilde{v}}{\partial x} = -\dfrac{\partial \tilde{p}}{\partial y} + \dfrac{\partial \tilde{T}_{xy}}{\partial x} + \dfrac{\partial \tilde{T}_{yy}}{\partial y} + \dfrac{\partial \tilde{T}_{yz}}{\partial z}, \\[2mm] \dfrac{\partial \tilde{w}}{\partial t} + U_B \dfrac{\partial \tilde{w}}{\partial x} = -\dfrac{\partial \tilde{p}}{\partial z} + \dfrac{\partial \tilde{T}_{xz}}{\partial x} + \dfrac{\partial \tilde{T}_{yz}}{\partial y} + \dfrac{\partial \tilde{T}_{zz}}{\partial z}, \end{cases} \tag{A.7}$$

where

$$\tilde{T}_{xx} = \frac{2}{Re_0} \frac{\partial \tilde{u}}{\partial x} + K_0 \left(2 \frac{\partial^2 \tilde{u}}{\partial t \partial x} + 2 U_B \frac{\partial^2 \tilde{u}}{\partial x^2} - 2 U_B' \frac{\partial \tilde{u}}{\partial y} \right),$$

$$\tilde{T}_{xy} = \frac{1}{Re_0} \left(\frac{\partial \tilde{u}}{\partial y} + \frac{\partial \tilde{v}}{\partial x} \right) + K_0 \left(\frac{\partial^2 \tilde{u}}{\partial t \partial y} + \frac{\partial^2 \tilde{v}}{\partial t \partial x} + U_B \frac{\partial^2 \tilde{u}}{\partial x \partial y} \right.$$
$$\left. + U_B'' \tilde{v} + U_B \frac{\partial^2 \tilde{v}}{\partial x^2} + U_B' \frac{\partial \tilde{u}}{\partial x} - U_B' \frac{\partial \tilde{v}}{\partial y} \right),$$

$$\tilde{T}_{xz} = \frac{1}{Re_0} \left(\frac{\partial \tilde{w}}{\partial x} + \frac{\partial \tilde{u}}{\partial z} \right) + K_0 \left(\frac{\partial^2 \tilde{w}}{\partial t \partial x} + \frac{\partial^2 \tilde{u}}{\partial t \partial z} + U_B \frac{\partial^2 \tilde{u}}{\partial x \partial z} \right.$$
$$\left. + U_B \frac{\partial^2 \tilde{w}}{\partial x^2} - U_B' \frac{\partial}{\partial y} \right),$$

$$\tilde{T}_{yy} = \frac{2}{Re_0} \frac{\partial \tilde{v}}{\partial y} + K_0 \left(2 \frac{\partial^2 \tilde{v}}{\partial t \partial y} + 2 U_B \frac{\partial^2 \tilde{v}}{\partial x \partial y} + 2 U_B' \frac{\partial \tilde{u}}{\partial y} \right),$$

$$\tilde{T}_{yz} = \frac{1}{Re_0} \left(\frac{\partial \tilde{w}}{\partial y} + \frac{\partial \tilde{v}}{\partial z} \right) + K_0 \left(\frac{\partial^2 \tilde{w}}{\partial t \partial y} + \frac{\partial^2 \tilde{v}}{\partial t \partial z} + U_B \frac{\partial^2 \tilde{v}}{\partial x \partial z} \right.$$
$$\left. + U_B \frac{\partial^2 \tilde{w}}{\partial x \partial y} + U_B' \frac{\partial \tilde{u}}{\partial z} \right),$$

$$\tilde{T}_{zz} = \frac{2}{Re_0} \frac{\partial \tilde{w}}{\partial z} + K_0 \left(2 \frac{\partial^2 \tilde{w}}{\partial t \partial z} + 2 U_B \frac{\partial^2 \tilde{w}}{\partial x \partial z} \right).$$

Taking the normal mode form for the perturbations

$$(\tilde{u}, \tilde{v}, \tilde{w}, \tilde{p}) = (\hat{u}(t, y), \hat{v}(t, y), \hat{w}(t, y), \hat{p}(t, y)) \, e^{i(\alpha x + \beta z)},$$

substituting and dividing by the exponential term, the components of the extra-stress tensor become

$$\hat{T}_{xx} = \frac{2}{Re_0} i\alpha\hat{u} + K_0 \left(2i\alpha\hat{u}_t - 2\alpha^2 U_B\hat{u} - 2U_B'\mathcal{D}\hat{u}\right),$$

$$\hat{T}_{xy} = \frac{1}{Re_0} \left(\mathcal{D}\hat{u} + i\alpha\hat{v}\right) + K_0\big(\mathcal{D}\hat{u}_t + i\alpha\hat{v}_t + i\alpha U_B\mathcal{D}\hat{u}$$
$$+ U_B''v - \alpha^2 U_B\hat{v} + i\alpha U_B'\hat{u} - U_B'\mathcal{D}\hat{v}\big),$$

$$\hat{T}_{xz} = \frac{1}{Re_0} \left(i\alpha\hat{w} + i\beta\hat{u}\right) + K_0\big(i\alpha\hat{w}_t + i\beta\hat{u}_t - \alpha\beta U_B\hat{u}$$
$$- \alpha^2 U_B\hat{w} - U_B'\mathcal{D}\hat{w}\big),$$

$$\hat{T}_{yy} = \frac{2}{Re_0}\mathcal{D}\hat{v} + K_0 \left(2\mathcal{D}\hat{v}_t + 2i\alpha U_B\mathcal{D}\hat{v} + 2U_B'\mathcal{D}\hat{u}\right),$$

$$\hat{T}_{yz} = \frac{1}{Re_0} \left(\mathcal{D}\hat{w} + i\beta\hat{v}\right) + K_0\big(\mathcal{D}\hat{w}_t + i\beta\hat{v}_t - \alpha\beta U_B\hat{v}$$
$$+ i\alpha U_B\mathcal{D}\hat{w} + i\beta U_B'\hat{u}\big),$$

$$\hat{T}_{zz} = \frac{2}{Re_0} i\beta\hat{w} + K_0 \left(2i\beta\hat{w}_t - 2\alpha\beta U_B\hat{w}\right),$$

where $\mathcal{D}$ denotes the derivative with respect to y and the subscript t denotes the derivative with respect to t. Therefore, the continuity equation in the system (A.7) becomes

$$i\alpha\hat{u} + \mathcal{D}\hat{v} + i\beta\hat{w} = 0,$$

and the equations of motion in the system (A.7) become

$$\hat{u}_t + i\alpha U_B\hat{u} + U_B'\hat{v} = -i\alpha\hat{p} + \frac{1}{Re_0} \left(\mathcal{D}^2\hat{u} - k^2\hat{u}\right)$$
$$+ K_0\big(\mathcal{D}^2\hat{u}_t - k^2\hat{u}_t - i\alpha k^2 U_B\hat{u} + i\alpha U_B\mathcal{D}^2\hat{u}$$
$$+ U_B'''\hat{v} - \alpha^2 U_B'\hat{v} + i\alpha U_B''\hat{u} + i\alpha U_B'\mathcal{D}\hat{u}\big), \quad \text{(A.8)}$$

$$\hat{v}_t + i\alpha U_B\hat{v} = -\mathcal{D}\hat{p} + \frac{1}{Re_0} \left(\mathcal{D}^2\hat{v} - k^2\hat{v}\right)$$
$$+ K_0\big(\mathcal{D}^2\hat{v}_t - k^2\hat{v}_t + i\alpha U_B''\hat{v} - i\alpha k^2 U_B\hat{v} - k^2 U_B'\hat{u}$$
$$+ i\alpha U_B'\mathcal{D}\hat{v} + i\alpha U_B\mathcal{D}^2\hat{v} + 2U_B''\mathcal{D}\hat{u} + 2U_B'\mathcal{D}^2\hat{u}\big), \quad \text{(A.9)}$$

$$\hat{w}_t + i\alpha U_B \hat{w} = -i\beta \hat{p} + \frac{1}{Re_0}\left(\mathcal{D}^2 \hat{w} - k^2 \hat{w}\right)$$
$$+ K_0\big(\mathcal{D}^2 \hat{w}_t - k^2 \hat{w}_t - i\alpha k^2 U_B \hat{w} - \alpha\beta U_B' \hat{v}$$
$$+ i\alpha U_B \mathcal{D}^2 \hat{w} + i\beta U_B'' \hat{u} + i\beta U_B' \mathcal{D}\hat{u}\big). \quad \text{(A.10)}$$

We eliminate the pressure from the equations by introducing the wall-normal vorticity $\hat{\eta} = i\beta\hat{u} - i\alpha\hat{w}$. First, we multiply equation (A.8) by $i\beta$ and subtract $i\alpha$ times equation (A.10), which yields the following equation for $\tilde{\eta}$

$$\hat{\eta}_t + K_0\left(k^2 - \mathcal{D}^2\right)\hat{\eta}_t = -i\alpha U_B \hat{\eta} - i\beta U_B' \hat{v} + \frac{1}{Re_0}\left(\mathcal{D}^2 - k^2\right)\hat{\eta} \quad \text{(A.11)}$$
$$+ K_0\left(i\alpha U_B \left(\mathcal{D}^2 - k^2\right)\hat{\eta} + i\beta U_B''' \hat{v}\right),$$

where $k^2 = \alpha^2 + \beta^2$. Then we multiply (A.8) by $i\alpha$ and sum $i\beta$ times (A.10) and we obtain

$$-\mathcal{D}\hat{v}_t - i\alpha U_B \mathcal{D}\hat{v} + i\alpha U_B' \hat{v} = k^2 \hat{p} + \frac{1}{Re_0}\left(k^2 - \mathcal{D}^2\right)\mathcal{D}\hat{v}$$
$$+ K_0\Big(\left(k^2 - \mathcal{D}^2\right)\mathcal{D}\hat{v}_t + i\alpha U_B''' \hat{v} - i\alpha k^2 U_B' \hat{v}$$
$$+ i\alpha k^2 U_B \mathcal{D}\hat{v} - i\alpha U_B \mathcal{D}^3 \hat{v} - k^2 U_B'' \hat{u} - k^2 U_B' \mathcal{D}\hat{u}\Big).$$

Deriving the last equation with respect to y, we get

$$-\mathcal{D}^2 \hat{v}_t - i\alpha U_B \mathcal{D}^2 \hat{v} + i\alpha U_B'' \hat{v} = k^2 \mathcal{D}\hat{p} + \frac{1}{Re_0}\left(k^2 - \mathcal{D}^2\right)\mathcal{D}^2 \hat{v}$$
$$+ K_0\Big(\left(k^2 - \mathcal{D}^2\right)\mathcal{D}^2 \hat{v}_t + i\alpha U_B^{iv} \hat{v} + i\alpha U_B''' \mathcal{D}\hat{v} - i\alpha k^2 U_B'' \hat{v}$$
$$+ i\alpha k^2 U_B \mathcal{D}^2 \hat{v} - i\alpha U_B' \mathcal{D}^3 \hat{v} - i\alpha U_B \mathcal{D}^4 \hat{v}$$
$$- k^2 U_B''' \hat{u} - 2k^2 U_B'' \mathcal{D}\hat{u} - k^2 U_B' \mathcal{D}^2 \hat{u}\Big).$$

We can now sum this equation to k^2 times (A.9) in order to derive the following equation for $\hat{v}$

$$k^2 \hat{v}_t + i\alpha k^2 U_B \hat{v} = \mathcal{D}^2 \hat{v}_t + i\alpha U_B \mathcal{D}^2 \hat{v} - i\alpha U_B'' \hat{v} - \frac{1}{Re_0}\left(k^2 - \mathcal{D}^2\right)^2 \hat{v}$$
$$+ K_0\Big(-\left(k^2 - \mathcal{D}^2\right)^2 \hat{v}_t + i\alpha U_B^{iv} \hat{v} + i\alpha U_B''' \mathcal{D}\hat{v} + 2i\alpha k^2 U \mathcal{D}^2 \hat{v}$$
$$- i\alpha U_B' \mathcal{D}^3 \hat{v} - i\alpha U_B \mathcal{D}^4 \hat{v} - i\alpha k^4 U_B \hat{v} + i\alpha k^2 U_B' \mathcal{D}\hat{v}$$
$$- k^4 U_B' \hat{u} - k^2 U_B''' \hat{u} + k^2 U_B' \mathcal{D}^2 \hat{u}\Big).$$

Rearranging terms and using $\hat{u} = \frac{i}{k^2}(\alpha\mathcal{D}\hat{v} - \beta\hat{\eta})$ we obtain

$$\left(k^2 - \mathcal{D}^2\right)\hat{v}_t + K_0\left(k^2 - \mathcal{D}^2\right)^2\hat{v}_t = -i\alpha U_B\left(k^2 - \mathcal{D}^2\right)\hat{v}$$
$$- i\alpha U_B''\hat{v} - \frac{1}{Re_0}\left(k^2 - \mathcal{D}^2\right)^2\hat{v} + K_0\Big(i\alpha U_B^{iv}\hat{v} - i\alpha k^4 U_B\hat{v}$$
$$+ 2i\alpha k^2 U_B\mathcal{D}^2\hat{v} - i\alpha U_B\mathcal{D}^4\hat{v} + i\beta k^2 U_B'\hat{\eta} + i\beta U_B'''\hat{\eta} - i\beta U_B'\mathcal{D}^2\hat{\eta}\Big).$$
$$(A.12)$$

Therefore, the coupled equations (A.11) and (A.12) for $\hat{\eta}$ and $\hat{v}$ will form the initial-value problem (2.5). We now assume a normal mode form also in time, as follows

$$(\hat{v}, \hat{\eta}) = (\hat{v}_1(y), \hat{\eta}_1(y))e^{-i\omega t},$$

and define $\mathbf{q} = (\hat{v}_1, \hat{\eta}_1)^T$. Then, we can rewrite equations (A.11) and (A.12) as an eigenvalue problem, as follows

$$\mathcal{L}\mathbf{q} = \omega\mathcal{M}\mathbf{q},$$

where $\mathcal{M}$ and $\mathcal{L}$ are linear operators defined as follows

$$\mathcal{L} = \left[\begin{array}{cc} \mathcal{L}_{OS} & \mathcal{L}_{CN} \\ \mathcal{L}_C & \mathcal{L}_{SQ} \end{array}\right],$$

$$\mathcal{M} = \left[\begin{array}{cc} k^2 - \mathcal{D}^2 + K_0\left(k^2 - \mathcal{D}^2\right)^2 & 0 \\ 0 & 1 + K_0\left(k^2 - \mathcal{D}^2\right) \end{array}\right],$$

where

$$\mathcal{L}_{OS} = \alpha U_B\left(k^2 - \mathcal{D}^2\right) + \alpha U_B'' + \frac{1}{iRe_0}\left(k^2 - \mathcal{D}^2\right)^2$$
$$+ K_0\Big(-\alpha U_B^{iv} + \alpha k^4 U_B - 2\alpha k^2 U_B\mathcal{D}^2 + \alpha U_B\mathcal{D}^4\Big),$$
$$\mathcal{L}_{CN} = K_0\left(-\beta k^2 U_B' - \beta U_B''' + \beta U_B'\mathcal{D}^2\right),$$
$$\mathcal{L}_C = \beta U_B' - K_0\beta U_B''',$$
$$\mathcal{L}_{SQ} = \alpha U_B + \frac{1}{iRe_0}\left(k^2 - \mathcal{D}^2\right) + \alpha K_0 U_B\left(k^2 - \mathcal{D}^2\right).$$

Therefore, we obtained the eigenvalue problem (1.27).

For two-dimensional disturbances $\beta = 0$ and the equation for the wall-normal velocity $\hat{v}_1$, when written in terms of the stream function

ϕ, reduces to the modified Orr-Sommerfeld equation (1.22), which is

$$(U_B - c)(\phi'' - \alpha^2 \phi) - U_B'' \phi = \frac{1}{i\alpha Re_0} \left\{ \phi^{iv} - 2\alpha^2 \phi'' + \alpha^4 \phi \right\}$$
$$+ K_0 \left\{ (U_B - c)(\phi^{iv} - 2\alpha^2 \phi'' + \alpha^4 \phi) - U_B^{iv} \phi \right\}.$$

These calculations have been checked with MAPLE [50].

A.5. Conservation of energy

In this section we show that nonlinear terms do not enter the evolution equation for the perturbation energy for the second grade models, similarly to Newtonian fluids (Drazin [23]). Therefore, nonlinear terms conserve energy and the energy balance can be obtained from the linearised equations. We show this for two-dimensional disturbances and we do not make any assumption on the mean flow nor on the domain.

Let us denote with u_i and U_i the perturbation velocity and the mean flow velocity in the x_i-direction, respectively. Then, we can write the equation of motion for a second grade model in the x_i-direction using Einstein summation convention as follows

$$\frac{\partial u_i}{\partial t} = -u_j \frac{\partial u_i}{\partial x_j} - U_j \frac{\partial u_i}{\partial x_j} - u_j \frac{\partial U_i}{\partial x_j} - \frac{\partial p}{\partial x_i} + \frac{1}{Re_0} \frac{\partial^2 u_i}{\partial x_j^2} + K_0 \frac{\partial \tau_{ij}}{\partial x_j},$$

where τ_{ij} are the components of the following tensor

$$\boldsymbol{\tau} = \mathbf{A}_2 - \mathbf{A}_1^2.$$

This formulation can be straightforwardly derived from equations (1.4), (1.5) and definition (1.1). We isolate the time derivatives in τ_{ij} as follows

$$\tau_{ij} = K_0 \frac{\partial}{\partial t} \left(\frac{\partial^2 u_i}{\partial x_j^2} \right) + \tau'_{ij},$$

where τ'_{ij} is the part of τ_{ij} that does not include any derivative with respect to time. Multiplying each motion equation by u_i and summing on the index i we obtain

$$\frac{1}{2} \frac{\partial \mathbf{u}^2}{\partial t} - K_0 \frac{\partial}{\partial t} \left(u_i \frac{\partial^2 u_i}{\partial x_j^2} \right) = - u_i u_j \frac{\partial u_i}{\partial x_j} - u_i U_j \frac{\partial u_i}{\partial x_j} - u_i u_j \frac{\partial U_i}{\partial x_j}$$

$$- u_i \frac{\partial p}{\partial x_i} + \frac{1}{Re_0} u_i \frac{\partial^2 u_i}{\partial x_j^2} + K_0 u_i \frac{\partial \tau'_{ij}}{\partial x_j}.$$

Using $\nabla \cdot \mathbf{U} = 0$ and $\nabla \cdot \mathbf{u} = 0$, we can rewrite it as follows

$$\frac{1}{2} \frac{\partial \mathbf{u}^2}{\partial t} - K_0 \frac{\partial}{\partial t} \left(\frac{\partial}{\partial x_j} \left(u_i \frac{\partial u_i}{\partial x_j} \right) - \left(\frac{\partial u_i}{\partial x_j} \right)^2 \right) =$$

$$- \frac{1}{2} \frac{\partial (u_i^2 u_j)}{\partial x_j} - \frac{1}{2} \frac{\partial (u_i^2 U_j)}{\partial x_j} - u_i u_j D_{ij} - \frac{\partial (u_i p)}{\partial x_i}$$

$$+ \frac{1}{Re_0} \left(\frac{\partial}{\partial x_j} \left(u_i \frac{\partial u_i}{\partial x_j} \right) - \left(\frac{\partial u_i}{\partial x_j} \right)^2 \right) + K_0 u_i \frac{\partial \tau'_{ij}}{\partial x_j}, \quad \text{(A.13)}$$

where D_{ij} is the mean rate-of-strain defined as follows

$$D_{ij} = \frac{1}{2} \left(\frac{\partial U_i}{\partial x_j} + \frac{\partial U_j}{\partial x_i} \right).$$

We define the total energy of the perturbation contained in a volume V as follows

$$E = \int_V \frac{1}{2} \mathbf{u}^2 dV + K_0 \int_V \left(\frac{\partial u_i}{\partial x_j} \right)^2 dV,$$

and the evolution equation for the disturbance kinetic energy is obtained by integrating equation (A.13) over the volume V. In the Newtonian case, where $K_0 = 0$, the energy E reduces to the kinetic energy and all cubic terms that derive from the nonlinear terms are integrated out by assuming the disturbance to be localised or spatially periodic and using Gauss' theorem.

In the non-Newtonian case, where $K_0 \neq 0$, integrating equation (A.13) over V we obtain

$$\frac{\partial E}{\partial t} = \int_V \left(-u_i u_j D_{ij} - \frac{1}{Re_0} \left(\frac{\partial u_i}{\partial x_j} \right)^2 + K_0 u_i \frac{\partial \tau'_{ij}}{\partial x_j} \right) dV.$$

We focus on two-dimensional disturbances, and we show that only the linear terms coming from the term $u_i \frac{\partial \tau'_{ij}}{\partial x_j}$ will appear in the energy evolution equation. We expand the non-Newtonian contribution to the energy equation (A.13) as follows

$$u_i \frac{\partial \tau'_{ij}}{\partial x_j} = N_{\mathrm{l}} + N_{\mathrm{nl}},$$

where N_l are the terms resulting from the linear terms that we do not report here for brevity and N_nl are cubic terms resulting from the nonlinear terms that can be written explicitly as follows

$$N_\text{nl} = \underbrace{2u\frac{\partial^2 f}{\partial x^2} + 2v\frac{\partial^2 g}{\partial y^2}}_{\text{A}} + \underbrace{u\frac{\partial^2 f}{\partial y^2} + v\frac{\partial^2 g}{\partial x^2}}_{\text{B}}$$

$$+ \underbrace{u\frac{\partial^2 g}{\partial x\partial y} + v\frac{\partial^2 f}{\partial x\partial y}}_{\text{C}} + \underbrace{2u\frac{\partial h}{\partial y} + 2v\frac{\partial h}{\partial x}}_{\text{D}}$$

$$+ \underbrace{u\frac{\partial l}{\partial x} + u\frac{\partial m}{\partial x} - v\frac{\partial l}{\partial y} + v\frac{\partial m}{\partial y}}_{\text{E}},$$

with f, g, h, l and m are functions introduced to simplify the calculations, defined as follows

$$f = u\frac{\partial u}{\partial x} + v\frac{\partial u}{\partial y},$$

$$g = u\frac{\partial v}{\partial x} + v\frac{\partial v}{\partial y},$$

$$h = \frac{\partial u}{\partial x}\frac{\partial u}{\partial y} + \frac{\partial v}{\partial x}\frac{\partial v}{\partial y},$$

$$l = \left(\frac{\partial v}{\partial x}\right)^2 - \left(\frac{\partial u}{\partial y}\right)^2,$$

$$m = -2\left(\frac{\partial u}{\partial x}\right)^2 - 2\frac{\partial v}{\partial x}\frac{\partial u}{\partial y}.$$

Using the continuity equation, A+C becomes

$$\text{A+C} = 2u\frac{\partial^2 f}{\partial x^2} + 2v\frac{\partial^2 g}{\partial y^2} + u\frac{\partial^2 g}{\partial x\partial y} + v\frac{\partial^2 f}{\partial x\partial y}$$

$$= \frac{\partial}{\partial x}\left(u\frac{\partial f}{\partial x}\right) + \frac{\partial}{\partial y}\left(v\frac{\partial f}{\partial x}\right) + \frac{\partial}{\partial x}\left(u\frac{\partial g}{\partial y}\right) + \frac{\partial}{\partial y}\left(v\frac{\partial g}{\partial y}\right)$$

$$+ \underbrace{u\frac{\partial^2 f}{\partial x^2} + v\frac{\partial^2 g}{\partial y^2}}_{\text{F}}.$$

All the terms that can be written as a divergence will be integrated out, therefore we consider only F that can be rewritten as

$$\text{F} = u\frac{\partial}{\partial x}\left(u\frac{\partial^2 u}{\partial x^2} + \left(\frac{\partial u}{\partial x}\right)^2 + v\frac{\partial^2 u}{\partial x \partial y} + \frac{\partial v}{\partial x}\frac{\partial u}{\partial y}\right)$$

$$+ v\frac{\partial}{\partial y}\left(u\frac{\partial^2 v}{\partial x \partial y} + \left(\frac{\partial v}{\partial y}\right)^2 + v\frac{\partial^2 v}{\partial y^2} + \frac{\partial v}{\partial x}\frac{\partial u}{\partial y}\right)$$

$$= u\frac{\partial}{\partial x}\left(u\frac{\partial^2 u}{\partial x^2} + v\frac{\partial^2 u}{\partial x \partial y}\right) - v\frac{\partial}{\partial y}\left(u\frac{\partial^2 u}{\partial x^2} + v\frac{\partial^2 u}{\partial x \partial y}\right)$$

$$+ \frac{\partial}{\partial x}\left(u\left(\frac{\partial u}{\partial x}\right)^2 + u\frac{\partial v}{\partial x}\frac{\partial u}{\partial y}\right) + \frac{\partial}{\partial y}\left(u\left(\frac{\partial u}{\partial x}\right)^2 + u\frac{\partial v}{\partial x}\frac{\partial u}{\partial y}\right)$$

$$= \frac{\partial}{\partial x}\left(u\left(\frac{\partial u}{\partial x}\right)^2 + u\frac{\partial v}{\partial x}\frac{\partial u}{\partial y} + u^2\frac{\partial^2 u}{\partial x^2} + uv\frac{\partial^2 u}{\partial x \partial y}\right)$$

$$+ \frac{\partial}{\partial y}\left(u\left(\frac{\partial u}{\partial x}\right)^2 + u\frac{\partial v}{\partial x}\frac{\partial u}{\partial y} - u^2\frac{\partial^2 u}{\partial x^2} - uv\frac{\partial^2 u}{\partial x \partial y}\right)$$

$$+ \underbrace{2\frac{\partial v}{\partial y}\left(u\frac{\partial^2 u}{\partial x^2} + v\frac{\partial^2 u}{\partial x \partial y}\right)}_{\text{G}}.$$

B becomes

$$\text{B} = u\frac{\partial}{\partial y}\left(u\frac{\partial^2 u}{\partial x \partial y} + v\frac{\partial^2 u}{\partial y^2}\right) + v\frac{\partial}{\partial x}\left(u\frac{\partial^2 v}{\partial x^2} + v\frac{\partial^2 v}{\partial x \partial y}\right)$$

$$= \frac{\partial}{\partial y}\left(u^2\frac{\partial^2 u}{\partial x \partial y} + uv\frac{\partial^2 u}{\partial y^2}\right) + \frac{\partial}{\partial x}\left(uv\frac{\partial^2 v}{\partial x^2} + v^2\frac{\partial^2 v}{\partial x \partial y}\right)$$

$$\underbrace{- \frac{\partial u}{\partial y}\left(u\frac{\partial^2 u}{\partial x \partial y} + v\frac{\partial^2 u}{\partial y^2}\right) - \frac{\partial v}{\partial x}\left(u\frac{\partial^2 v}{\partial x^2} + v\frac{\partial^2 v}{\partial x \partial y}\right)}_{\text{H}}.$$

D becomes

$$\text{D} = 2\frac{\partial uh}{\partial y} + 2\frac{\partial vh}{\partial x} - 2\frac{\partial u}{\partial y}h - 2\frac{\partial v}{\partial x}h$$

$$= 2\frac{\partial uh}{\partial y} + 2\frac{\partial vh}{\partial x} \underbrace{- 2\left(\frac{\partial u}{\partial y}\right)^2\frac{\partial u}{\partial x} - 2\left(\frac{\partial v}{\partial x}\right)^2\frac{\partial v}{\partial y}}_{\text{I}}.$$

E becomes

$$E = \frac{\partial um}{\partial x} + \frac{\partial vm}{\partial y} + \frac{\partial ul}{\partial x} - \frac{\partial vl}{\partial y} - l\frac{\partial u}{\partial x} + l\frac{\partial v}{\partial y}$$

$$= \frac{\partial um}{\partial x} + \frac{\partial vm}{\partial y} + \frac{\partial ul}{\partial x} - \frac{\partial vl}{\partial y} + \underbrace{2l\frac{\partial v}{\partial y}}_{J}.$$

Now, adding all the terms that are not yet expressed as a divergence, we obtain

$$G + H + I + J = 2\frac{\partial v}{\partial y}\left(u\frac{\partial^2 u}{\partial x^2} + v\frac{\partial^2 u}{\partial x \partial y}\right)$$

$$- \frac{\partial u}{\partial y}\left(u\frac{\partial^2 u}{\partial x \partial y} + v\frac{\partial^2 u}{\partial y^2}\right) - \frac{\partial v}{\partial x}\left(u\frac{\partial^2 v}{\partial x^2} + v\frac{\partial^2 v}{\partial x \partial y}\right)$$

$$= u\left(2\frac{\partial v}{\partial y}\frac{\partial^2 u}{\partial x^2} - \frac{\partial u}{\partial y}\frac{\partial^2 u}{\partial x \partial y} - \frac{\partial v}{\partial x}\frac{\partial^2 v}{\partial x^2}\right)$$

$$+ v\left(2\frac{\partial v}{\partial y}\frac{\partial^2 u}{\partial x \partial y} - \frac{\partial u}{\partial y}\frac{\partial^2 u}{\partial y^2} - \frac{\partial v}{\partial x}\frac{\partial^2 v}{\partial x \partial y}\right)$$

$$= -u\frac{\partial}{\partial x}\left(\left(\frac{\partial u}{\partial x}\right)^2 + \frac{1}{2}\left(\frac{\partial u}{\partial y}\right)^2 + \frac{1}{2}\left(\frac{\partial v}{\partial x}\right)^2\right)$$

$$- v\frac{\partial}{\partial y}\left(\left(\frac{\partial v}{\partial y}\right)^2 + \frac{1}{2}\left(\frac{\partial u}{\partial y}\right)^2 + \frac{1}{2}\left(\frac{\partial v}{\partial x}\right)^2\right)$$

$$= -\frac{\partial}{\partial x}\left(u\left(\frac{\partial u}{\partial x}\right)^2 + \frac{1}{2}u\left(\frac{\partial u}{\partial y}\right)^2 + \frac{1}{2}u\left(\frac{\partial v}{\partial x}\right)^2\right)$$

$$- \frac{\partial}{\partial y}\left(v\left(\frac{\partial v}{\partial y}\right)^2 + \frac{1}{2}v\left(\frac{\partial u}{\partial y}\right)^2 + \frac{1}{2}v\left(\frac{\partial v}{\partial x}\right)^2\right).$$

All the nonlinear terms have been written as divergence. Using Gauss' divergence theorem and the boundary conditions, these terms will disappear once they are integrated over the domain.

A.6. Energy balance

In this section, we derive an energy balance for the second order fluids. Consider the modified Orr-Sommerfeld equation (1.22)

$$(U_B - c)\left(\phi'' - \alpha^2\phi\right) - U_B''\phi = \frac{1}{i\alpha Re_0}\left\{\phi^{iv} - 2\alpha^2\phi'' + \alpha^4\phi\right\}$$
$$+ K_0\left\{(U_B - c)\left(\phi^{iv} - 2\alpha^2\phi'' + \alpha^4\phi\right) - U_B^{iv}\phi\right\}. \quad (A.14)$$

Multiplying by the complex conjugate $\bar{\phi}$, integrating with respect to y and using the homogeneous boundary conditions the left hand side of Equation (A.14) becomes

$$\int_0^\infty \left((U_B - c)\phi''\bar{\phi} - \alpha^2(U_B - c)|\phi|^2 - U_B''|\phi|^2\right)\,dy =$$
$$= c\left(I_1^2 + \alpha^2 I_0^2\right) - \int_0^\infty \left(U_B'\phi'\bar{\phi} + U_B|\phi'|^2 + \left(U_B'' + \alpha^2 U_B\right)|\phi|^2\right)\,dy,$$

where we defined

$$I_k^2 = \int_0^\infty |\phi^{(k)}|^2\,dy \qquad \text{for } k = 0, 1, 2.$$

Integration of the viscous terms in Equation (A.14) gives

$$\int_0^\infty \left(\phi^{iv}\bar{\phi} - 2\alpha^2\phi''\bar{\phi} + \alpha^4|\phi|^2\right)\,dy = I_2^2 + 2\alpha^2 I_1^2 + \alpha^4 I_0^2.$$

The non-Newtonian terms, multiplied by K_0, in Equation (A.14) become

$$\int_0^\infty \left((U_B - c)\left(\phi^{iv} - 2\alpha^2\phi'' + \alpha^4\phi\right) - U_B^{iv}\phi\right)\,dy =$$
$$= -c\left(I_2^2 + 2\alpha^2 I_1^2 + \alpha^4 I_0^2\right) + \int_0^\infty \left(U_B''\phi''\bar{\phi} + 2U_B'\phi''\bar{\phi}' + 2\alpha^2 U_B'\phi'\bar{\phi}\right)\,dy$$
$$+ \int_0^\infty \left(U_B|\phi''|^2 + 2\alpha^2 U_B|\phi'|^2 + \left(\alpha^4 U_B - U_B^{iv}\right)|\phi|^2\right)\,dy.$$

Thus, we get

$$-i\alpha Re_0 c\left(I_1^2 + \alpha^2 I_0^2\right) = (-1 + i\alpha c K_0 Re_0)\left(I_2^2 + 2\alpha^2 I_1^2 + \alpha^4 I_0^2\right)$$
$$-i\alpha Re_0 \int_0^\infty \left(U_B'\phi'\bar{\phi} + U_B|\phi'|^2 + \left(U_B'' + \alpha^2 U_B\right)|\phi|^2\right)\,dy$$
$$-i\alpha K_0 Re_0 \int_0^\infty \left(U_B''\phi''\bar{\phi} + 2U_B'\phi''\bar{\phi}' + 2\alpha^2 U_B'\phi'\bar{\phi} + U_B|\phi''|^2\right)\,dy$$

$$- i\alpha K_0 Re_0 \int_0^\infty \left(2\alpha^2 U_B |\phi'|^2 + \left(\alpha^4 U_B - U_B^{iv}\right) |\phi|^2\right) \, dy.$$

We take the real part of this equation and use the following identities for a complex number $z = z_r + iz_i$

$$\Re(iz) = \Re(iz_r - z_i) = -z_i,$$

$$z_i = \frac{z - \bar{z}}{2i} = -\frac{i}{2}(z - \bar{z}).$$

We find

$$\alpha Re_0 c_i \left(I_1^2 + \alpha^2 I_0^2\right) = - \left(1 + \alpha c_i K_0 Re_0\right) \left(I_2^2 + 2\alpha^2 I_1^2 + \alpha^4 I_0^2\right)$$

$$- \frac{i\alpha Re_0}{2} \int_0^\infty \left(U_B' \left(\phi' \bar{\phi} - \phi \bar{\phi}'\right)\right) \, dy$$

$$- \frac{i\alpha K_0 Re_0}{2} \int_0^\infty \left(U_B'' \left(\phi'' \bar{\phi} - \phi \bar{\phi}''\right) + 2\alpha^2 U_B' \left(\phi' \bar{\phi} - \phi' \bar{\phi}\right)\right) \, dy$$

$$- \frac{i\alpha K_0 Re_0}{2} \int_0^\infty \left(2 U_B' \left(\phi'' \bar{\phi}' - \phi' \bar{\phi}''\right)\right) \, dy.$$

Using integration by part, we obtain the energy balance (1.24):

$$\alpha Re_0 c_i \left(I_1^2 + \alpha^2 I_0^2\right) + K_0 \alpha Re_0 c_i \left(I_2^2 + 2\alpha^2 I_1^2 + \alpha^4 I_0^2\right) =$$

$$- \left(I_2^2 + 2\alpha^2 I_1^2 + \alpha^4 I_2^2\right) - \frac{i\alpha Re_0}{2} \int_0^\infty \left(U_B' \left(\phi' \bar{\phi} - \phi \bar{\phi}'\right)\right) \, dy$$

$$- \frac{i\alpha K_0 Re_0}{2} \int_0^\infty \left(2 U_B' \left(\phi'' \bar{\phi}' - \phi' \bar{\phi}''\right) + \left(2\alpha^2 U_B' - U_B'''\right) \left(\phi' \bar{\phi} - \phi' \bar{\phi}\right)\right) \, dy.$$

A.7. Non-dimensional governing equations for the PTT and Giesekus models

The ASBL equations for the PTT and the Giesekus models need to be solved numerically. For the purpose of the linear stability analysis, we non-dimensionalise the ASBL equations using the following transformations (4.8). Therefore, the equations obtained in Section 4.3.8 for the linear PTT model become

$$\frac{du}{dy} + \frac{d\tau_{xy}}{dy} + \beta \frac{d^2 u}{dy^2} = 0$$

$$- \frac{\partial p}{\partial y} + \frac{1}{Re} \frac{d\tau_{yy}}{dy} = 0$$

where $Re = \frac{U_e}{V_0}$ is the Reynolds number and the components of the polymeric stress tensor are governed by

$$\tau_{xx} - K\frac{d\tau_{xx}}{dy} - 2\,Wi\frac{du}{dy}\tau_{xy} + \xi\,Wi\frac{du}{dy}\tau_{xy} + \epsilon\frac{Wi}{1-\beta}\tau_{xx}\left(\tau_{xx} + \tau_{yy}\right) = 0$$

$$\tau_{xy} - K\frac{d\tau_{xy}}{dy} - Wi\frac{du}{dy}\tau_{yy} + \xi\frac{Wi}{2}\frac{du}{dy}\left(\tau_{xx} + \tau_{yy}\right)$$
$$+ \epsilon\frac{Wi}{1-\beta}\tau_{xy}\left(\tau_{xx} + \tau_{yy}\right) - (1-\beta)\frac{du}{dy} = 0$$

$$\tau_{yy} - K\frac{d\tau_{yy}}{dy} + \xi\,Wi\frac{du}{dy}\tau_{xy} + \epsilon\frac{Wi}{1-\beta}\tau_{yy}\left(\tau_{xx} + \tau_{yy}\right) = 0.$$

where $Wi = \frac{\lambda_1 U_e}{\delta_*} = \frac{\rho\lambda_1 U_e V_0}{\eta_0}$ is the Weissenberg number and $K = \frac{\rho\lambda_1 V_0^2}{\eta_0}$.

For the exponential PTT model, the motion equations do not change from the linear case. However the elastic stress equations obtained in Section 4.3.9 become

$$\tau_{xx} - K\frac{d\tau_{xx}}{dy} - 2\,Wi\frac{du}{dy}\tau_{xy} + \xi\,Wi\frac{du}{dy}\tau_{xy}$$
$$+ \left[\exp\left(\epsilon\frac{Wi}{1-\beta}(\tau_{xx} + \tau_{yy})\right) - 1\right]\tau_{xx} = 0$$

$$\tau_{xy} - K\frac{d\tau_{xy}}{dy} - Wi\frac{du}{dy}\tau_{yy} + \xi\frac{Wi}{2}\frac{du}{dy}\left(\tau_{xx} + \tau_{yy}\right)$$
$$+ \left[\exp\left(\epsilon\frac{Wi}{1-\beta}(\tau_{xx} + \tau_{yy})\right) - 1\right]\tau_{xy} - (1-\beta)\frac{du}{dy} = 0$$

$$\tau_{yy} - K\frac{d\tau_{yy}}{dy} + \xi\,Wi\frac{du}{dy}\tau_{xy} + \left[\exp\left(\epsilon\frac{Wi}{1-\beta}(\tau_{xx} + \tau_{yy})\right) - 1\right]\tau_{yy} = 0.$$

For the Giesekus model, the equations obtained in Section 4.3.10 become

$$\tau_{xx} - K\frac{d\tau_{xx}}{dy} - 2\,Wi\frac{du}{dy}\tau_{xy} + \alpha\frac{Wi}{1-\beta}\left(\tau_{xx}^2 + \tau_{xy}^2\right) = 0$$

$$\tau_{xy} - K\frac{d\tau_{xy}}{dy} - Wi\frac{du}{dy}\tau_{yy} + \alpha\frac{Wi}{1-\beta}\tau_{xy}\left(\tau_{xx} + \tau_{yy}\right) - (1-\beta)\frac{du}{dy} = 0$$

$$\tau_{yy} - K\frac{d\tau_{yy}}{dy} + \alpha\frac{Wi}{1-\beta}\left(\tau_{xy}^2 + \tau_{yy}^2\right) = 0.$$

Bibliography

[1] ABBASBANDY, S., HAYAT, T., ALSAEDI, A., AND RASHIDI, M. M. Numerical and analytical solutions for Falkner-Skan flow of MHD Oldroyd-B fluid. *International Journal of Numerical Methods for Heat & Fluid Flow 24*, 2 (2014), 390–401.

[2] ALFREDSSON, P., AND MATSUBARA, M. Free-stream turbulence, streaky structures and transition in boundary layer flows. In *Fluids 2000 Conference and Exhibit* (Reston, Virigina, 2000), American Institute of Aeronautics and Astronautics.

[3] ANDERSON, J. D. Ludwig Prandtl's Boundary Layer. *Physics Today 58*, 12 (2005), 42–48.

[4] BARNES, H. A., HUTTON, J. F., AND WALTERS, K. *An Introduction to Rheology*. Rheology Series. Elsevier Science, 1989.

[5] BATCHELOR, G. K. *An Introduction to Fluid Dynamics*. Cambridge Mathematical Library. Cambridge University Press, 2000.

[6] BEARD, D. W., AND WALTERS, K. Elastico-viscous boundary-layer flows I. Two-dimensional flow near a stagnation point. *Mathematical Proceedings of the Cambridge Philosophical Society 60*, 3 (1964), 667–674.

[7] BHATNAGAR, R. K., GUPTA, G., AND RAJAGOPAL, K. R. Flow of an Oldroyd-B fluid due to a stretching sheet in the presence of a free stream velocity. *International Journal of Non-Linear Mechanics 30*, 3 (1995), 391–405.

[8] BISTAGNINO, A., BOFFETTA, G., CELANI, A., MAZZINO, A., PULIAFITO, A., AND VERGASSOLA, M. Nonlinear dynamics of the viscoelastic Kolmogorov flow. *Journal of Fluid Mechanics 590* (2007), 61–80.

[9] BLASIUS, H. Grenzschichten in flüssigkeiten mit kleiner reibung (The boundary layers in fluids with little friction). *Zeitschrift für Mathematik und Physik 56*, 1 (1950), 1–37.

[10] BOGER, D., AND WALTERS, K. *Rheological Phenomena in Focus*. ISSN. Elsevier Science, 2012.

[11] BRANDT, L. The lift-up effect: the linear mechanism behind transition and turbulence in shear flows. *European Journal of Mechanics - B/Fluids 47* (2014), 80–96.

[12] BRANDT, L., SCHLATTER, P., AND HENNINGSON, D. S. Transition in boundary layers subject to free-stream turbulence. *Journal of Fluid Mechanics 517* (2004), 167–198.

[13] BRIDGES, T. J., AND MORRIS, P. J. Differential eigenvalue problems in which the parameter appears nonlinearly. *Journal of Computational Physics 55*, 3 (1984), 437–460.

[14] BUTLER, K. M., AND FARRELL, B. F. Three-dimensional optimal perturbations in viscous shear flow. *Physics of Fluids A: Fluid Dynamics 4*, 8 (1992), 1637–1650.

[15] CHUN, D. H., AND SCHWARZ, W. H. Stability of a plane Poiseuille flow of a second order fluid. *Physics of Fluids 11*, 1 (1968), 5–9.

[16] CORBETT, P., AND BOTTARO, A. Optimal perturbations for boundary layers subject to stream-wise pressure gradient. *Physics of Fluids 12*, 1 (2000), 120–130.

[17] CRIMINALE, W. O., JACKSON, T. L., AND JOSLIN, R. D. *Theory and Computation of Hydrodynamic Stability*. Cambridge Monographs on Mechanics. Cambridge University Press, 2003.

[18] DAVIES, C. Numerical simulation of boundary layer disturbance evolution. *Philosophical Transactions of the Royal Society A: Mathematical, Physical and Engineering Sciences 363*, 1830 (2005), 1109–1118.

[19] DAVIES, C., AND CARPENTER, P. W. A novel velocity–vorticity formulation of the Navier–Stokes equations with applications to boundary layer disturbance evolution. *Journal of Computational Physics 172*, 1 (2001), 119–165.

[20] DE ANGELIS, E., CASCIOLA, C. M., L'VOV, V. S., PIVA, R., AND PROCACCIA, I. Drag reduction by polymers in turbulent channel flows: Energy redistribution between invariant empirical modes. *Physical Review E - Statistical Physics, Plasmas, Fluids, and Related Interdisciplinary Topics 67*, 5 (2003), 056312.

[21] DE ANGELIS, E., CASCIOLA, C. M., L'VOV, V. S., POMYALOV, A., PROCACCIA, I., AND TIBERKEVICH, V. Drag reduction by a linear viscosity profile. *Physical Review E - Statistical Physics, Plasmas, Fluids, and Related Interdisciplinary Topics 70*, 5 (2004), 055301.

[22] DEALY, J. M. Weissenberg and Deborah numbers – their definition and use. *Rheology Bulletin 79*, 2 (2010), 14–18.

[23] DRAZIN, P. G. *Introduction to Hydrodynamic Stability*. Cambridge Texts in Applied Mathematics. Cambridge University Press, 2002.

[24] DRISCOLL, T. A., HALE, N., AND TREFETHEN, L. N. *Chebfun Guide*, 2014. Chebfun Version 5. `www.chebfun.org`.

[25] DUNN, J. E., AND FOSDICK, R. L. Thermodynamics, stability, and boundedness of fluids of complexity 2 and fluids of second grade. *Archive for Rational Mechanics and Analysis 56*, 3 (1974), 191–252.

[26] DUNN, J. E., AND RAJAGOPAL, K. R. Fluids of differential type: critical review and thermodynamic analysis. *International Journal of Engineering Science 33*, 5 (1995), 689–729.

[27] ELLINGSEN, T., AND PALM, E. Stability of linear flow. *Physics of Fluids 18*, 4 (1975), 487–488.

[28] FALKNER, V. M., AND SKAN, S. W. Some approximate solutions of the boundary layer equations. *Philosophical Magazine 12* (1931), 865–896.

[29] FOSDICK, R. L., AND RAJAGOPAL, K. R. Anomalous features in the model of second order fluids. *Archive for Rational Mechanics and Analysis 70*, 2 (1979), 145–152.

[30] FRANSSON, J. H. M. Investigations of the asymptotic suction boundary layer. Tech. rep., Royal Institute of Technology, Stockholm, Sweden, 2001.

[31] GARG, V. K., AND RAJAGOPAL, K. R. Stagnation point flow of a non-Newtonian fluid. *Mechanics Research Communications 17*, 6 (1990), 415–421.

[32] GARG, V. K., AND RAJAGOPAL, K. R. Flow of a non-Newtonian fluid past a wedge. *Acta Mechanica 88*, 1 (1991), 113–123.

[33] GIESEKUS, H. A simple constitutive equation for polymer fluids based on the concept of deformation-dependent tensorial mobility. *Journal of Non-Newtonian Fluid Mechanics 11*, 1-2 (1982), 69–109.

[34] GRIFFITHS, P. T. Stability of the shear-thinning boundary-layer flow over a flat inclined plate. *Proceedings of the Royal Society of London. Series A, Mathematical and Physical Sciences 473*, 2205 (2017), 20170350.

[35] GROSCH, C. E., AND ORSZAG, S. A. Numerical solution of problems in unbounded regions: Coordinate transforms. *Journal of Computational Physics 25*, 3 (1977), 273–295.

[36] GUSTAVSSON, L. H. Initial-value problem for boundary layer flows. *Physics of Fluids 22*, 9 (1979), 1602–1605.

[37] GUSTAVSSON, L. H. Excitation of direct resonances in plane Poiseuille flow. *Studies in Applied Mathematics 75*, 3 (1986), 227–248.

[38] HARRIS, J. *Rheology and non-Newtonian flow.* Longman, 1977.

[39] HAYAT, T., IMTIAZ, M., AND ALSAEDI, A. Boundary layer flow of Oldroyd-B fluid by exponentially stretching sheet. *Applied Mathematics and Mechanics 37*, 5 (2016), 573–582.

[40] HERRON, I. H. The Orr-Sommerfeld equation on infinite intervals. *SIAM Review 29*, 4 (1987), 597–620.

[41] HO, T. C., AND DENN, M. M. Stability of plane Poiseuille flow of a highly elastic liquid. *Journal of Non-Newtonian Fluid Mechanics 3*, 2 (1977), 179–195.

[42] HODA, N., JOVANOVIC, M. R., AND KUMAR, S. Energy amplification in channel flows of viscoelastic fluids. *Journal of Fluid Mechanics 601* (2008), 407–424.

[43] HODA, N., JOVANOVIC, M. R., AND KUMAR, S. Frequency responses of streamwise-constant perturbations in channel flows of Oldroyd-B fluids. *Journal of Fluid Mechanics 625* (2009), 411–434.

[44] JAMES, D. F. Boger fluids. *Annual Review of Fluid Mechanics 41*, 1 (2009), 129–142.

[45] JOSEPH, D. D. Viscous potential flow. *Journal of Fluid Mechanics 479* (2003), 191–197.

[46] JOSEPH, D. D. Potential flow of viscous fluids: historical notes. *International Journal of Multiphase Flow 32*, 3 (2006), 285–310.

[47] JOSEPH, D. D., AND LIAO, T. Y. Potential flows of viscous and viscoelastic liquids. *Journal of Fluid Mechanics 265* (1994), 1–23.

[48] KHAPKO, T. Transition to turbulence in the asymptotic suction boundary layer. Tech. rep., Royal Institute of Technology, Stockholm, Sweden, 2014.

[49] LANDAHL, M. T. A note on an algebraic instability of inviscid parallel shear flows. *Journal of Fluid Mechanics 98*, 2 (1980), 243–251.

[50] MAPLESOFT, A DIVISION OF WATERLOO MAPLE INC., WATERLOO, ONTARIO. Maple 2018.1, 2018. www.maplesoft.com.

[51] MORGAN, S. *Stability of Periodically Modulated Rotating Disk Boundary Layers.* PhD thesis, Cardiff University, 2018.

[52] OLDROYD, J. G. On the formulation of rheological equations of state. *Proceedings of the Royal Society of London. Series A. Mathematical and Physical Sciences 200*, 1063 (1950), 523–541.

[53] ORSZAG, S. A. Accurate solution of the Orr-Sommerfeld stability equation. *Journal of Fluid Mechanics 50*, 4 (1971), 659–703.

[54] OWENS, R. G., AND PHILLIPS, T. N. *Computational Rheology.* Imperial College Press, 2002.

[55] PAKDEMIRLI, M. Conventional and multiple deck boundary layer approach to second and third grade fluids. *International Journal of Engineering Science 32*, 1 (1994), 141–154.

[56] PALMER, A. *Linear Stability Analyses of Poiseuille Flows of Viscoelastic Liquids.* PhD thesis, The University of Wales, Aberystwyth, 2007.

[57] PALMER, A., AND PHILLIPS, T. N. Numerical approximation of the spectra of Phan-Thien Tanner liquids. *Numerical Algorithms 38* (2005), 133–153.

[58] PEDLOSKY, J. *Geophysical Fluid Dynamics.* Springer New York, 2013.

[59] PHAN-THIEN, N. *Understanding Viscoelasticity.* Graduate Texts in Physics. Springer-Verlag Berlin Heidelberg, 2002.

[60] POOLE, R. J. The Deborah and Weissenberg numbers. *Rheology Bulletin 53*, 2 (2012), 32–39.

[61] PORTEOUS, K. C., AND DENN, M. M. Linear stability of plane Poiseuille flow of viscoelastic liquids. *Transactions of the Society of Rheology 16*, 2 (1972), 295.

[62] PRANDTL, L. Über flüssigkeitsbewegung bei sehr kleiner reibung (Motion of fluids with very little viscosity). In *Verhandlungen des III internationalen Mathematiker-Kongresses in Heidelberg, 1904* (1905), A. Krazer, Ed., pp. 484–491.

[63] RAFIKI, A., HIFDI, A., OUAZZANI TOUHAMI, M., AND TAGHAVI, S. M. Hydrodynamic stability of plane Poiseuille flow of non-Newtonian fluids in the

presence of a transverse magnetic field. *Journal of the Society of Rheology, Japan 42*, 1 (2014), 51–60.

[64] RAJAGOPAL, K. On boundary conditions for fluids of the differential type. In *Navier–Stokes Equations and Related Nonlinear Problems*, A. Sequeira, Ed. Plenum Press, 1995.

[65] RAJAGOPAL, K. R., GUPTA, A. S., AND NA, T. Y. A note on the Falkner-Skan flows of a non-Newtonian fluid. *International Journal of Non-Linear Mechanics 18*, 4 (1983), 313–320.

[66] RAJAGOPAL, K. R., GUPTA, A. S., AND WINEMAN, A. S. On a boundary layer theory for non-Newtonian fluids. *International Journal of Engineering Science 18*, 6 (1980), 875–883.

[67] RAJAGOPAL, K. R., AND KALONI, P. N. Some remarks on boundary conditions for flows of fluids of the differential type. In *Continuum Mechanics and its Applications*, G. A. C. Graham and S. K. Malik, Eds. Hemisphere Press, 1989.

[68] RAYLEIGH, L. On the stability, or instability, of certain fluid motions. *Proceedings of the London Mathematical Society s1-11*, 1 (1879), 57–72.

[69] REDDY, S. C., AND HENNINGSON, D. S. Energy growth in viscous channel flows. *Journal of Fluid Mechanics 252*, 2006 (1993), 209–238.

[70] RIVLIN, R. S., AND ERICKSEN, J. L. Stress deformation relations for isotropic materials. *Journal of Rational Mechanics and Analysis 4* (1955), 323–425.

[71] SADEGHY, K., TAGHAVI, S. M., KHABAZI, N., MIRZADEH, M., AND KARIMFAZLI, I. On the use of hydrodynamic instability test as an efficient tool for evaluating viscoelastic fluid models. *Advanced Studies in Theoretical Physics 1*, 8 (2007), 367–379.

[72] SAJID, M., ABBAS, Z., JAVED, T., AND ALI, N. Boundary layer flow of an Oldroyd-B fluid in the region of a stagnation point over a stretching sheet. *Canadian Journal of Physics 88*, 9 (2010), 635–640.

[73] SCHLICHTING, H., AND GERSTEN, K. *Boundary-Layer Theory*. Springer-Verlag Berlin Heidelberg, 2000.

[74] SCHMID, P. J. Linear stability theory and bypass transition in shear flows. *Physics of Plasmas 7*, 5 (2000), 1788–1794.

[75] SCHMID, P. J. Nonmodal stability theory. *Annual Review of Fluid Mechanics 39*, 1 (2007), 129–62.

[76] SCHMID, P. J., AND BRANDT, L. Analysis of Fluid Systems: Stability, Receptivity, Sensitivity: Lecture notes from the FLOW-NORDITA Summer School on Advanced Instability Methods for Complex Flows, Stockholm, Sweden, 2013. *Applied Mechanics Review 66*, 2 (2014), 024803–024824.

[77] SCHMID, P. J., AND HENNINGSON, D. S. *Stability and Transition in Shear Flows*. Applied Mathematical Sciences. Springer New York, 2000.

[78] SIBLEY, D. N. *Viscoelastic Flows of PTT Fluids*. PhD thesis, University of Bath, 2010.

[79] SPEZIALE, C. G. On the advantages of the vorticity-velocity formulation of the equations of fluid dynamics. *Journal of Computational Physics 73*, 2 (1987), 476–480.

[80] SURESHKUMAR, R., AND BERIS, A. N. Linear stability analysis of viscoelastic Poiseuille flow using an Arnoldi-based orthogonalization algorithm. *Journal of Non-Newtonian Fluid Mechanics 56*, 2 (1995), 151–182.

[81] TANI, I. History of Boundary Layer Theory. *Annual Review of Fluid Mechanics 9*, 1 (1977), 87–111.

[82] TANNER, R. I. *Engineering rheology*. Oxford Engineering Science Series. Oxford University Press, 2000.

[83] THIEN, N. P., AND TANNER, R. I. A new constitutive equation derived from network theory. *Journal of Non-Newtonian Fluid Mechanics 2*, 4 (1977), 353–365.

[84] TOLLMIEN, W. Über die entstehung der turbulenz (The production of turbulence). In *Vorträge aus dem Gebiete der Aerodynamik und verwandter Gebiete*, A. Gilles, L. Hopf, and T. V. Kármán, Eds. Springer, Berlin, Heidelberg, 1930, pp. 18–21.

[85] TREFETHEN, L. N. Pseudospectra of matrices. In *Numerical Analysis*, D. F. Griffiths and G. A. Watson, Eds. Longman Scientific & Technical, 1991.

[86] TREFETHEN, L. N. *Finite Difference and Spectral Methods for Ordinary and Partial Differential Equations*. Cambridge University Press, 1996. Unpublished text, available at http://people.maths.ox.ac.uk/trefethen/pdetext.html.

[87] TREFETHEN, L. N. *Spectral Methods in MATLAB*. Society for Industrial and Applied Mathematics, 2000.

[88] TREFETHEN, L. N. *Approximation Theory and Approximation Practice*. Other Titles in Applied Mathematics. SIAM, 2013.

[89] TREFETHEN, L. N., AND EMBREE, M. *Spectra and pseudospectra: The behaviour of nonnormal matrices and operators*. Princeton University Press, 2005.

[90] TREFETHEN, L. N., TREFETHEN, A. E., REDDY, S. C., AND DRISCOLL, T. A. Hydrodynamic stability without eigenvalues. *Science 261*, 5121 (1993), 578–584.

[91] VAJRAVELU, K., AND ROLLINS, D. Hydromagnetic flow of a second grade fluid over a stretching sheet. *Applied Mathematics and Computation 148*, 3 (2004), 783–791.

[92] VAJRAVELU, K., AND ROPER, T. Flow and heat transfer in a second grade fluid over a stretching sheet. *International Journal of Non-Linear Mechanics 34*, 6 (1999), 1031–1036.

[93] VAN DYKE, M. *Perturbation Methods in Fluid Mechanics*. Parabolic Press, 1975.

[94] WHITE, C. M., AND MUNGAL, M. G. Mechanics and prediction of turbulent drag reduction with polymer additives. *Annual Review of Fluid Mechanics 40*, 1 (2008), 235–256.

[95] White, J. L. Dynamics of viscoelastic fluids, melt fracture, and the rheology of fiber spinning. *Journal of Applied Polymer Science 8*, 5 (1964), 2339–2357.

[96] Zhang, M., Lashgari, I., Zaki, T. A., and Brandt, L. Linear stability analysis of channel flow of viscoelastic Oldroyd-B and FENE-P fluids. *Journal of Fluid Mechanics 737* (2013), 249–279.